

ROLE OF DISTANT, INTRASUBUNIT RESIDUES IN CATALASE-PEROXIDASE  
CATALYSIS: TRACING THE ROLE OF GENE DUPLICATION  
AND FUSION IN ENZYME STRUCTURE AND FUNCTION

Except where reference is made to the work of others, the work described in  
This dissertation is my own or was done in collaboration with my  
Advisory committee. This dissertation does not include  
proprietary or classified information.

---

Carma Oshea Cook

Certificate of Approval:

---

Holly R. Ellis  
Associate Professor  
Chemistry and Biochemistry

---

Douglas C. Goodwin, Chair  
Associate Professor  
Chemistry and Biochemistry

---

Evert C. Duin  
Assistant Professor  
Chemistry and Biochemistry

---

Edward J. Parish  
Professor  
Chemistry and Biochemistry

---

George T. Flowers  
Dean  
Graduate School

ROLE OF DISTANT, INTRASUBUNIT RESIDUES IN CATALASE-PEROXIDASE  
CATALYSIS: TRACING THE ROLE OF GENE DUPLICATION  
AND FUSION IN ENZYME STRUCTURE AND FUNCTION

Carma Oshea Cook

A Dissertation

Submitted to

the Graduate Faculty of

Auburn University

in Partial Fulfillment of the

Requirements for the

Degree of

Doctor of Philosophy

Auburn, Alabama  
May 9, 2009

ROLE OF DISTANT, INTRASUBUNIT RESIDUES IN CATALASE-PEROXIDASE  
CATALYSIS: TRACING THE ROLE OF GENE DUPLICATION  
AND FUSION IN ENZYME STRUCTURE AND FUNCTION

Carma Oshea Cook

Permission is granted to Auburn University to make copies of this dissertation at its discretion, upon request of individuals or institutions and at their expense.  
The author reserves all publication rights.

---

Signature of Author

---

Date of Graduation

## VITA

Carma Oshea Cook, daughter of Mary S. Cook and the late William Cook, Sr., was born on November 3, 1969. She graduated from B.B. Comer High School, Sylacauga, AL, in May of 1988. She then attended Auburn University, Auburn, AL, where she received a Bachelor of Chemical Engineering degree in March of 1993. Ms. Cook relocated to Denver, CO where she worked as a high school science and math teacher as well as a chemist in the pharmaceutical and environmental industries. In August of 2003 she entered graduate school at Auburn University in the Department of Chemistry and Biochemistry in pursuit of the Ph.D. degree.

DISSERTATION ABSTRACT

ROLE OF DISTANT, INTRASUBUNIT RESIDUES IN CATALASE-PEROXIDASE  
CATALYSIS: TRACING THE ROLE OF GENE DUPLICATION  
AND FUSION IN ENZYME STRUCTURE AND FUNCTION

Carma Oshea Cook

Doctor of Philosophy, May 9, 2009  
(Bachelor Chemical Engineering, Auburn University, Auburn, AL, March 1993)

257 Typed Pages

Directed by Douglas C. Goodwin

In spite of being positioned 30 Å away from the active site, the C-terminal domain is essential for catalase-peroxidase (KatG) function. Addition of equimolar amounts of separately expressed and isolated C-terminal domain (KatG<sup>C</sup>) to the active-site bearing N-terminal domain (KatG<sup>N</sup>) restores KatG function. There are highly conserved interdomain residue interactions that could be essential for the reactivation of KatG<sup>N</sup>. Kinetic and spectroscopic studies indicate that the Arg 117-Asp597 (R117-D597) salt-bridge interaction is not essential for KatG catalytic function. However

R117 and D597 individually appear to play a significant role in stabilizing a loop that connects the N-terminal B (contains the active site distal histidine (His 106)) and C helices. This loop (BC) could play a role in maintaining the structural integrity of the active site.

To further explore the significance of these residues, R117A, R117D, D597A and D597R variants were created using site-directed mutagenesis and expressed for the separately isolated domains. A major phase of reactivation kinetics is absent for R117A, leading to a substantial decrease in the rate and extent of reactivation. This implicates the residue as having a role in orienting the BC interhelical loop on the N-terminal domain for proper interaction with the C-terminal domain. The R117D KatG<sup>N</sup> variant was reactivated by KatG<sup>C</sup> by a slow monophasic process. The peroxidase activity observed following reactivation was indistinguishable from that of reactivated KatG<sup>N</sup>. Conversely, reactivated R117D KatG<sup>N</sup> showed only 30% of the catalase activity of the unmodified KatG<sup>N</sup>. Spectroscopic measurements indicated a substantial increase in high-spin states consistent with the observed return of peroxidase activity in R117D KatG<sup>N</sup>. However, EPR measurements showed a distinct difference in the distribution of high-spin states in comparison to wild-type KatG and reactivated KatG<sup>N</sup>. In contrast to far-UV CD measurements for R117D KatG<sup>N</sup>, D597R KatG<sup>C</sup> showed a substantial disruption of secondary structural content. Consistent with this observation, D597R KatG<sup>C</sup> was unable to drive reactivation of KatG<sup>N</sup> or R117D KatG<sup>N</sup>. These results show important roles for R117 and D597 in catalase-peroxidase function, but confirm that this has less to do with their interaction with one another and is more attributed to their effects on the structure

and function of the individual domains. The disruption of KatG<sup>C</sup> structure by the D597R substitution indicates the importance of the residue to the structural integrity of a normally robust domain. Moreover, the result suggests that while KatG<sup>C</sup> is able to reactivate multiple conformers of KatG<sup>N</sup>, neither KatG<sup>N</sup> nor its R117D variant is able to facilitate the refolding of D597R KatG<sup>C</sup>.

We also investigated the strictly conserved Tyr111 (Y111) residue on the N-terminal domain BC loop and the strictly conserved Arg484 (R484) on the B'C' loop of the C-terminal domain. Spectroscopic and kinetic evaluation revealed minimal changes in the catalase and peroxidase activities upon reactivation of the Y111A KatG<sup>N</sup> variant with KatG<sup>C</sup>. However, the kinetics of Y111A catalase recovery were considerably slower than all other features of reactivation, indicating that a feature unique to catalase activity was impaired by the substitution. On the other hand, a 10-fold decrease in catalase and a total loss of peroxidase activity was observed for the reactivation of KatG<sup>N</sup> and Y111A KatG<sup>N</sup> with the R484A variant. These results suggest that R484 may play a role in supporting the B'C' loop structure. This loop may be essential for proper interaction with the N-terminal domain's BC loop, which in turn plays a major role in maintaining proper active site architecture for KatG function.

## ACKNOWLEDGEMENTS

The research conducted in this dissertation was made possible through the assistance and support of many individuals. First, I would like to extend my gratitude to my research advisor, Dr. Douglas C. Goodwin. His guidance and motivation throughout my graduate school research career has inspired me to pursue a career in academic research with the goal of training young scientists and giving back what he has so generously given to me. Second, I would like to thank my committee members, Drs. Holly Ellis, Evert Duin, and Edward Parish for their constructive feedback and professional assistance throughout all stages of the research and dissertation process. To all of my co-workers, past and present, in the Goodwin Laboratory at Auburn University, especially Dr. Ruletha Baker-Hartfield, Dr. Cornelius Varnado, Dr. Yongjiang Li, Kimberly Laband, Robert Moore, and Jaryce Nabors, thank you for your thought-provoking discussions, tireless scientific and technical assistance, and most of all, camaraderie. I would like to give an extra special thanks to my daughter, Jaimeela Cook, for her patience and unconditional love and support throughout this process. Finally, I would like to thank the Department of Chemistry and Biochemistry at Auburn University and the National Science Foundation Bridge to the Doctorate and GK-12 Fellowship programs as well as grant MCB 641614 for funding my graduate school career.



Style manual used: Biochemical and Biophysical Research Communications

Computer software used: Microsoft Word, Microsoft Excel, Prism,  
ChemDraw, SwissPdbViewer, and MegaPOV

## TABLE OF CONTENTS

LIST OF FIGURES .....	xiii
LIST OF TABLES .....	xviii
CHAPTER ONE: LITERATURE REVIEW .....	1
1.1 Reactive Oxygen Species in Biological Systems.....	2
1.2 Catalases .....	9
1.3 Peroxidases .....	16
1.4 Catalase-Peroxidases.....	32
CHAPTER TWO: RESTRUCTURING OF THE CATALASE-PEROXODASE ACTIVE SITE BY A DISTANT AND INACTIVE DOMAIN.....	46
2.1 Abstract.....	46
2.2 Introduction.....	47
2.3 Materials and Methods.....	51
2.4 Results.....	70
2.5 Discussion.....	83
CHAPTER THREE: THE EFFECT OF R117 AND D597 INTERDOMAIN RESIDUE SUBSTITUTIONS ON THE REACTIVATION OF ESCHERICHIA COLI CATALASE-PEROXIDASE .....	92
3.1 Abstract.....	92
3.2 Introduction.....	93
3.3 Materials and Methods.....	101

3.4 Results.....	105
3.5 Discussion.....	115
CHAPTER FOUR: REVERSING THE POLARITY OF THE R117/D597 ION PAIR: EFFECT ON CATALASE-PEROXIDASE REACTIVATION .....	120
4.1 Abstract.....	120
4.2 Introduction.....	122
4.3 Materials and Methods.....	125
4.4 Results.....	130
4.5 Discussion.....	154
CHAPTER FIVE: ROLE OF Y111 AND R484 IN CATALASE-PEROXIDASE REACTIVATION.....	158
5.1 Abstract.....	158
5.2 Introduction.....	159
5.3 Materials and Methods.....	163
5.4 Results.....	168
5.5 Discussion.....	197
CHAPTER SIX: DISCUSSION .....	202
6.1 Role of the C-terminal Domain in Catalase-Peroxidase Structure and Function.....	204
6.2 Effect of N-terminal Domain Substitutions on Catalase-Peroxidase Reactivation .....	209
6.3 Effect of C-terminal Domain Substitutions on Catalase-Peroxidase Reactivation .....	218
6.4 Advancing catalytic function by gene-duplication and fusion .....	219
6.5 Catalase-peroxidases: Novel roles for Gene Duplication and Fusion in Advancing Catalytic Function .....	223

6.6 Impact of Gene Duplication and Fusion on Catalase-peroxidase Reactivation .....	226
--	-----

## LIST OF FIGURES

Scheme 1.1 Radiolysis of Water .....	4
Scheme 1.2 Interrelationship Between Superoxide, Hydrogen Peroxide, Superoxide Dismutase, and Catalase .....	10
Figure 1.1 Structure of Heme <i>b</i> and Heme <i>d</i> .....	15
Figure 1.2 Catalytic Cycle of Heme Peroxidases .....	21
Figure 1.3 Active Site of Peanut Peroxidase .....	23
Figure 1.4 Active Site of Cytochrome <i>c</i> Peroxidase.....	25
Figure 1.5 Modulation of the Two Forms of Compound II from Ascorbate Peroxidase.....	27
Figure 1.6 Comparison of Cytochrome <i>c</i> Peroxidase and Manganese Peroxidase.....	30
Figure 1.7 Active Site of Peanut Peroxidase .....	33
Figure 1.8 Dual Catalytic Cycle of Catalase-Peroxidases .....	35
Figure 1.9 Comparison of the Active Sites of Catalases and Catalase-peroxidases .....	36
Figure 1.10 Comparison of the Active Sites of Peroxidases and Catalase-peroxidases.....	38
Figure 1.11 Catalase-peroxidase Peripheral Active Site Structures .....	40
Figure 1.12 Catalase-peroxidase Trp-Tyr-Met Covalent Adduct.....	42
Scheme 2.1 Representation of the Dual Catalytic Cycle of Catalase-Peroxidases.....	49

Figure 2.1 General Method of PCR Cloning Using the Type-II Endonuclease <i>Eam</i> 1104I.....	53
Figure 2.2 Recognition Sequence 5'-CTCTTC and Cleavage Sites of <i>Eam</i> 1104I.....	54
Figure 2.3 Structure of IPTG and Lactose.....	57
Figure 2.4 Structural Scheme of Ni-NTA Resin and Bound Six-His Tag.....	66
Figure 2.5 Far-UV CD of wtKatG and its Separately Expressed And Isolated Domains.....	72
Figure 2.6 Reactivation of KatG <sup>N</sup> in the presence of KatG <sup>C</sup> .....	74
Figure 2.7 Catalase and Peroxidase Activities Over Time For an Equimolar Mixture of KatG <sup>N</sup> and KatG <sup>C</sup> .....	75
Figure 2.8 Effect of pH on the apparent rate constant and amplitude For KatG <sup>N</sup> Reactivated with KatG <sup>C</sup> .....	78
Figure 2.9 Effect of Separately Expressed and Isolated KatG <sup>C</sup> on the Visible Absorption Spectrum of KatG <sup>N</sup> .....	80
Figure 2.10 Effect of Separately Expressed and Isolated KatG <sup>C</sup> on the EPR Spectrum of KatG <sup>N</sup> .....	82
Figure 2.11 Interfaces Between the N- and C-terminal Domains of KatG.....	86
Scheme 3.1 Representation of the Dual Catalytic Cycle of Catalase-Peroxidases.....	95
Figure 3.1 Comparison of the Active Sites of a Monofunctional Peroxidase and a Catalase-peroxidase.....	96
Figure 3.2 Catalase-peroxidase Peripheral Structures.....	97
Figure 3.3 Interdomain Interactions Between the C-terminal Domain and the BC Loop of the N-terminal Domain.....	100
Figure 3.4 Far-UV CD of KatG <sup>C</sup> , D597A KatG <sup>C</sup> , KatG <sup>N</sup> , and R117A KatG <sup>N</sup> .....	107
Figure 3.5 Reactivation of KatG <sup>N</sup> and R117A KatG <sup>N</sup> .....	108
Figure 3.6 Ferric MCD Spectra of KatG <sup>N</sup> and R117A KatG <sup>N</sup> Reactivated with KatG <sup>C</sup> and D597A KatG <sup>C</sup> .....	112

Figure 3.7 Ferric MCD Kinetics for KatG <sup>N</sup> Reactivated with KatG <sup>C</sup> and D597A KatG <sup>C</sup> .....	113
Figure 3.8 Ferrous MCD Spectra of KatG <sup>N</sup> and R117A KatG <sup>N</sup> Reactivated with KatG <sup>C</sup> and D597A KatG <sup>C</sup> .....	114
Figure 3.9 Comparison of wild-type KatG EPR spectrum with that of Recombined Domains.....	116
Figure 4.1 CD Spectra of KatG <sup>N</sup> and R117D KatG <sup>N</sup> .....	131
Figure 4.2 CD Spectra of KatG <sup>C</sup> and D597R KatG <sup>C</sup> .....	132
Figure 4.3 Heme Absorption Spectra of KatG <sup>N</sup> compared to R117D KatG <sup>N</sup> .....	134
Figure 4.4 Change in the Soret Band of the Heme Absorption Spectra of KatG <sup>N</sup> and R117D KatG <sup>N</sup> After Incubation with KatG <sup>C</sup> and Variants Thereof.....	135
Figure 4.5 Contribution of the Charge Transfer and $\alpha$ and $\beta$ Bands to the Heme Absorption Spectra of KatG <sup>N</sup> and R117D KatG <sup>N</sup> after Incubation with KatG <sup>C</sup> and Variants Thereof.....	136
Figure 4.6 Ferrous MCD Spectra of R117D KatG <sup>N</sup> .....	141
Figure 4.7 High-spin EPR spectra of R117D KatG <sup>N</sup> Recombined with KatG <sup>C</sup> and D597A KatG <sup>C</sup> .....	142
Figure 4.8 Comparison of EPR Spectra of KatG <sup>N</sup> and R117D KatG <sup>N</sup> Reactivated with D597R KatG <sup>C</sup> .....	143
Figure 4.9 Catalase Reactivation of KatG <sup>N</sup> and R117D KatG <sup>N</sup> .....	145
Figure 4.10 Comparison of Catalase Activity of KatG <sup>N</sup> and R117D KatG <sup>N</sup> after a 24-hr incubation period with the C-terminal domain and variants thereof.....	147
Figure 4.11 Peroxidase Reactivation of KatG <sup>N</sup> and R117D KatG <sup>N</sup> .....	149
Figure 4.12 Comparison of Peroxidase Activity of KatG <sup>N</sup> and R117D KatG <sup>N</sup> after a 24-hr incubation period with the C-terminal domain and variants thereof.....	152
Figure 5.1 Far-UV CD Spectra of KatG <sup>N</sup> and Y111A KatG <sup>N</sup> .....	170

Figure 5.2 Far-UV CD Spectra of KatG <sup>C</sup> and R484A KatG <sup>C</sup> .....	171
Figure 5.3 UV-visible Absorption Spectra of Ferric Y111A KatG <sup>N</sup> Before and After Incubation with KatG <sup>C</sup> .....	172
Figure 5.4 UV-visible Absorption Spectra of Ferrous Y111A KatG <sup>N</sup> Before and After Incubation with KatG <sup>C</sup> .....	174
Figure 5.5 UV-visible Absorption Spectra of Ferric KatG <sup>N</sup> and Y111A KatG <sup>N</sup> Before and After Incubation with R484A KatG <sup>C</sup> .....	177
Figure 5.6 UV-visible Absorption Spectra of Ferrous KatG <sup>N</sup> and Y111A KatG <sup>N</sup> Before and After Incubation with R484A KatG <sup>C</sup> .....	178
Figure 5.7 Ferrous MCD Spectra of Y111A KatG <sup>N</sup> Before and After Incubation with KatG <sup>C</sup> .....	179
Figure 5.8 Ferrous MCD Spectra of Y111A KatG <sup>N</sup> Before and After Incubation with R484A KatG <sup>C</sup> .....	181
Figure 5.9 EPR spectra of Y111A KatG <sup>N</sup> recombined with KatG <sup>C</sup> .....	182
Figure 5.10 EPR spectra of Y111A KatG <sup>N</sup> recombined with R484A KatG <sup>C</sup> .....	183
Figure 5.11 Catalase Reactivation of KatG <sup>N</sup> and Y111A KatG <sup>N</sup> .....	185
Figure 5.12 Comparison of Catalase Activity of KatG <sup>N</sup> and Y111A KatG <sup>N</sup> with Respect to H <sub>2</sub> O <sub>2</sub> as a substrate .....	187
Figure 5.13 Peroxidase Reactivation of KatG <sup>N</sup> and Y111A KatG <sup>N</sup> .....	190
Figure 5.14 Comparison of Peroxidase Activity of KatG <sup>N</sup> and Y111A KatG <sup>N</sup> with Respect to H <sub>2</sub> O <sub>2</sub> as the Substrate .....	193
Figure 5.15A Change in Ferric MCD Spectra of Y111A KatG <sup>N</sup> Over a 24-hr Incubation Period with KatG <sup>C</sup> .....	195
Figure 5.15B Comparison of the Rates of Return of Catalase and Peroxidase Activities with the Rate of Change of Ferric MCD Spectra of Y111A KatG <sup>N</sup> recombined with KatG <sup>C</sup> .....	195
Scheme 6.1 Model for the Reactivation of KatG <sup>N</sup> in the Presence of KatG <sup>C</sup> .....	206
Scheme 6.2 Proposed Mechanism for the Reactivation of R117A KatG <sup>N</sup> with KatG <sup>C</sup> .....	210



Figure 6.1 Normalized Return of Catalase Activity for KatG <sup>N</sup> , R117A KatG <sup>N</sup> , and Y111A KatG <sup>N</sup> in the Presence of KatG <sup>C</sup> .....	212
Scheme 6.3 Proposed Mechanism for the Reactivation of R117D KatG <sup>N</sup> with KatG <sup>C</sup> .....	213
Scheme 6.4 Proposed Mechanism for the Reactivation of Y111A KatG <sup>N</sup> with KatG <sup>C</sup> .....	214

## LIST OF TABLES

Table 2.1 Apparent Kinetic Parameters for Catalase and Peroxidase Activities of Coincubated KatG <sup>N</sup> and KatG <sup>C</sup> .....	76
Table 3.1 Rate Constants for Reactivation of KatG <sup>N</sup> and R117A KatG <sup>N</sup> with KatG <sup>C</sup> and D597A KatG <sup>C</sup> .....	109
Table 4.1 UV-Visible Spectral Features for the Ferric Heme States of KatG <sup>N</sup> and R117D KatG <sup>N</sup> .....	137
Table 4.2 Rate Constants and Catalase Activity Recovered for KatG <sup>N</sup> and R117D KatG <sup>N</sup> .....	146
Table 4.3 Apparent Kinetic Parameters for the Catalase Activity Recovered for KatG <sup>N</sup> and R117D KatG <sup>N</sup> .....	148
Table 4.4 Rate Constants and Peroxidase Activity Recovered for KatG <sup>N</sup> and R117D KatG <sup>N</sup> .....	150
Table 4.5 Apparent Kinetic Parameters for the Peroxidase Activity Recovered for KatG <sup>N</sup> and R117D KatG <sup>N</sup> .....	153
Table 5.1 Ferric Spectral Features of KatG <sup>N</sup> and Y111A KatG <sup>N</sup> Recombined with KatG <sup>C</sup> and R484A KatG <sup>C</sup> .....	173
Table 5.2 Ferrous Spectral Features of KatG <sup>N</sup> and Y111A KatG <sup>N</sup> Recombined with KatG <sup>C</sup> and R484A KatG <sup>C</sup> .....	175
Table 5.3 Rate Constants and Catalase Activity Recovered for KatG <sup>N</sup> and Y111A KatG <sup>N</sup> .....	186
Table 5.4 Apparent Kinetic Parameters for the Catalase Activity Recovered for KatG <sup>N</sup> and Y111A KatG <sup>N</sup> .....	189
Table 5.5 Rate Constants and Peroxidase Activity Recovered for KatG <sup>N</sup> and Y111A KatG <sup>N</sup> .....	191

Table 5.6 Apparent Kinetic Parameters for the Peroxidase Activity Recovered for KatG <sup>N</sup> and Y111A KatG <sup>N</sup> .....	194
--	-----

## **CHAPTER ONE**

### **LITERATURE REVIEW**

This dissertation addresses questions surrounding the role of protein structures in modulating the catalytic abilities of a distant active site. Examples of such questions are: To what extent do such structures direct catalytic function? What mechanisms are employed to communicate the effects of distant structures to the active site? How does nature introduce new enzyme activities into existing protein scaffolds? How can this be duplicated to accomplish the rational redesign of enzymes for new catalytic function? A lack of suitable models has made such questions quite difficult to address. For reasons that will be explored in this Literature Review, the bifunctional catalase-peroxidases (frequently referred to as KatGs) provide excellent models to explore these fundamental questions. This chapter will first establish why enzymes with catalase and/or peroxidase activity are essential for survival of organisms that require molecular oxygen or even just live in its presence. The mechanisms by which aerobic organisms form and dispose of reactive oxygen species will be described. In addition, the enzymes that catalyze these reaction pathways will be discussed with particular attention to structure/function comparisons of the enzymes nature uses to dispose of hydrogen peroxide. The research described in this dissertation is framed by these comparisons. It is here that the importance of the two-domain structure, bifunctionality, and evolutionary origin of

catalase-peroxidases surfaces. Through this, the rationale for this work on the roles of the distant, and seemingly inactive C-terminal domain in catalase-peroxidase active site function come into focus.

### *1.1 Reactive Oxygen Species in Biological Systems*

At the core of every organism's ability to interact with their environment is the need for energy in order for biological processes to occur. A significant amount of this required energy is obtained, ultimately, by electron transfer from a food source to a terminal electron acceptor, a process referred to generally as respiration. A variety of terminal electron acceptors are used in nature, but oxygen is the most efficient due to the fact that it produces the greatest yield of adenosine triphosphate (ATP). Thus, aerobic respiration refers to the oxidative catabolism of nutrients and transfer of those electrons to molecular oxygen to produce water. The free energy derived from the process is coupled to the generation of ATP. Organisms that utilize oxygen for respiration are aerobic, whereas those that rely on another terminal electron acceptor are anaerobic. Organisms to which molecular oxygen is toxic are strict anaerobes, and those that do not require oxygen but survive in its presence are facultative anaerobes.

The high yields of ATP from nutrient carbon sources represent the positive side of molecular oxygen. The negative side is the propensity for the formation of reactive oxygen species. Any organism that survives in the presence of molecular oxygen (whether or not it uses molecular oxygen as a terminal electron acceptor) must be able to

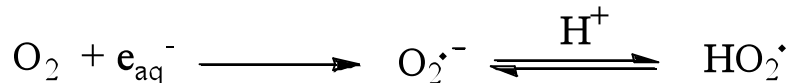
dispose of the reactive entities derived from molecular oxygen. Indeed, these organisms have multiple mechanisms to remove these detrimental species.

In an environment containing molecular oxygen, organisms are persistently subjected to an array of reactive entities collectively referred to as reactive oxygen species (ROS). A large portion of these entities are derived as a result of two major reaction processes: (1) the reduction of molecular oxygen, and (2) the reaction of molecular oxygen with carbon-centered radicals [1]. The latter produces peroxy radicals ( $\text{RO}_2\cdot$ ), alkoxy radicals ( $\text{RO}\cdot$ ), and organic hydroperoxides (ROOH). The reduction of molecular oxygen produces superoxide/hydroperoxyl radicals ( $\text{O}_2^{\cdot-}/\text{HO}_2\cdot$ ), hydrogen peroxide ( $\text{H}_2\text{O}_2$ ), and the hydroxyl radical ( $\cdot\text{OH}$ ). Reactive oxygen species can also be divided down other lines. Some are free radicals (i.e., possess an unpaired electron) such as  $\cdot\text{OH}$ ,  $\cdot\text{O}_2\text{H}$ , and  $\text{O}_2^{\cdot-}$ , while others are fully covalent  $\text{O}_2$  containing species (like  $\text{H}_2\text{O}_2$ , and ROOH).

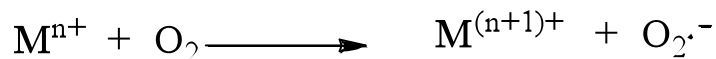
#### *1.1.1. Formation of superoxide/hydroperoxyl radicals*

Free radicals are formed due to the homolytic cleavage of chemical bonds by thermal energy, photochemical energy, one-electron transfer reactions, molecule-assisted homolysis, or ionizing radiation sources [2]. Superoxide anion is formed most often by the one electron reduction of molecular oxygen, although one-electron oxidation of  $\text{H}_2\text{O}_2$  is also possible. For example, the addition of one solvated electron to molecular oxygen

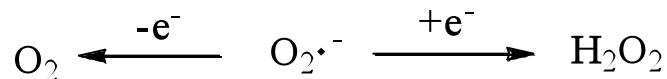
produces a superoxide radical species ( $O_2^{\cdot-}$ ) and its conjugate acid (hydroperoxyl radical,  $HO_2^{\cdot}$ ,  $pK_a = 4.8$ ) as follows:

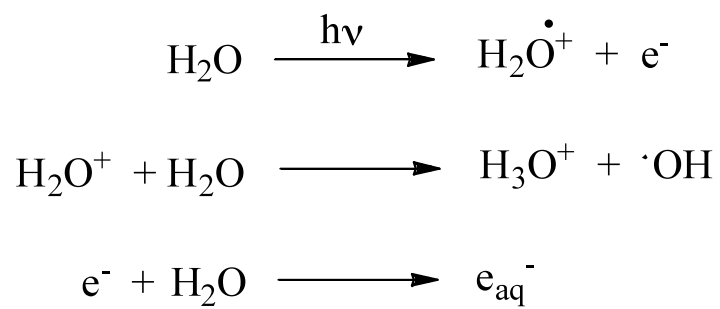


At physiological pH, this radical exists predominantly in the unprotonated form. The solvated electron ( $e_{aq}^-$ ) is generated by radiolysis of water as shown in Scheme 1.1 [3, 4]. This reaction has been used by oncologists to increase the destruction of tumor cells by utilizing radiation to increase the production of oxygen-derived radicals [2]. The superoxide radical can also be produced by reacting oxygen with different metal ions such as  $Fe^{2+}$  or  $Cu^+$ , this is one of many reasons why metals such as iron and copper are so tightly controlled in biological systems:



Superoxide can react as an oxidizing or reducing agent when it disproportionates into hydrogen peroxide and oxygen. In essence, this radical can lose its unpaired electron by either donating it or it can accept another electron as shown below:





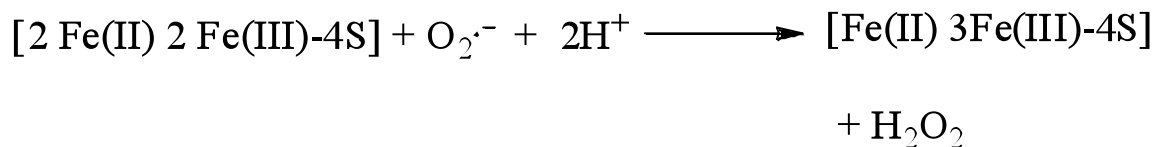
Scheme 1.1 Radiolysis of Water



The reducing properties of superoxide led to its identification by McCord and Fridovich [15, 16]. They observed the reduction of ferric cytochrome *c* during oxidation of xanthine catalyzed by milk xanthine oxidase. The  $O_2^{\cdot-}$  produced from  $O_2$  reduction resulted in reduction of cytochrome *c* to its ferrous state as indicated by a change in absorption spectrum of the heme.

The superoxide radical is formed in all aerobic cells. It is generated by a number of mechanisms including the mistransfers of electrons in the respiratory electron transport chain (especially at complexes I and III) [149]. Enzymes like xanthine oxidase generate superoxide as mentioned above. Indeed, a central player in the antibacterial response of neutrophils is the generation of enormous quantities of superoxide by NADPH oxidase [150]. This in itself is an indicator of the deleterious nature of the molecule.

Surprisingly, superoxide is not an especially reactive molecule, but it is, at the same time, highly toxic. Nanomolar concentrations of superoxide can be lethal to cells. More often than not, superoxide initiates reaction cascades that have dire consequences. For example, superoxide reacts with some Fe-S cluster-containing enzymes via oxidation to produce hydrogen peroxide and release of free iron [6-13]. This mechanism has been shown for dihydroxy acid dehydratase [7], 6-phosphogluconate dehydratase [8], aconitase [9], and fumarase A and B [10-12]. The native enzyme clusters (containing two Fe(II) and two Fe(III) atoms) are oxidized according to the following reaction:



The oxidized cluster then releases Fe(II), which now is capable of catalyzing the formation of additional reactive oxygen species. The abundant presence of reductants and molecular oxygen allows for iron-catalyzed formation of hydroxyl radical, a species with a reduction potential of +2.3V. This is capable of oxidizing virtually any biological molecule. Other examples, of deleterious processes starting with superoxide include reaction with nitric oxide to form peroxynitrite (ONOO<sup>-</sup>) [14], and the protonated form of superoxide (the hydroperoxyl radical) is an initiator of lipid peroxidation [17].

Given the lethal consequences of even small concentrations of superoxide, it makes sense that cells would have in place defenses to head off its downstream reactions. In 1968 and 1969, McCord and Fridovich discovered that the enzyme xanthine oxidase produces the superoxide radical in biological systems, and erythrocytes contain an enzyme (which later became known as superoxide dismutase (SOD)) that dismutates superoxide to hydrogen peroxide and molecular oxygen according to the following reaction [15, 16]:



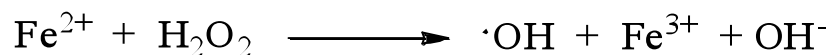
The reaction is catalyzed at diffusion-limited rates at neutral pH where the non-enzymatic dismutation reaction is considerably slower than its optimum at pH 4.8.

Fridovich and coworkers discovered that there are two classes of SODs. One class contains Cu(II) and Zn(II) (i.e., Cu/Zn SOD) while the other class utilizes a single metal ion, either Mn(III) or Fe(III), at its catalytic center [15, 16]. Studies involving *E. coli* mutants that have lost the ability to produce the MnSOD (SodA) or the FeSOD

(SodB) enzymes have greater hypersensitivity towards molecular oxygen and superoxide [18, 19]. Furthermore, the human disease amyotrophic lateral sclerosis (ALS or Lou Gehrig's disease) is often associated with a genetic defect in the Cu/ZnSOD gene [20-22]. Superoxide is an entity that all aerobic cells encounter and must address. SOD is central to that defense as indicated by the consequences of its absence or impaired function.

### *1.1.2 Formation of Hydrogen Peroxide*

Although it is essential to successful defense against reactive oxygen species, in many respects SOD only pushes back the problem by one step. The reduction of superoxide produces H<sub>2</sub>O<sub>2</sub>, another toxic molecule. In addition, several oxidases are known to generate H<sub>2</sub>O<sub>2</sub> as a product such as glucose oxidase and fatty acyl-coA oxidase. The reduction potential for H<sub>2</sub>O<sub>2</sub> is quite high (+1.3 V), yet, as with superoxide, H<sub>2</sub>O<sub>2</sub> is not a particularly reactive molecule. However, this changes dramatically in the presence of redox active metals. Hydrogen peroxide is a known inactivator of numerous metalloenzymes. Importantly, H<sub>2</sub>O<sub>2</sub> can react further via the Fenton reaction that is facilitated by a one-electron transfer provided by certain metal ions:



The Fenton reaction exploits the fact that many metals can exist in multiple oxidation states. Reduction of the peroxide O-O bond by the metal generates the highly reactive

hydroxyl radical. Due to the high reactivity of the hydroxyl radical, it causes extensive damage to biological molecules of all types at rates limited only by diffusion. Therefore, the existence of SOD in all aerobic organisms is not enough to protect against oxidative damage. The production of hydrogen peroxide and, subsequently, hydroxyl radicals poses further danger to these organisms. It is crucial for aerobic organisms to possess mechanisms to degrade toxic hydrogen peroxide in addition to superoxide in order to avoid the formation of hydroxyl radical.

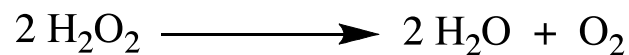
In the course of evolution aerobic species have developed defenses against this toxic threat. In the metabolic sequence:  $O_2 \rightarrow O_2^{\cdot-} \rightarrow H_2O_2 \rightarrow \cdot OH$ , aerobic organisms have built in defenses that can impede this pathway at different stages. SOD degrades the superoxide radical, however, the toxic hydrogen peroxide molecule is produced, which further reacts via a one-electron reduction to form the hydroxyl radical that threatens the integrity of cells. Once the hydroxyl radical is formed, there is little that can be done (outside of the use of high concentration scavengers) to prevent its reaction with biomolecules. Therefore, it is crucial for aerobic organisms to have built-in mechanisms to safely degrade hydrogen peroxide before it can be cleaved to form hydroxyl radical.

Some form of catalase and/or peroxidase enzyme is present in virtually every cell exposed to oxygen. These enzymes facilitate the reduction of hydrogen peroxide to water, and in the case of catalase oxidation of a second equivalent of  $H_2O_2$  to molecular oxygen. Therefore, these enzymes act synergistically with SOD help protect aerobic organisms from oxidative damage as shown in Scheme 1.2. SOD decreases the yield of  $H_2O_2$  by preventing superoxide from causing the destructive release of iron and other redox active transition metals. SOD also eliminates superoxide, a known inhibitor of

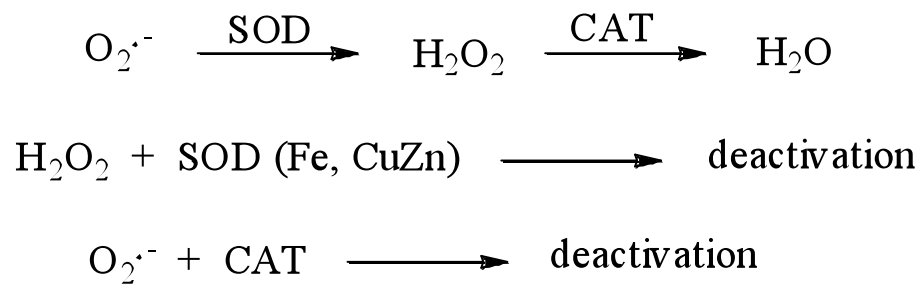
catalases and peroxidases [23, 24]. Catalases and peroxidases remove hydrogen peroxide heading off the many deleterious reactions it can initiate. Interestingly, one of these is the inactivation of the Cu/ZnSOD and FeSOD enzymes. In summary, SOD on one hand and catalases and peroxidases on the other represent a mutually protective set of antioxidant enzymes that work in concert to protect cells from oxidative damage [2].

## 1.2 Catalases

Catalases are enzymes that are critical in protecting cells against damage mediated by hydrogen peroxide [2]. Due to their striking ability to evolve molecular oxygen, catalases have been studied for over 100 years, with the first characterization and naming of the enzyme occurring in 1900 [25]. The overall reaction for all catalases (heme and non-heme) enzymes is the same:



Likewise there are two distinct stages in the reaction pathway for the heme and non-heme catalases, however the mechanisms contributing to these two stages differ considerably for heme-containing or “classical” catalases versus that for non-heme catalases [26].

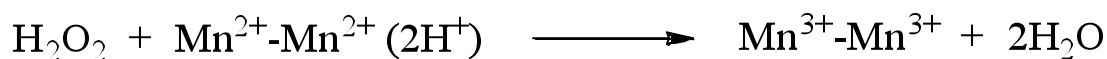


Scheme 1.2 The interrelationship between superoxide, hydrogen peroxide, superoxide dismutase (SOD) and catalase (CAT).

### 1.2.1 Non-heme catalases

The non-heme catalases are of bacterial origin and are the smallest class. They are unrelated by sequence, structure, and mechanism to other enzymes with catalase activity, and so, are only briefly discussed here. The active site of these enzymes contains a bridged binuclear manganese-rich reaction center rather than a heme group [27]. Because of this, non-heme catalases have been referred to as “pseudo” catalases as well as manganese catalases. The H<sub>2</sub>O<sub>2</sub> dismutation rates are lower for manganese catalases compared with typical catalases. Moreover, the apparent K<sub>m</sub> values are reported to be ~220 mM [28], suggesting a low catalytic efficiency at low H<sub>2</sub>O<sub>2</sub> concentrations. This could explain why they may not have become as widespread in nature [29]. The activity varies only slightly over the pH range from 5 to 10, and in this one respect, they are very similar to typical catalases.

There have been three non-heme catalases characterized, and the crystal structures of two of them have been determined (*Lactobacillus plantarum* and *Thermus thermophilus*) [27]. Clearly, the mechanism for manganese catalases must differ substantially from that of classical catalases. The dimanganese cluster is stable in either the Mn<sup>2+</sup>-Mn<sup>2+</sup> or Mn<sup>3+</sup>-Mn<sup>3+</sup> oxidation states. The reaction cycle can be written as a two-stage mechanism. During catalytic turnover, the active site has to support both the reduced and the oxidized state of the dimanganese core. The Mn<sup>2+</sup>-Mn<sup>2+</sup> cluster is expected to polarize the O-O bond of hydrogen peroxide, favoring a heterolytic cleavage of the peroxidic bond and release of water as follows [30]:



Hydrogen peroxide oxidation and dioxygen release occurs by a simple electron transfer

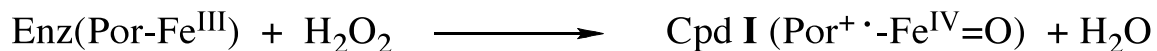


For the most part, no sequential order exists in the reduction and oxidation stages [151].

In contrast to heme-containing catalases, no reactive intermediate is formed, and both water molecules are formed in one reaction [151]. Furthermore, no evidence exists for involvement of free radicals in manganese catalase turnover.

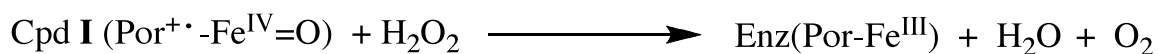
### 1.2.2 Monofunctional Catalases

As with the non-heme catalases, two stages are evident in the catalase mechanism of the classical enzymes. The first stage involves oxidation of the heme iron using hydrogen peroxide as substrate to form compound I (Cpd I), a ferryl species with one oxidizing equivalent located on the iron and a second oxidizing equivalent delocalized in a porphyrin radical:





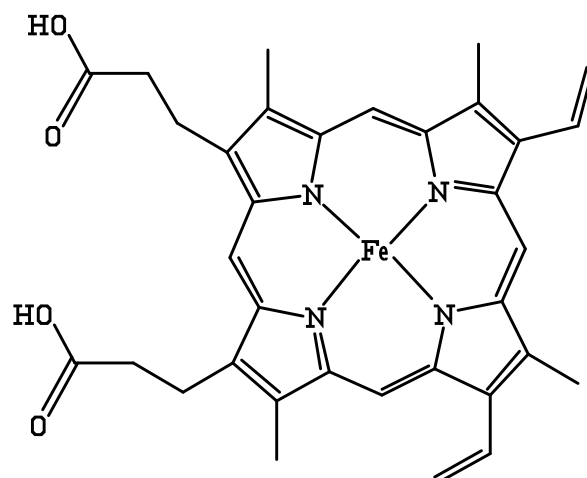
The second phase for heme-containing catalases involves the reduction of compound **I** and utilizes a second molecule of hydrogen peroxide as an electron donor supplying two reducing equivalents to the heme:



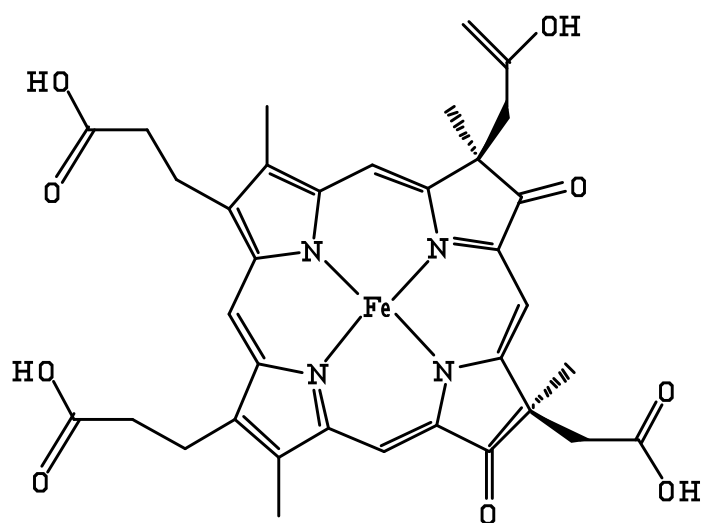
The largest and most widely investigated group of catalases are those which are monofunctional, heme-containing enzymes. The dismutation of hydrogen peroxide is their predominant function. The most suitable way of subcategorizing this group is based on the subunit size and the type of heme present in the active site. Based on subunit size, there are two distinct subgroups, one containing a small subunit (55 to 69 kDa) with heme *b* associated with it, and one containing a large subunit (75 to 84 kDa) with heme *d* (Figure 1.1). These subunits of catalases have been shown to mainly be associated in a tetrameric manner, and a phylogenetic analysis of 70 monofunctional catalase sequences [31] has revealed a subdivision of monofunctional catalases into three distinct groups or clades. Clade I is comprised of the plant catalases and one branch of bacterial catalases. Clade II consists of only the large subunit catalases with bacterial and fungal origins. Clade III contains a third group of bacterial catalases as well as fungal and animal catalases and one enzyme with an archaebacterial origin. Interestingly, it is proposed that these main clades arose from a progenitor catalase through a minimum of at least two gene duplication events [26]. The nature of this progenitor enzyme as far as subunit size and heme type present remains the subject of much research and discussion.

### *1.3 Peroxidases*

Peroxidases are abundant enzymes present in all organisms and participate in a wide variety of biological processes, the most important of which are involved in the response to oxidative stress [32, 33]. Heme peroxidases were first detected in plants and animals in the 19<sup>th</sup> century [34] and named as such by Linossier [35]. The catalytic mechanism for the decomposition of hydrogen peroxide by heme peroxidases was determined to be similar to that of catalases. Furthermore, up until the mid-20<sup>th</sup> century, all peroxidases were considered to be heme peroxidases. However, in 1954 Gordon C. Mills described a novel peroxidase that lacked a colored prosthetic group [36]. Nevertheless, his observations were accepted with great cynicism. Mills' glutathione peroxidase (GPx) is now a part of a large family of non-heme peroxidases that have been proven to react and consist of two types of enzymes: those that utilize glutathione as an electron-donor substrate and those that have high specificity for thioredoxin (i.e., thioredoxin-type proteins known as peroxiredoxins), not glutathione [37]. The characteristic feature of this superfamily of enzymes is a redox-active selenocysteine (Sec) residue (cysteine for peroxiredoxins) that is integrated into the protein and forms the center of a catalytic triad (Sec, Gln, Trp) or tetrad (Sec, Gln, Asn, Trp) [38, 39]. The non-heme peroxidases are largely outside the scope of this dissertation, and so are only briefly considered here.



**Heme *b***



**Heme *d***

Figure 1.1. Structures of Heme *b* and Heme *d*

### 1.3.1 *Non-heme Peroxidases (Glutathione Peroxidases and Thioredoxin Peroxidases)*

The heme-free thiol peroxidases include glutathione peroxidases (GPxs) and peroxiredoxins and catalyze the reduction of H<sub>2</sub>O<sub>2</sub> and organic hydroperoxides to water or analogous alcohols [40]. Collectively, they belong to the glutathione peroxidase superfamily of proteins and are found in many organisms throughout all kingdoms of life [41]. They differ in the type of electron-donating substrate that is used to reduce hydrogen peroxide and the amino acid present in the redox center to complete the catalytic triad or tetrad.

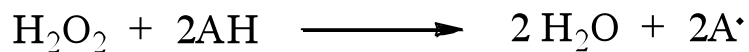
The reduction of hydroperoxides and the simultaneous oxidation of thiols to disulfides by GPxs have been studied extensively [39]. Seven members of the GPx superfamily have been discovered in mammals and it has been determined that they have high sequence similarity, conserved sequence patterns, similar biochemical function, and characteristic catalytic triad formed by selenocysteine or cysteine, glutamine, and tryptophan [38]. The glutathione peroxidase family is named after bovine tetrameric GPx-1, the first GPx described [36] and the first mammalian protein in which selenocysteine was identified in the active site [42].

The last member of the mammalian GPx family to be discovered, GPx-7, is cysteine-based and has low glutathione-dependent peroxidase activity. Since the discovery of GPx-7, a large number of similar sequences from organisms ranging from bacteria to vertebrates have been observed, most of them containing a Cys residue corresponding to the Sec present in most of the mammalian enzymes. It thus became evident that the members of the GPx family, with a Sec as redox active moiety, are just a

minor group, confined to vertebrates, with some scattered presence in lower organisms. Despite structural similarities, not all of the GPx homologues are preferentially reduced by GSH but by thioredoxin (Trx). The majority of nonvertebrate GPxs share structural features indicating a preferential reactivity with Trx [40].

### 1.3.2 Heme Peroxidases

Heme peroxidases are abundant enzymes present in all living things that participate in a variety of physiological processes [32, 33]. All heme peroxidases participate in a similar reaction mechanism involving the degradation of H<sub>2</sub>O<sub>2</sub> according to the following simplified reaction mechanism:



The first step in the removal of H<sub>2</sub>O<sub>2</sub> by heme peroxidases is identical to that for heme catalases and starts with the reaction of the ferric (resting) enzyme with one equivalent of H<sub>2</sub>O<sub>2</sub>, generating H<sub>2</sub>O and a ferryl porphyrin/protein radical intermediate known as compound I (Figure 1.2). In the second step, compound I undergoes reduction via two one-electron donating steps to return the enzyme to its resting state. The first reduction involves the exogenous electron donor substrate transferring an electron to compound I, which typically reduces the porphyrin/protein radical to leave a ferryl intermediate known as compound II and a substrate radical. In the second reduction step, the

exogenous electron donor returns the enzyme to its resting state, producing a second equivalent of substrate radical.

Heme peroxidases use heme *b* containing high-spin ferric iron as a prosthetic group, have been extensively studied, and are observed in all five kingdoms of life. They have been categorized in broad terms as mammalian and plant peroxidases [43].

### *1.3.2.1 Mammalian Heme Peroxidases*

The active site heme and the global tertiary structure of mammalian/animal heme peroxidases differ significantly from plant/fungi/bacteria heme peroxidases [44].

Mammalian peroxidases likely arose from a different ancestral gene than plant peroxidases [45]. However, convergent evolution allowed the two families of proteins to possess a common function [44]. The two most common mammalian peroxidases are myeloperoxidase (MPO) and lactoperoxidase (LPO).

Myeloperoxidase is a major component of neutrophils, which are cells that provide a front line of defense for the immune system against invading microbes [44]. Myeloperoxidase is a 146 kDa cationic, dimeric protein consisting of two monomer units (73 kDa each) connected by a disulfide bridge at Cys 153 [46] that are identical and functionally independent [47]. Each monomer is composed of a heavy, glycosylated chain (58.5 kDa, 467 amino acids) and a light chain (14.5 kDa, 106 amino acids) [46].

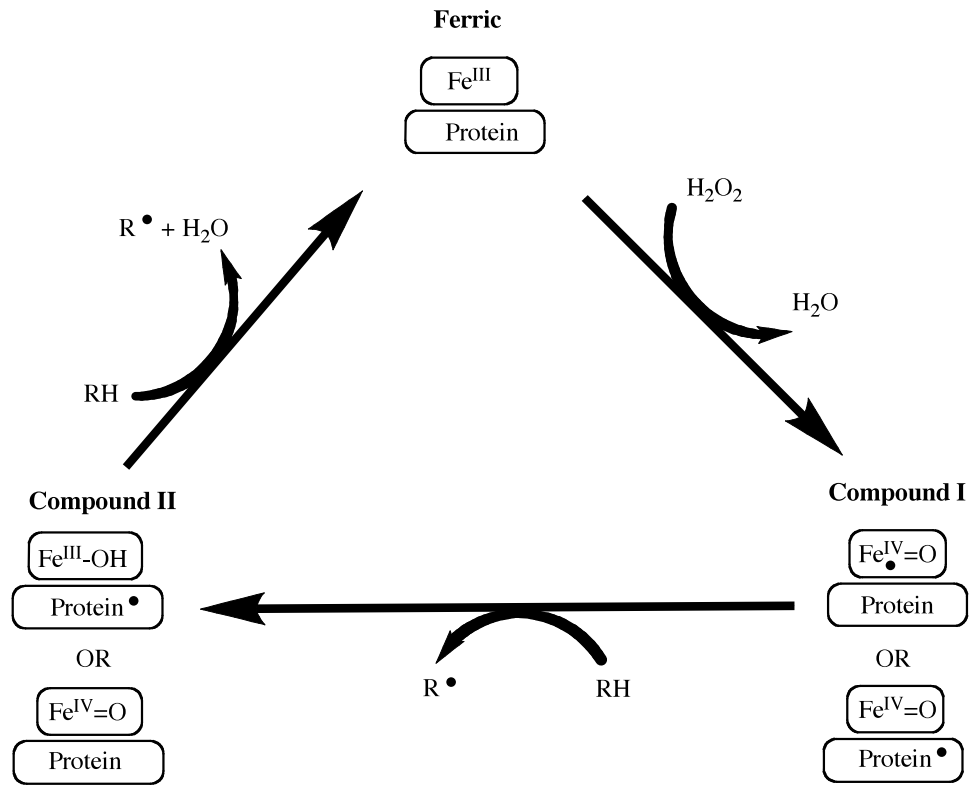


Figure 1.2 Catalytic cycle of heme peroxidases

The active site is located in the heavy chains and contains a modified iron protoporphyrin IX derivative that yields a distinctive green color [44]. This modified heme is positioned at the bottom of a deep crevice which allows only H<sub>2</sub>O<sub>2</sub> and small anions to access the iron atom [48]. Myeloperoxidase compound I formation with hydrogen peroxide is reversible thus requiring larger concentrations of hydrogen peroxide to observe its formation than is typical of other peroxidases. The truly unique and significant feature of myeloperoxidase is the ability of its compound I intermediate to oxidize Cl<sup>-</sup> to the hypochlorite anion (ClO<sup>-</sup>). The ability of this enzyme to, in essence, form bleach is a critical part of the neutrophil response to bacterial invasion. In this respect it is closely tied to superoxide and hydrogen peroxide formation by NADPH oxidase mentioned previously.

Lactoperoxidase is green in color like myeloperoxidase due to a covalently linked modified protoporphyrin IX type heme. There is one heme group per molecule of lactoperoxidase which consists of an approximately 80-kDa single polypeptide chain. The resting ferric enzyme has a pentacoordinate iron with the imidazole of the proximal histidine residue being the fifth ligand. A compound I-like intermediate is also formed upon the reaction between lactoperoxidase and hydrogen peroxide. Lactoperoxidase compound I is unable to oxidize Cl<sup>-</sup>, but is capable of oxidizing other halides and pseudohalides (e.g., thiocyanate) to the corresponding hypohalite ions. This is also purported to have a role in antimicrobial defense.



### *1.3.2.2 The Plant Peroxidases*

The plant peroxidase superfamily is not entirely appropriately named. It contains members from plants, yeasts and other fungi, and bacteria. Across three classes of the plant peroxidases there is remarkable conservation of active site structure and catalytic capabilities. All of the plant peroxidases use the heme *b* prosthetic group ligated by way of the  $\epsilon$  nitrogen of a histidine on the proximal side of the heme [49]. A hydrogen bond involving the  $\delta$  nitrogen of the imidazole ring is formed with a highly conserved aspartate residue [50]. This increases the anionic character of the histidine ligand and is proposed to help peroxidases stabilize the ferryl heme intermediates of catalysis [50]. On the distal side, a strictly conserved histidine is positioned about 5 Å above the heme iron. This residue serves as a general base for catalysis and is particularly important for the formation of compound I intermediates [51]. Likewise, an arginine residue is strictly conserved on the distal side. This also supports compound I formation by acting as an electrostatic catalyst to offset a negative charge that develops across the O-O bond of the hydrogen peroxide substrate [51]. A structure depicting the typical peroxidase active site is shown in Figure 1.3. In spite of the high degree of conservation of active site structure and catalytic capability, there is equally remarkable diversity of cellular function, much of which depends on cellular environment and the identity of available electron donors. The plant peroxidases have been further divided into three subclasses according to their cellular location and function.

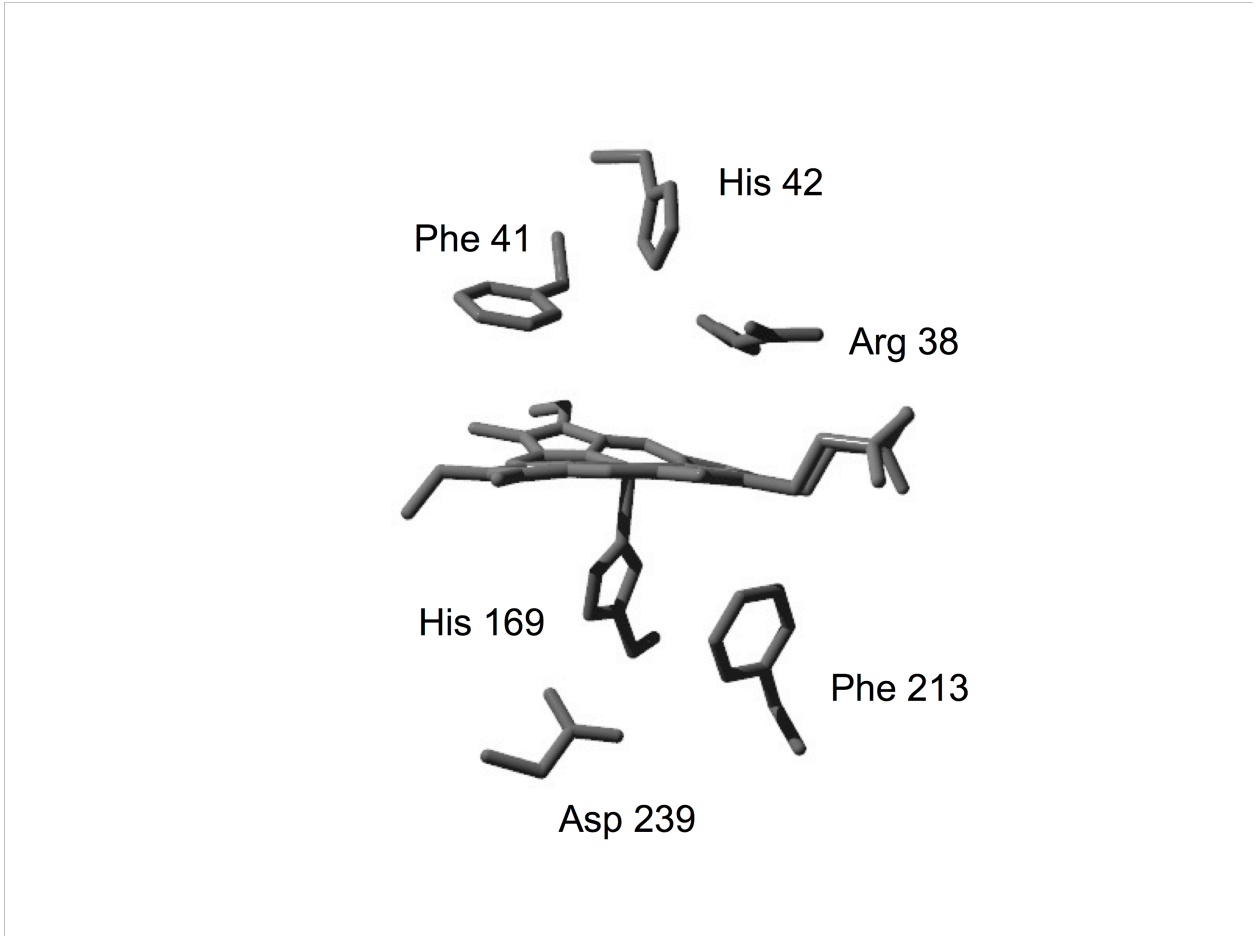


Figure 1.3. The active site of peanut peroxidase, a typical plant peroxidase.

Examples of Class I plant peroxidases have been identified in a wide range of prokaryotes and eukaryotes. They include cytochrome *c* peroxidase and ascorbate peroxidase [52]. The supposed function of these peroxidases is the detoxification of hydrogen peroxide, analogous to the role of the catalases. However, rather than oxidizing a second equivalent of hydrogen peroxide, these peroxidases oxidize substrates that produce low-potential radicals (e.g., monodehydroascorbate) or otherwise minimally reactive products. Yeast cytochrome *c* peroxidase reduces hydrogen peroxide to water and oxidizes two equivalents of reduced ( $\text{Fe}^{\text{II}}$ ) cytochrome *c*. It contains one heme group bound to a single polypeptide chain with a molecular weight of approximately 34 kDa [53]. As is typical of most plant peroxidases, it is composed of 10 alpha helices (A-J), and the heme is bound between helices B (on its distal side) and F (on its proximal side), as shown in Figure 1.4. The imidazole ring of the histidine 175 is the proximal fifth ligand to the iron. The distal sixth position is vacant.

The first step in the catalytic mechanism of yeast cytochrome *c* peroxidase involves the reduction of hydrogen peroxide to water and the oxidation of cytochrome *c* peroxidase to compound **I**, which is a ferryl heme/protein radical intermediate where the initial radical formed is centered at Trp 191 ( $\text{Fe}^{\text{IV}}=\text{O}$ , Trp $\cdot$ ) [54]. Cytochrome *c* peroxidase is returned to its ferric state by two sequential reductions by an exogenous electron donor, forming compound **II** as an intermediate in this process. The reduction of compound **II** is also controlled by the formation of a radical at the proximal Trp191 residue [55]. The reduction of compound **II** to return the enzyme to its ferric state

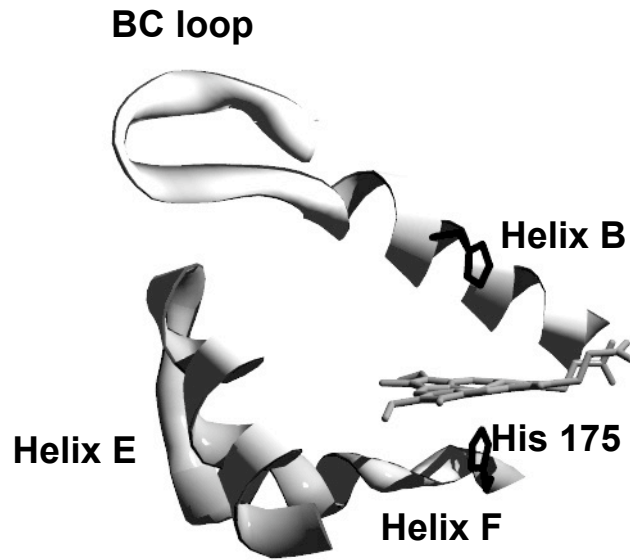


Figure 1.4 Active site of cytochrome *c* peroxidase

appears to be modulated by the equilibrium between  $\text{Fe}^{\text{IV}}=\text{O}$ , Trp and  $\text{Fe}^{\text{III}}$ ,  $\text{Trp}^{\cdot+}$  forms of compound II as shown in Figure 1.5 [56].

The active site of ascorbate peroxidase is highly similar to cytochrome c peroxidase except that it has a metal binding site near the proximal tryptophan residue, which is occupied by a potassium ion [57]. The presence of the potassium is suggested to make the tryptophan (analogous to Trp 191 in CcP) more difficult to oxidize. Consequently, in compound I of ascorbate peroxidase the free radical component is retained as a porphyrin radical rather than transferred to the protein [57]. This among other features facilitates the oxidation of the much smaller substrate, ascorbate, near the heme edge. The primary role of ascorbate peroxidase is to catalyze the removal of hydrogen peroxide by ascorbate according to the following reaction:



The monodehydroascorbyl radical is a low potential species that rapidly disproportionates, and thus, diffuses the substantial oxidizing power of  $\text{H}_2\text{O}_2$ . An added advantage is that hydrogen peroxide is removed without the production of molecular oxygen (as opposed to catalases). This is advantageous for the two most prominent locations of the enzyme: root nodules of legumes which have nitrogenase activity and chloroplasts of plants where photosynthesis occurs. Molecular oxygen is inhibitory to photosynthesis, and its production by ascorbate peroxidase would block glucose

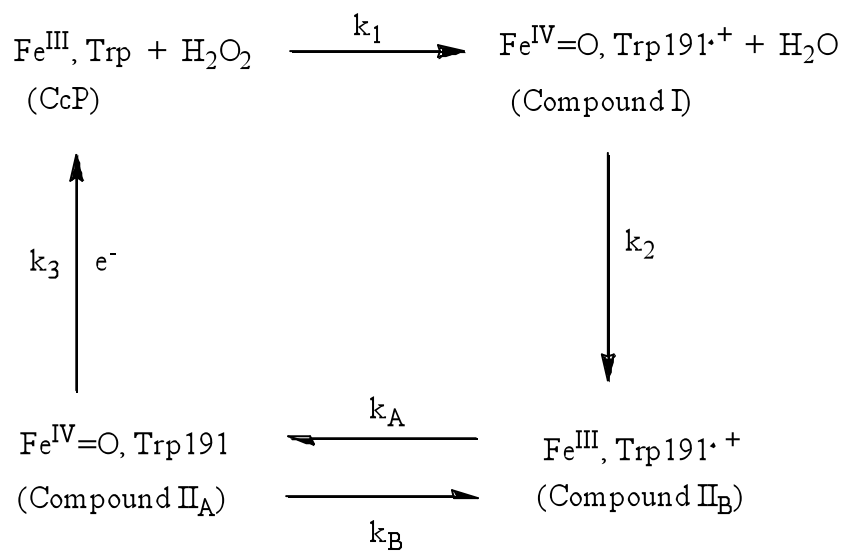


Figure 1.5 Modulation of the two forms of compound II from ascorbate peroxidase.

production. The root nodules of legumes are constantly subjected to oxidative water stress, which activates its antioxidant defense system. However, its defense system cannot handle an overproduction of reactive oxygen species. Under these conditions, nitrogen fixation occurs which is accompanied by irreversible inactivation of nitrogenase.

#### *1.3.2.3 Class II Plant Peroxidases*

Class II peroxidases are secreted fungal enzymes. They have a signal peptide sequence at the N-terminus for secretion via the endoplasmic reticulum. Lignin and manganese peroxidases from *Phanerochaete chrysosporium* are two of the most widely studied class II peroxidases. They differ from class I peroxidases in that two tryptophans, one on the proximal side of the heme and one on the distal side of the heme are replaced most often by phenylalanine (Phe), or in limited cases a leucine (Leu) residue. Consistent with their extracellular location, these enzymes have multiple disulfide bonds. Furthermore, class II peroxidases, such as manganese peroxidase, have two calcium binding sites, whereas class I peroxidases, like cytochrome c peroxidase, have none (Figure 1.6). One calcium ion is near the proximal Phe or Leu residue. The second calcium is located on the distal side of the heme just to the C-terminal end of the B-helix [58]. Interestingly, the loss of this calcium ion causes a change in the active site such that the distal histidine, which is present in all plant peroxidases as a general base, actually becomes a direct ligand to the heme iron [59]. This disrupts its ability to act as a general base and also prevents hydrogen peroxide from accessing the active site.

Lignin peroxidase has a protein fold similar to that of yeast cytochrome c peroxidase [58]. However, the approach to the distal side of the heme is much more constricted because of the calcium ions near the distal Phe [58]. In its active conformation, the ferric heme iron of lignin peroxidase is in a high-spin pentacoordinate state. Compound I formation follows the conventional pathway of other heme peroxidases. Compound II can form spontaneously from compound I, indicating that electron transfer from the protein does occur albeit at comparatively slow rates to cytochrome c peroxidase. Lignin peroxidase is capable of oxidizing a wide range of electron donors, but veratryl alcohol (produced and excreted by *P. chrysosporium*) is viewed as a preferred substrate. It follows the typical peroxidatic path, reducing compound I to compound II and compound II back to the native state in one-electron steps [60].

Manganese peroxidase differs from lignin peroxidase in having a more open active site and five, rather than four, disulfide bonds. The native enzyme exists in the hexacoordinate high-spin state with histidine as the proximal fifth ligand and a weakly bound water molecule as the sixth [59]. As the name suggests, the preferred electron donor for this enzyme is  $Mn^{II}$  complexed with organic acids (e.g., oxalate) [61]. The



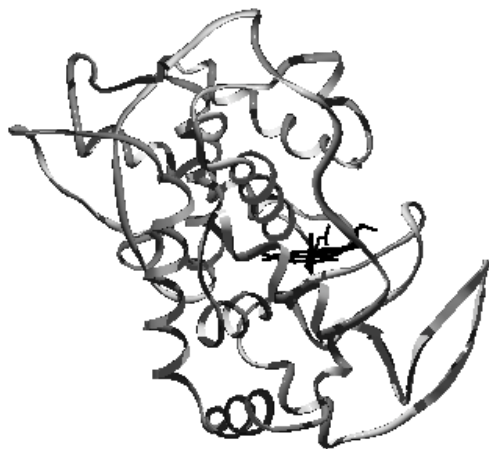
**A****B**

Figure 1.6 Comparison of (A) cytochrome c peroxidase and (B) manganese peroxidase. The black spheres in panel B indicate the location of calcium ions.

protein-derived binding ligands to the  $Mn^{2+}$  ion have been identified as Asp179, Glu35, Glu39, a heme propionate, and two water molecules [59]. These residues are catalytically significant and mutations to these residues affect the stability of the B helix and, subsequently, the binding of calcium on the distal side [62]. Furthermore, it has been shown that MnP is susceptible to thermal inactivation due to the loss of the distal calcium [108]. Loss of activity due to thermal inactivation caused distinct changes in the heme coordination to a low-spin state. These changes are indicative of a sixth ligand being bound to the distal side of the heme iron [108].

#### *1.3.2.4 Class III Heme Peroxidases*

Class III peroxidases are the secretory plant peroxidases that include horseradish peroxidase and peanut peroxidase. Indeed, these enzymes encode an N-terminal excretory signal peptide. The active form of horseradish peroxidase is pentacoordinate, with the fifth ligand being the proximal imidazole side chain of histidine 170. The other active site residues and their arrangement are highly similar to the other two classes, particularly Class II peroxidases. The outer substrate access channel to the heme is hydrophobic with either one or three phenylalanine residues near the C18 methyl at the heme edge for peanut peroxidase and horseradish peroxidase, respectively. As with the Class II enzymes, Class III peroxidases contain two calcium ions in analogous positions. Four disulfide bridges are present, though they are in different locations from those in class II enzymes [63]. Interestingly, the cysteines of one of these disulfide bonds are on either side of ligands to the distal side calcium at the C-terminal end of the B-helix

(Figure 1.7). As with the Class II enzymes, the heme environment is sensitive to the presence and absence of calcium. In its absence there is diminished activity but the effects are not nearly as dramatic as observed with the fungal enzymes [64]. Apparently, the disulfide bond serves to provide additional stability to this region of the peroxidase structure [65].

#### *1.4 Catalase-Peroxidases*

In addition to catalases and peroxidases there is an additional group of enzymes that catalyze the rapid decomposition of hydrogen peroxide. They are primarily bacterial enzymes, but several examples have been observed in lower eukaryotes [152]. They require heme as a prosthetic group. In fact, these enzymes use a single active site to accomplish both catalase *and* peroxidase activities. The bifunctionality of catalase-peroxidases (also frequently referred to as KatGs) is unique because enzymes that exhibit strong peroxidase activity generally possess weak catalase activity and catalase enzymes are typically poor peroxidases [80].

The catalytic disproportionation of hydrogen peroxide begins with the KatG in its resting state reacting with one equivalent of hydrogen peroxide to yield water and Compound I (Figure 1.8). Compound I is then reduced back to resting enzyme by a second equivalent of hydrogen peroxide, forming water and molecular oxygen. The first step of the peroxidatic cycle is identical to the catalase in forming Compound I.

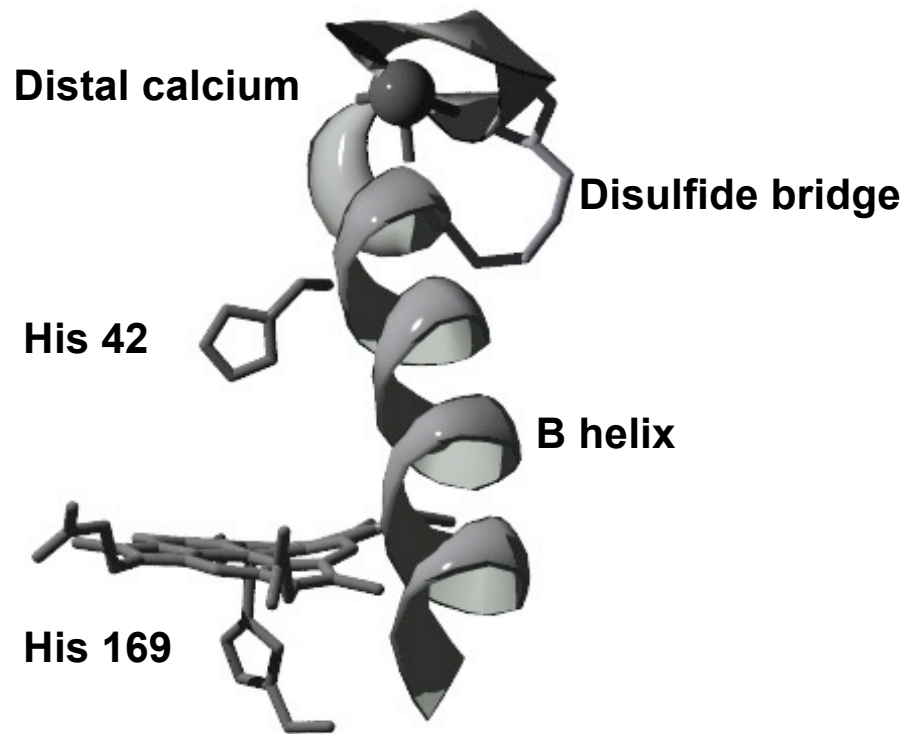


Figure 1.7 Active site of peanut peroxidase. The disulfide bonds on either side of ligands to the distal calcium atom (grey ball) are located at the C-terminal end of the B-helix.

However, the resting enzyme is regenerated via two sequential one-electron reduction steps by an exogenous electron donor. The first reduction produces a substrate radical and an Fe<sup>III</sup>-OH/protein radical complex (or ferryl intermediate) known as compound II [66]. The second reductive step produces the resting enzyme and a second equivalent of substrate radical.

In light of the preceding discussion, this raises several interesting questions. The first and most obvious is: which group of enzymes do the catalase-peroxidases most resemble, heme catalases or heme peroxidases? The answer to this question is unequivocal. On one hand catalase-peroxidases bear virtually no similarity to heme catalases (also referred to as monofunctional catalases). This can be observed at the amino acid sequence level as well as the overall folds of the two groups of proteins. Even the active sites bear little resemblance to one another (Figure 1.9). Monofunctional catalases can use either heme *b* or *d* as the prosthetic group (depending on the type of catalase) whereas catalase-peroxidases exclusively use heme *b*. Furthermore, the monofunctional catalase active site residues consist of distal serine, asparagine and histidine residues. The only residue in common with catalase-peroxidases is the histidine but between the two groups of enzymes the histidine is oriented differently. In typical catalases, the imidazole ring is parallel with the heme, but in catalase-peroxidases it is perpendicular. On the proximal side of the heme, monofunctional catalases ligate the heme through a tyrosine phenolate modulated by an adjacent arginine. Catalase-peroxidases have a histidine as the proximal ligand.

On the other hand, the catalase-peroxidases bear a strong resemblance to the typical (or monofunctional) heme peroxidases. Indeed, they are so closely related that

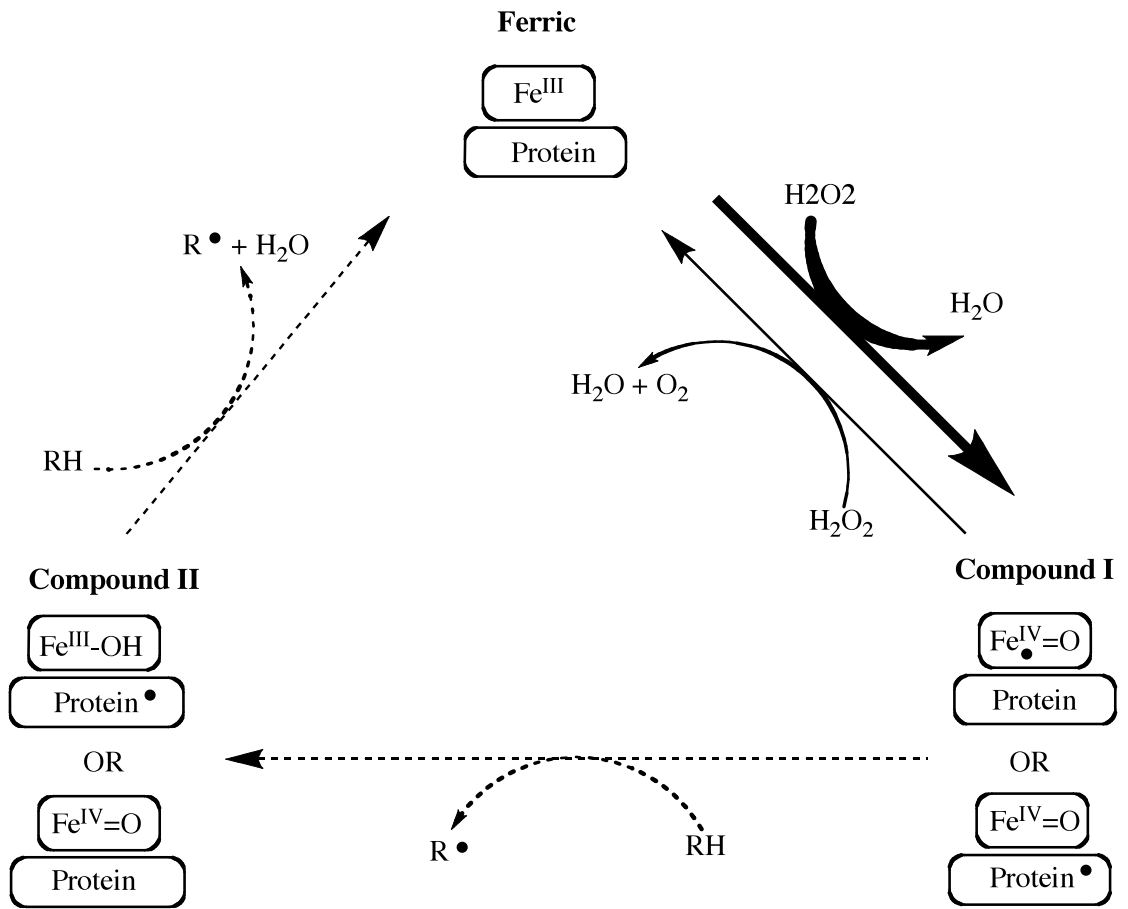


Figure 1.8 The dual catalytic cycle of catalase-peroxidases

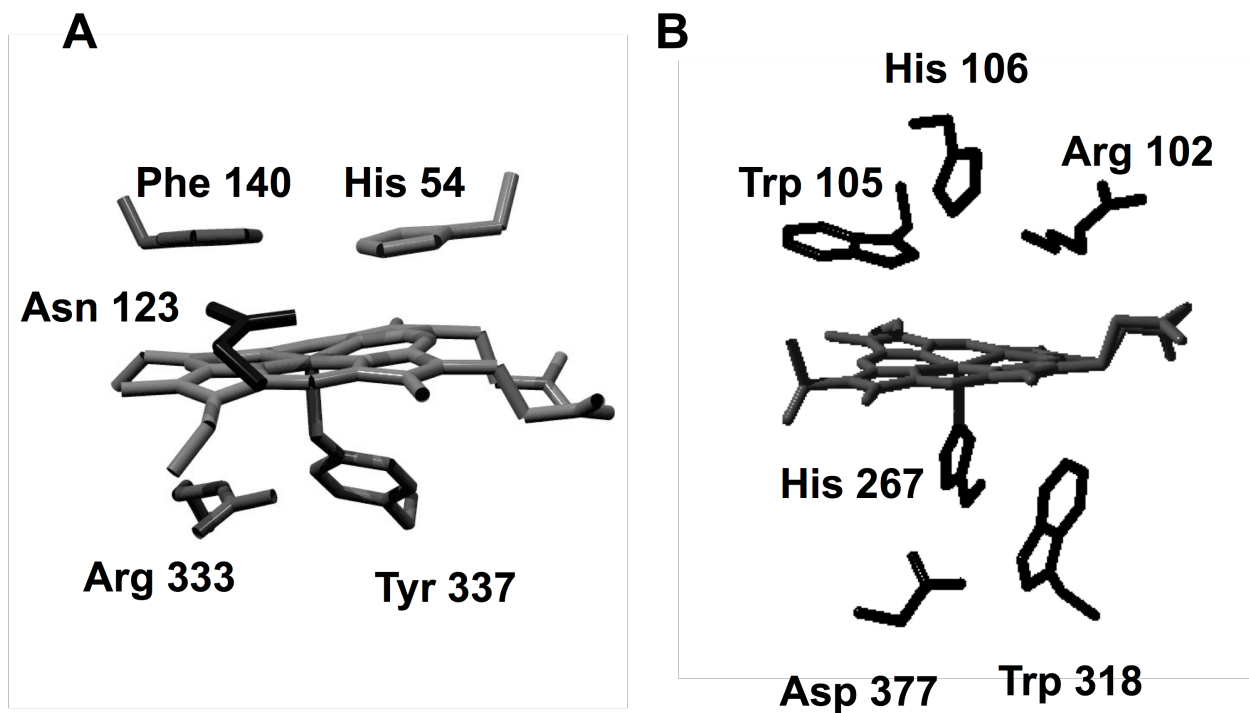


Figure 1.9 Structural comparison of the active sites of (A) catalase (PDB Accession number 1IPH) [153] and (B) catalase-peroxidase (PDB Accession number 1MWV)[68].

they are classified as Class I plant peroxidases. The active site of KatGs consists of a distal and a proximal catalytic triad that are identical to the active site catalytic residues of monofunctional peroxidases. Furthermore, the active sites of monofunctional peroxidases and KatGs are nearly superimposable on one another [67, 68] (Figure 1.10). Therefore, the difference in function between the monofunctional peroxidases and catalase-peroxidases must be due to structures peripheral to and at a distance from the active site. One would expect such structures to be absent from the monofunctional peroxidases. These structures could have an active site structural support role and/or a direct role in KatG catalysis.

To get a view of such features, one must take a step back from the active site and view the catalase-peroxidase protein as a whole. They exist actively as dimers or tetramers and are composed 80 kDa subunits consisting of two domains, roughly twice as large as the typical peroxidase subunit. Moreover, most peroxidases are monomeric. The N-terminal domain binds heme and contains the active site. The C-terminal domain lacks heme and does not appear to catalyze any reaction on its own. It is, nevertheless, a structure conserved across all catalase-peroxidases. The N-terminal domain appears as a typical peroxidase (10 alpha helices, etc.) with the exception of two interhelical insertions of about 35 amino acids each.

Clearly, catalase-peroxidases are evolutionarily related to monofunctional peroxidases, not catalases. The substantial catalase activity of these enzymes is a more recent addition, and the features that distinguish the typical peroxidase from the monofunctional enzyme are rather obvious. Thus, the catalase-peroxidases provide great



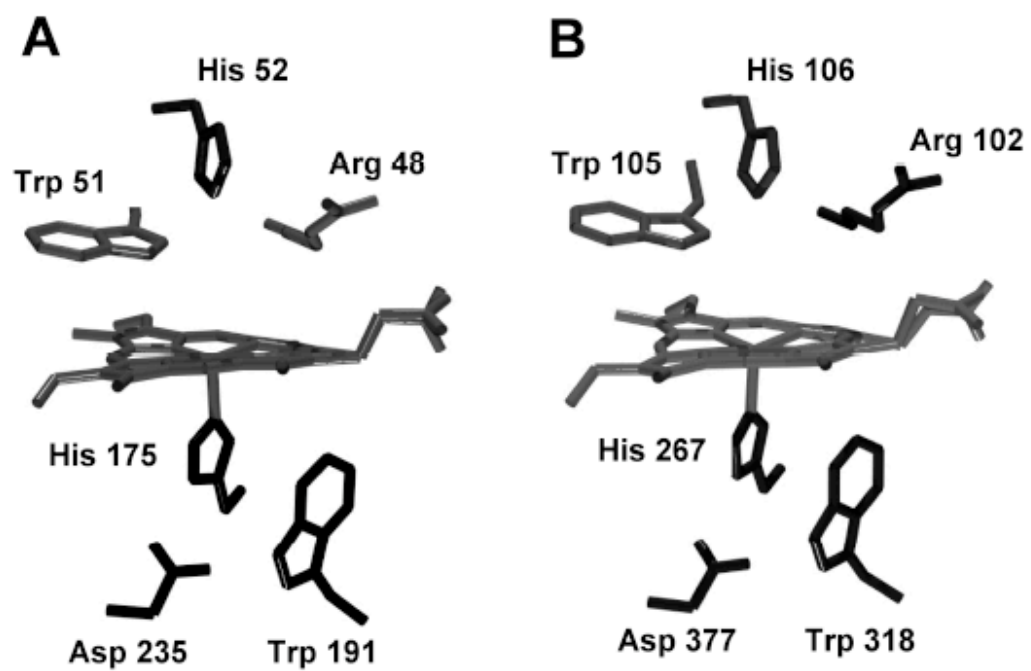


Figure 1.10 Comparison of the active sites of (A) cytochrome c peroxidase (PDB Accession number 1CCP [154] and (B) catalase-peroxidase (PDB Accession number 1MWV)[68].

models to investigate questions surrounding how an existing structural framework is co-opted for the generation of new enzymatic activities. What structural changes must be introduced? By what mechanisms are such changes introduced? How are these effectively accommodated by the existing protein? What structural changes must be made to “shore up” modifications leading to new activities? By what mechanisms do newly added structures communicate with the active site?

#### *1.4.1 Interhelical Insertions*

Although the active site and overall tertiary structural arrangement of the catalase-peroxidase N-terminal domain closely resembles that of monofunctional class I peroxidases, comparison of these two groups of enzymes reveals two interhelical insertions that are unique to the N-terminal domain of bifunctional catalase-peroxidases but absent from monofunctional peroxidases (Figure 1.11) [69, 70]. Both insertions are peripheral to the active site [67, 68]. The first insertion, with a length of 36-43 residues, is positioned between conserved helices D and E. The second insertion, with a length of 35-36 residues, is located between helices F and G. Despite their peripheral locations to the active site, these two insertions are believed to play important functional roles based on the facts that the first three structural levels of catalase-peroxidases and peroxidases are almost superimposable (i.e., type of heme, heme ligands, and non-heme ligand environment). A variant of KatG produced by removing the DE insertion (KatG<sup>ΔDE</sup>) resulted in elevated peroxidase activities compared to wild-type KatG (wtKatG) that were similar to monofunctional peroxidases [71]. However, a total loss of

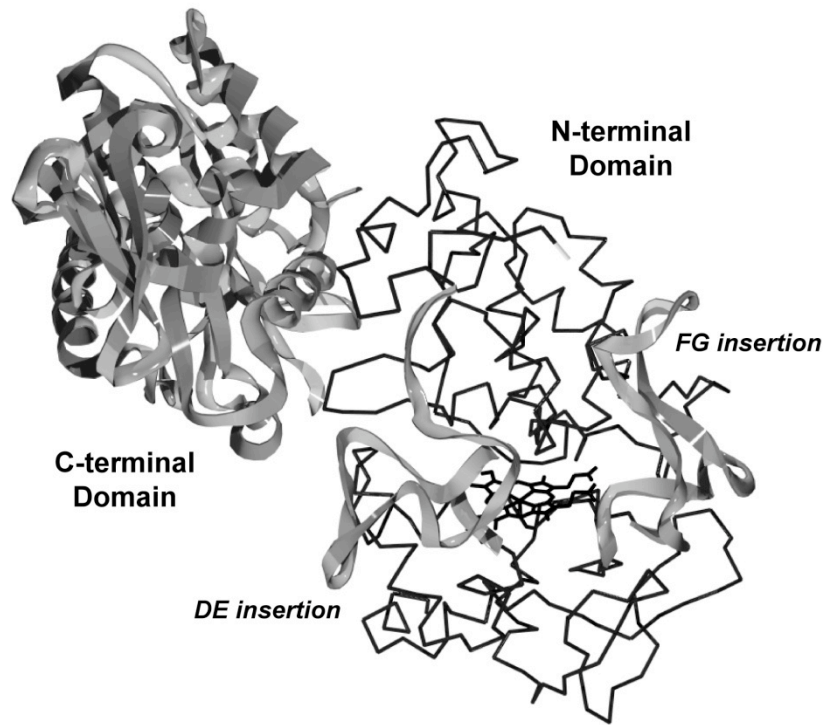


Figure 1.11 Catalase-peroxidase peripheral active structures

catalase activity was observed as a result of removing this peripheral structure. Another variant was created by removing the FG insertion (KatG<sup>ΔFG</sup>). This variant resulted in similar peroxidase activity compared to wtKatG and a 99% reduction in catalase activity. Clearly, these insertions are vital for imparting catalase activity to the bifunctional KatG active site.

#### 1.4.2 *Trp-Tyr-Met Covalent Adduct*

With the revelation of the first crystal structure of a catalase-peroxidase (*Haloarcula marismortui* KatG), a novel Trp-Tyr-Met adduct was identified [67] (Figure 1.12). This has been observed in two other catalase-peroxidase structures, and the residues involved are strictly conserved, suggesting that this covalent adduct is common to all catalase-peroxidases [69, 72]. The bonds are formed between C<sup>η2</sup> of Trp and C<sup>ε1</sup> of Tyr, and between C<sup>ε2</sup> of Tyr and S<sup>δ</sup> of Met. Alterations of the Trp [73, 74] or Tyr [75, 76] result in the loss of catalase activity with little effect upon the peroxidase activity of the enzymes, indicating the role of this adduct is to maintain the catalase activity of these bifunctional enzymes. Furthermore, the central residue of this covalent adduct (Tyr) is located in the DE insertion. This suggests that the loss of catalase activity in the KatG<sup>ΔDE</sup> variant is due to the loss of this tyrosine, which is critical for maintaining the structural integrity of the active site. In addition, it has been shown that disruption of this covalent linkage weakens the binding of heme to the active site, which is instrumental in partially converting the heme iron state from pentacoordinate high-spin to hexacoordinate low-spin [77].

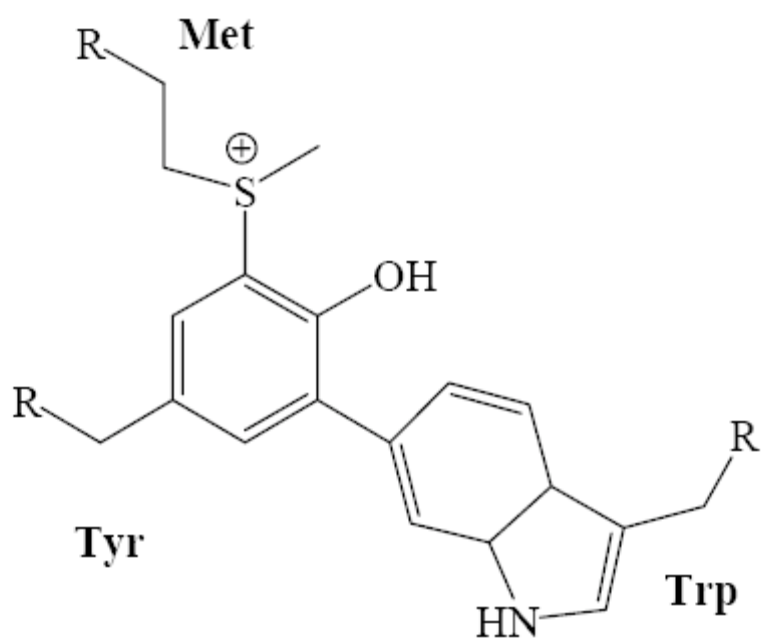


Figure 1.12 Catalase-peroxidase Trp-Tyr-Met covalent adduct

### 1.4.3 The C-terminal Domain

Interestingly, the two-domain structure of catalase-peroxidase is the result of a gene duplication and fusion. Catalase-peroxidases contain two fused copies of a primordial peroxidase gene [70, 78]. As mentioned previously, the N-terminal domain is similar to monofunctional peroxidases and contains the heme prosthetic group for catalysis. The C-terminal domain is also structurally similar to monofunctional peroxidases, but it has no direct catalytic role. It no longer has the ability to bind heme though the architecture of an active site is present. It has no other apparent catalytic activity of its own. Nevertheless, this structure is conserved across all catalase-peroxidases, suggesting it has a role in enzyme function.

The purpose of this dissertation is to determine the role of the C-terminal domain in restructuring the active site of KatG by producing to stand-alone protein domains. A variant of *E. coli* catalase-peroxidase lacking the C-terminal domain (KatG<sup>N</sup>) [79] as well as a variant lacking the N-terminal domain (KatG<sup>C</sup>) were separately expressed and isolated. Spectroscopic, catalytic, and binding properties of KatG<sup>N</sup> demonstrate that the C-terminal domain is essential for activation of KatG<sup>N</sup>. Despite being  $\geq 30\text{\AA}$  away from the active site, the C-terminal domain supports its structure by preventing the coordination of the distal histidine to the heme iron.

To determine the extent and rate of reactivation of KatG<sup>N</sup> by KatG<sup>C</sup>, we co-incubated equimolar amounts of each protein [80]. Addition of KatG<sup>C</sup> to KatG<sup>N</sup> decreased the inactive, hexacoordinate low-spin heme species typical of KatG<sup>N</sup> and increased the mixture of high-spin species of typical of wtKatG. Consistent with the

restructuring of the active site, both catalase and peroxidase activities were detected.

This indicates that the reactivation process involved the interaction of specific residues and/or structures between the domains and that these interactions play a vital role in proper structure and function of KatG.

The C-terminal domain makes highly conserved intrasubunit interdomain contacts with the BC loop of the N-terminal domain [67-68, 81-82]. Because the BC loop extends from the B helix, a major part of the KatG active site, these contacts between the BC loop and the C-terminal domain may be necessary for the proper structural integrity of the heme-dependent active site. Furthermore, the N-terminal domain makes several interactions with the B'C' loop of the C-terminal domain. To determine whether interactions between residues and/or structures between the domains play a role in KatG function, we have used site-directed mutagenesis to make substitutions to several interdomain residues. The purpose of this dissertation is to determine the effect of these substitutions on the reactivation and the structural integrity of the catalase-peroxidase active site.

## CHAPTER TWO

### RESTRUCTURING OF THE CATALASE-PEROXIDASE ACTIVE SITE BY A DISTANT AND INACTIVE DOMAIN

#### 2.1 *Abstract*

Catalase-peroxidases are composed of two peroxidase-like domains. The N-terminal domain contains the heme-dependent, bifunctional active site. The C-terminal domain does not bind heme, has no catalytic activity, and is separated from the active site by  $>30$  Å. Nevertheless, without the C-terminal domain, the N-terminal domain exhibits neither catalase nor peroxidase activity due to the apparent coordination of the distal histidine to the heme iron. Here we report the ability of the separately expressed and isolated C-terminal domain (KatG<sup>C</sup>) to restructure the N-terminal domain (KatG<sup>N</sup>) to its bifunctional conformation. Addition of equimolar KatG<sup>C</sup> to KatG<sup>N</sup> decreased the hexacoordinate low-spin heme complex and increased the high-spin species (penta-coordinate and hexacoordinate). EPR spectra of the domain mixture showed a distribution between high-spin species nearly identical to that of wild-type KatG. The CD spectrum for the 1:1 physical mixture of the domains was identical to an arithmetic composite of individual spectra for KatG<sup>N</sup> and KatG<sup>C</sup>. Both physical and arithmetic mixtures were nearly identical to the spectrum for wild-type KatG, suggesting that major



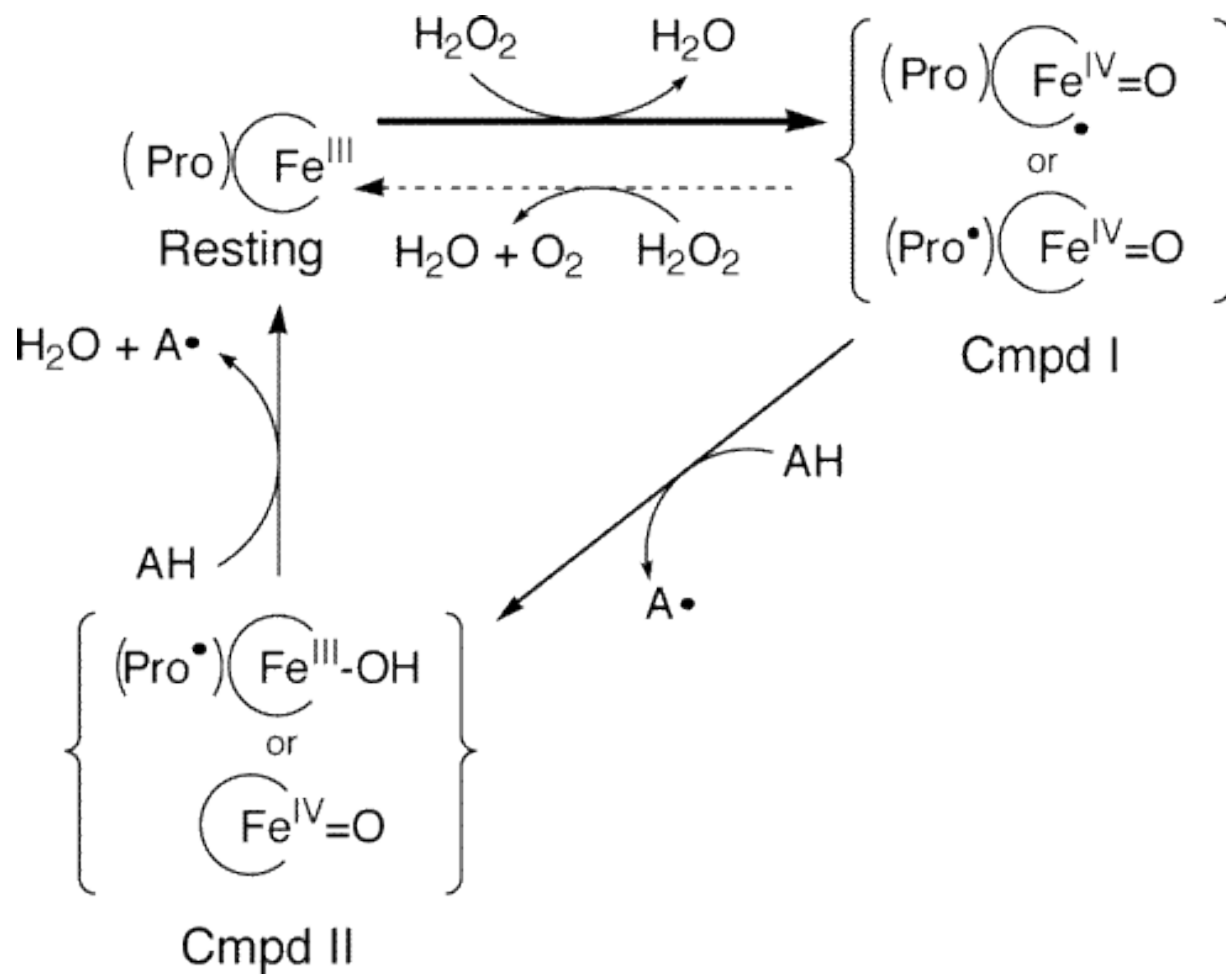
shifts in secondary structure did not accompany active site reconfiguration. With the shift in heme environment, the parallel return of catalase *and* peroxidase activity was observed. Inclusion of bovine serum albumin instead of KatG<sup>C</sup> produced no activity, indicating that specific interdomain interactions were required to reestablish the bifunctional active site. Apparent constants for reactivation ( $k_{\text{react}} \sim 4 \times 10^{-3} \text{ min}^{-1}$ ) indicate that a slow process like movement of established structural elements may precede the restructuring of the heme environment and return of catalytic activity.

## 2.2 Introduction

Catalase-peroxidases have a single multifunctional active site that facilitates efficient catalase *and* peroxidase activities. These enzymes have generated considerable biomedical interest. Catalase-peroxidase (KatG) from *Mycobacterium tuberculosis* has been exploited for the activation of the front-line antitubercular agent isoniazid to its antibiotic form. Interestingly, the increasing prevalence of isoniazid-resistant *M. tuberculosis* is strongly tied (over 70% of resistant strains) to mutations that compromise the ability of KatG to catalyze activation [83]. It is also interesting to note that a novel group of periplasmic catalase-peroxidases have been identified as potential virulence factors in dangerous pathogens such as the enterohemorrhagic *Escherichia coli* strain O157:H7 [84] and *Yersinia pestis* [85-87], both of which are recognized as high priority threats as agents of bioterrorism. Nevertheless, the mechanisms by which these enzymes may operate as virulence factors have not been illuminated. Clearly, there are important

benefits to be derived from understanding the structure and function of the catalase-peroxidases.

The disproportionation of  $\text{H}_2\text{O}_2$  (i.e., catalase activity) by heme-dependent catalases, including the catalase-peroxidases, starts with reaction of resting enzyme with 1 equiv of  $\text{H}_2\text{O}_2$  to yield  $\text{H}_2\text{O}$  and an oxoferryl porphyrin/protein radical intermediate (compound **I**) (Scheme 2.1). Compound **I** is then reduced back to resting enzyme by a second equivalent of  $\text{H}_2\text{O}_2$ , generating  $\text{O}_2$  and  $\text{H}_2\text{O}$ . The peroxidase catalytic cycle also begins with compound **I** formation. However, compound **I** is reduced in two sequential one-electron steps by an exogenous electron donor to return the enzyme to its ferric state. The first reduction produces 1 equivalent of substrate radical and, with typical peroxidases (e.g., horseradish peroxidase), the oxoferryl intermediate known as compound **II**. However, recent evidence suggests that in catalase-peroxidases the heme iron is reduced first to yield an  $\text{Fe}^{\text{III}}\text{-OH}$ /protein radical complex [66]. In both cases, the second reductive step produces the resting enzyme and a second equivalent of substrate radical. Though these two catalytic processes are similar, the bifunctional ability of the catalase-peroxidases is highly unusual. Heme enzymes with substantial catalase activity typically exhibit poor peroxidase activity. Likewise, the heme enzymes known for their strong peroxidase activity tend to show very weak catalase activity. The lack of catalase activity in typical peroxidases (e.g., cytochrome *c* peroxidase) is noteworthy because, with few exceptions [88], the active sites of these enzymes and the catalase-peroxidases are virtually superimposable on one another [67] and [72]. This striking functional difference between two enzymes that are so structurally similar provides a robust system



Scheme 2.1. Representation of the Dual Catalytic Cycle of Catalase-Peroxidases. Catalase activity involves cycling between the resting and compound I (Cmpd I) forms. Peroxidase activity includes the reactions involving compound II (Cmpd II).

for unraveling the subtle perturbations of heme enzyme active sites that lead to profound differences in mechanism and function.

Along these lines, catalase-peroxidases have three prominent structural features that are absent from monofunctional peroxidases. All three structures are peripheral to the enzyme active site, and evidence suggests that all three are essential for catalase-peroxidase function [67], [71], [68], and [79]. One of these features is a 300 amino acid C-terminal domain. The C-terminal domain also structurally resembles a monofunctional peroxidase, suggesting that its presence in the catalase-peroxidases is due to an ancient gene-duplication event; however, this domain does not bind heme and does not catalyze any discernible reaction. Nevertheless, we have shown that this "inactive" domain is essential for catalase-peroxidase catalysis [79]. A catalase-peroxidase variant containing only its N-terminal domain (KatG<sup>N</sup>) lacks catalase *and* peroxidase activities [79]. Results of site-directed mutagenesis and spectroscopic studies indicate that, in the absence of the C-terminal domain, an active site histidine (the so-called distal histidine) acts as a ligand to the heme iron, interrupting its ability to act as a general base in catalase-peroxidase catalysis.

Here we demonstrate the ability of the separately expressed and isolated C-terminal domain (KatG<sup>C</sup>) to restructure the active site found within the N-terminal domain (KatG<sup>N</sup>). Addition of equimolar KatG<sup>C</sup> to KatG<sup>N</sup> resulted in a shift in the active site heme coordination environment. There was a decrease in the inactive hexacoordinate low-spin heme typical of KatG<sup>N</sup> and a concomitant increase in the high-spin species typical of wild-type catalase-peroxidases. Consistent with these alterations in active site structure, both catalase *and* peroxidase activities were detected. A generic protein, bovine

serum albumin, was unable to restore either catalase or peroxidase activities when it was incubated with KatG<sup>N</sup> in place of KatG<sup>C</sup>, indicating that specific interdomain interactions were required for KatG<sup>N</sup> activation.

## 2.3 *Materials and Methods*

### 2.3.1 *Materials*

Hydrogen peroxide (30%), imidazole, phenyl-Sepharose resin, ampicillin, chloramphenicol, phenylmethanesulfonyl fluoride (PMSF), and 2,2'-azinobis(3-ethylbenzothiazoline-6-sulfonic acid) (ABTS) were purchased from Sigma (St. Louis, MO). Isopropyl  $\beta$ -D-thiogalactopyranoside (IPTG), urea, and tetracycline hydrochloride were obtained from Fisher (Pittsburgh, PA). All restriction enzymes were purchased from New England Biolabs (Beverly, MA), and all oligonucleotide primers were purchased from Invitrogen (Carlsbad, CA). All *E. coli* strains [BL-21(DE3) pLysS and XL-1 Blue] and Pfu polymerase were obtained from Stratagene (La Jolla, CA). Nickel nitrilotriacetic acid (Ni-NTA resin) was obtained from Qiagen (Valencia, CA). All buffers and media were prepared using water purified through a Millipore Q-PakII system (18.2 M $\Omega$ /cm resistivity).

## 2.3.2 Cloning and Expression of wtKatG and its Domain Variants

### 2.3.2.1 Seamless<sup>®</sup> cloning (Stratagene) Method

The purpose of the Stratagene Seamless<sup>®</sup> cloning method is to eliminate the N-terminal domain and generate a free C-terminal domain expression construct with seamless junctions that are independent of naturally occurring restriction sites. This cloning method is based upon PCR (polymerase chain reaction) and the capacity of the type-IIIS restriction endonuclease (ENase) *Eam1104I* to cleave any DNA sequence located at a defined distance from its recognition sequence. This allows the cloning and/or modification of any DNA sequence independent of naturally occurring restriction sites (Figure 2.1). Insert and vector DNA are prepared by long PCR, which allows for least 35 kb to be amplified to high yields from 1 ng of DNA template. Primers designed to amplify the vector backbone, plus any portion of a gene residing within it, easily permit the exclusion of any DNA segment. The omitted section can subsequently be replaced with a mutated form or exchanged with a corresponding sequence from another source by amplifying the region with primers that include the *Eam1104I* recognition sequence 5'-CTCTTC (Figure 2.2).

The unique feature of *Eam1104I* is that its cleavage site is one nucleotide down on the upper strand in the 3' direction and four nucleotides down on the lower strand in the 5' direction (cleavage sites shown as arrows in Figure 2.2). The *Eam1104I*

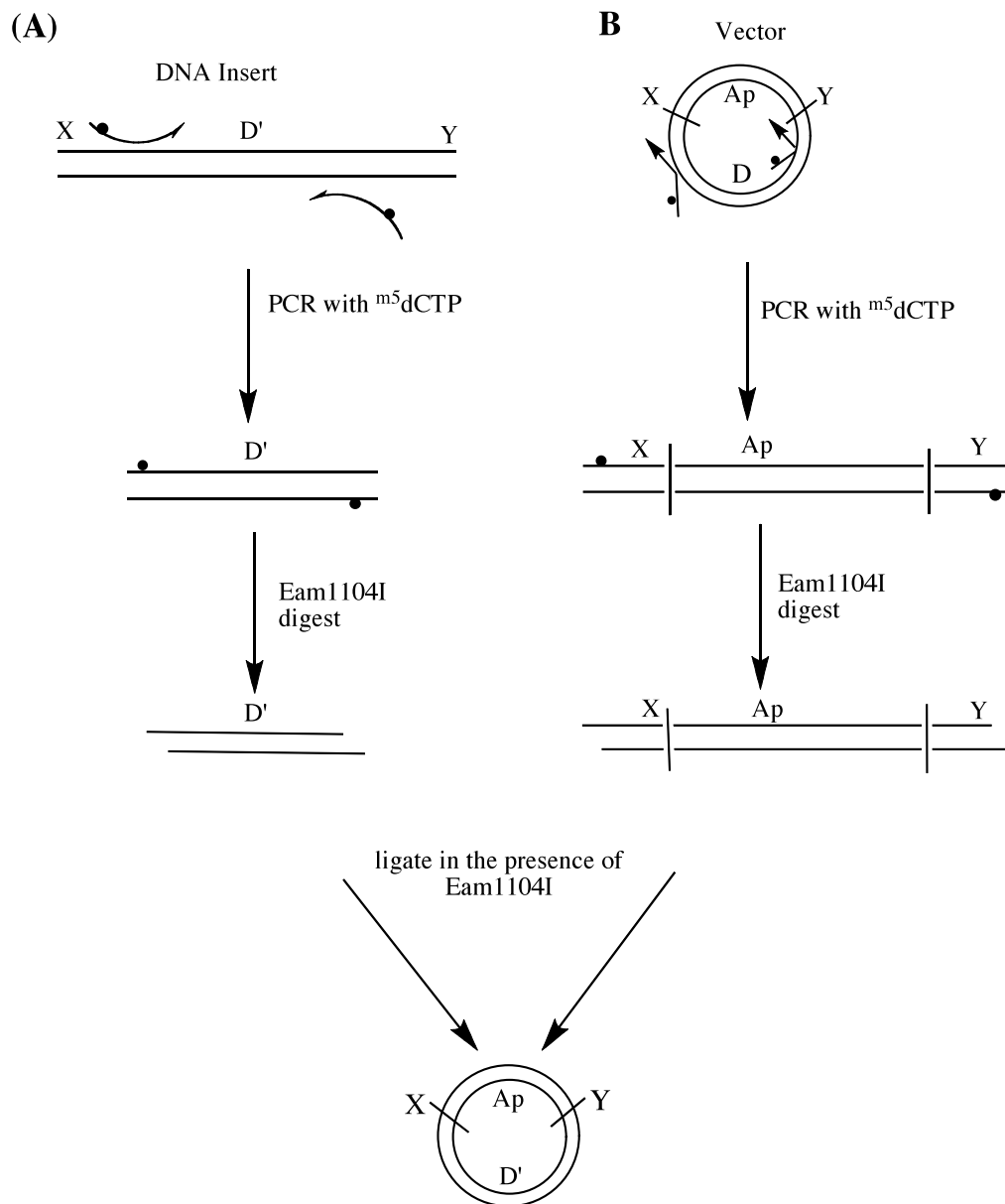


Figure 2.1. General method of PCR cloning using the Type-IIS endonuclease *Eam1104I*.

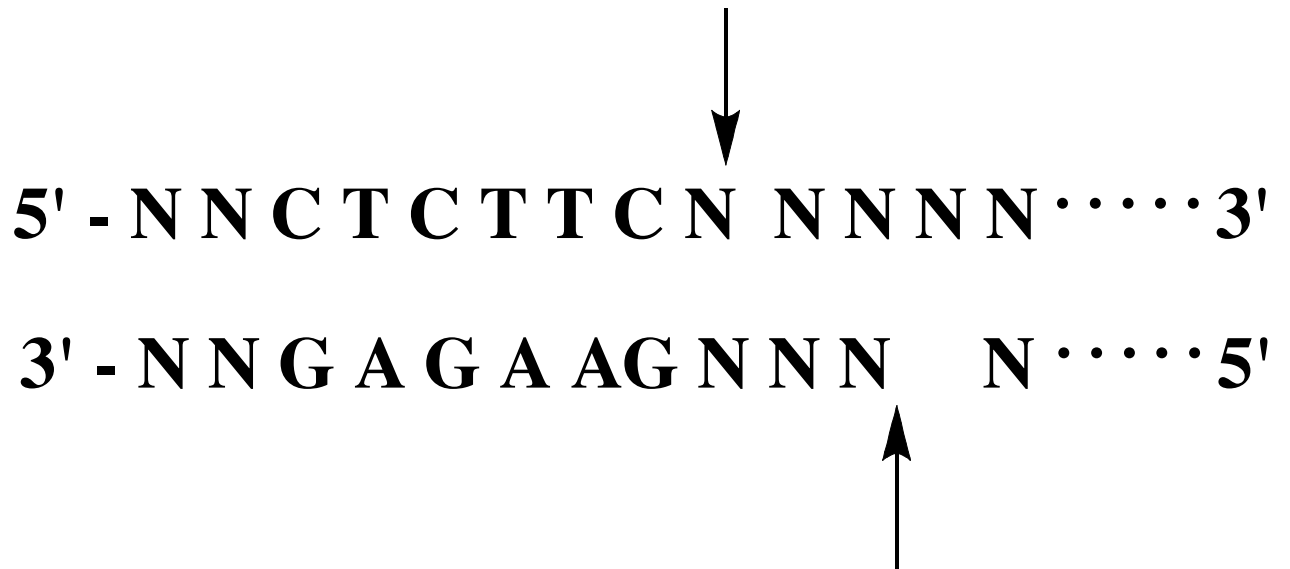


Figure 2.2. Recognition sequence 5'-CTCTTC and cleavage sites (arrows) of *Eam1104I*.



endonuclease activity is inhibited when the deoxycytosine (dCTP) residues in the recognition site are replaced with 5-methyl-deoxycytosine (<sup>m5</sup>dCTP). Incorporation of <sup>m5</sup>dCTP into the DNA results in a PCR product that is resistant to cleavage at the naturally occurring *Eam*1104I sites. Since the *Eam*1104I recognition sites built into the PCR primers contain non-methylated dCTP, and there are no dCTP residues in the complementary strand of an *Eam*1104I site (5'-GAAGAG-3'), the PCR reaction does not incorporate <sup>m5</sup>dCTP into either strand of the primer-encoded recognition sequence. The terminal restriction sites are thus efficiently digested while the internal positions are protected. Thus, digestion of the PCR product with *Eam*1104I detaches the recognition sequence from each terminus, which generates termini containing three nucleotides in their 5' overhang sequences. The digested PCR products are then ligated with a pET-20b plasmid DNA vector using T4 DNA ligase.

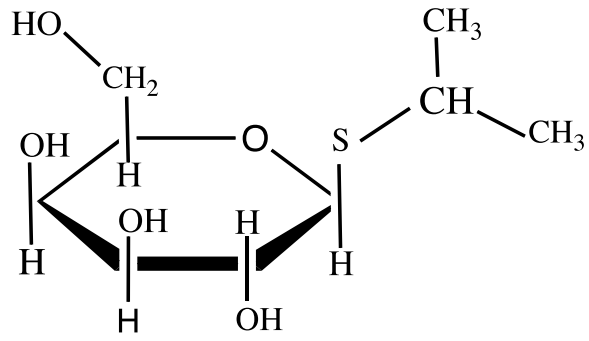
#### 2.3.2.2 *The pET expression system*

The pET expression system is a method developed for the cloning and expression of recombinant proteins. Target genes are cloned into pET plasmids under control of bacteriophage T7 transcription selectivity, which converts predominantly all of the cell resources to target gene expression. Target genes are initially cloned using non-expression hosts lacking the T7 RNA polymerase gene. Plasmids are then transferred into expression hosts containing a chromosomal copy of the T7 RNA polymerase gene under *lacUV5* control. Target genes are maintained in a transcriptionally silent mode prior to induction. Expression is induced by the addition of isopropyl-β-D-

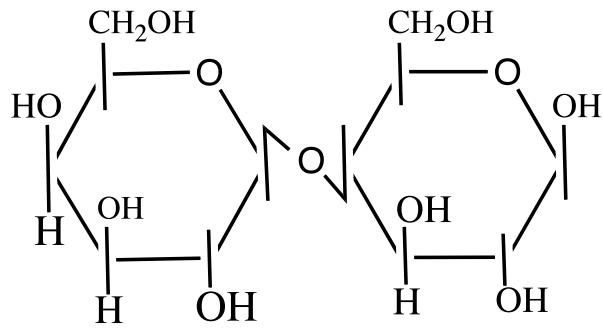
thiogalactopyranoside (IPTG), a lactose analog (Figure 2.3). The desired product comprises more than 50% of the total cell protein a few hours after induction. The pET plasmid used in the studies in this dissertation was pET-20b. The gene of interest was inserted following the T7 RNA polymerase promoter. All genes were placed in the plasmid so that expression would result in a C-terminal 6-histidine tag. For selection purposes, the pET-20b plasmid encodes an ampicillin resistance gene, conferring ampicillin resistance on cells carrying the plasmid.

#### 2.3.2.3 Non-expression host *E. coli* XL-1 Blue

Ligated plasmid DNA was amplified by transforming it with the *E. coli* XL-1 Blue non-expression host. All transformations for the C-terminal domain and variants thereof using *E. coli* XL-1 Blue were carried out using the following heat-shock method: the XL-1 Blue supercompetent cells were incubated with target plasmid on ice for 30 minutes. The transformation mixture was then heat pulsed in a 42°C water bath for 45 seconds, followed by quenching on ice for 2 minutes. All transformation for the N-terminal domain and variants using *E. coli* XL-1 were done by electroporation using a Biorad Micropulser<sup>TM</sup>. The XL-1 Blue electroporation competent cells were incubated on ice with target plasmid for 1 minute. The transformation mixture was then micropulsed in a 0.2 cm electroporation cuvette. The transformants were allowed to recover in Hanahan's broth (SOB medium) supplemented with glucose, MgCl•6H<sub>2</sub>O, and MgSO<sub>4</sub>•7H<sub>2</sub>O (SOC medium) for 1 hour at 37°C with agitation at 240 rpm. Following



IPTG



Lactose

Figure 2.3. Structure of IPTG and Lactose

recovery, cells were plated on LB (Luria-Bertani) agar plates supplemented with ampicillin. In all molecular cloning described in this dissertation, transformed *E. coli* XL-1 Blue strains were grown on LB-agar plates and in LB broth in the presence of ampicillin (100 mg/mL).

#### 2.3.2.4 Protein expression host *E. coli* BL-21 Gold [DE3] pLysS

The proteins in this dissertation were expressed using the *E. coli* strain BL-21 [DE3] pLysS. *E. coli* strain BL-21Gold [DE3] pLysS was transformed with pET-20b plasmid containing the gene for *E. coli* catalase-peroxidase (KatG) variants. The expression strain is a  $\lambda$ DE3 phage lysogen, which contains a chromosomal copy of the gene for T7 RNA polymerase under control of the *lac* UV5 promoter. Therefore, when lactose or any of its analogs (e.g., IPTG, Figure 2.3) are absent, the *lac* repressor binds to the *lac* promoter, blocking expression of the target protein. However, in the presence of lactose or a suitable analog, the *lac* repressor dissociates from the *lac* promoter, resulting in the expression of T7 RNA polymerase, which facilitates the expression of the target protein. The protein expressions discussed in this dissertation utilized isopropyl- $\beta$ -D-thiogalactopyranoside (IPTG) as a lactose analog. The expression strain also consists of a plasmid that encodes T7 lysozyme (hence the pLysS designation). Lysozyme is an inhibitor of T7 RNA polymerase, which prevents “leakage” expression of the target protein by the *lac* UV5 promoter. “Leakage” expression refers to the small amount of T7 RNA polymerase that is expressed in the absence of lactose or one of its analogs. The presence of T7 RNA polymerase in turn induces expression of the target protein. If the

protein being over-expressed is toxic, “leakage” expression will diminish cell growth. Consequently, the cell density levels may be insufficient for abundant expression of the target protein. Therefore, the presence of the plasmid that encodes T7 lysozyme is an important feature that allows for the expression of target proteins in a tightly controlled manner.

The transformation procedure for *E. coli* BL-21 Gold [DE3] pLysS cells used for all studies described in this dissertation is as follows: the cells were incubated with the target plasmid on ice for 30 minutes. Then the mixture was heat shocked at 42°C for 20 seconds in a water bath, followed by quenching on ice for 2 minutes. Cells were allowed to recover for 1 hour at 37°C in SOC medium with gentle agitation. Following recovery, the cells were inoculated on LB agar plates supplemented with ampicillin (100 mg/mL) (N-terminal domain variants) or ampicillin (100 mg/mL) and chloramphenicol 34.5 mg/mL) (C-terminal domain variants and wtKatG).

#### 2.3.2.5 Cloning and expression of wild-type *KatG* (wtKatG)

The cloning of wtKatG was accomplished previously by Dr. Douglas Goodwin utilizing the *katG* gene that was acquired from *E. coli* (K-12) genomic DNA. Two primers, ECCPa03 (GTA GAG GGG AGC ACA CAT ATG AGC ACG TCA GAC GAT ATC C), and ECCPa06 (CTG AAC GCG GTC AGA CTC GAG CAG GTC GAA ACG GTC) were used to amplify the *katG* gene, using PCR techniques. To incorporate the *katG* gene into pET-20b, the resulting PCR product and the pET-20b plasmid were digested with endonucleases *NdeI* and *XhoI*, and the proper fragments were ligated

together according to standard procedures [89]. Candidate plasmids were sequenced to verify that no accidental mutations had accumulated during the cloning process. By using the XhoI restriction site in the multiple cloning sequence of pET-20b, the katG gene was followed by six codons for histidine and a stop codon. Thus, wtKatG is expressed with a six-histidine tag on its C-terminus. The *E. coli* protein expression host (BL-21 [DE3]pLysS) was transformed with the pKatG1 plasmid and transformants were selected based on ampicillin resistance.

Expression of wtKatG and data thereof obtained for comparison in this dissertation was done by Yongjiang Li. WtKatG expression was achieved by growing in transformed expression host in LB broth (2L) with 100 mg/mL ampicillin. Cells were grown to mid-log phase ( $OD_{600} = 0.4 \sim 0.6$ ) and expression of wtKatG was induced by addition of 1 mM IPTG. At the time of induction, cultures were also supplemented with 0.5 mM  $\delta$ -amino levulinic acid and 0.5 mM ferrous ammonium sulfate for biological synthesis of heme. The expression was carried out at 37°C with constant shaking for four hours after induction. Cells were harvested by centrifugation (13,000 x g), and the cell pellets were stored at -80°C until purification.

WtKatG expression was analyzed by treating samples of cells with equal volumes of 10% trichloroacetic acid (4°C) followed by centrifugation. The pellet was then washed with 1 mL acetone, dried on a 95°C heating block, and re-suspended in SDS-PAGE loading buffer. The pH of the resuspended pellet was adjusted with trizma base and separated by SDS-PAGE using 7.5% acrylamide resolving gel.

### 2.3.2.6 Cloning and Expression of *KatG<sup>C</sup>*

Constructs for the expression of *KatG<sup>ΔNterm</sup>* (wt*KatG* lacking its N-terminal domain) were generated from a deletion mutagenesis procedure developed in our laboratory adapted from Seamless<sup>®</sup> cloning (Stratagene). The plasmid for expression of recombinant His-tagged *E. coli* *KatG* (p*KatG*1) was used as a template. Primers were designed to: (1) amplify p*KatG*1 excluding codons for the N-terminal domain (Ser 2–Asp 431), (2) include a restriction site for *Eam*1104 I, and (3) yield the necessary *Eam*1104 I overhanging sequence. Because *Eam*1104I is a type IIS endonuclease, it cleaves target DNA downstream of its recognition sequence. Thus, the resulting overhanging sequences were designed for religation such that only the codons corresponding to the target deletion were removed. Neither the addition of new restrictions sites and extra codons, nor the removal of codons outside the target sequence was required. We used the forward primer ECCP D301 (GCC GGA CTC TTC G ***ATG*** GAA GAT CTG ATC TGG CAA GAT CC) and the reverse primer ECCP D302 (CGT CTG CTC TTC T ***CAT*** ATG TAT ATC TCC TTC TTA AAG). The *Eam*1104 I recognition sequence is underlined and the overhanging sequence generated upon hydrolysis by *Eam*1104 I is in bold italics. 5-methyl dNTPs were added to the PCR reactions during the 19<sup>th</sup> cycle of the elongation phase. The PCR products were purified with ethanol and digested with *Eam*1104 I and ligated with T4 DNA ligase. The ligated plasmid was used to transform *E. coli* XL-1 Blue. Colonies were selected on the basis of ampicillin resistance, and candidate plasmids were verified by DNA sequence analysis to ensure the accuracy of the seamless mutagenesis procedure. The expression host *E. coli* BL-21 [DE3] pLysS was

transformed with the  $KatG^{\Delta N^{term}}$  construct as previously described.

Expression of  $KatG^C$  was achieved by growing the transformed *E. coli* BL-21 [DE3] pLysS expression host in LB broth supplemented with 100 mg/L ampicillin. Cells were grown to mid-log phase ( $OD_{600} = 0.4 - 0.6$ ) and expression of  $KatG^C$  was induced by addition of 1mM IPTG. The expression was carried out at 37°C with constant agitation for four hours after induction. Cells were then harvested by centrifugation (13,000 x g), and the cell pellets were stored at -80°C until purification was performed.

$KatG^{\Delta N^{term}}$  expression was evaluated by treating a sample of cells with an equal volume of 10% trichloroacetic acid (4°C) followed by centrifugation. The pellet was then washed with 1 ml acetone, dried at 90°C, and then re-suspended in SDS-PAGE loading buffer. The pH of the re-suspended pellet was adjusted with trizma base (pH 8.0) and separated by SDS-PAGE using a 7.5% acrylamide resolving gel.

#### 2.3.2.7 Cloning and expression of $KatG^N$

A construct for the expression of  $KatG$  lacking its C-terminal domain ( $KatG^N$ ) was produced by using site-directed mutagenesis primers ECCPm08(+) (GCC GAA AGA AGA TCT GCT CGA GTA AGA TCC GCT GCC) and ECCPm08(-) (GGC AGC GGA TCT TAC TCG AGC AGA TCT TCT TTC GGC) to introduce a *XhoI* restriction site following codon 432 (Leu) (Quik Change, Stratagene) by Ruletha D. Baker. Plasmids from candidate colonies (*E. coli* XL-1 Blue) were treated with *XhoI*, and fragments were separated by agarose gel electrophoresis. The band corresponding to the pET20b plasmid plus the codons of the N-terminal domain was excised, extracted from



the gel, and religated using T4 DNA ligase. The product was used to transform *E. coli* (XL-1 Blue). Candidate plasmids were evaluated by diagnostic restriction digests and DNA sequence analysis. The resulting expression construct (pKatG<sup>N</sup>) included codons 1 (Met) through 432 (Leu) followed by codons for Leu, Glu, and a six-histidine tag. This plasmid was used to transform *E. coli* (BL-21 [DE3] pLysS) as previously described.

Expression of KatG<sup>N</sup> was achieved by growing the transformed *E. coli* BL-21 [DE3] pLysS expression host in LB broth supplemented with 100 mg/l ampicillin and 35 mg/l chloramphenicol. Cells were grown to mid-log phase (OD<sub>600</sub> = 0.4-0.6) and expression of KatG<sup>C</sup> was induced by addition of 1mM IPTG. The expression was carried out at 37°C with constant agitation for four hours after induction. Cells were then harvested by centrifugation (13,000 x g), and the cell pellets were stored at -80°C until purification was performed.

### 2.3.3 Purification of wtKatG and the KatG domains (KatG<sup>N</sup> and KatG<sup>C</sup>)

Purification of wtKatG was performed by Yongjiang Li and data obtained from this purified protein were used for comparison purposes. WtKatG Cell pellets were resuspended in Bugbuster<sup>™</sup> reagent supplemented with 0.1 mM PMSF. Following homogenization, benzonase (250 units) was added, and the mixture was incubated at 23°C with gentle stirring for 1 hour. The cell lysate was then centrifuged at 12,000 rpm for 20 minutes.

KatG<sup>C</sup> cell pellets were resuspended in buffer A (200 mM phosphate buffer, pH 7.0) supplemented with 0.1 mM PMSF and 0.1 mg/mL lysozyme. Following

homogenization, the suspension was sonicated with a Branson 250 sonifier at constant output, 3.5 duty, for eight cycles consisting of 45 seconds on and 45 seconds off.

Following the sonification, benzonase (500 units) was added to the cell lysate, and the mixture was incubated at 23°C with gentle stirring for 1 hour. The cell lysates were then centrifuged at 12,000 rpm for 20 minutes.

WtKatG and KatG<sup>C</sup> were then purified using a Ni-NTA column. The Ni-NTA resin is utilized for purification of proteins with a six-histidine tag. Nitriloacetic acid (NTA) is the chelator, which is covalently bound to the resin. Immobilized Ni<sup>2+</sup> cations are coordinated by the NTA moiety. The target protein, designed to contain a His-tag can tightly bind to the Ni<sup>2+</sup> cations (Figure 2.4). All other cellular proteins that either do not bind or only slightly bind to the resin can be washed off with low concentration imidazole solution. The target protein can subsequently be eluted with high concentration imidazole. This procedure allows us to purify six-histidine tagged proteins in either native or denatured forms.

For wtKatG and KatG<sup>mC</sup>, the supernatant was loaded onto a Ni-NTA column by recirculating the solutions at 1 ml/min through the column bed overnight. After the target protein had been loaded onto the Ni-NTA, the column was washed with buffer **B** (50 mM phosphate buffer, pH 8.0; 200 mM NaCl) for wtkatG or buffer **A** for KatG<sup>C</sup>, supplemented with 2 mM imidazole to remove contaminant non-target proteins lacking the six-histidine tag. A second wash was then performed with buffer **A** or buffer **B** supplemented with 20 mM imidazole to wash off more tightly bound non-target proteins. Finally, protein was eluted off the column with buffer **A** or buffer **B** supplemented with 200 mM imidazole. Excess imidazole was then removed by gel filtration (Sephacryl 300

HR) chromatography (wtkatG) or dialysis (KatG<sup>C</sup>). By dialysis, the target protein was dialyzed against buffer **A** for 18-36 hours. Appropriate fractions as determined by SDS-PAGE were combined, aliquoted, and stored at -80°C.

#### 2.3.4 Purification of KatG<sup>N</sup>

For KatG<sup>N</sup>, cell pellets were resuspended in buffer **B** supplemented with 0.1 mM PMSF. Following homogenization, the suspension was sonicated with a Branson 250 sonifier at constant output, 3.5 duty, for eight cycles consisting of 42 seconds on and 42 seconds off. Following sonification, benzonase (500 units) was added to the cell lysate, and the mixture was incubated at room temperature with gentle stirring for 1 hour. The cell lysate was then centrifuged at 10,000 rpm for 10 minutes. KatG<sup>N</sup> was expressed in inclusion bodies. . Because of this, following the centrifugation of the lysate, the supernatant was discarded, and the pellet was re-suspended in 8M urea, re-homogenized, and re-centrifuged. After the second centrifugation, the supernatant was diluted 1:2 with 1M NaCl and Ni-NTA resin was added to the supernatant solution, and the resultant mixture was incubated overnight at 23°C with constant, gentle agitation. The Ni-NTA resin was then collected on a column and washed with 10 column volumes of 10 mM imidazole in 8 M urea. The target protein was then eluted from the column using 8 M urea supplemented with 200 mM imidazole. The purity of each fraction was estimated by Coomassie-stained SDS-PAGE, and the appropriate fractions (95% pure) were pooled and dialyzed against buffer **B** for 24 h with five changes.

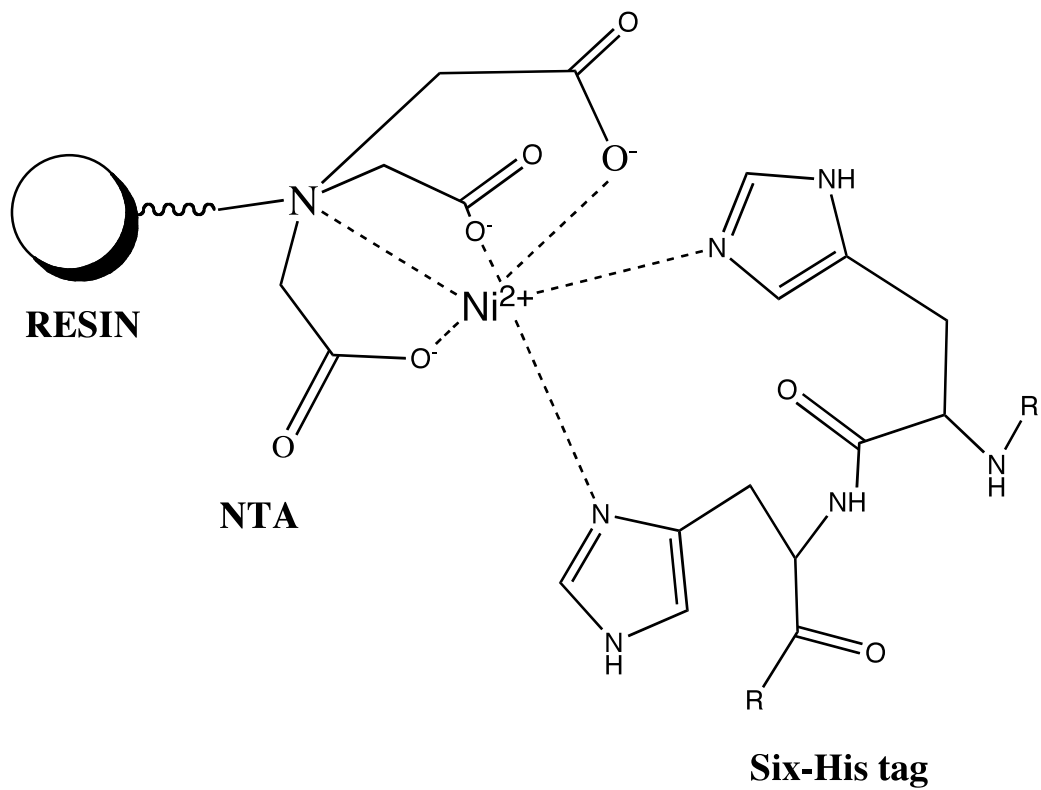


Figure 2.4. Structural scheme of Ni-NTA resin and bound Six-His tag.

### 2.3.5 Reconstitution of wtKatG and KatG<sup>N</sup>

Heme binding or reconstitution was accomplished by incubating the protein at 4°C overnight with an amount of hemin solution after purification. Due to its poor solubility at neutral or acidic pH, hemin reconstitution solutions were prepared by dissolving them in 0.1 M KOH. Hemin concentrations were determined by the method of Falk [90]. Reconstitution converts the apo-protein (heme free) to holo-protein (heme-bound) when incubated with hemin. Spectra for a given KatG protein was recorded from 750-250 nm using a Shimadzu UV1601 spectrophotometer (Columbia, MD) before and after incubation with 0.75 (wtKatG) or 0.95 (KatG<sup>N</sup>) equivalents of hemin solution. Heme binding was determined by shifts in spectral lineshapes and molar absorptivities.

### 2.3.6 Domain mixing and incubation procedures

The concentrations of KatG<sup>N</sup> and KatG<sup>C</sup> were calculated using the molar absorptivities below. Solutions containing KatG<sup>N</sup> and KatG<sup>C</sup> were incubated at 4°C for times ranging from 0 to 72 h. Reactivation was also measured as a function of pH. In each case, KatG<sup>N</sup> and KatG<sup>C</sup> were incubated in the presence of 120 mM buffer (citrate or phosphate) at the appropriate pH. Following a given incubation time, aliquots were removed, and activity was measured according to the assays described below. Assay conditions were such that the added aliquot volume did not significantly affect the pH of the assay. Apparent rate constants for reactivation ( $k_{\text{react}}$ ) as a function of pH were fit to

equation (1), where  $a$  and  $b$  are the theoretical maximum and minimum  $k_{\text{react}}$  values, respectively.

$$y = a + (b - a)/(1 + 10^{\text{pK}_a - \text{pH}}) \quad (2.1)$$

### 2.3.7 Catalase and Peroxidase Activity Assays

Peroxidase activity was evaluated by monitoring the production of the ABTS radical over time at 417 nm ( $34.7 \text{ mM}^{-1} \text{ cm}^{-1}$ ) [91]. All assays were carried out at room temperature in 50 mM acetate buffer, pH 5.0. Catalase activity was evaluated by monitoring the decrease in  $\text{H}_2\text{O}_2$  concentration with time at 240 nm ( $39.4 \text{ M}^{-1} \text{ cm}^{-1}$ ) [92]. All assays were carried out at room temperature in 100 mM phosphate buffer, pH 7.0. All catalase and peroxidase activities were normalized on the basis of heme content.

### 2.3.8 UV-Visible Absorption Spectroscopy

All UV-visible absorption spectra were recorded using a Shimadzu UV1601 spectrophotometer (Columbia, MD). The molar absorptivities of  $\text{KatG}^{\text{N}}$  (prior to heme addition) and  $\text{KatG}^{\text{C}}$  at 280 nm were estimated according to the method of Gill and von Hippel [94]:  $\epsilon_{280}(\text{KatG}^{\text{N}}) = 1.11 \times 10^5 \text{ M}^{-1} \text{ cm}^{-1}$  and  $\epsilon_{280}(\text{KatG}^{\text{C}}) = 3.36 \times 10^4 \text{ M}^{-1} \text{ cm}^{-1}$ . Concentrations of holo-wtKatG and holo- $\text{KatG}^{\text{N}}$  were determined on the basis of the molar absorptivity of the Soret band  $\lambda_{\text{max}}$ :  $\epsilon_{408}(\text{wtKatG}) = 1.21 \times 10^5 \text{ M}^{-1} \text{ cm}^{-1}$  [71] and  $\epsilon_{416}(\text{KatG}^{\text{N}}) = 9.8 \times 10^4 \text{ M}^{-1} \text{ cm}^{-1}$  [79].

### 2.3.9 *Circular Dichroism Spectropolarimetry*

Far-UV (185-300 nm) circular dichroism (CD) spectra were recorded for wtKatG, KatG<sup>N</sup>, KatG<sup>C</sup>, and a 1:1 mixture of KatG<sup>N</sup> and KatG<sup>C</sup> using a Jasco J-810 spectropolarimeter (Tokyo, Japan). To minimize buffer interference at wavelengths below 200 nm, all spectra were recorded using 10 mM phosphate buffer, pH 7.0, and Suprasil quartz cells (0.1 mm path length). All spectra were recorded at 23°C.

### 2.3.10 *Electron Paramagnetic Resonance Spectroscopy*

Spectra were recorded using a Bruker EMX instrument equipped with an Oxford ESR 900 cryostat and ITC temperature controller. Additional sample concentration, if necessary, was performed using Amicon Ultra-4 centrifugal filter devices (Beverly, MA). The settings for the spectrometer were as follows: temperature, 10 K; microwave frequency, 9.38 GHz; microwave power, 0.1 mW; modulation amplitude, 10G; modulation frequency, 100 kHz; time constant, 655.36 ms; conversion time, 655.36 ms; and receiver gain,  $1.0 \times 10^5$ .

## 2.4 Results

### 2.4.1 Far-UV Circular Dichroism (CD) Spectroscopy

To gain additional insight into the role of the C-terminal domain in KatG structure and catalysis, we measured the CD response of KatG<sup>N</sup> to the separately expressed and isolated C-terminal domain (KatG<sup>C</sup>). All data are reported in terms of mean residue ellipticity (MRE). The concentration of each protein was 5  $\mu$ M. All spectra were recorded at 23°C using 10 mM phosphate buffer, pH 7.0. Far-UV CD spectra for KatG<sup>N</sup> (Figure 2.5, trace a) and KatG<sup>C</sup> (trace b) indicate secondary structural content substantially different from each other and wild-type KatG (trace c). However, a CD spectrum for the physical mixture of KatG<sup>N</sup> and KatG<sup>C</sup> (1:1 ratio) (trace d) was highly similar to that of wtKatG. The composite spectrum derived arithmetically from the separate spectra for KatG<sup>N</sup> and KatG<sup>C</sup> were superimposable on the spectrum obtained from the physical mixture of the domains (Figure 2.5 inset). These data suggest that (1) preparation of the separated domains, KatG<sup>N</sup> and KatG<sup>C</sup>, does not result in major disruption of secondary structural content from that which is expected for each domain from the wild-type enzyme and (2) the physical mixture of KatG<sup>N</sup> and KatG<sup>C</sup> did not appreciably change the secondary structural content of either protein.



#### 2.4.2 Catalase and Peroxidase Activity Assays

An equimolar mixture of KatG<sup>N</sup> and KatG<sup>C</sup> had appreciable catalase and peroxidase activities (Figure 2.6). Catalase activity was measured for a 100 nM concentration of each protein in the presence of 10 mM H<sub>2</sub>O<sub>2</sub> and 100 mM phosphate buffer, pH 7.0. Peroxidase activity was measured for a 50 nM concentration of each protein in the presence of 1 mM H<sub>2</sub>O<sub>2</sub>, 1 mM ABTS, and 50 mM acetate buffer, pH 5.0. All assays were carried out at 23°C. Individually, neither KatG<sup>N</sup> nor KatG<sup>C</sup> had either catalase or peroxidase activity. Furthermore, incubation of KatG<sup>N</sup> with a generic protein such as bovine serum albumin (BSA) did not restore either catalase or peroxidase activity, indicating that specific interactions between the domains were essential for restoration of the catalase-peroxidase active site in KatG<sup>N</sup>.

Further examination revealed that catalase and peroxidase activities increased with time of coincubation of the two domains (Figure 2.7). At 4°C, increases in peroxidase and catalase activities were observed over the first 20 h. Interestingly, both activities were observed to return at similar rates. Fits of the observed data to a single exponential equation produced rate constants for reactivation ( $k_{\text{react}}$ ) of  $3.4 \times 10^{-3}$  and  $2.5 \times 10^{-3} \text{ min}^{-1}$  for catalase and peroxidase activities, respectively. We measured steady-state kinetic parameters for the catalase activity of the equimolar mixture of KatG<sup>N</sup> and KatG<sup>C</sup> following 30 min, 24 h, and 48 h incubations at 4°C (Table 2.1). These data show that the increase in activity over time (see Figure 2.7) was due primarily to an effect on

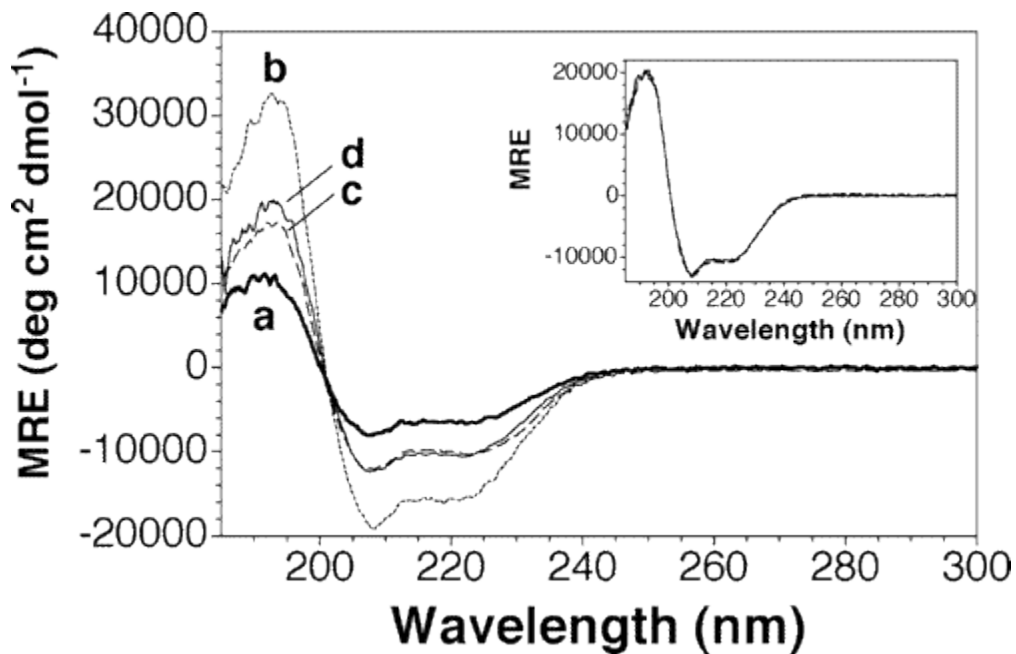


Figure 2.5. Far-UV circular dichroism spectra of wtKatG and each of its separately expressed and isolated domains. Spectra were recorded for KatG<sup>N</sup> (a, bold line), KatG<sup>C</sup> (b, dotted line), wtKatG (c, dashed line), and an equimolar mixture of KatG<sup>N</sup> and KatG<sup>C</sup> (d, solid line). The inset shows a comparison of the equimolar mixture of KatG<sup>N</sup> and KatG<sup>C</sup> to the composite spectrum derived arithmetically from the individual spectra for KatG<sup>N</sup> and KatG<sup>C</sup>. All data are reported in terms of mean residue ellipticity (MRE). The concentration of each protein was 4.3  $\mu$ M. All spectra were recorded at 23°C using 10 mM phosphate buffer, pH 7.0.

the apparent  $k_{\text{cat}}$ , increasing from roughly  $90 \text{ s}^{-1}$  following a 30 min incubation with KatG<sup>C</sup> to about  $2000 \text{ s}^{-1}$  following 24 and 48 h incubations. The latter values represent 20% of those obtained by our laboratory for wild-type KatG [71, 93] and fall between 15% and 60% of the values obtained for catalase-peroxidases from other organisms. Incubation with KatG<sup>C</sup> showed relatively little effect on the apparent  $K_M$  for H<sub>2</sub>O<sub>2</sub>. A value of about 2.5 mM was observed following all three coincubation times. This is very similar to the apparent  $K_M$  of wild-type KatG for H<sub>2</sub>O<sub>2</sub> [94-96] and well within the range for that observed for other catalase-peroxidases. The apparent second-order rate constant obtained for the recovered catalase activity was about  $9 \times 10^5 \text{ M}^{-1} \text{ s}^{-1}$ .

Likewise, we evaluated the steady-state peroxidase activity of the coincubated domains as a function of H<sub>2</sub>O<sub>2</sub>. The peroxidase kinetics for wild-type KatG and our KatG<sup>N</sup>/KatG<sup>C</sup> mixture were complex. Nevertheless, the maximum peroxidase activity (the apparent  $k_{\text{cat}}$ ) followed a trend similar to that determined for catalase activity (Table 2.1). Following 24 and 48 h incubations with KatG<sup>C</sup>, values of about  $13 \text{ s}^{-1}$  were determined and represent about 22% of the value that we have recorded for wild-type KatG [71, 93].

The effect of pH on the rate of KatG<sup>N</sup> reactivation by KatG<sup>C</sup> was also explored (Figure 2.8, closed symbols). KatG<sup>N</sup> and KatG<sup>C</sup> (1  $\mu\text{M}$  each) were incubated together at 4°C in 120 mM phosphate (squares) or 120 mM citrate (triangles) at various pHs. Aliquots were removed periodically to measure catalase activity at pH 7.

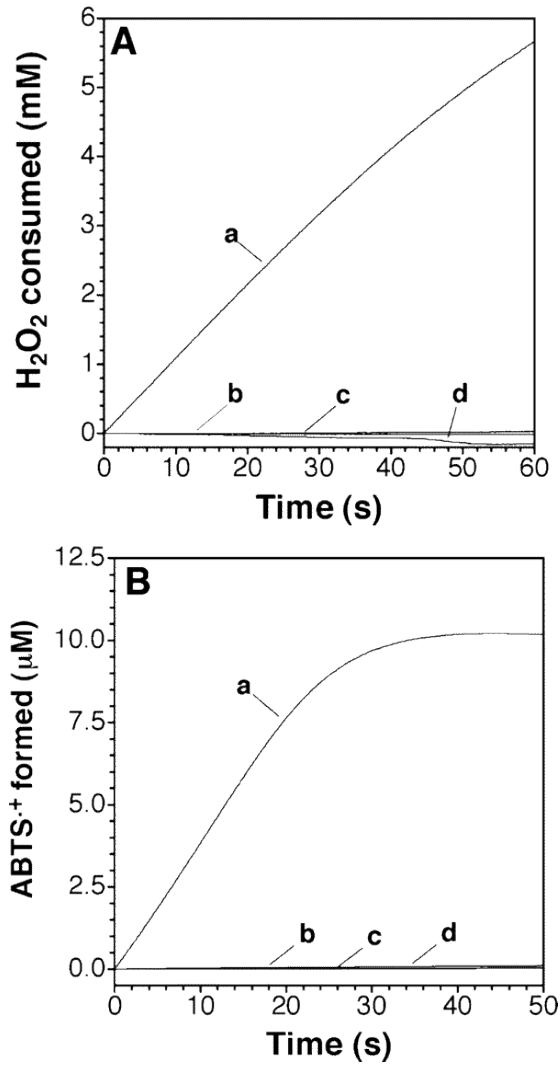


Figure 2.6. Reactivation of KatG<sup>N</sup> in the presence of KatG<sup>C</sup>. Catalase (A) and peroxidase (B) activities were measured for an equimolar mixture of KatG<sup>N</sup> and KatG<sup>C</sup> (a), KatG<sup>N</sup> alone (b), KatG<sup>C</sup> alone (c), and an equimolar mixture of KatG<sup>N</sup> and bovine serum albumin (d).

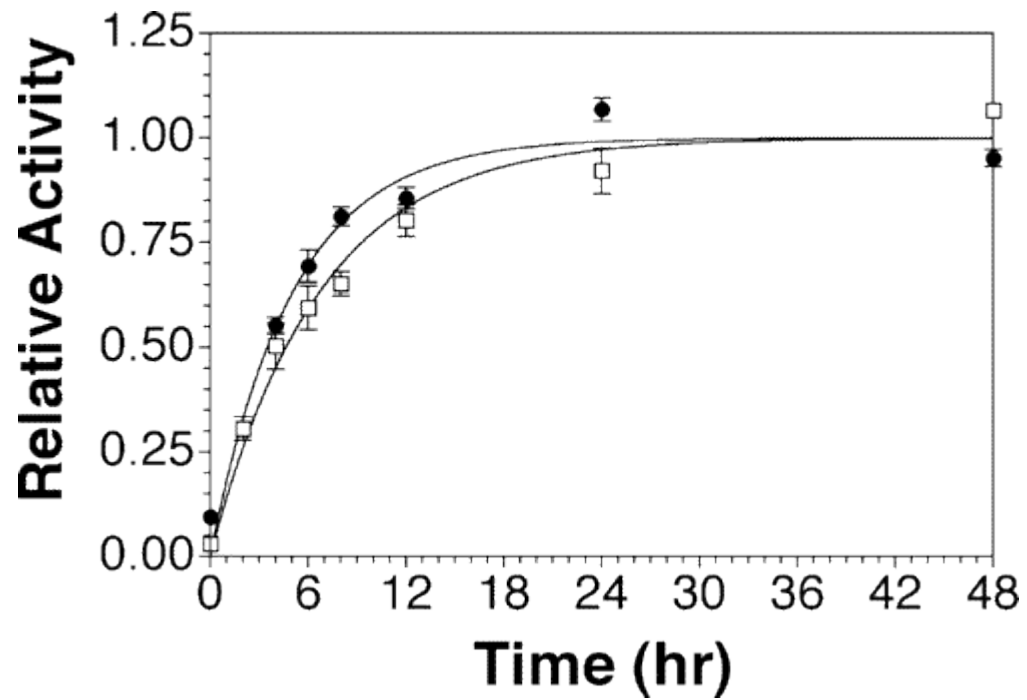


Figure 2.7. Catalase and peroxidase activities over time for an equimolar mixture of  $KatG^N$  and  $KatG^C$ . An equimolar mixture of  $KatG^N$  and  $KatG^C$  was incubated at 4 C for an increasing length of time prior to measurement of its catalase (closed circles) and peroxidase (open squares) activities.

Table 2.1. Apparent kinetic parameters for catalase and peroxidase activities for coincubated KatG<sup>N</sup> and KatG<sup>C</sup>.

Protein	Catalase <sup>a</sup>			Peroxidase <sup>b</sup>
	$k_{\text{cat}}$ (s <sup>-1</sup> )	$K_M$ (mM)	$k_{\text{cat}}/K_M$ (M <sup>-1</sup> s <sup>-1</sup> )	$k_{\text{cat}}$ (s <sup>-1</sup> )
<b>wtKatG<sup>c</sup></b>	$1.2 \pm 0.2 \times 10^4$	$4.0 \pm 0.4$	$3.1 \pm 0.5 \times 10^6$	$58 \pm 3$
<b>N + C (0.5)<sup>d</sup></b>	$86 \pm 18$	$3.1 \pm 0.8$	$2.9 \pm 0.3 \times 10^4$	$8 \pm 5 \times 10^{-3}$
<b>N + C (24)</b>	$2270 \pm 18$	$2.2 \pm 0.2$	$1.0 \pm 0.1 \times 10^6$	$13 \pm 1$
<b>N + C (48)</b>	$1900 \pm 160$	$2.2 \pm 0.1$	$8.7 \pm 0.6 \times 10^5$	$14 \pm 1$

<sup>a</sup> Catalase assays included 50 nM KatG<sup>N</sup>, 50 nM KatG<sup>C</sup>, and 100 mM phosphate, pH 7.0, 23°C.

<sup>b</sup> Peroxidase assays included 20 nM KatG<sup>N</sup>, 20 nM KatG<sup>C</sup>, and 50 mM acetate, pH 5.0, 23°C.

<sup>c</sup> From ref [97]

<sup>d</sup> KatG<sup>N</sup> and KatG<sup>C</sup> (1:1) incubated at 4 C in 120 mM phosphate, pH 7.0, for x hours (in parentheses).

From single exponential fits of the data,  $k_{\text{react}}$  values corresponding to rate (solid symbols) and amplitude values corresponding to maximum recovered activity (open symbols) were obtained. The bold solid line represents a fit of  $k_{\text{react}}$  (pH 6-8) to eq 2.1. The general trends of  $k_{\text{react}}$  (pH 6 and below) and amplitude (pH 5-8) are highlighted by the dashed and light solid lines, respectively. Catalase activity was measured in the presence of 8.5 mM  $\text{H}_2\text{O}_2$  at 23°C. The units for the amplitude are in reciprocal seconds because they are taken from rates of catalase activity divided by  $[\text{KatG}^{\text{N}}]$ . As the pH decreased from 8.0, there was a progressive increase in the apparent rate constant ( $k_{\text{react}}$ ) for reactivation. The maximum observed  $k_{\text{react}}$  ( $9.4 \times 10^{-3} \text{ min}^{-1}$ ) was obtained at pH 6.0, representing a 7-fold increase in rate. A fit of the data (pH 8-6) to eq 1 yielded an apparent  $\text{p}K_{\text{a}}$  of 6.2 and predicted a maximum  $k_{\text{react}}$  of  $1.4 \times 10^{-2} \text{ min}^{-1}$ . However, below pH 6.0 there was an abrupt decrease in  $k_{\text{react}}$ , precluding a more complete data set to directly observe the true maximum and more accurately determine the  $\text{p}K_{\text{a}}$ . Nevertheless, the data suggest 6.5 as an upper limit for the apparent  $\text{p}K_{\text{a}}$  governing the reactivation of  $\text{KatG}^{\text{N}}$  by  $\text{KatG}^{\text{C}}$ .

In a similar manner, the extent of reactivation was determined from the amplitudes of the single exponential data obtained at each pH. The amplitude remained essentially constant from pH 8 to at least pH 6.5. Furthermore, in a trend resembling  $k_{\text{react}}$ , there was an abrupt decrease in amplitude at low pH. The parallel and dramatic disruption of rate and extent of activation suggests that, at low pH, the structural integrity of the free  $\text{KatG}^{\text{N}}$  or  $\text{KatG}^{\text{C}}$  may be compromised. Along these lines, we have observed by UV-vis an increased propensity of  $\text{KatG}^{\text{N}}$  toward unfolding and aggregation at low pH. Within error,  $k_{\text{react}}$  and amplitude values obtained in the presence of phosphate or

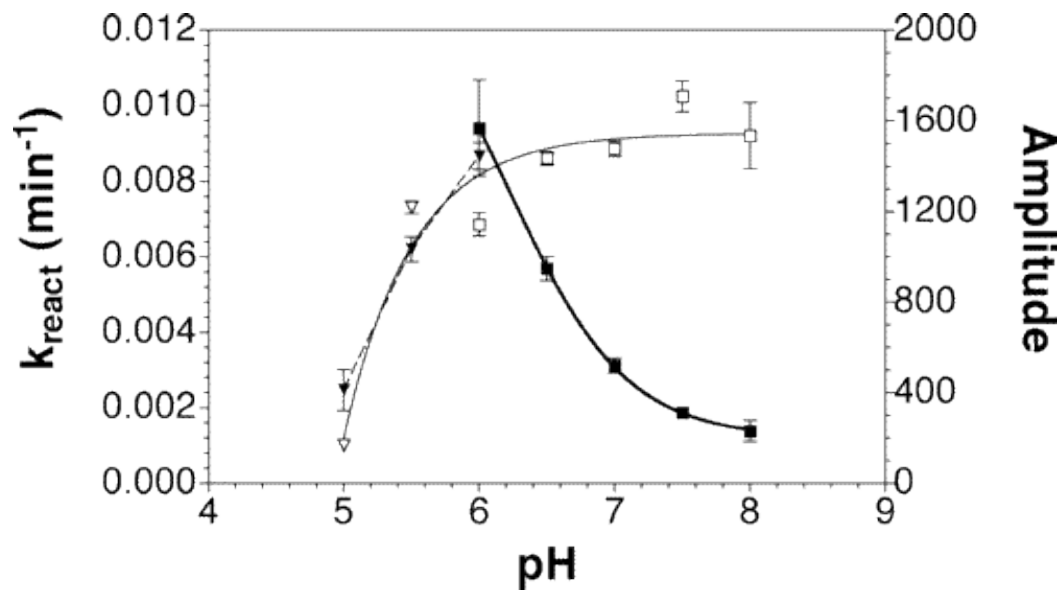


Figure 2.8. Effect of pH on the apparent rate constant ( $k_{\text{react}}$ ) and amplitude for  $\text{KatG}^{\text{N}}$  reactivation by  $\text{KatG}^{\text{C}}$ .



citrate buffers were the same, indicating that the behavior at low pH was not due to the buffer itself.

#### 2.4.3 *UV-visible Heme Absorption Spectroscopy*

Visible absorption spectra corresponding to the  $\alpha$ ,  $\beta$ , and charge transfer transitions for KatG<sup>N</sup> changed little immediately following the addition of an equimolar concentration of the C-terminal domain (Figure 2.9). However, following a 48 h incubation at 4°C, increases in absorption corresponding to the short- and long-wavelength charge transfer transitions (near 500 and 645 nm, respectively) were observed. Decreases in the intensities of KatG<sup>N</sup>, along with increases in the high-spin species (hexacoordinate and pentacoordinate), that are typically observed for wild-type KatG. Comparison of the spectrum obtained at 48 hour to those of wild-type KatG and KatG<sup>N</sup> has undergone active site restructuring in the presence of KatG<sup>C</sup>.

#### 2.4.4 *Electron paramagnetic resonance (EPR) spectroscopy*

In the absence of the KatG<sup>C</sup>, the EPR spectrum of KatG<sup>N</sup> is dominated by signals consistent with a hexacoordinate low-spin heme complex (Figure 2.10, spectrum A). Indeed, the  $g_1$  (2.92),  $g_2$  (2.28), and  $g_3$  (1.53) values obtained from the spectrum suggest that the strong-field sixth ligand in the coordination sphere is a histidine residue [98, 99

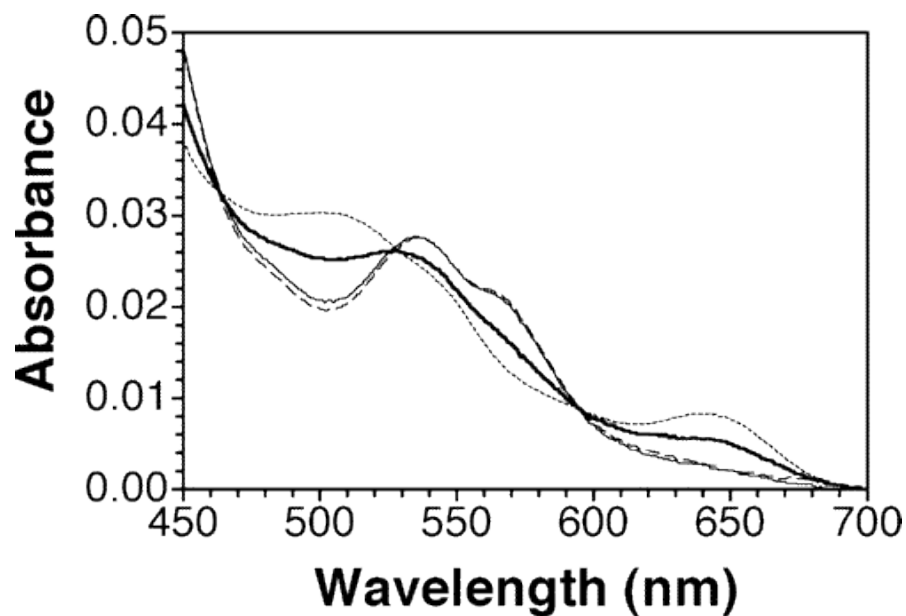


Figure 2.9 Effect of separately expressed and isolated KatG<sup>C</sup> on the visible absorption spectrum of KatG<sup>N</sup>. A spectrum corresponding to the charge transfer and  $\alpha$  and  $\beta$  transitions of the heme prosthetic group were recorded for KatG<sup>N</sup> alone (solid line), an equimolar mixture of KatG<sup>N</sup> and KatG<sup>C</sup> immediately after mixing (dashed line), and an equimolar mixture of KatG<sup>N</sup> and KatG<sup>C</sup> following a 48 h incubation at 4°C (bold line). A typical spectrum for wtKatG is also shown (dotted line).

90, 91]. Previous work from this laboratory strongly suggests that this histidine is the so-called distal histidine within the active site of catalase-peroxidases [79]. Addition of an equimolar concentration of KatG<sup>C</sup> to KatG<sup>N</sup> resulted in the appearance of EPR signals corresponding to high-spin pentacoordinate and hexacoordinate heme iron, as evident from a group of signals with *g*-values around 6 and increased amplitude near *g* = 2 (Figure 2.10, spectrum B); however, the hexacoordinate low-spin complex was still the dominant species present. Following 48-hr incubation (4°C) of the two domains, a dramatic increase in the high-spin species was observed along with the concomitant decrease in the hexacoordinate low-spin complex (Figure 2.10, spectrum c). Consistent with our UV-vis results, some hexacoordinate low-spin complex was still observable after the 48 h incubation. However, the distribution of high-spin components in the spectrum bore a strong resemblance to that of wild-type KatG (compare signals at *g* ~ 6 in spectra C and D).

To investigate the discrepancy between restored KatG<sup>N</sup> active sites by activity (~20%) and by spectroscopy (~50%), we evaluated the effect of added H<sub>2</sub>O<sub>2</sub> on the EPR spectrum of KatG<sup>N</sup> following its restructuring by KatG<sup>C</sup>. H<sub>2</sub>O<sub>2</sub> (20 equiv) was added and allowed to react for 1 h before the sample was frozen and a spectrum recorded. The signals corresponding to the pentacoordinate and hexacoordinate high-spin species were highly similar to the unreacted KatG<sup>N</sup>/KatG<sup>C</sup> mixture. However, the signal intensity was diminished by roughly 30%. With the exception of a weak free radical signal at *g* ~ 2, no other obviously new species were detected.

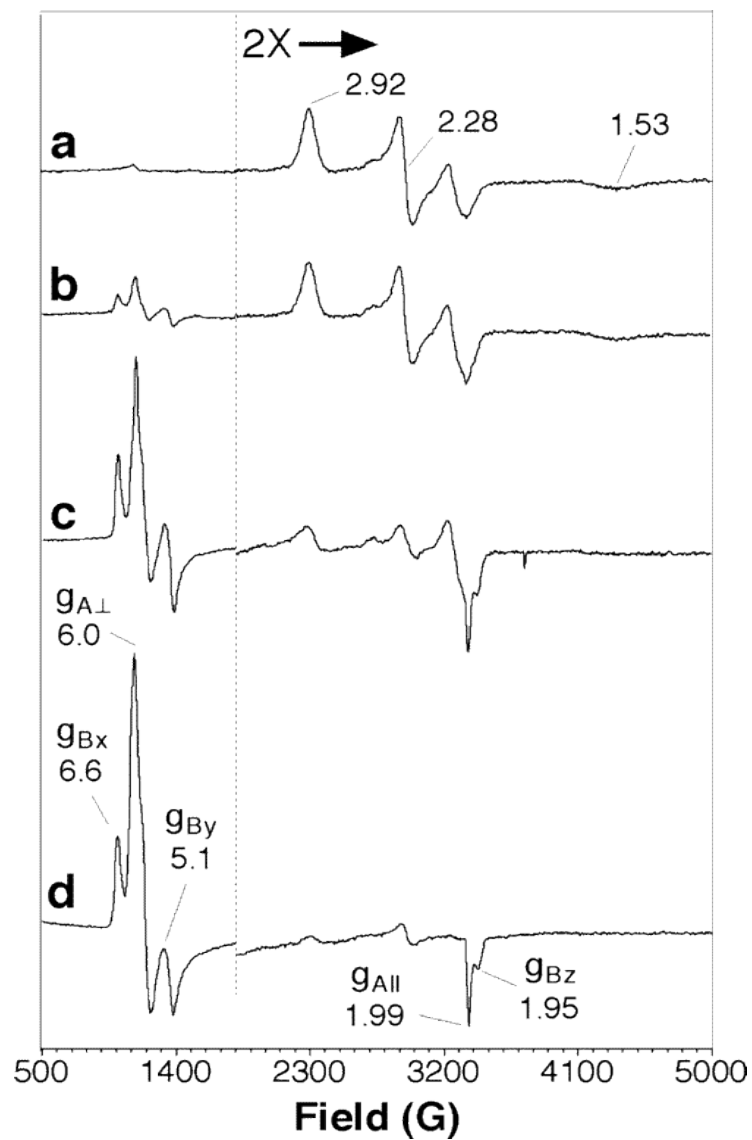


Figure 2.10. Effect of separately expressed and isolated  $KatG^C$  on the EPR spectrum for  $KatG^N$ . An EPR spectrum was recorded for  $KatG^N$  alone (a),  $KatG^N$  immediately following mixture with equimolar  $KatG^C$  (b),  $KatG^N$  following a 48-hr incubation ( $4^\circ\text{C}$ ) with equimolar  $KatG^C$  (c), and wtKatG (d).

## 2.5 Discussion

Despite its substantial distance from the active site and lack of any identifiable catalytic activity of its own, the C-terminal domain is clearly an integral component of catalase-peroxidase structure and catalysis. In the absence of the C-terminal domain, the N-terminal domain, which contains the active site, has no apparent activity. The active site heme is in a hexacoordinate low-spin state, and the strong field sixth ligand is likely supplied by the so-called distal histidine. Because heterolytic cleavage of hydroperoxide substrates requires their direct access to the heme iron, and because the distal histidine is required as a general base for the reaction, the loss of catalase and peroxidase activity is a reasonable expectation for active site rearrangement of this type.

These effects are at least partially reversed by the reintroduction of the C-terminal domain as a separate protein. The restructuring of the active site is evident, first of all, from spectroscopic analyses of the coordination environment of the heme. The UV-visible spectra clearly reveal an increase in high-spin heme species, and this comes at the expense of the hexacoordinate low-spin complex. The EPR spectra confirm these conclusions and also show a distribution between high-spin species nearly identical to that of the wild-type enzyme. The mixed population of coordination states for ferric catalase-peroxidases is a peculiarity of these enzymes, one that is highly sensitive to subtle changes around the active site induced by mutagenesis and, in some cases, aging, buffer conditions, etc. [100-101]. It is striking that this distribution is so precisely reproduced by domain recombination.

The more exacting measure of active site reconstruction, however, is the presence of not only peroxidase activity but catalase activity as well. Recent studies by our laboratory and others indicate that the catalase activity of the catalase-peroxidases exists due to a precarious balance of factors. Precisely ordered hydrogen-bonding networks are required for catalase activity. These are either dependent upon (at least in part) or act in concert with a novel covalent cross-link between active site Trp 105, Tyr 226, and Met 252 (*E. coli* KatG numbering). Many catalase-peroxidase variants created by site-directed mutagenesis [66, 88, 74, 102, 76, 75, 73, 103-105] and deletion mutagenesis [72] exhibit little or no catalase activity. Spectroscopic evaluation of these variants often indicates that only rather subtle modifications of the heme environment have resulted from these modifications [66, 88, 71, 74, 102, 76, 75, 73, and 103]. Indeed, the vast majority of these variants retain peroxidase activity equal to or better than their wild-type counterparts ([88, 67, 74, 102, 93, 75-76, 73, 103-105]. The substantial catalase activity observed from KatG<sup>N</sup> upon incubation with KatG<sup>C</sup> indicates that the separate C-terminal domain supports a very precise restructuring of the active site environment.

Visual inspection of the reported catalase-peroxidase structures [67-68, 72] and comparison to the known behavior of similar monofunctional peroxidases supports a connection between the presence or absence of the C-terminal domain and the coordination state of the heme iron, particularly as it involves the distal histidine (His 106). Prominent *intrasubunit* interactions are observed between the B'C' loop and E' helix of the C-terminal domain and the BC loop of the N-terminal domain (Figure 2.11). Structures from the N-terminal domain are shown as a blue ribbon. Structures from the *intrasubunit* C-terminal domain are shown as red -carbon traces. Structures from the

*intersubunit* C-terminal domain are shown as green-carbon traces. The heme (orange) and distal histidine (cyan) are also shown. All C-terminal domain structures are labeled with primed letters (e.g., B'C' loop), and all structures from the N-terminal domain are shown with unaccented letters (e.g., AB loop). The approximate analogous location of the Ca<sup>2+</sup> ion found in monofunctional peroxidases is indicated (\*). Coordinates from the structure of *Burkholderia pseudomallei* KatG were used (PDB accession number 1MWV) [68]. Substantial *intersubunit* interactions are also observed between the AB loop and C helix of the N-terminal domain and a structure encompassing helices G' through I' of the C-terminal domain. On both sides of these interdomain interfaces, many of the individual residues involved in the interactions are strictly conserved across the catalase-peroxidases.

Interestingly, many of the monofunctional peroxidases use a completely different strategy to support the BC loop and B helix. In the fungal secretory peroxidases (i.e., the class II peroxidases), a calcium ion is coordinated by residues from the BC loop and B helix [106-107]. The loss of this calcium results in the coordination of the distal histidine to the heme iron, yielding a hexacoordinate low-spin heme in the active site and the concomitant loss of peroxidase activity [108-110]. It is interesting to note that in our system  $k_{\text{react}}$  increases as pH decreases with an apparent  $pK_a$  of 6.2. This would be consistent with the protonation of a histidine residue to disfavor its coordination to the heme iron and thus achieve activation of KatG<sup>N</sup>. Indeed, the bishistidine coordinated

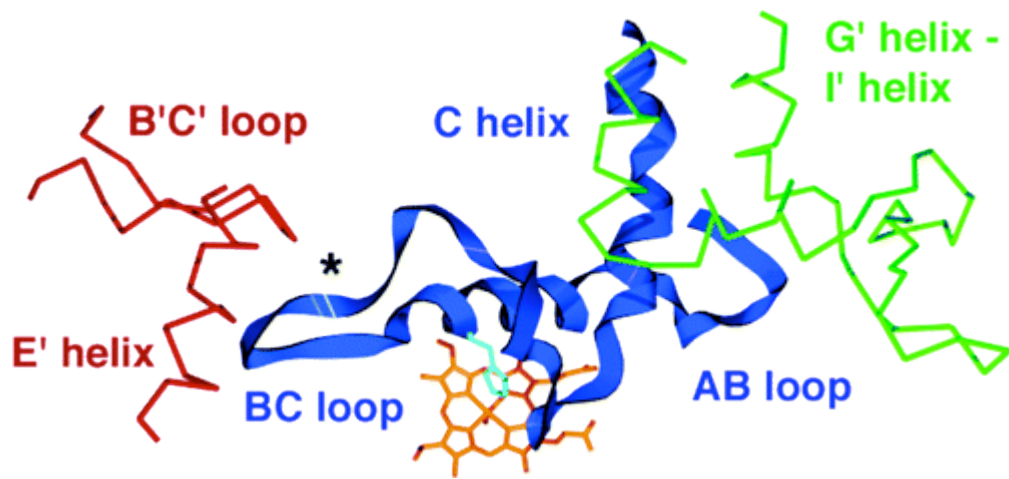


Figure 2.11. Interfaces between the N- and C-terminal domains of KatG.



heme of  $\text{Ca}^{2+}$ -deficient manganese peroxidase (a class II peroxidase) loses a histidine ligand with decreasing pH according to a  $\text{pK}_a$  of 5.7 [108].

In the class III peroxidases (plant secretory peroxidases such as horseradish peroxidase and peanut peroxidase), the BC loop and B helix are further stabilized by a disulfide bond that straddles the calcium coordination site [63, 111]. Thus, the loss of calcium by these enzymes produces a much less dramatic outcome. Less activity is lost, and a more subtle alteration of the heme environment occurs [112-113]. Indeed, greater active site stability has been imparted to the class II manganese peroxidase (MnP) by using site-directed mutagenesis to introduce an analogous disulfide bond to that observed in the class III enzymes [65].

Among the class II and class III peroxidases, the shifts in heme coordination environment and loss of activity are reversible upon the reintroduction of calcium. Likewise, we demonstrate that the same consequences for structure and activity that are observed in catalase-peroxidase upon removal of the C-terminal domain can be reversed by reintroduction of the domain as a separately expressed and isolated protein.

The striking difference between these reactivation processes is the time course for active site restructuring. Reintroduction of calcium to the class II and III peroxidases leads to rapid restoration of active site architecture and peroxidase activity. For example, incubation of inactivated MnP with calcium restores activity within a matter of minutes [114]. Conversely, active site restructuring in  $\text{KatG}^{\text{N}}$ , as evident from shifts in heme coordination environment *and* catalytic activity, takes on the order of 24 h. This may be partially accounted for by the fact that reactivation of  $\text{KatG}^{\text{N}}$  was accomplished with a single equivalent of  $\text{KatG}^{\text{C}}$ , whereas reactivation of MnP was carried out using over 30

equiv of  $\text{Ca}^{2+}$  [114]. Nevertheless, to a first approximation,  $\text{KatG}^{\text{N}}$  reactivation occurs at about one-tenth the rate of  $\text{Ca}^{2+}$ -dependent MnP reactivation. This is suggestive of slow structural rearrangements that may precede the spectroscopic and catalytic evidence of reactivation. One possible process is the establishment of the Trp-Tyr-Met covalent adduct unique to catalase-peroxidases [67-68, 72, 115, and 104]. However, this seems unlikely because establishment of the covalent adduct is peroxide dependent and occurs via formation of compound **I** [66, 103]. In our studies, no peroxide was added to induce activation, and compound **I** formation is not supported by the hexacoordinate low-spin complex observed in  $\text{KatG}^{\text{N}}$ . Thus, formation of the covalent adduct could not precede the reorganization of the active site.

A second explanation is that structural perturbation of  $\text{KatG}^{\text{N}}$  and/or  $\text{KatG}^{\text{C}}$  is required to establish a productive conformation that allows for the subsequent restructuring of the active site. This would be consistent with the suggestion of Carpena *et al.* that the C-terminal domain serves as a platform to ensure the proper folding of the N-terminal domain [116]. Indeed, there are several points of contact between the two domains, including those mentioned above. Although the precise sequence of events leading to active site restructuring remains to be established, our data suggest that large-scale unfolding and refolding of either domain at the secondary structural level are unlikely. Our  $\text{KatG}^{\text{N}}$  and  $\text{KatG}^{\text{C}}$  have CD spectra that are consistent with what is expected from the wild-type enzyme. The folded arrangement of  $\text{KatG}^{\text{N}}$  is such that both active site histidines appear to serve as axial ligands to the heme iron [79]. Importantly, there are no changes observed in CD upon coincubation of the separated domains. In any

case, it is clear that KatG<sup>C</sup> is able to induce whatever structural changes in the N-terminal domain are necessary to restore its active conformation.

Interestingly, a rearrangement that involves shifts in preexistent structural elements could account for the observed data. All known catalase-peroxidase structures show an intricate association between the first 30 amino acids of both N-terminal domains. Each C-terminal domain also contributes to this part of the dimer interface [67-68, 72]. It is reasonable to suggest that, in the absence of the C-terminal domain, the first amino acids of the N-terminal domain adopt an alternative conformation that does not allow for the correct interaction across the dimer interface. It is anticipated that the switch out of such an alternative conformation could present a significant kinetic barrier to active site restructuring. Indeed, precedent for such slow conformational changes of exactly this type has been observed in the substrate-induced interconversion of quaternary isoforms of human porphobilinogen synthase. Rate constants for this interconversion as measured by substrate-induced reactivation of the enzyme were on the order of  $1.7 \times 10^{-2} \text{ min}^{-1}$  (reported as  $1.05 \text{ h}^{-1}$ ) [117], very similar to what we have observed for KatG<sup>N</sup> reactivation.

Whether measured spectroscopically (~50%) or by catalytic activity (~20%), active site restructuring by KatG<sup>N</sup> is not complete. It is possible that a fraction of the N-terminal domain is locked in a conformational state that is recalcitrant to the actions of KatG<sup>C</sup>. We suggest that this is reported by the fraction that remains in its hexacoordinate low-spin state (~50%). At the present time, we have not identified conditions that address this population.

It also appears that although a proportion of KatG<sup>N</sup> is spectroscopically responsive to KatG<sup>C</sup>-dependent restructuring, it either produces a less active conformation or produces a mixed population of active and inactive states. Two possible explanations are currently under investigation in our laboratory. One is that restructuring of KatG<sup>N</sup> by KatG<sup>C</sup> produces a proportion of active sites that, while spectroscopically similar to wild-type KatG, do not react correctly with H<sub>2</sub>O<sub>2</sub>. Indeed, the fact that reaction with a low concentration of H<sub>2</sub>O<sub>2</sub> produces an appreciable change in EPR spectrum evident a full hour after addition suggests that at least some proportion of restructured KatG<sup>N</sup> is compromised with respect to catalytic consumption of the substrate.

A second and potentially related possibility is that some KatG<sup>N</sup> structural elements outside the active site are not arranged correctly by KatG<sup>C</sup> to yield full activity. Indeed, we have produced a KatG<sup>N</sup> variant lacking an interhelical insertion known as large loop 2 (LL2) [67]; it is also known as the FG insertion because it is located between the F and G helices of the N-terminal domain [71]. KatG lacking this interhelical insertion has little or no catalase activity but retains substantial peroxidase activity [71]. This modified KatG<sup>N</sup> has no catalytic activity and forms a hexacoordinate low-spin complex just like KatG<sup>N</sup>. Spectroscopically, the active site of this variant is restored to a similar extent (~50%) by equimolar KatG<sup>C</sup>. However, unlike KatG<sup>N</sup>, the peroxidase activity of this KatG<sup>N</sup> variant is restored to a commensurate level (50%) in comparison to the intact KatG lacking the same insertion [118]. Interestingly, an *intersubunit* point of contact between the domains occurs between the LL2 interhelical insertion of one subunit and the C-terminal domain of a second subunit. It is possible that KatG<sup>C</sup> does not fully or correctly address this structural feature in KatG<sup>N</sup>.

In conclusion, the essential nature of the C-terminal domain to catalase-  
peroxidase structure and catalysis is demonstrated by its ability to restore, at least in part,  
the N-terminal domain to its bifunctionally active conformation. Reactivation of the  
enzyme in this manner provides a unique opportunity to probe the mechanisms by which  
the C-terminal domain directs the folding and maintenance of this uniquely bifunctional  
active site.

## CHAPTER THREE

### THE EFFECT OF R117 AND D597 INTERDOMAIN RESIDUE SUBSTITUTIONS ON THE REACTIVATION OF *ESCHERICHIA COLI* CATALASE-PEROXIDASE

#### 3.1 *Abstract*

Catalase-peroxidases are multifunctional enzymes composed of two domains. One of the domains contains the active site while the other is “inactive”. Our previous investigations show that catalase-peroxidase expressed without a C-terminal domain lacks activity due to a structural collapse inside of the active site. To determine if these structural shifts and the corresponding loss of activity for the N-terminal domain (KatG<sup>N</sup>) were reversible, we used deletion mutagenesis to separately express and isolate the C-terminal domain (KatG<sup>C</sup>). KatG<sup>N</sup> reactivates upon incubation with equimolar concentrations of KatG<sup>C</sup> as the active site is restructured. The intrasubunit interface between the domains is dominated by highly conserved interactions between the C-terminal domain and a loop connecting the B and C helices of the N-terminal domain. Because the BC loop extends from the B helix, which is a major part of the KatG active site, these contacts between the BC loop and the C-terminal domain may be essential for the proper structural integrity of this heme-dependent active site. A highly conserved

intrasubunit salt-bridge consisting of an Arg117 (R117) on the active domain and an Asp597 (D597) on the inactive domain is positioned 30Å away from the active site. Using site-directed mutagenesis, the R117A and D597A variants were expressed for the separately isolated domains. Kinetic and spectroscopic evaluation of these proteins showed that D597 does not play a major role in active site reactivation. Therefore, the salt-bridge interaction between R117 and D597 is not necessary for maintaining the proper active site architecture for KatG function. On the other hand, R117 is necessary for active site restructuring. A major phase of reactivation kinetics is absent for R117A, leading to a substantial decrease in the rate and extent of reactivation. This implicates the residue as having a role in orienting the BC interhelical loop on the N-terminal domain for proper interaction with the C-terminal domain.

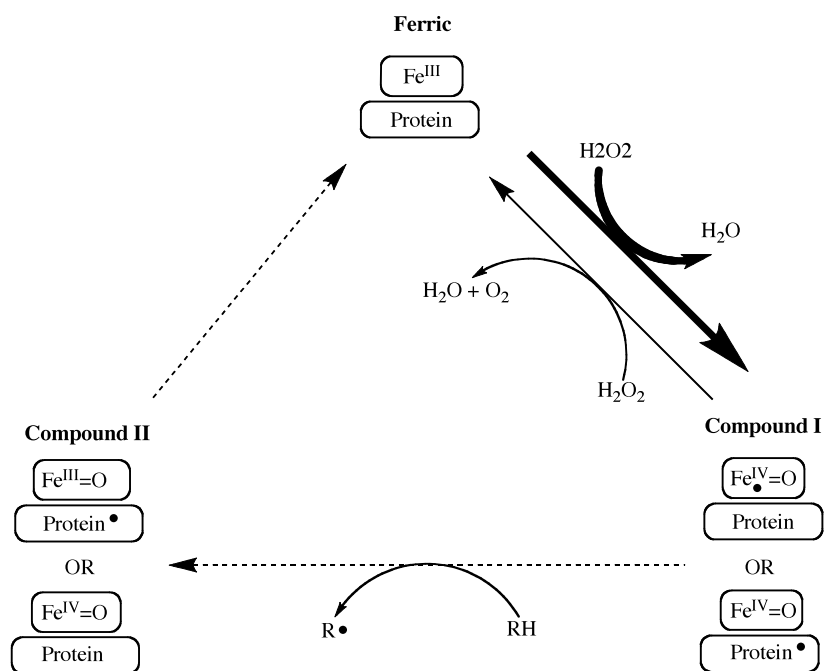
### 3.2 *Introduction*

Catalase-peroxidases (KatGs) have a multifunctional active site that facilitates the decomposition of hydrogen peroxide and other reactive oxygen-based species in or around the cell by two distinct reaction pathways. The catalase reaction, typical of monofunctional catalases and catalase-peroxidases, begins with the oxidation of the enzyme in its resting or ferric state with one equivalent of H<sub>2</sub>O<sub>2</sub> to produce H<sub>2</sub>O and an oxoferryl porphyrin/protein radical intermediate known as compound **I** (Scheme 3.1). This intermediate is reduced back to ferric enzyme by a second equivalent of H<sub>2</sub>O<sub>2</sub>, generating O<sub>2</sub> and H<sub>2</sub>O. The peroxidase reaction pathway also begins with the formation of compound **I**. However, the return of the enzyme to its ferric state is accomplished by

the reduction of compound **I** in two sequential one-electron steps by an exogenous electron donor (RH). The first reduction step produces one equivalent of substrate radical (R•) and compound **II**. In typical peroxidases (e.g., horseradish peroxidase), compound **II** is an oxoferryl intermediate ( $\text{Fe}^{\text{IV}}=\text{O}$ ). Questions still surround the exact electronic structures of compounds I and II in catalase-peroxidases and are beyond the scope of the research reported here. In any case, the second reductive step is the same for monofunctional peroxidases and catalase-peroxidases in that it produces a second equivalent of substrate radical and returns the enzyme to its ferric state.

The bifunctional nature of the KatG active site is unique due to the fact that the catalytic and peroxidatic reaction cycles are highly similar yet these activities very rarely overlap in enzyme catalysis. Typical heme enzymes that have substantial catalase activity usually exhibit poor peroxidase activity. Likewise, enzymes that have strong peroxidase activity usually have weak catalase activity. The lack of catalase activity exhibited by monofunctional peroxidases is interesting because the active sites of monofunctional peroxidases and catalase-peroxidases are nearly superimposable on one another (Figure 3.1). Therefore, the striking difference in function between these two types of enzymes with highly similar active sites is due to structures peripheral to and at a distance from the active site. Catalase-peroxidases consist of three structural features absent from monofunctional peroxidases that are vital for KatG function: two interhelical insertions and a C-terminal domain. The interhelical insertions each contain about 35 amino acids. One (the DE insertion) connects helices D and E and the other (the FG insertion) connects helices F and G (Figure 3.2).





Scheme 3.1. Representation of the dual catalytic cycle of catalase-peroxidases. The first step in catalase and peroxidase reactions (bold arrow) involves cycling between ferric and compound I forms. Catalase activity (solid arrow) involves cycling from compound I back to the ferric form. Peroxidase activity (dashed arrows) involves cycling from compound I to compound II to the ferric form.

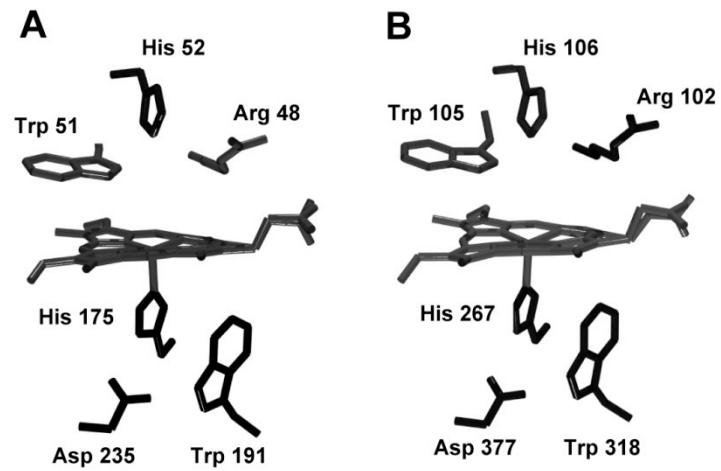


Figure 3.1. Structural comparison of the active sites of a monofunctional peroxidase (cytochrome c peroxidase) (A) and a catalase-peroxidase (B). The numbering of the amino acids in panel B is according to their appearance in the sequence of *E. coli* KatG. Coordinates are from the protein data bank, accession numbers 1ccp (panel A), and 1itk (panel B).

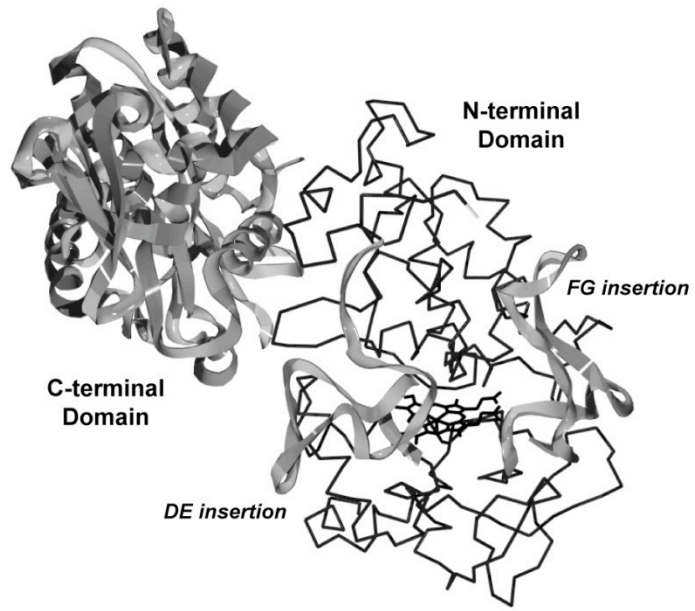


Figure 3.2. Catalase-Peroxidase Peripheral Structures (in ribbon format).

A variant of KatG produced by removing the DE insertion (KatG<sup>ΔDE</sup>) resulted in elevated peroxidase activities compared to wtKatG that were similar to monofunctional peroxidases [118]. However, a total loss of catalase activity occurred as a result of removing the DE insertion. Previous studies have shown that a novel covalent link (Trp 105, Tyr 226, and Met 252) is essential for catalase and not peroxidase activity [73-76]. Substitution of Tyr 226 to a Phe causes the total loss of catalase activity [75-76]. The central residue of this covalent adduct (Tyr 226) is located in the DE insertion. This suggests that the loss of catalase activity is due to the loss of this tyrosine, which is critical for this covalent adduct that uniquely supports the catalase activity. On the other hand, the variant produced by removal of the FG insertion (KatG<sup>ΔFG</sup>) resulted in similar peroxidase activity as compared to wild-type KatG (wtKatG) and a 99% reduction of catalase activity [71]. The removal of this insertion is believed to change the heme environment due to the distal histidine being positioned closer to the active site and, consequently, hindering substrate accessibility.

Catalase-peroxidases contain two fused copies of the primordial peroxidase gene [43, 78]. The copy translated into the N-terminal domain is similar to monofunctional peroxidases and contains the heme prosthetic group to participate in catalysis. The C-terminal domain is also structurally similar to monofunctional peroxidases, but it does not bind heme or catalyze any discernable reaction. Nevertheless, this structure is conserved across all catalase-peroxidases, suggesting that it has a role in enzyme function.

To determine the role of the C-terminal domain in catalase-peroxidase structure and function, we produced a variant of *E. coli* catalase-peroxidase (KatG) lacking the C-terminal domain (KatG<sup>N</sup>) [79] as well as a variant lacking the N-terminal domain

(KatG<sup>C</sup>). Spectroscopic, catalytic, and ligand binding properties of KatG<sup>N</sup> demonstrate that the C-terminal domain is essential for catalase-peroxidase to function as either a catalase or a peroxidase. Despite being  $\geq 30$  Å away from the active site, the C-terminal domain supports its structure by preventing the coordination of the distal histidine to the heme iron.

To determine the ability of KatG<sup>C</sup> to restructure the active site of KatG<sup>N</sup>, we co-incubated equimolar amounts of each protein [80]. Addition of KatG<sup>C</sup> to KatG<sup>N</sup> decreased the hexacoordinate low-spin species typical of inactive KatG<sup>N</sup> and increased the mixture of high spin species typical of wtKatG. Consistent with the restructuring of the active site, both catalase and peroxidase activities were detected. To determine if the restructuring of the active site was exclusively due to the presence of KatG<sup>C</sup>, we incubated a generic protein, bovine serum albumin, with KatG<sup>N</sup>. Neither catalase nor peroxidase activities were restored. This indicates that specific interdomain residue interactions are necessary for the proper structure and function of KatG.

The C-terminal domain makes several highly conserved intrasubunit interdomain contacts with the BC loop of the N-terminal domain (Figure 3.3) [67-68, 72, 82]. Because the BC loop extends from the B helix, a major part of the KatG active site, these contacts between the BC loop and the C-terminal domain may be necessary for the proper structural integrity of the heme-dependent active site. A highly conserved intrasubunit salt-bridge consisting of an Arg117 (R117) on the active domain and an Asp597 (D597) on the inactive domain is positioned 30Å away from the active site. Using site-directed

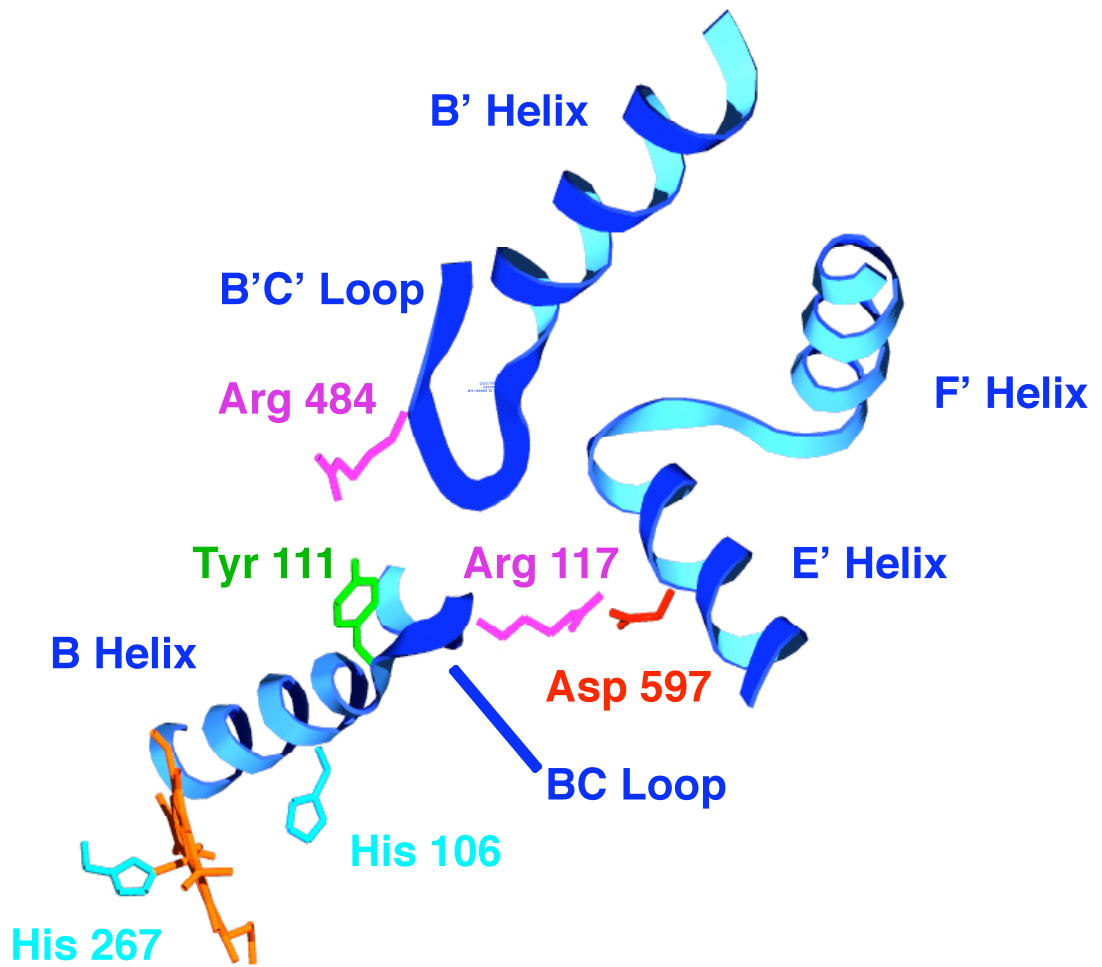


Figure 3.3. Interdomain interactions between C-terminal domain and the BC loop of the N-terminal domain.

mutagenesis, the R117A and D597A variants were expressed for the separately isolated domains. Here, we report the effect of these substitutions on reactivation of KatG.

### 3.3 *Materials and Methods*

#### 3.3.1 *Materials*

Hydrogen Peroxide (30%), imidazole, hemin, ampicillin, chloramphenicol, sodium dithionite, and 2,2'-azino-bis(3-ethylbenzthiazoline-6-sulfonic acid) (ABTS) were purchased from Sigma (St. Louis, MO). Isopropyl- $\beta$ -D-thiogalactopyranoside (IPTG), mono- and di-basic sodium phosphate, acetic acid, and sodium acetate were obtained from Fisher (Pittsburgh, PA). Potassium cyanide was purchased from Mallinckrodt (Paris, KY). Benzonase was purchased from Novagen (Madison, WI). All restriction enzymes were purchased from New England Biolabs (Beverly, MA). All oligonucleotide primers were purchased from Invitrogen (Carlsbad, CA). All *E. coli* strains (BL-21 [DE3] and XL-1 Blue) and *Pfu* polymerase were obtained from Stratagene (La Jolla, CA). Nickel-nitrilotriacetic acid (Ni-NTA) resin was purchased from Qiagen (Valencia, CA). All buffers and media were prepared using water purified through a Millipore QPak-II system (18.2 M $\Omega$ /cm resistivity).

### 3.3.2 *Cloning of KatG<sup>C</sup> and D597A KatG<sup>C</sup> Expression Plasmids*

Generation of an expression construct for KatG<sup>C</sup> was accomplished using a deletion mutagenesis procedure developed in our laboratory [71] as previously described [79]. Site-directed mutagenesis was used to produce the D597A KatG<sup>C</sup> variant utilizing primers ECCP M 310+ (ACT GCT GAT CGC GAA AGC ACA GC) AND ECCP M 310- (GCT GTG CTT TCG CGA TCA GCA GT).

### 3.3.3 *Cloning of KatG<sup>N</sup> and R117A KatG<sup>N</sup> Expression Plasmids*

Generation of an expression construct for KatG<sup>N</sup> was accomplished as previously described [79]. Site-directed mutagenesis was used to produce the R117A KatG<sup>N</sup> variant utilizing primers ECCP M 103+ (GTT CAA TCG ATG GCG CCG GTG GCG) and ECCP M 103- (CCC GCG CCA CCG GCG CCA TCG ATT GAA C).

### 3.3.4 *Expression and Purification of the KatG Domains and their Variants*

Expression of the KatG domains and their variants were carried out as previously described [79]. Isolation of KatG<sup>C</sup> and D597A KatG<sup>C</sup> was carried out as previously described for another catalase-peroxidase [93]. Purification of KatG<sup>N</sup> and R117A KatG<sup>N</sup> was performed as previously described [79], except that the supernatant was diluted 1:2 with 1M NaCl prior to being added to the Ni-NTA resin.



### 3.3.5 *Domain Mixing and Incubation Procedures*

The concentrations of KatG<sup>N</sup> and KatG<sup>C</sup> were determined using molar absorptivities below. Solutions containing KatG<sup>N</sup> and KatG<sup>C</sup> were incubated at 4°C for times ranging from 0 to 48 hours in the presence of 100 mM phosphate buffer, pH 7.0. Following a given incubation time, aliquots were removed, and activity was measured according to the assays described below.

### 3.3.6 *UV-Visible absorption spectra and activity assays.*

Enzyme was reconstituted with 0.95 equivalents of hemin. Reconstituted enzyme solution incubated for 72 hours at 4°C to allow unincorporated heme to precipitate out of solution. The solution was then spun and removed from the precipitated heme. This was to ensure that free heme did not interfere with any spectral or kinetic data. Concentration of reconstituted enzyme was determined using the pyridine hemichrome assay [16]. The determined concentration was used to convert absorption into molar absorptivity according to Beer's Law. Protein containing heme in the ferrous state was prepared by adding a small (< 10 mg) amount of sodium dithionite to the native enzyme. All spectra were obtained at room temperature on a Shimadzu UV-1601 spectrophotometer (Columbia, MD) with a cell pathlength of 1.0 cm. Catalase and peroxidase activity assays were performed as previously described [80].

### 3.3.7 *Circular Dichroism Spectroscopy (CD).*

All spectra were obtained using 5  $\mu$ M enzyme in 5 mM phosphate (pH 7.0.) Spectra were recorded at 23 °C in a quartz cell (0.5 mm path length) from 250 – 195 nm on a Jasco J-810 spectrophotometer (Tokyo, Japan.) Baselineing and analysis were done using Jasco J-720 software.

### 3.3.8 *Magnetic Circular Dichroism Spectroscopy (MCD).*

All spectra were obtained using 15  $\mu$ M enzyme in 50 mM phosphate 50 mM NaCl buffer, pH 7.0. Enzyme containing ferrous heme was prepared by adding a small amount (<10 mg) of sodium dithionite to the native enzyme. Spectra were recorded at 23 °C in a quartz cell (5.0 mm path length) with 1.4 Tesla magnetic cell holder from 700 – 350 nm on a Jasco J-810 spectrophotometer (Tokyo, Japan). Baselineing and analysis were done using Jasco J-720 software.

### 3.3.9 *Electron Paramagnetic Resonance Spectroscopy.*

Spectra were recorded using a Bruker EMX instrument equipped with an Oxford ESR 900 cryostat and ITC temperature controller. Additional sample concentration was performed using Amicon Ultra-4 centrifugal filter devices (Beverly, MA). The settings for the spectrometer were as follows: temperature, 10 K; microwave frequency, 9.38 GHz; microwave power, 0.1 mW; modulation amplitude, 10 G; modulation frequency,

100 kHz; time constant, 655.36 ms; conversion time, 655.36 ms; and receiver gain,  $1.0 \times 10^5$ .

### 3.4 Results

#### 3.4.1 Circular Dichroism Spectroscopy

To determine the role of R117 and D597 in KatG structure and function, we measured the response of KatG<sup>N</sup> to the separately expressed and isolated D597A KatG<sup>C</sup> and the response of R117A KatG<sup>N</sup> to KatG<sup>C</sup>. Mutagenesis, protein expression, and protein purification were accomplished for the individual proteins (KatG<sup>N</sup>, KatG<sup>C</sup>, R117A KatG<sup>N</sup>, and D597A KatG<sup>C</sup>) as described in *Materials and Methods*. R117A KatG<sup>N</sup> and D597A KatG<sup>C</sup> were each compared to their unmodified versions KatG<sup>N</sup> and KatG<sup>C</sup>, respectively. By circular dichroism, D597A KatG<sup>C</sup> was indistinguishable from KatG<sup>C</sup> (Figure 3.4A). Because the KatG<sup>N</sup> and its variants bind heme, UV-visible absorption spectra were compared for R117A KatG<sup>N</sup> and unmodified KatG<sup>N</sup>. Spectra for ferric, ferri-cyano, ferrous, and ferro-cyano complexes were highly similar for both proteins, and indicated that the dominant species isolated in both cases was a hexacoordinate low-spin complex (data not shown). Though the CD spectrum for R117A KatG<sup>N</sup> was highly similar to KatG<sup>N</sup>, it did show deviation from that for the unmodified protein, particularly below 200 nm (Figure 3.4B). This indicates the possibility of some local misfolding in the R117A KatG<sup>N</sup> variant, though it should be pointed out that this region of the CD spectrum is notorious for substantial reduction in signal to noise ratios.

### 3.4.2 Reactivation Kinetics

Equimolar concentrations of each domain were incubated together and the reactivation of the N-terminal domain active site was monitored by changes in catalase activity. Incubation of KatG<sup>N</sup> with D597A KatG<sup>C</sup> (Figure 3.5B, solid line) resulted in a return of activity similar to that obtained upon mixing KatG<sup>N</sup> with KatG<sup>C</sup> (Figure 3.5A, solid line). The reactivation process was biphasic. The more rapid phase was governed by a rate constant of about  $5 \times 10^{-4} \text{ s}^{-1}$ , while the slower phase showed a rate constant of about  $2 \times 10^{-5} \text{ s}^{-1}$  (Table 3.1). Approximately 50% of the total recovered activity (i.e., amplitude) was observed with each phase. In stark contrast, an equimolar mixture of R117A KatG<sup>N</sup> and KatG<sup>C</sup> (Figure 3.5A, dashed line) showed the recovery of very little activity. Although two phases were evident, activity was only observed in the second phase. A fit of the data to a single exponential produced rate constants of about  $2 \times 10^{-5} \text{ s}^{-1}$ . The initial lag phase and the second phase were also fit by an equation describing two sequential irreversible reactions. Two rate constants of about  $5 \times 10^{-5} \text{ s}^{-1}$  were obtained, though the error for each was rather large. Reactivation involving both variants (i.e., R117A KatG<sup>N</sup> plus D597A KatG<sup>C</sup>) (Figure 3.5B, dashed line) did not show an appreciably different rate or extent of reactivation in comparison to R117A KatG<sup>N</sup> plus KatG<sup>C</sup>. A summary of the kinetic data is shown in Table 3.1. Peroxidase activity was also monitored (data not shown). The same results were observed as with catalase activity with the exception that no peroxidase activity was observed with any combination involving R117A KatG<sup>N</sup>.

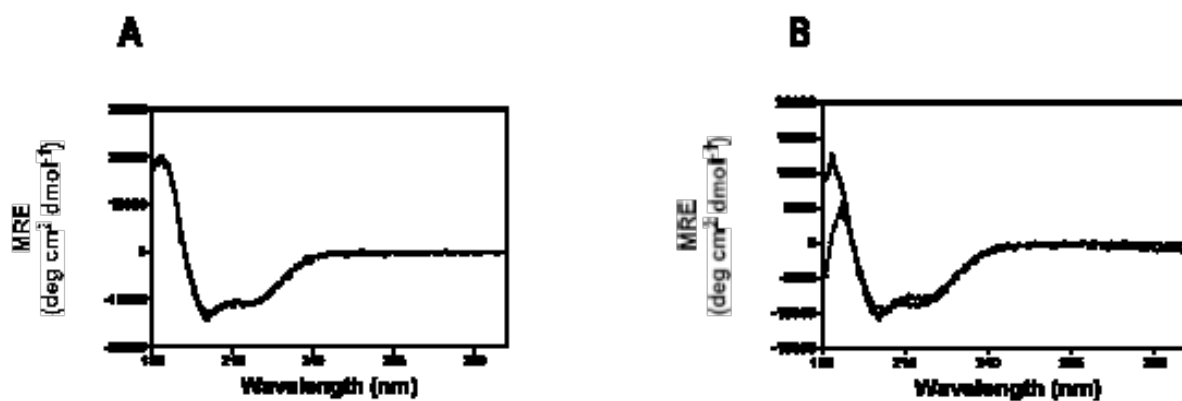


Figure 3.4. Far-UV circular dichroism spectra for KatG<sup>C</sup> (solid line) and D597A KatG<sup>C</sup> (dashed line) (panel A), and KatG<sup>N</sup> (solid line) and R117A KatG<sup>N</sup> (dashed line) (panel B). All spectra were recorded at 23°C using 5 μM protein in 5 mM phosphate buffer, pH 7.0.

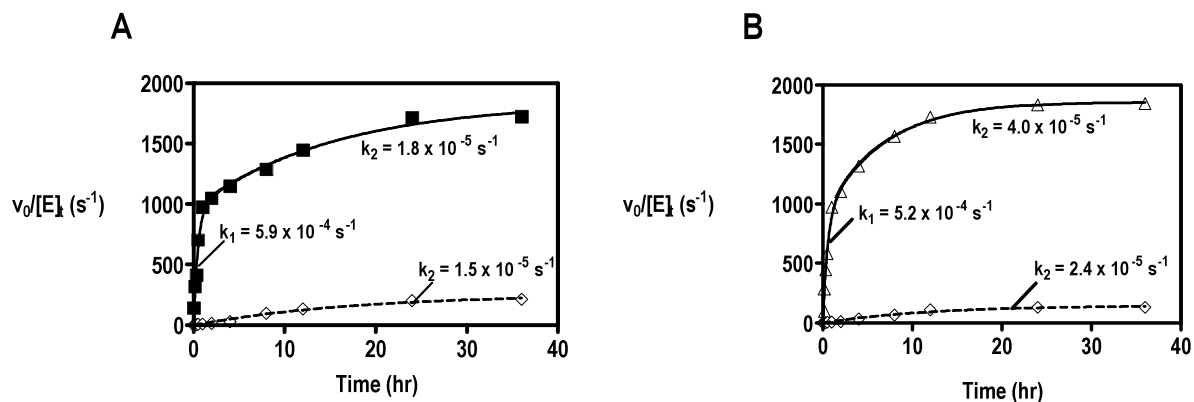


Figure 3.5. Reactivation of KatG<sup>N</sup> and (R117A) KatG<sup>N</sup>. Catalase activities were measured for equimolar mixtures of (A) KatG<sup>N</sup> + KatG<sup>C</sup> (squares) and R117A KatG<sup>N</sup> + KatG<sup>C</sup> (diamonds) and (B) KatG<sup>N</sup> + D597A KatG<sup>C</sup> (triangles) and R117A KatG<sup>N</sup> + D597A KatG<sup>C</sup> (diamonds). See footnote in Table 3.1 on  $k_2$  rate constants for R117A KatG<sup>N</sup> reactivation.

Table 3.1. Rate constants for reactivation of KatG<sup>N</sup> and R117A KatG<sup>N</sup> with KatG<sup>C</sup> or D597A KatG<sup>C</sup>.

Proteins	Rate Constants (s <sup>-1</sup> )		Amplitudes [v <sub>o</sub> /[E] <sub>T</sub> (s-I)] <sup>a</sup>		
	k <sub>1</sub>	k <sub>2</sub>	Amp <sub>1</sub>	Amp <sub>2</sub>	Amp <sub>T</sub>
N + C	5.9 x 10 <sup>-4</sup>	4.0 x 10 <sup>-5</sup>	970	870	1840
N + C <sup>D597A</sup>	5.2 x 10 <sup>-4</sup>	1.8 x 10 <sup>-5</sup>	910	963	1873
N <sup>R117A</sup> + C <sup>(b)</sup>	-----	1.6 x 10 <sup>-5</sup>	-----	257	257
N <sup>R117A</sup> + C <sup>D597A(b)</sup>	-----	2.4 x 10 <sup>-5</sup>	-----	145	145

<sup>a</sup>Amplitudes correspond to catalase activity recovered and are reported as (v<sub>o</sub>/[E]<sub>T</sub>). Amplitude corresponding to k<sub>1</sub> (Amp<sub>1</sub>) and k<sub>2</sub> (Amp<sub>2</sub>) are summed to give the total recovered catalase activity (Amp<sub>T</sub>).

<sup>b</sup>Two phases were evident in reactivation of R117A KatG<sup>N</sup>, the first was silent. A fit of the data to a single exponential produced the k<sub>2</sub> rate constants reported. A fit to two sequential irreversible steps produced two rate constants with large errors of approximately 5 x 10<sup>-5</sup> s<sup>-1</sup>.

The reactivation process was also monitored by magnetic circular dichroism (MCD) in order to monitor changes in the heme environment. Low-spin ferric heme shows a strong derivative-like signal centered near 414 nm. The high-spin ferric state has only much weaker signals in this wavelength range [121]. The MCD spectra for KatG<sup>N</sup> incubated with either KatG<sup>C</sup> or D597A KatG<sup>C</sup> (Figure 3.6A and 3.6C, respectively) revealed a decrease in low-spin heme over a 24-hr incubation period. Consistent with the activity data, the decrease in intensity of the 414 nm MCD band also followed biphasic kinetics (Figure 3.7). The rate constants obtained from the data were comparable to those obtained monitoring KatG reactivation by catalase activity (Table 3.1). These results reveal that the D597A substitution does not affect the C-terminal domain's ability to convert the heme in KatG<sup>N</sup> from its inactive low-spin state to its active high-spin species. In contrast, no significant change in the low-spin state was detected for R117A KatG<sup>N</sup> after a 24-hr incubation with either KatG<sup>C</sup> or D597A KatG<sup>C</sup> (Figure 3.6B and 3.6D, respectively).

### 3.4.3 *Ferrous Magnetic Circular Dichroism (MCD) Spectroscopy*

In order to ensure that the decrease in low-spin heme monitored by MCD of the ferric state corresponded to an increase in the high-spin state. MCD spectra for the ferrous states were obtained at the end of the domain incubations. The ferrous MCD spectra allow the relatively straightforward observation of high- and low-spin species even in mixtures of the two [121-123]. Bis-histidine coordinated low-spin ferrous heme proteins show a very intense derivative band near 558 nm, and ferrous high-spin heme



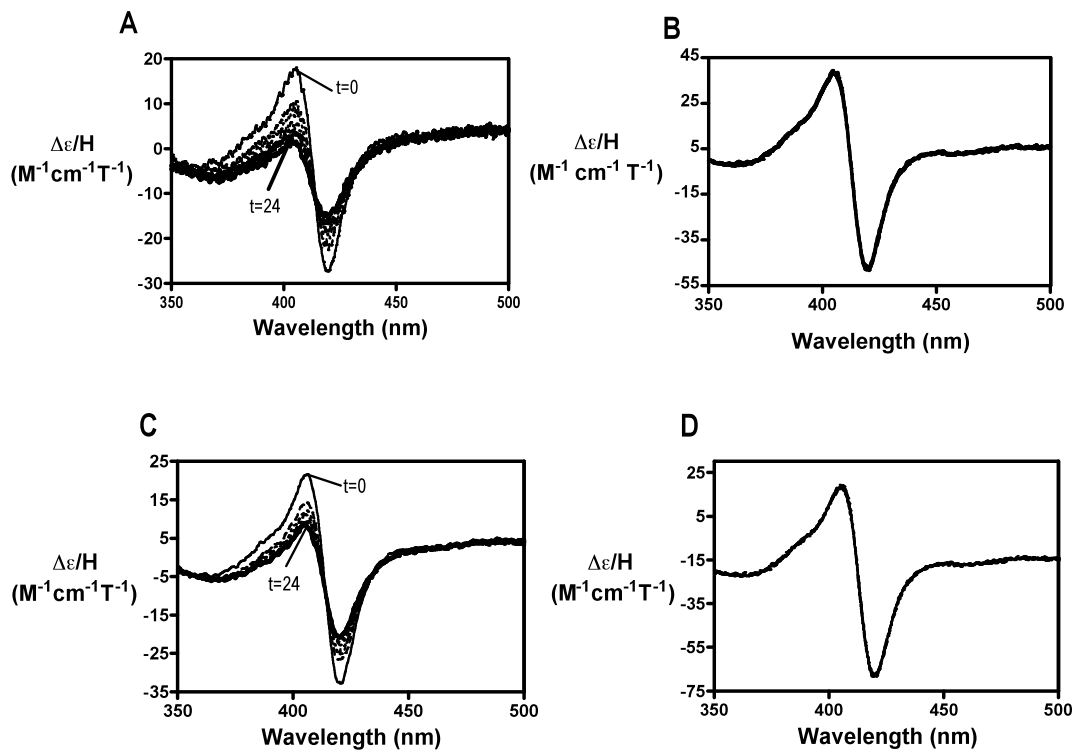


Figure 3.6. Ferric MCD spectra for KatG<sup>N</sup> and R117A KatG<sup>N</sup> reactivated with KatG<sup>C</sup> (panels A and B, respectively) and for KatG<sup>N</sup> and R117A KatG<sup>N</sup> reactivated with D597A KatG<sup>C</sup> (panels C and D, respectively). All spectra were recorded at 23°C in 200 mM phosphate buffer, pH 7.0, over a 24-hr period with a magnetic field strength of 1.4 T and a pathlength of 0.5 cm.

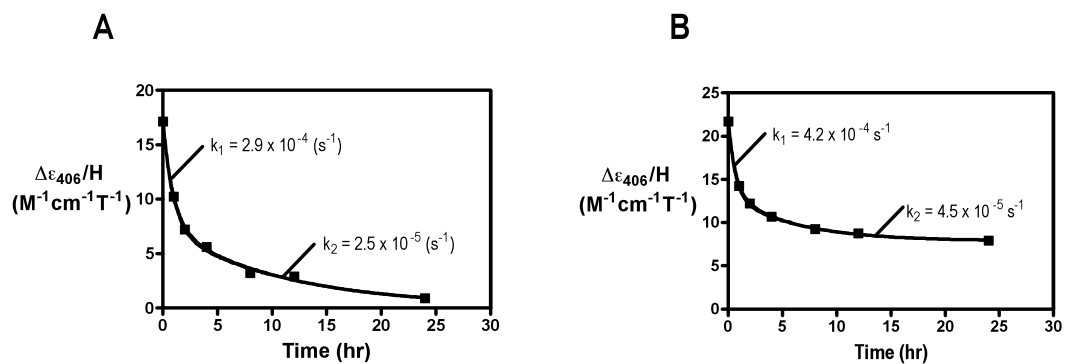


Figure 3.7. Ferric MCD reactivation kinetics for KatG<sup>N</sup> incubated with KatG<sup>C</sup> and D597A KatG<sup>C</sup> (Panels A and B, respectively). All data were recorded under same conditions as Figure 3.6.

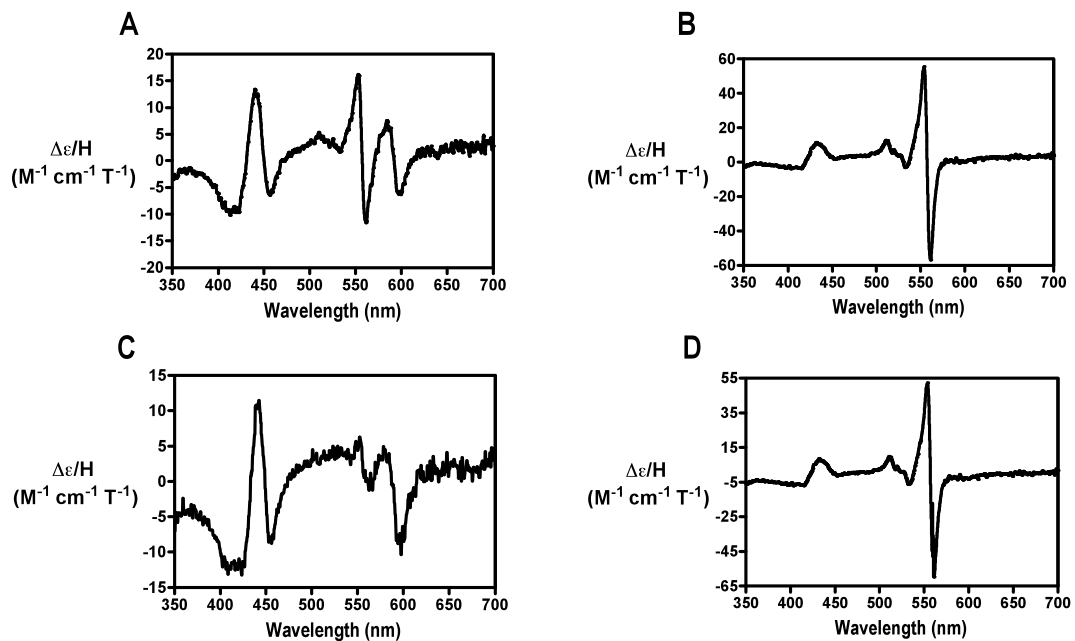


Figure 3.8. MCD spectra of ferrous KatG<sup>N</sup> + KatG<sup>C</sup> (A), (R117A)KatG<sup>N</sup> + KatG<sup>C</sup> (B), KatG<sup>N</sup> + (D597A)KatG<sup>C</sup> (C), (R117A)KatG<sup>N</sup> + (D597A)KatG<sup>C</sup> (D) following a 24-hr incubation period. All data are reported in terms of the difference in molar absorptivity ( $\Delta\epsilon$ ) per Tesla (T). Spectra were recorded under same conditions reported for Figure 6.

proteins show an intense band with maximum near 440 nm. The ferrous forms of KatG<sup>N</sup> incubated with either KatG<sup>C</sup> (Figure 3.8A) or D597A KatG<sup>C</sup> (Figure 3.8C) show substantial contribution from the high-spin states, consistent with the extent of catalase activity recovery. However, the ferrous form of R117A KatG<sup>N</sup> incubated with either KatG<sup>C</sup> or D597A KatG<sup>C</sup> (Figure 3.8B and 8D, respectively) reveal spectra that are consistent with pure bis-histidine coordinated low-spin heme.

#### 3.4.4 *Electron paramagnetic resonance (EPR) spectroscopy*

EPR was used to further explore ferric spectral changes upon recombining KatG<sup>N</sup> with KatG<sup>C</sup> and D597A KatG<sup>C</sup>. The spectrum for wild-type KatG (Figure 3.9A) displays strong high-spin signals and very little low-spin. The large axial signal in these spectra ( $g_{\perp} = 5.97$ ,  $g_{\parallel} = 1.99$ ) are typical of a hexacoordinate high-spin state, the dominant species observed in wild-type KatG [100, 124]. A rhombic high-spin signal was also observed in these spectra with  $g_x = 6.65$ ,  $g_z = 1.95$ , and  $g_y \sim 5.0$  though somewhat obscured by the axial signal. The rhombic component has been assigned to a pentacoordinate high-spin heme species [100, 124]. When KatG<sup>N</sup> is recombined with either KatG<sup>C</sup> or D597A KatG<sup>C</sup> (Figure 3.9B and 3.9C, respectively), spectra similar to wild-type KatG are observed. The most notable difference was the modest increase in pentacoordinate high-spin heme relative to the hexacoordinate high-spin state.

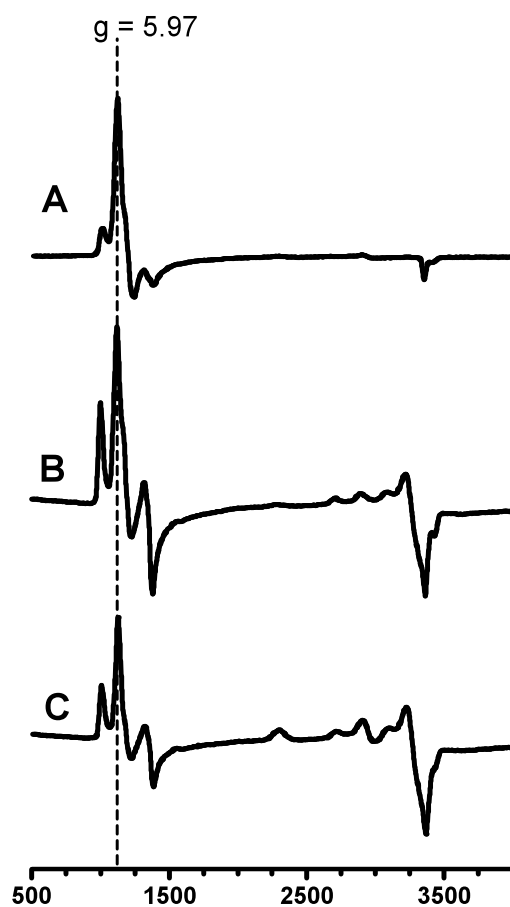


Figure 3.9. Comparison of wild-type KatG EPR spectrum with that of recombined domains after a 24-hr incubation period. Spectrometer settings: temperature, 10K; microwave frequency, 9.38 GHz; microwave power, 0.1 mW; modulation amplitude, 10 G; modulation frequency, 100 kHz. Panel A: wtKatG; Panel B: KatG<sup>N</sup> recombined with KatG<sup>C</sup>; Panel C: KatG<sup>N</sup> recombined with D597A KatG<sup>C</sup>.

### 3.5 *Discussion*

Our initial hypothesis was that the conserved R117-D597 interdomain salt-bridge interaction could be essential for maintaining the structural integrity of the active site since the N-terminal domain's R117 is part of the BC loop, which extends from the active site's B helix. Deletion of the C-terminal domain results in the coordination of His 106 (a residue of the B-helix) to the heme iron, leading to the loss of all catalytic activity. However, the kinetic and spectroscopic results suggest that the R117-D597 salt-bridge interaction is not required for the C-terminal domain, from its remote position, to direct restructuring of the KatG<sup>N</sup> active site. If such were the case, substitutions for either R117 or D597 would disrupt reactivation. Instead, all our data show that D597 substitution imposes no restriction to active site restructuring. Conversely, only very limited reactivation is observed for any combination involving the R117A substitution. Our results suggest that the role of R117 is essentially independent of its participation in the ion pair with D597. Though the precise role of R117 is not yet clear, it is reasonable to suggest that it helps to maintain the conformation of the entire BC loop, and therefore, the totality of its interactions with the C-terminal domain partner. We propose that the absence of the R117 side chain renders this loop unable to adopt a conformation that can respond to the C-terminal domain. Indeed, our far-UV CD spectrum for R117A KatG<sup>N</sup>, though identical at most wavelengths, does not exactly match that of KatG<sup>N</sup>. This may be indicative of local misfolding. All of the so-called plant peroxidase enzymes (including KatG) have a similarly structured BC loop, and even a cursory evaluation of these protein structures reveals that the conformation of this loop is highly important for

enzyme function. Class II plant peroxidases (e.g., manganese peroxidase) require calcium coordination to the structure to maintain the active heme coordination state [108, 116], and Class III plant peroxidases go a step further by using calcium coordination and a disulfide bond to maintain the structure of the BC loop [111-112]. In manganese peroxidase, the mechanism of thermal inactivation of the enzyme is the release of calcium and a shift to the inactive bis-histidine hexacoordinate low-spin heme. This structural rearrangement is also detectable by Far UV CD spectroscopy [62].

Our activity and MCD data both indicated biphasic reactivation of  $\text{KatG}^{\text{N}}$  by  $\text{KatG}^{\text{C}}$ . MCD, reporting shifts in heme coordination environment, produced highly similar rate constants for each phase as those observed by monitoring catalase activity. This suggests that the shift in coordination environment and the return of activity share the same rate-determining step, either dissociation of histidine from the heme iron, or some preceding event. In either case, there are, thus far, no discernable steps between restoration of proper heme coordination and the ability to carry out hydrogen peroxide decomposition by either catalase or peroxidase activities.

The mechanism underlying the observed biphasic reactivation is unknown. One possibility is that  $\text{KatG}^{\text{N}}$  exists in multiple conformational states. The rapid reactivation phase would correspond to a more facile conformational shift easily amenable to adjustment by the C-terminal domain, while the second would be more involved. Interestingly, R117A  $\text{KatG}^{\text{N}}$  shows no evidence of the rapid phase, and though there is a rate constant which corresponds to the slow phase for  $\text{KatG}^{\text{N}}$ , it has considerably lower amplitude. Apparently, substitution of R117 produces a small proportion of protein in a

conformation that can be reactivated by KatG<sup>C</sup> (albeit slowly) and a larger proportion that cannot be reactivated on the time scale of our experiments.

### 3.6 *Conclusion*

Thus far, our results indicate that D597 does not play a substantial role in the reactivation process. More important is the conformation of the BC loop. Supposing that the BC loop is correctly oriented, it remains to be seen whether D597 is one among a group of residues whose cumulative contribution is essential for reactivation. At this point, we can conclude that its absence alone is not sufficient to impede KatG<sup>N</sup> reactivation.



## CHAPTER FOUR

### REVERSING THE POLARITY OF THE R117/D597 INTERDOMAIN ION PAIR: EFFECT ON CATALASE-PEROXIDASE REACTIVATION

#### 4.1 Abstract

The catalase-peroxidase subunit is composed of two domains that arose due to gene duplication and fusion of a progenitor monofunctional peroxidase. The N-terminal domain contains the heme-dependent bifunctional active site, but the C-terminal domain lacks catalytic and heme binding capability. Without the C-terminal domain, the N-terminal domain (KatG<sup>N</sup>) is inactive due to the coordination of an active site general base (His 106) to the heme iron. However, KatG<sup>N</sup> can be reactivated upon incubation with equimolar concentrations of the separately expressed and isolated C-terminal domain (KatG<sup>C</sup>). The interface between these domains (some 30 Å from the active site) is populated by strictly conserved interactions. Among these is a salt-bridge between Arg117 (N-terminal domain) and Asp597 (C-terminal domain). Our previous studies have shown that the R117A substitution is highly disruptive to active site restructuring by KatG<sup>C</sup>, but surprisingly, the D597A substitution with KatG<sup>C</sup> is much less so. To further explore the components and interactions necessary for KatG<sup>N</sup> reactivation and the nature of their participation in the process, substitutions were introduced to reverse the polarity

of the ion pair (i.e., R117D KatG<sup>N</sup> and D597R KatG<sup>C</sup>). The R117D KatG<sup>N</sup> variant was reactivated by KatG<sup>C</sup> by a slow monophasic process. The peroxidase activity observed following reactivation was indistinguishable from that of reactivated KatG<sup>N</sup>. Conversely, reactivated R117D KatG<sup>N</sup> showed only 30% of the catalase activity of the unmodified KatG<sup>N</sup>. UV-visible and MCD spectroscopic measurements indicated a substantial increase in high-spin states consistent with the observed return of peroxidase activity in R117D KatG<sup>N</sup>. However, EPR measurements showed a distinct difference in the distribution of high-spin states in comparison to wild-type KatG and reactivated KatG<sup>N</sup>. In contrast to far-UV CD measurements for R117D KatG<sup>N</sup>, D597R KatG<sup>C</sup> showed a substantial disruption of secondary structural content. Consistent with this observation, D597R KatG<sup>C</sup> was unable to drive reactivation of KatG<sup>N</sup> or R117D KatG<sup>N</sup>. These results show important roles for R117 and D597 in catalase-peroxidase function, but confirm that this has less to do with their interaction with one another and is more attributed to their effects on the structure and function of their own domains. R117D KatG<sup>N</sup> maintains a conformation that can be activated by KatG<sup>C</sup>, but the substitution selectively diminishes the catalase activity of the uniquely bifunctional active site. The disruption of KatG<sup>C</sup> structure by the D597R substitution indicates the importance of the residue to the structural integrity of a normally robust domain. Moreover, the result suggests that while KatG<sup>C</sup> is able to reactivate multiple conformers of KatG<sup>N</sup>, neither KatG<sup>N</sup> nor its R117D variant is able to facilitate the refolding of D597R KatG<sup>C</sup>.

## 4.2 *Introduction*

Catalase-peroxidases (KatGs) have a multifunctional active site that facilitates the decomposition of hydrogen peroxide by two distinct reaction pathways. The catalase reaction, typical of monofunctional catalases and catalase-peroxidases, is divided into two steps. In the first,  $\text{H}_2\text{O}_2$  is reduced by two electrons to produce water and a highly oxidized heme intermediate referred to as compound I. In the second step a second equivalent of  $\text{H}_2\text{O}_2$  is oxidized to  $\text{O}_2$  as the enzyme returns to its resting ferric state. The typical peroxidase differs from catalase in that instead of oxidizing  $\text{H}_2\text{O}_2$ , another exogenous electron donor is oxidized. Most typically, two equivalents of an aromatic electron donor are oxidized in two sequential steps to generate two equivalents of a free radical product.

Surprisingly, despite the close chemical similarities of these two enzymatic activities, catalase and peroxidase activity rarely overlap in nature. Typical heme enzymes that have extensive catalase activity usually exhibit weak peroxidase activity [155]. Likewise, enzymes that have strong peroxidase activity usually have insubstantial catalase activity. The catalase-peroxidases facilitate high levels of catalase activity using an active site that is highly similar to monofunctional peroxidases [67, 68, 88]. To reconcile this substantial difference in function carried out by two highly similar structures, it has been noted that catalase-peroxidases possess structural features absent from the typical peroxidase enzymes [69, 70, 79]. These structural features are peripheral to and at a distance from the active site [69, 70, 79].

Catalase-peroxidases consist of three structural features absent from monofunctional peroxidases that are vital for KatG function: two interhelical insertions and a C-terminal domain [67, 71, 68, 79]. The interhelical insertions each contain about 35 amino acids. One (the DE insertion) connects helices D and E and the other (the FG insertion) connects helices F and G [71, 81]. Variants produced by removing both insertions resulted in loss of catalase activity whereas peroxidase activity was maintained [81]. The mechanism by which the FG insertion contributes to bifunctional activity remains unknown. Many (but not all) of the catalytic properties displayed by variants lacking the DE insertion can be accounted for by the loss of a unique three amino acid crosslink between an active site tryptophan, a strictly conserved tyrosine (part of the DE insertion) and an adjacent methionine [73-76].

Catalase-peroxidases contain two fused copies of the primordial peroxidase gene [43, 78]. The N-terminal domain copy is similar to monofunctional peroxidase. The interhelical insertions mentioned above would be the primary exception. The N-terminal domain contains a heme cofactor for catalysis. The C-terminal domain is also structurally similar to monofunctional peroxidases, but does not bind heme. Nevertheless, this domain is a conserved structure across all catalase-peroxidases, suggesting that it has a role in enzyme function.

Catalase-peroxidase (KatG) lacking its C-terminal domain (KatG<sup>N</sup>) has neither catalase nor peroxidase activity and the ability of small ligands to bind to the heme is dramatically diminished [79]. It appears that the C-terminal domain from its distant position (> 30 Å from the heme iron) supports N-terminal domain structure by preventing the coordination of the active site distal histidine (His 106) to the heme iron [79]. The

process has been shown to be reversible (see Chapter 2) as addition of the separately expressed and isolated C-terminal domain (KatG<sup>C</sup>) results in catalase and peroxidase recovery coincident with a shift in heme coordination to that observed in wild-type KatG.

The C-terminal domain makes several highly conserved intrasubunit interdomain contacts with the BC loop of the N-terminal domain [67-68, 72, 82]. This loop extends from the B helix, which is a major part of the KatG active site. An arginine residue sits at the apex of the BC loop and interacts with an aspartate residue (D597) on the E' helix of the C-terminal domain. We have capitalized on the ability of KatG<sup>C</sup> to reactivate KatG<sup>N</sup> as a novel means to evaluate the function of these conserved interactions. Rates and extents of reactivation and shifts in heme environment potentially allow for mechanistic insights not available with the intact KatG enzyme. Our studies on the alanine substituted variants produced surprising results indicating that the interaction itself was not the important feature in catalase-peroxidase catalytic function.

To gain further insight into the nature of this interaction and the influence of the interacting residues on catalase-peroxidase structure and function, we produced KatG<sup>N</sup> and KatG<sup>C</sup> variants that would reverse the polarity of the interaction (i.e, R117D KatG<sup>N</sup> and D597R KatG<sup>C</sup>). Kinetic and spectroscopic evaluation resulting from incubation of R117D KatG<sup>N</sup> with KatG<sup>C</sup> and D597A KatG<sup>C</sup> resulted in a two- to three-fold decrease in the return of catalase activity. The former substitution had no effect on the peroxidase activity, whereas the latter resulted in a two-fold decrease in peroxidatic function compared to the wild-type recombined domains. Therefore, in the presence of D597, the R117D substitution produces spectral and kinetic properties similar to that of monofunctional peroxidases. The D597R KatG<sup>C</sup> showed only minimal ability to restore

catalase or peroxidase activity to either KatG<sup>N</sup> or its R117D variant. The substantial disruption of secondary structural content suggests the substitution cannot be sustained by the normally highly stable C-terminal domain. These results suggest that R117 not only has an important role in maintaining a reactivatable structure in KatG<sup>N</sup>, but also has a specific influence on the bifunctional capabilities of the unique catalase-peroxidase active site. Furthermore, this study reveals that while the C-terminal domain may be serving as a folding platform for multiple conformational states of KatG<sup>N</sup>, the process does not appear to work in reverse.

### 4.3 *Materials and Methods*

#### 4.3.1 *Materials*

Hydrogen Peroxide (30%), imidazole, hemin, ampicillin, chloramphenicol, sodium dithionite, and 2,2'-azino-bis(3-ethylbenzthiazoline-6-sulfonic acid) (ABTS) were purchased from Sigma (St. Louis, MO). Isopropyl- $\beta$ -D-thiogalactopyranoside (IPTG), mono- and di-basic sodium phosphate, acetic acid, and sodium acetate were obtained from Fisher (Pittsburgh, PA). Potassium cyanide was purchased from Mallinckrodt (Paris, KY). Benzonase was purchased from Novagen (Madison, WI). All restriction enzymes were purchased from New England Biolabs (Beverly, MA). All oligonucleotide primers were purchased from Invitrogen (Carlsbad, CA). All *E. coli* strains (BL-21 [DE3] and XL-1 Blue) and *Pfu* polymerase were obtained from Stratagene (La Jolla, CA). Nickel-nitrilotriacetic acid (Ni-NTA) resin was purchased from Qiagen

(Valencia, CA). All buffers and media were prepared using water purified through a Millipore QPak-II system (18.2 MΩ/cm resistivity).

#### *4.3.2 Cloning of KatG<sup>C</sup>, D597A KatG<sup>C</sup>, and D597R KatG<sup>C</sup> Expression Plasmids*

Generation of an expression construct for KatG<sup>C</sup> was accomplished using a deletion mutagenesis procedure developed in our laboratory [71] as previously described [79]. Site-directed mutagenesis was used to produce the D597A KatG<sup>C</sup> variant utilizing primers ECCP M 310+ (ACT GCT GAT CGC GAA AGC ACA GC) and ECCP M 310- (GCT GTG CTT TCG CGA TCA GCA GT). Site-directed mutagenesis was also used to produce the D597R KatG<sup>C</sup> variant utilizing blunt-end primers mLECCP M 02+ (ATA CGT AAA GCA CAG CAA CTG ACG CTG ACC G) AND mLECCP M 03- (GAG CAG TGA CTC GGT GGT GGA AAC).

#### *4.3.3 Cloning of KatG<sup>N</sup> and R117D KatG<sup>N</sup> Expression Plasmids*

Generation of an expression construct for KatG<sup>N</sup> was accomplished as previously described [79]. Site-directed mutagenesis was used to produce the R117D KatG<sup>N</sup> variant utilizing blunt-end primers mLECCP M 05+ (GTT CAA TCG ACG GAG ATG GTG GCG GG) and mLECCP M 04- (CCC GCG CCA CCA TCT CCG TCG ATT GAA C).

#### 4.3.4 Expression and Purification of the KatG Domains and their Variants

Expression of the KatG domains and their variants were carried out as previously described [79]. Isolation of KatG<sup>C</sup> and D597A KatG<sup>C</sup> was carried out as previously described for another catalase-peroxidase [93]. Purification of KatG<sup>N</sup> and R117A KatG<sup>N</sup> was performed as previously described [79], except that the supernatant was diluted 1:2 with 1M NaCl prior to being added to the Ni-NTA resin.

#### 4.3.5 Domain Mixing and Incubation Procedures

The concentrations of KatG<sup>N</sup> and KatG<sup>C</sup> were determined using molar absorptivities below. Solutions containing KatG<sup>N</sup> and KatG<sup>C</sup> were incubated at 4°C for times ranging from 0 to 48 hours in the presence of 100 mM phosphate buffer, pH 7.0. Following a given incubation time, aliquots were removed, and activity was measured according to the assays described below. The return of enzyme activities over time were fit two one- or two-exponential equations to obtain reactivation rate constants ( $k$ ) and amplitudes ( $A$ ). The constant  $C$  accounts for baseline activity/signal.

$$\frac{v_o}{[E]_T} = A(1 - e^{-kt}) + C \quad (\text{Equation 4.1})$$

$$\frac{v_o}{[E]_T} = A_1(1 - e^{-k_1t}) + A_2(1 - e^{-k_2t}) + C \quad (\text{Equation 4.2})$$



#### 4.3.6 UV-Visible absorption spectra and activity assays

Enzyme was reconstituted with 0.95 equivalents of hemin. Reconstituted enzyme solution incubated for 24 hours at 4°C to allow unincorporated heme to precipitate out of solution. The solution was then spun and removed from the precipitated heme. This was to ensure that free heme did not interfere with any spectral or kinetic data. Concentration of reconstituted enzyme was determined using the pyridine hemichrome assay [90]. The determined concentration was used to convert absorption into molar absorptivity according to Beer's Law. Protein containing heme in the ferrous state was prepared by adding a small (< 10 mg) amount of sodium dithionite to the native enzyme. All spectra were obtained at room temperature on a Shimadzu UV-1601 spectrophotometer (Columbia, MD) with a cell pathlength of 1.0 cm. Catalase and peroxidase activity assays were performed as previously described [80]. Initial velocities were fit to Michaelis-Menten equation by non-linear regression analysis to determine the apparent kinetic parameters. If inhibition was evident for the peroxidase assays, the fitting equation was modified to a general excess substrate dependent inhibition model:

$$v_o = \frac{k_{cat}[S]}{K_M + [S] + \frac{[S]^2}{K_N}} \quad (\text{Equation 4.3})$$

Where  $K_N$  is a macroscopic constant that reflects the ability of the substrate to act as an inhibitor.

#### 4.3.7 *Circular Dichroism Spectroscopy (CD)*

All spectra were obtained using 5  $\mu$ M enzyme in 5 mM phosphate, pH 7.0. Spectra were recorded at 23 °C in a quartz cell (0.5 mm path length) from 300 – 190 nm on a Jasco J-810 spectrophotometer (Tokyo, Japan.) Baseline and analysis were done using Jasco J-720 software.

#### 4.3.8 *Magnetic Circular Dichroism Spectroscopy (MCD)*

All ferric and ferrous spectra were obtained using 1.0 and 15  $\mu$ M recombined proteins, respectively, in 100 mM phosphate buffer, pH 7.0. Enzyme containing ferrous heme was prepared by adding a small amount (<10 mg) of sodium dithionite to the native enzyme. Spectra were recorded at 23 °C in a quartz cell (5.0 mm path length) with 1.4 Tesla magnetic cell holder from 700 – 350 nm on a Jasco J-810 spectrophotometer (Tokyo, Japan). Baseline and analysis were done using Jasco J-720 software.

#### 4.3.9 *Electron Paramagnetic Resonance Spectroscopy*

Spectra were recorded using a Bruker EMX instrument equipped with an Oxford ESR 900 cryostat and ITC temperature controller. Additional sample concentration was performed using Amicon Ultra-4 centrifugal filter devices (Beverly, MA.) The settings for the spectrometer were as follows: temperature, 10 K; microwave frequency, 9.38 GHz; microwave power, 0.1 mW; modulation amplitude, 10 G; modulation frequency,

100 kHz; time constant, 655.36 ms; conversion time, 655.36 ms; and receiver gain,  $1.0 \times 10^5$ .

#### 4.4 Results

##### 4.4.1 Spectroscopic Evaluation of Reactivated R117D KatG<sup>N</sup>

###### 4.4.1.1 Far-UV Circular Dichroism (CD) Spectra of R117D KatG<sup>N</sup> and D597R KatG<sup>C</sup>

To evaluate the composition of secondary structural features in R117D KatG<sup>N</sup> and D597R KatG<sup>C</sup>, far-UV CD spectra of the substituted domains were recorded using a Jasco J-810 Spectrapolarimeter (Tokyo, Japan) and compared to the far-UV CD spectra of their respective wild-type domain. The CD spectrum of R117D KatG<sup>N</sup> resembles that of KatG<sup>N</sup> (Figure 4.1). The strong negative signals at around 222 nm and 208 nm represent substantial  $\alpha$ -helical content in the structure, and the positive signal at 190 nm is contributed by both  $\alpha$ -helix and  $\beta$ -sheet. On the other hand, the CD spectrum of D597R KatG<sup>C</sup> reveals weaker negative  $\alpha$ -helical signals at 222 nm and 208 nm as well as reduced  $\alpha$ -helicity and  $\beta$ -sheet character at 190 nm in contrast to KatG<sup>C</sup> (Figure 4.2).

###### 4.4.1.2 UV-visible spectroscopy

The heme absorption spectra for the ferric forms of KatG<sup>N</sup> and R117A KatG<sup>N</sup> are both dominated by hexacoordinate low-spin heme. Such spectra are characterized by a

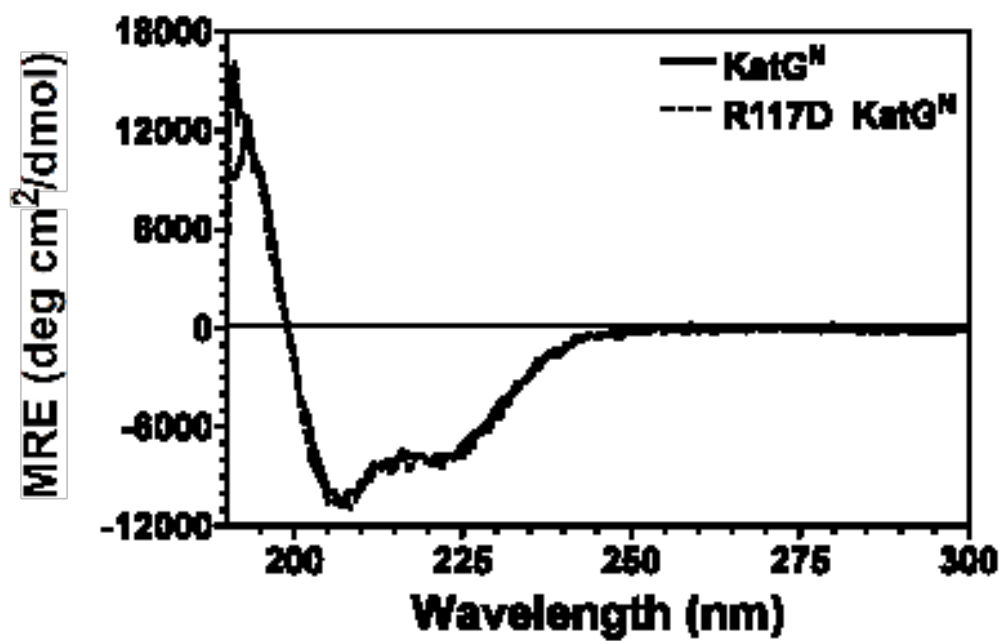


Figure 4.1. CD spectra of KatG<sup>N</sup> and R117D KatG<sup>N</sup>

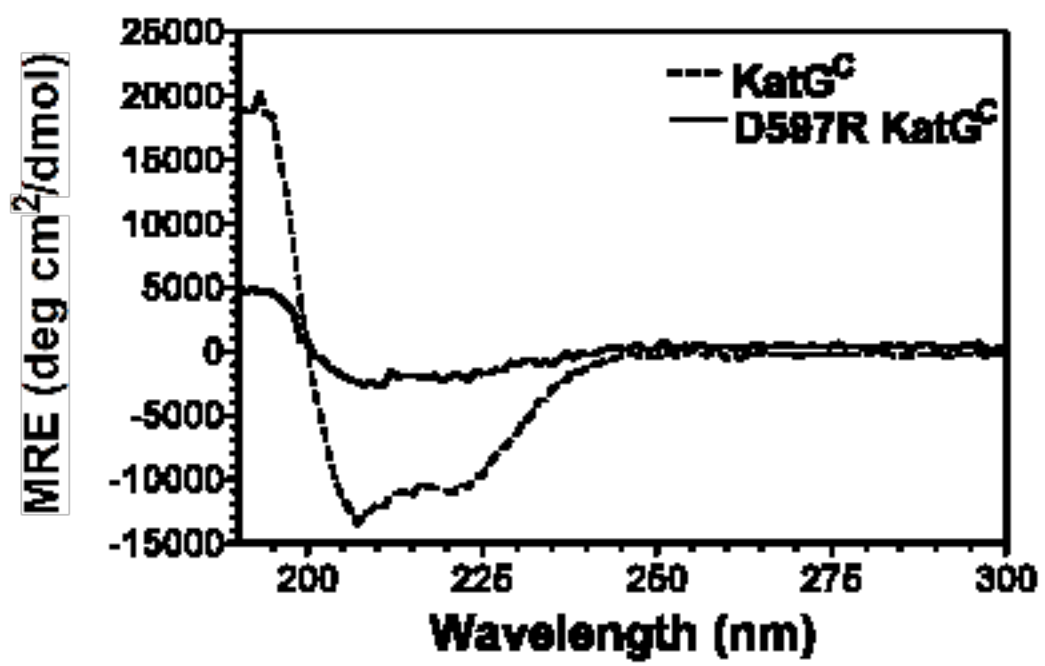


Figure 4.2. CD spectra of KatG<sup>C</sup> and D597R KatG<sup>C</sup>

sharp Soret ( $\gamma$ ) band at 416 nm and prominent  $\beta$  and  $\alpha$  bands at 536 nm and 568 nm, respectively. The absorption spectrum of R117D KatG<sup>N</sup> shows similar features (Figure 4.3, top view). Following incubation with KatG<sup>C</sup>, the heme in R117D KatG<sup>N</sup> showed a slow but substantial shift (Figure 4.3B). The  $\alpha$  and  $\beta$  bands diminished in intensity along with an increase in charge transfer bands at 640 nm (CT1) and 500 nm (CT2). The Soret ( $\gamma$ ) band broadened, decreased in intensity, and blue shifted, giving a new  $\lambda_{\text{max}}$  near 410 nm.

The pairing of KatG<sup>N</sup> variants (unmodified and R117D KatG<sup>N</sup>) and KatG<sup>C</sup> variants (unmodified, D597A KatG<sup>C</sup>, and D597R KatG<sup>C</sup>) resulted in a dramatic differentiation of heme spectra (Figure 4.4 and 4.5 and Table 4.1). Combining the unmodified domains (KatG<sup>N</sup> + KatG<sup>C</sup>) results in a shift of the Soret band to 408 nm (Figure 4.4). Likewise, there is a considerable decrease in the intensity of the  $\alpha$  and  $\beta$  bands concomitant with the appearance of two charge transfer bands (CT1 and CT2) at 645 nm and 507 nm, respectively (Figure 4.5). These spectral properties are consistent with a mixture of species dominated by penta- and hexa-coordinate high spin heme iron [81]. For R117D KatG<sup>N</sup> following its incubation with KatG<sup>C</sup>, the Soret band shifted to 412 nm (Figure 4.4), and further into the visible range, a noteworthy increase in absorption at 645 nm and 500 nm was detected (Figure 4.5), indicating the presence of the CT1 and CT2 transitions, respectively. However, in the case of the latter, the absorption maximum was at 523 nm. This is suggestive of simultaneous contributions

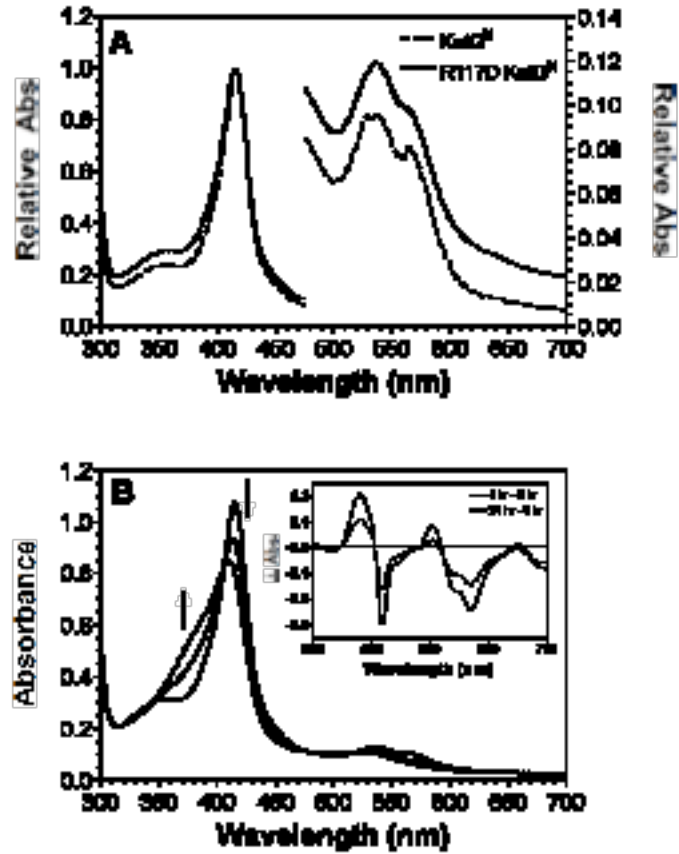


Figure 4.3. Heme absorption spectra of KatG<sup>N</sup> compared to R117D KatG<sup>N</sup>. (A) The heme absorption spectrum of separately expressed and isolated KatG<sup>N</sup> and R117D KatG<sup>N</sup> showed similar spectral features. (B) The change in heme absorption spectra of KatG<sup>N</sup> and R117D KatG<sup>N</sup> after incubation with KatG<sup>C</sup>. A set of difference spectra calculated from part B is shown in the inset.

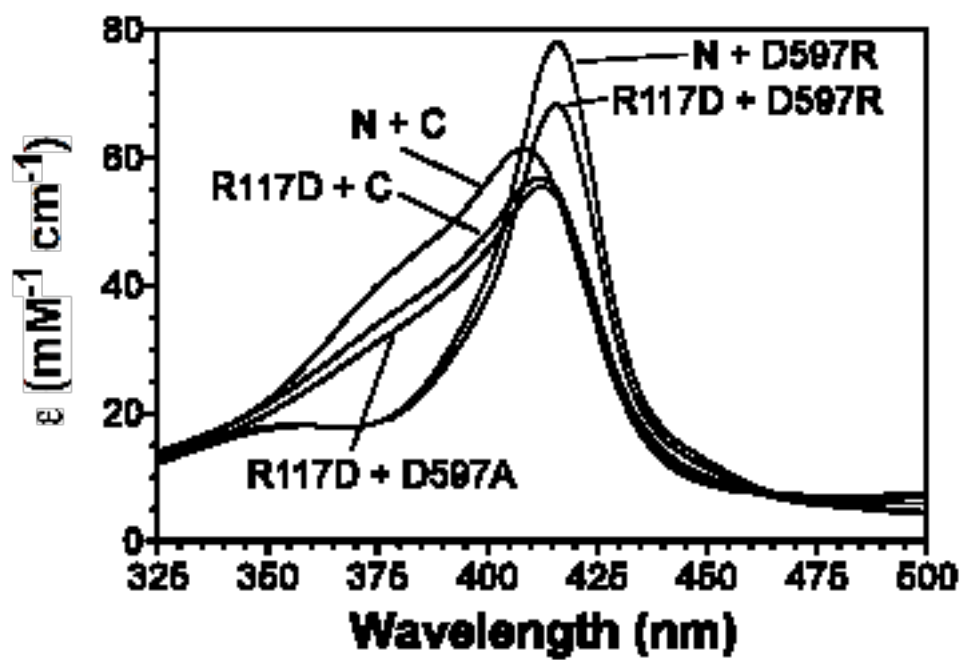


Figure 4.4. Change in the Soret band of the heme absorption spectra of KatG<sup>N</sup> and R117D KatG<sup>N</sup> after incubation with the C-terminal domain and variants thereof.



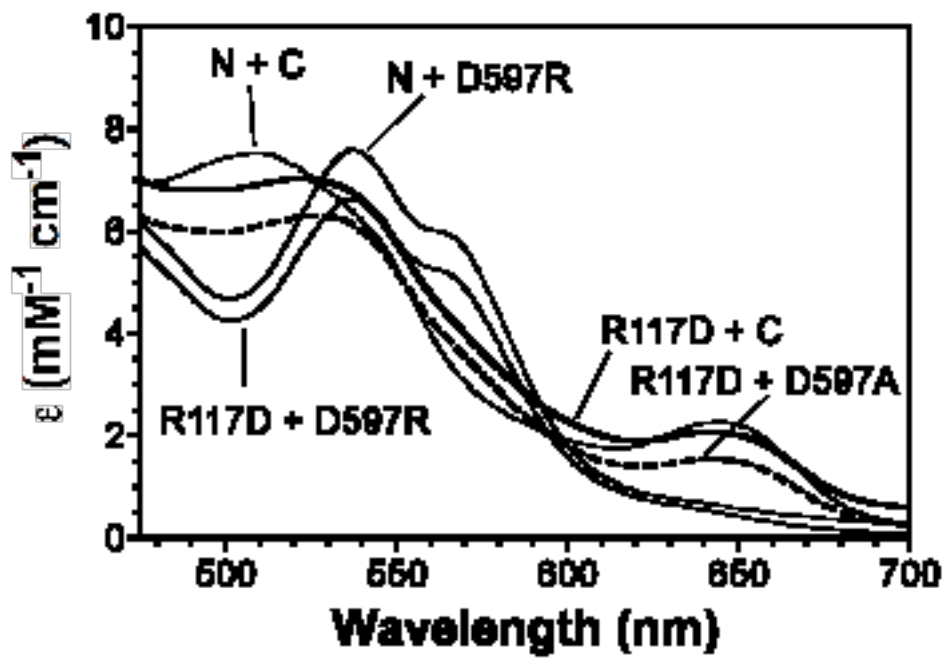


Figure 4.5. Contribution of the charge transfer and  $\alpha$  and  $\beta$  bands to the heme absorption spectra of KatG<sup>N</sup> and R117D KatG<sup>N</sup> after incubation with KatG<sup>C</sup> and variants thereof.

**Table 4.1.** UV-visible spectral features for the ferric heme states of KatG<sup>N</sup> or R117D KatG<sup>N</sup> paired with KatG<sup>C</sup>, D597A KatG<sup>C</sup>, or D597R KatG<sup>C</sup>.<sup>a</sup>

Domain Variants <sup>b</sup>		Absorption band maxima (nm [mM <sup>-1</sup> cm <sup>-1</sup> ])				
N	C	$\gamma$ (Soret)	CT2 <sup>c</sup>	$\beta$	$\alpha$	CT1 <sup>d</sup>
KatG <sup>N</sup>	KatG <sup>C</sup>	408 (61.4)	507 (7.52)	- <sup>e</sup>	-	645 (2.27)
R117D	KatG <sup>C</sup>	412 (56.8)	-	523 (7.04)	-	646 (2.07)
R117D	D597A	413 (55.4)	-	527 (6.31)	-	642 (1.55)
R117D	D597R	416 (68.3)	-	537 (6.63)	570	-
KatG <sup>N</sup>	D597R	416 (78.0)	-	537 (7.59)	570	-

<sup>a</sup>Spectra were recorded in 50 mM phosphate buffer, pH 7.0 following a 24 hour incubation of each combination at 4°C.

<sup>b</sup>One representative of each domain was present in each combination. KatG<sup>N</sup> and KatG<sup>C</sup> refer to the unmodified domains.

<sup>c</sup>CT2, short wavelength charge transfer transition (usually between 490 and 510 nm).

<sup>d</sup>CT1, long wavelength charge transfer transition (usually between 600 and 650 nm).

<sup>e</sup>Absorption bands that were not observed or were too weak to make unequivocal assignments are indicated by a dash.

from CT2 and  $\beta$  band absorption. Nearly identical results were obtained when R117D KatG<sup>N</sup> was incubated with D597A KatG<sup>C</sup>. In both domain pairings, the results suggest a substantial increase in high-spin heme species (pentacoordinate and hexacoordinate), but an appreciable amount of hexacoordinate low-spin heme appears to remain. In contrast, incubation of either KatG<sup>N</sup> or its R117D variant with D597R KatG<sup>C</sup> (Figures 4.4 and 4.5), resulted in little if any spectral shift compared to the KatG<sup>N</sup> or R117D KatG<sup>N</sup> alone. The Soret band absorption maximum remained at 416 nm and the absorption of the  $\beta$  and  $\alpha$  bands were clearly evident at 537 nm and 570 nm.

#### *4.4.1.3 Magnetic Circular Dichroism Spectroscopy (MCD)*

MCD was used to more readily distinguish between the high- and low-spin heme species present in the reactivated R117D KatG<sup>N</sup> proteins. In MCD, low-spin ferrous heme is present around 550 nm has a strong A-term that represents the Q- or  $\alpha$ -band. This signal is absent in high-spin ferrous heme. The B- or Soret bands for high- and low-spin hemes are also distinguishable from each other. Examples of low- and high-spin ferrous hemes can be found in [119-120] and [125-127]. The individually expressed and isolated domains were recombined and incubated at 4°C for 24 hours. Following the incubation period, dithionite was added to reduce the heme species present. The ferrous spectra of R117D KatG<sup>N</sup> recombined with KatG<sup>C</sup> and D597A KatG<sup>C</sup> (Figure 4.6A and 6B, respectively) both show strong A-term signals around 550 nm indicating that low-spin heme is present. However, there are also spectral features in the 575–625 nm range consistent with high-spin heme. Furthermore, a strong signal at 440 nm is typical of

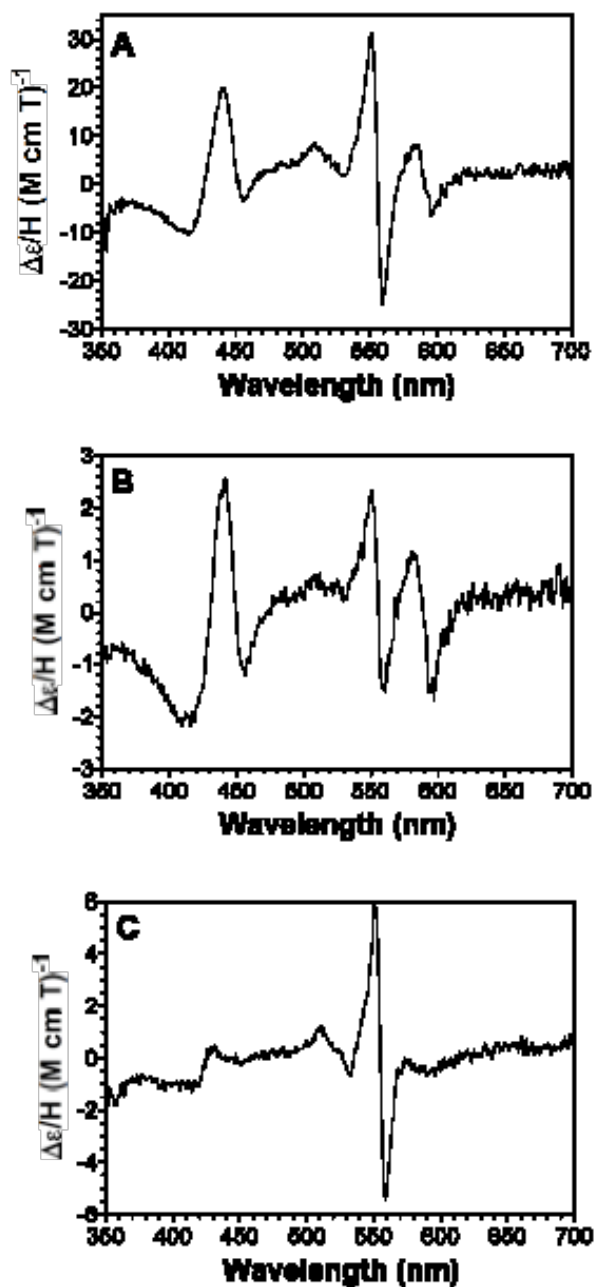


Figure 4.6. Ferrous magnetic circular dichroism (MCD) spectra of R117D KatG<sup>N</sup>. MCD of R117D KatG<sup>N</sup> reactivated with (a) KatG<sup>C</sup>, (b) D597A KatG<sup>C</sup>, and (c) D597R KatG<sup>C</sup> following a 24-hour incubation period.

high-spin ferrous hemes, but with a lower intensity for the D597A substitution. These ferrous MCD spectral results are consistent with those observed for the unmodified KatG<sup>N</sup> and KatG<sup>C</sup> following their incubation together for 24 hours [124]. In striking contrast, the ferrous spectra of R117D KatG<sup>N</sup> + D597R KatG<sup>C</sup> (Figure 4.6C) is that of an exclusively hexa-coordinate low-spin heme complex similar to that of KatG<sup>N</sup> prior to any incubation with KatG<sup>C</sup> [128].

#### *4.4.1.4 Electron paramagnetic resonance (EPR) spectroscopy*

Application of EPR to evaluate the ferric state can be used to corroborate the results of our UV-vis and MCD studies; however, it also allows one to distinguish between the high-spin species present in a given KatG preparation. A hallmark of KatG enzymes isolated from a variety of sources is that a mixed population of pentacoordinate and hexacoordinate high-spin hemes is almost always observed. A typical spectrum for active catalase-peroxidases includes contributions from rhombic ( $g_{x,y,z} = 6.69, 4.97, 1.95$ ) and axial ( $g_{\perp} = 5.97, g_{\parallel} = 1.99$ ) signals, assigned as pentacoordinate and hexacoordinate high-spin heme species, respectively. Furthermore, in the typical KatG spectrum the axial (i.e., hexacoordinate high-spin) form dominates. The EPR spectrum for KatG<sup>N</sup> following its reactivation by KatG<sup>C</sup> shows a similar pattern (Figure 4.7). The EPR spectrum for R117D KatG<sup>N</sup> following its incubation with either KatG<sup>C</sup> or D597A KatG also showed a strong contribution from high spin heme species; however, there is a

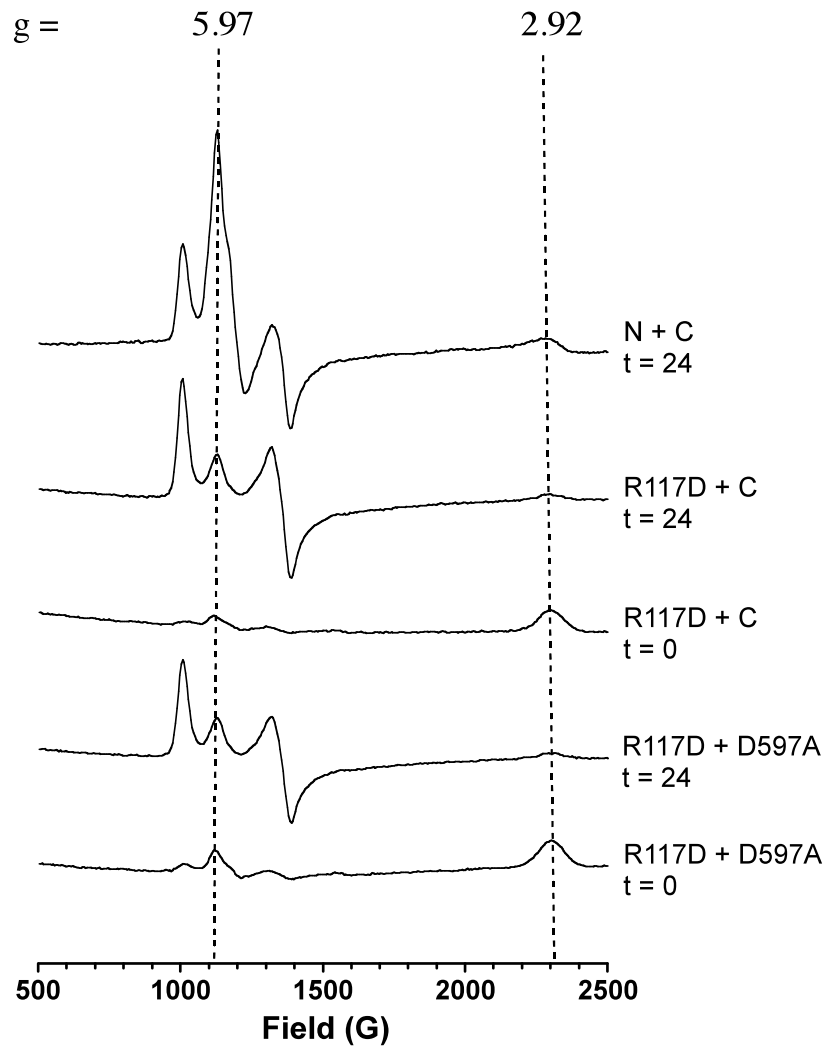


Figure 4.7. High-spin EPR spectra of R117D KatG<sup>N</sup> recombined with KatG<sup>C</sup> and D597A KatG<sup>C</sup> following a 24-hr incubation period. All spectra were recorded at 10K. Spectrometer settings were as described in the *Materials and Methods* section.

marked departure from the typical KatG spectrum, or even that obtained from incubation of the unmodified KatG<sup>N</sup> and KatG<sup>C</sup> domains. The dominant signal is clearly that of the rhombic form, indicating that reactivation of R117D KatG<sup>N</sup> produces substantially more of the pentacoordinate high-spin form. Although the rhombic signal is also present for KatG<sup>N</sup> recombined with KatG<sup>C</sup>, the more prominent feature is the axial signal [80]. In contrast to the wild-type recombined domains, low-spin signals are significant features for R117D KatG<sup>N</sup> recombined with KatG<sup>C</sup> and D597A KatG<sup>C</sup>, similar to those present in the EPR spectra of KatG<sup>N</sup> + KatG<sup>C</sup> after a 24-hr incubation period [80]. On the other hand, recombination of KatG<sup>N</sup> and R117D KatG<sup>N</sup> with D597R KatG<sup>C</sup> (Figure 4.8) produces an exclusively low-spin ( $g = 2.92, 2.27, 1.53$ ) heme environment as with KatG<sup>N</sup> [128].

#### 4.4.2 *Kinetic Evaluation of Reactivated R117D KatG<sup>N</sup>*

##### 4.4.2.1 *Reactivation Kinetics*

To further evaluate the effect of interdomain residue substitution on active site conformational rearrangements, the rate and extent of catalase and peroxidase activity recovery was evaluated. Equimolar mixtures pairing KatG<sup>N</sup> (or variants thereof) and KatG<sup>C</sup> (or variants thereof) were tested for their catalase activity periodically over a 24 to 36-hour period (Figure 4.9). Incubation of R117D KatG<sup>N</sup> with KatG<sup>C</sup> resulted in a monophasic return of catalase activity in contrast to the biphasic reactivation of KatG<sup>N</sup> by

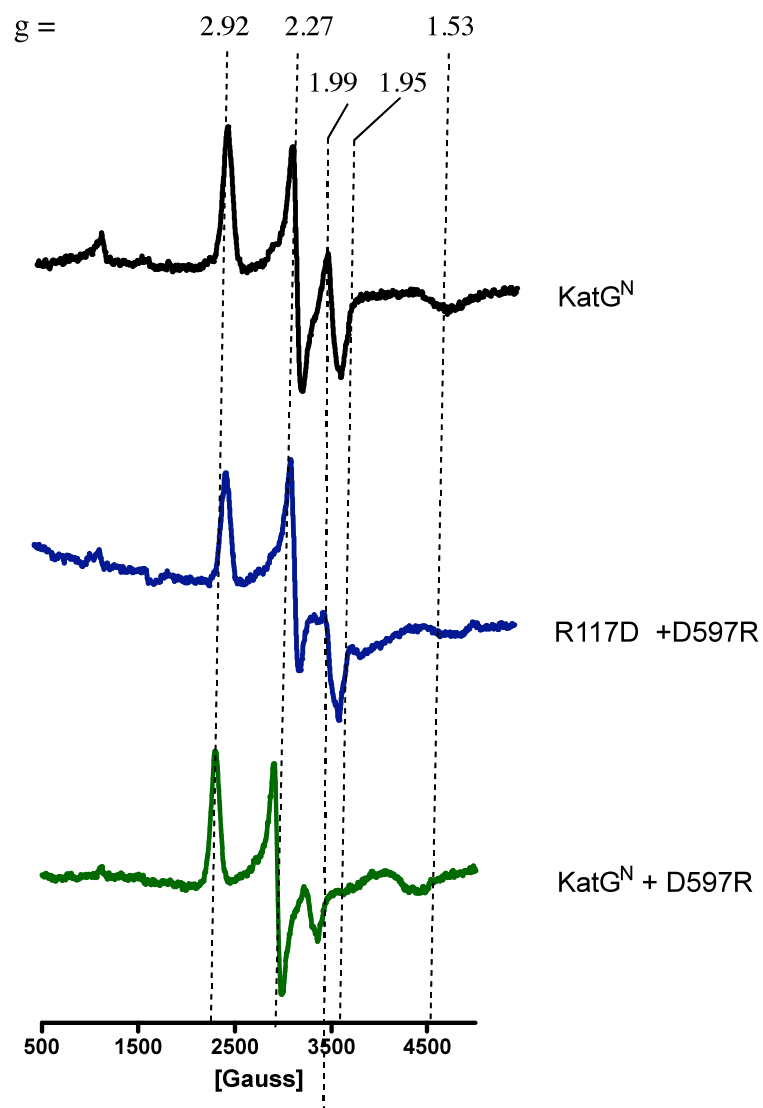


Figure 4.8. Comparison of EPR spectra of R117D KatG<sup>N</sup> and KatG<sup>N</sup> reactivated with D597R KatG<sup>C</sup> following a 24-hr incubation period. All spectra were recorded at 10K. Spectrometer settings were as described in the *Materials and Methods* section.



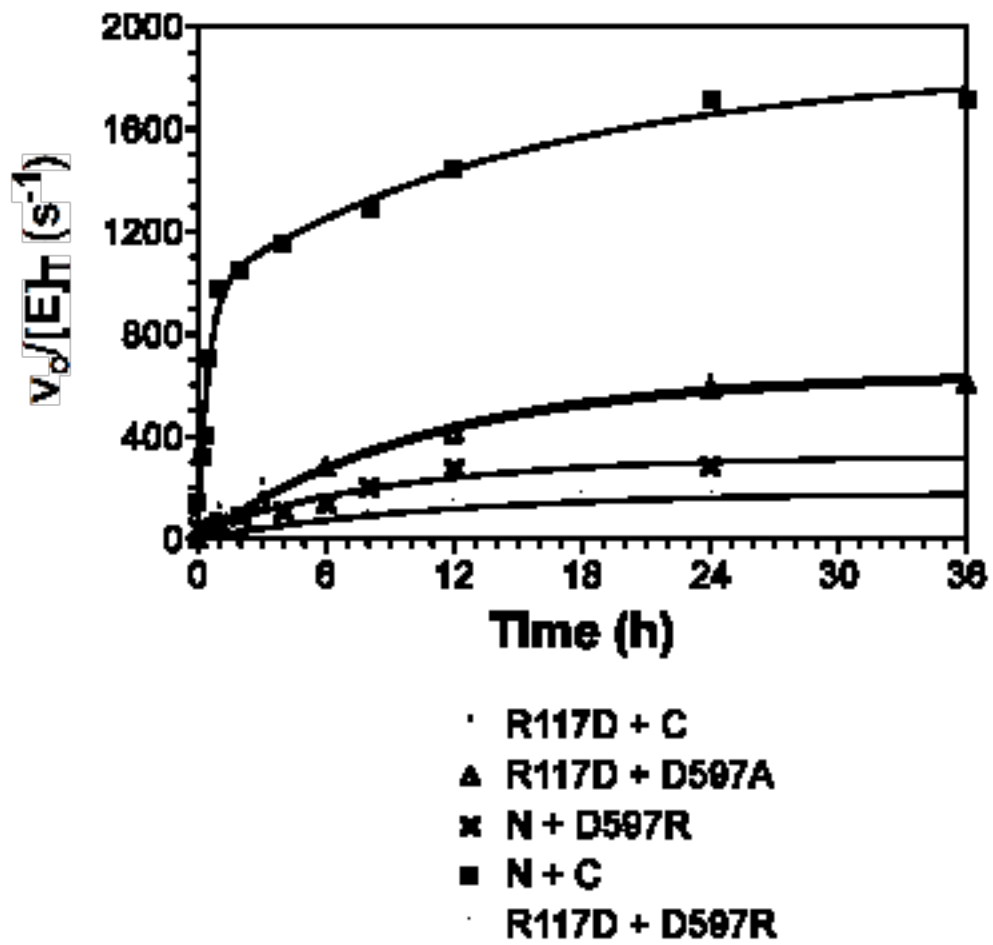


Figure 4.9. Reactivation of KatG<sup>N</sup> and R117D KatG<sup>N</sup>.

Catalase activities were measured for equimolar mixtures of each domain.

of KatG<sup>N</sup>, a 3-fold reduction in total recovered catalase activity (i.e., amplitude) was observed. Interestingly, reactivation of R117D KatG<sup>N</sup> by D597A KatG<sup>C</sup> also occurred in a monophasic process with a nearly identical rate constant and amplitude as those observed with unmodified KatG<sup>C</sup>. The D597R substitution in KatG<sup>C</sup> compromised the extent of recovery of catalase activity in KatG<sup>N</sup> (decreased ~ 6 fold) and its R117D variant (~ 3.5 fold). Interestingly, monophasic reactivation kinetics were also observed here, and the rate constant was highly similar to those observed for the other domain combinations (Table 4.2).

The effect of H<sub>2</sub>O<sub>2</sub> concentration on the catalase activity of each domain pairing was evaluated (Figure 4.10). From these data steady-state kinetic parameters were obtained (Table 4.3). In general, the most markedly affected parameter was  $k_{cat}$  which followed very closely the trend observed in the amplitude of catalase recovery. There was also some diversity in the apparent  $K_M$  values obtained, however, comparisons of maximum catalytic output (apparent  $k_{cat}$ ) and catalytic efficiency (apparent  $k_{cat}/K_M$ ) showed the domain pairs falling into three distinct groups. Any domain pairing involving D597R KatG<sup>C</sup> showed the lowest catalytic output and catalytic efficiencies, about an order of magnitude lower than KatG<sup>N</sup> + KatG<sup>C</sup> by either parameter. R117D KatG<sup>N</sup> reactivated by either KatG<sup>C</sup> or D597A KatG<sup>C</sup> fell in the middle with 2 to 3 fold lower  $k_{cat}$  and  $k_{cat}/K_M$  values than the pairing of the unmodified domains.

**Table 4.2.** Rate constants and catalase activity recovered for KatG<sup>N</sup> or R117D KatG<sup>N</sup> paired with KatG<sup>C</sup>, D597A KatG<sup>C</sup>, or D597R KatG<sup>C</sup>.

Domain Variants		Rate constants (s <sup>-1</sup> )		Amplitudes { $v_0/[E]_T$ (s <sup>-1</sup> )} <sup>a</sup>		
N	C	$k_1$ (s <sup>-1</sup> )	$k_2$ (s <sup>-1</sup> )	$Amp_1$	$Amp_2$	$Amp_T$
<sup>a</sup> KatG <sup>N</sup>	KatG <sup>C</sup>	5.9 x 10 <sup>-4</sup>	1.8 x 10 <sup>-5</sup>	970	870	1840
R117D	KatG <sup>C</sup>	-	2.3 x 10 <sup>-5</sup>	-	644	644
R117D	D597A	-	2.5 x 10 <sup>-5</sup>	-	638	638
R117D	D597R	-	2.2 x 10 <sup>-5</sup>	-	185	185
KatG <sup>N</sup>	D597R	-	2.9 x 10 <sup>-5</sup>	-	295	295

<sup>a</sup>Amplitudes correspond to catalase activity recovered and are reported as ( $v_0/[E]_T$ ).

Amplitude corresponding to  $k_1$  ( $Amp_1$ ) and  $k_2$  ( $Amp_2$ ) are summed to give total recovered catalase activity ( $Amp_T$ ).

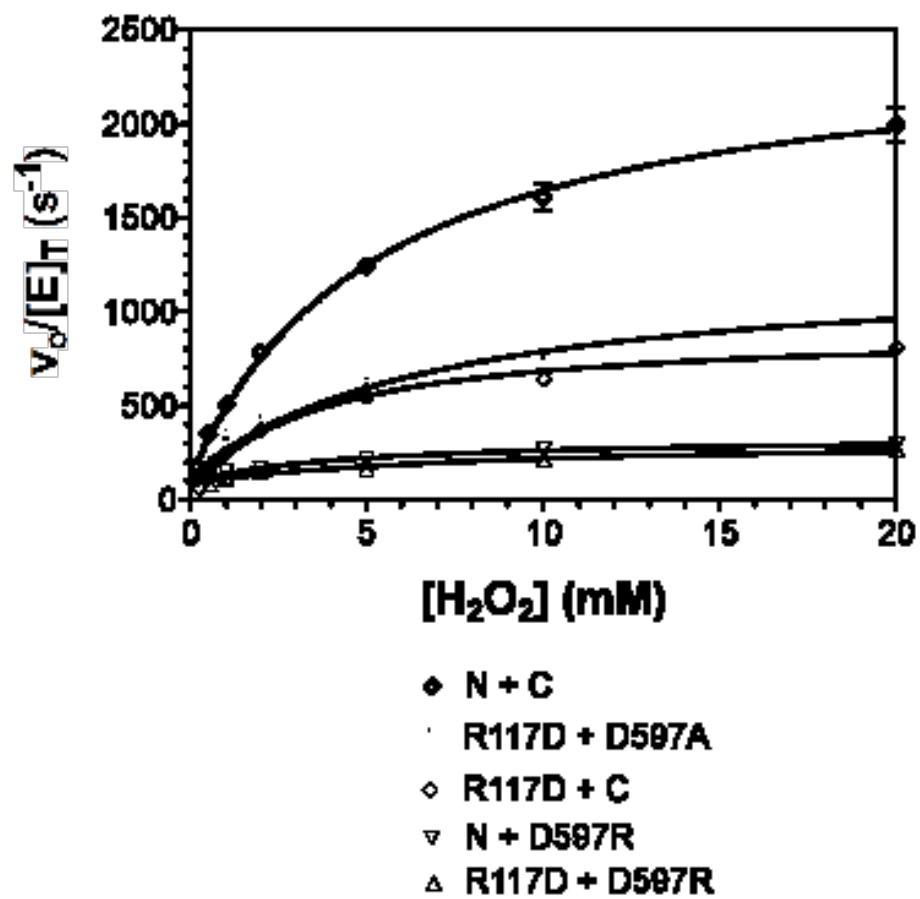


Figure 4.10. Comparison of Catalase Activity of KatG<sup>N</sup> and R117D KatG<sup>N</sup> after a 24-hr incubation period with the C-terminal domain and variants thereof with respect to H<sub>2</sub>O<sub>2</sub> as the substrate.

**Table 4.3.** Apparent kinetic parameters for the recovered catalase activity in KatG<sup>N</sup> or R117D KatG<sup>N</sup> paired with KatG<sup>C</sup>, D597A KatG<sup>C</sup>, or D597R KatG<sup>C</sup>.

Domain Variants		Catalase kinetic parameters		
N	C	$k_{cat}$ (s <sup>-1</sup> )	$K_M$ (mM H <sub>2</sub> O <sub>2</sub> )	$k_{cat}/K_M$ (M <sup>-1</sup> s <sup>-1</sup> )
KatG <sup>N</sup>	KatG <sup>C</sup>	2312 ± 78	3.9 ± 0.4	5.9 x 10 <sup>5</sup>
R117D	KatG <sup>C</sup>	845 ± 19	3.1 ± 0.3	2.8 x 10 <sup>5</sup>
R117D	D597A	1127 ± 37	7.0 ± 0.9	1.6 x 10 <sup>5</sup>
R117D	D597R	242 ± 12	9.0 ± 1.9	2.7 x 10 <sup>4</sup>
KatG <sup>N</sup>	D597R	245 ± 12	4.3 ± 0.9	5.7 x 10 <sup>4</sup>

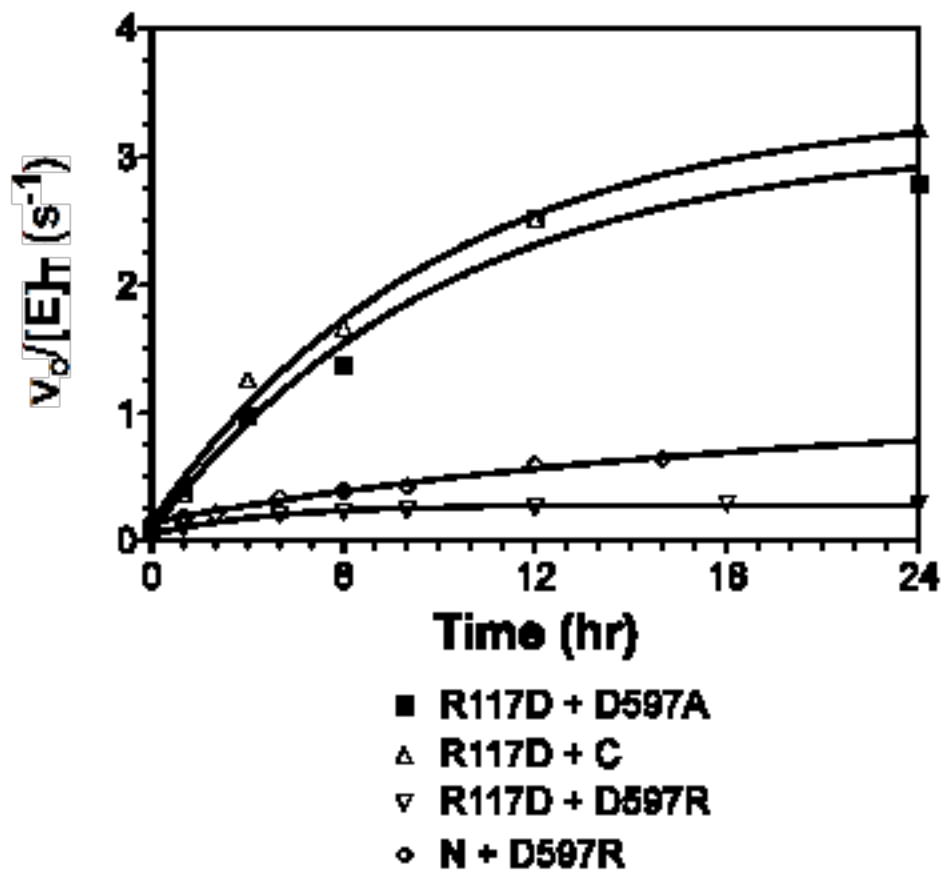


Figure 4.11. Reactivation of KatG<sup>N</sup> and R117D KatG<sup>N</sup>.

Peroxidase activities were measured for equimolar mixtures of each domain.

**Table 4.4.** Rate constants and activity recovered for the peroxidase restoration in KatG<sup>N</sup> or R117D KatG<sup>N</sup> paired with KatG<sup>C</sup>, D597A KatG<sup>C</sup>, or D597R KatG<sup>C</sup>.

Domain Variants		Rate constants (s <sup>-1</sup> )		Amplitudes { $v_o/[E]_T$ (s <sup>-1</sup> )} <sup>a</sup>		
N	C	$k_1$ (s <sup>-1</sup> )	$k_2$ (s <sup>-1</sup> )	$Amp_1$	$Amp_2$	$Amp_T$
<sup>a</sup> KatG <sup>N</sup>	KatG <sup>C</sup>	1.3 x 10 <sup>-4</sup>	4.0 x 10 <sup>-5</sup>	1.50	1.20	2.70
R117D	KatG <sup>C</sup>	-	3.0 x 10 <sup>-5</sup>	-	3.28	3.28
R117D	D597A	-	3.0 x 10 <sup>-5</sup>	-	3.07	3.07
R117D	D597R	-	7.5 x 10 <sup>-5</sup>	-	0.231	0.231
KatG <sup>N</sup>	D597R	-	1.5 x 10 <sup>-5</sup>	-	0.88	0.88

<sup>a</sup>Amplitudes correspond to peroxidase activity recovered and are reported as ( $v_o/[E]_T$ ). Amplitude corresponding to  $k_1$  ( $Amp_1$ ) and  $k_2$  ( $Amp_2$ ) are summed to give total recovered peroxidase activity ( $Amp_T$ ).

The kinetics of peroxidase activity recovery by KatG<sup>N</sup> or R117D KatG<sup>N</sup> in the presence of KatG<sup>C</sup> and its variants (Figure 4.11) was similar to that of catalase recovery in that a rate constant of about  $3 \times 10^{-5} \text{ s}^{-1}$  was observed in all cases (Table 4.4). As observed with catalase recovery, combinations involving D597R KatG<sup>C</sup> returned considerably less peroxidase activity (i.e., had lower amplitudes) than pairings involving KatG<sup>C</sup> or D597A KatG<sup>C</sup>. In contrast, to the kinetics of catalase recovery, the amplitudes observed for KatG<sup>N</sup> + KatG<sup>C</sup>, R117D KatG<sup>N</sup> + KatG<sup>C</sup>, and R117D KatG<sup>N</sup> + D597A KatG<sup>C</sup> were all similar to one another.

The effect of H<sub>2</sub>O<sub>2</sub> concentration on the peroxidase activity of the domain pairs was evaluated (Figure 4.12). The kinetic parameters for the recovered peroxidase activity from either KatG<sup>N</sup> or R117D KatG<sup>N</sup> incubated with KatG<sup>C</sup> were essentially identical in  $k_{cat}$ ,  $K_M$ , and even in the peroxide-dependent inhibition parameter  $K_N$  (Table 4.5). For the R117D KatG<sup>N</sup>/D597A KatG<sup>C</sup> combination, the observed  $k_{cat}$  was cut in half; however, the same was observed for the  $K_M$ , yielding a  $k_{cat}/K_M$  that was essentially the same as that for combinations involving unmodified KatG<sup>C</sup>. In contrast, any combination involving D597R KatG<sup>C</sup> showed at least a 25-fold decrease in  $k_{cat}$  and at least the same increase in  $K_M$ . As a result the  $k_{cat}/K_M$  for these combinations was decreased by three to four orders of magnitude.



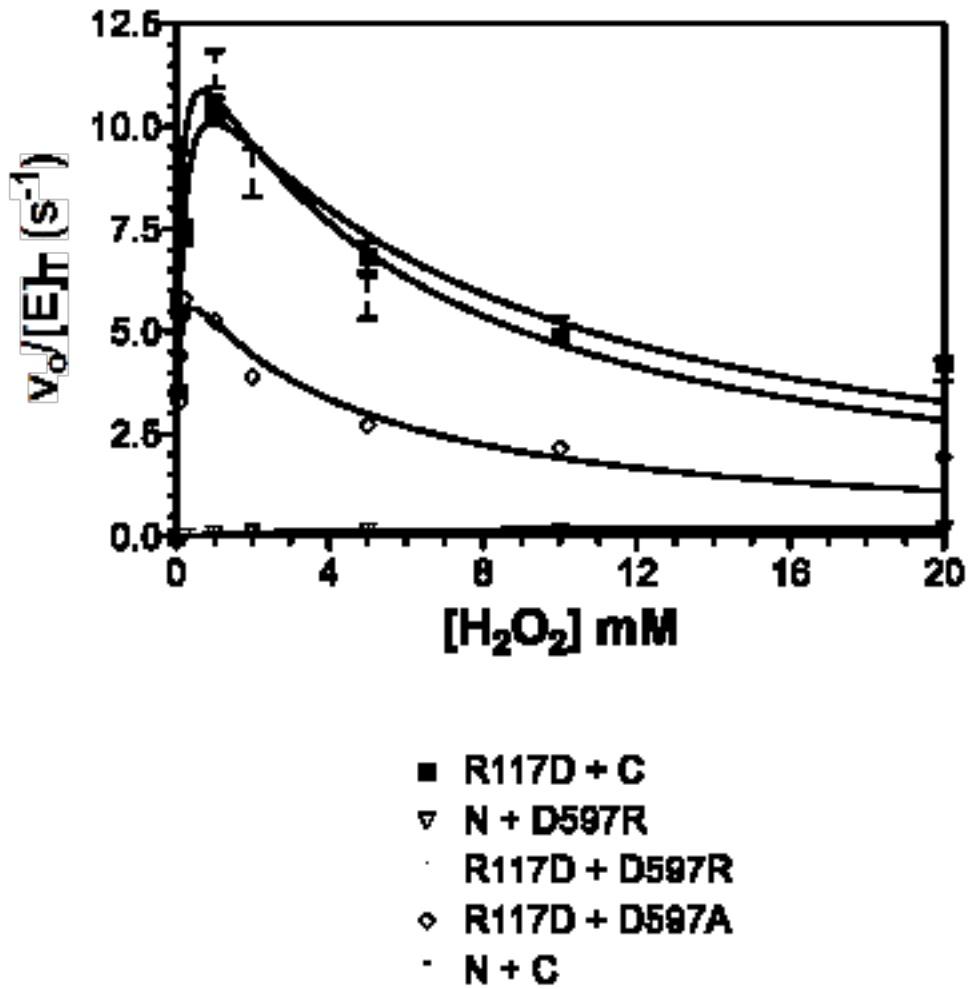


Figure 4.12. Comparison of peroxidase activity of R117D KatG<sup>N</sup> after a 24-hr incubation period with KatG<sup>C</sup> and variants thereof with respect to H<sub>2</sub>O<sub>2</sub> as the substrate.

**Table 4.5.** Apparent kinetic parameters for the recovered peroxidase activity in KatG<sup>N</sup> or R117D KatG<sup>N</sup> paired with KatG<sup>C</sup>, D597A KatG<sup>C</sup>, or D597R KatG<sup>C</sup>.

Domain Variants		Peroxidase kinetic parameters			
N	C	$k_{\text{cat}}$ (s <sup>-1</sup> )	$K_M$ (mM H <sub>2</sub> O <sub>2</sub> )	$k_{\text{cat}}/K_M$ (M <sup>-1</sup> s <sup>-1</sup> )	$K_N$ (mM H <sub>2</sub> O <sub>2</sub> )
KatG <sup>N</sup>	KatG <sup>C</sup>	13.6 ± 0.9	0.084 ± 0.02	1.6 x 10 <sup>5</sup>	5.3 ± 0.9
R117D	KatG <sup>C</sup>	12.9 ± 0.66	0.13 ± 0.02	1.0 x 10 <sup>5</sup>	6.9 ± 0.9
R117D	D597A	6.8 ± 0.45	0.05 ± 0.01	1.4 x 10 <sup>5</sup>	4.0 ± 0.71
R117D	D597R	0.46 ± 0.03	44 ± 7	1.0 x 10 <sup>1</sup>	-
KatG <sup>N</sup>	D597R	0.23 ± 0.01	2.8 ± 0.3	8.2 x 10 <sup>1</sup>	-

#### 4.5 Discussion

Reactivation of the KatG N-terminal domain by a separately expressed and isolated C-terminal domain conclusively demonstrates the importance of distant protein structures in modulating the catalytic abilities of an active site. The effect of substitutions at the interdomain interface on the reactivation process provide insight into the mechanisms of communication through protein structural components. Substitution of arginine 117 with aspartate in KatG<sup>N</sup> and/or the substitution of aspartate 597 with arginine in KatG<sup>C</sup>, produced surprising effects on the kinetics of reactivation and on the nature of the reactivated enzyme.

The R117D substitution in KatG<sup>N</sup> eliminated the biphasic kinetics of catalase reactivation, regardless of the form of KatG<sup>C</sup> used (KatG<sup>C</sup>, D597A KatG<sup>C</sup>, or D597R KatG<sup>C</sup>). The more rapid ( $k = \sim 6 \times 10^{-4} \text{ s}^{-1}$ ) of two phases appeared to be absent, leaving only a slow phase  $k = \sim 2.5 \times 10^{-5} \text{ s}^{-1}$ . At first glance, this appeared to largely account for the decreased extent of catalase recovery. The pairing of R117D KatG<sup>N</sup> with KatG<sup>C</sup> or D597A KatG<sup>C</sup> showed only about 30% of the catalase recovery obtained with KatG<sup>N</sup> + KatG<sup>C</sup>. The relatively low catalase activity was confirmed by a comparison of the steady-state kinetic parameters for the different domain pairings. The  $k_{cat}$  and  $k_{cat}/K_M$  values obtained for the unmodified domains were 2 to 3 fold greater than those obtained for R117D KatG<sup>N</sup> in the presence of either KatG<sup>C</sup> or its D597A variant.

Interestingly, the recovery of R117D KatG<sup>N</sup> peroxidase activity followed a similar kinetic pattern with a single phase governed by a rate constant near  $3 \times 10^{-5} \text{ s}^{-1}$ . The striking contrast, however, was the extent of peroxidase activity recovered following

the incubation of R117D KatG<sup>N</sup> with either KatG<sup>C</sup> or its D597A variant. It was highly similar to the pairing of the unmodified domains, KatG<sup>N</sup> and KatG<sup>C</sup>. This also was confirmed by the steady-state kinetic parameters for peroxidase activity following reactivation. Reactivation of KatG<sup>N</sup> or R117D KatG<sup>N</sup> by KatG<sup>C</sup> produced peroxidase activity with essentially the same kinetic parameters across the board ( $k_{cat}$ ,  $K_M$ ,  $k_{cat}/K_M$ , and  $K_N$ ). While R117D KatG<sup>N</sup> peroxidase activity recovered by D597A KatG<sup>C</sup> showed a significantly lower  $k_{cat}$ , a comparative decrease in  $K_M$  yielded a  $k_{cat}/K_M$  nearly identical to the other two domain pairings.

This indicates that full restructuring of the active site coordination environment is possible with the R117D substitution, but the catalytic abilities of this active site are altered relative to the unmodified KatG<sup>N</sup> following its reactivation. As indicated by all of our spectroscopic results, KatG<sup>C</sup> (or its D597A variant) are able to shift the architecture of the active site, removing a strong field ligand (presumably His106) from the coordination sphere of the heme iron. This is indicated by the increase high-spin heme species and the decrease in hexacoordinate low-spin species. However, our EPR results clearly indicate that the distribution of high-spin species obtained following reactivation of R117D is different from reactivated KatG<sup>N</sup> or even the intact wild type KatG. The axial component of the typical catalase-peroxidase spectrum is substantially diminished in R117D KatG<sup>N</sup> reactivated by either KatG<sup>C</sup> or D597A KatG<sup>C</sup>. The axial signal has been assigned as a hexacoordinate high-spin heme, and the rhombic component has been assigned as pentacoordinate high-spin heme. [124]. These results would suggest that upon reactivation the R117D substitution tends to favor pentacoordinate high spin heme more readily than the typical catalase-peroxidase active site.

The distribution between these high spin species has been suggested to reflect the arrangement of active site water molecules and their hydrogen bonding to the heme iron and active site residues [124, 134]. As such it is sensitive to a variety of factors, most prominently pH. The spectrum dominated by rhombic distortion tends to prevail at lower pH, while the axial signal dominates at higher pH values. It is noteworthy that peroxidase activity is optimal at lower pH values while catalase activity is greater at higher pH values [134]. Moreover, we have observed in several of our variants that an active site that tends to favor the pentacoordinate over hexacoordinate high-spin state also tends to have selectively diminished catalase activity. Reactivated R117D KatG<sup>N</sup> would seem to be another protein that falls in this category.

Our previous studies on R117A KatG<sup>N</sup> clearly indicated an important role for this residue in KatG<sup>N</sup> reactivation. The results with R117D KatG<sup>N</sup> confirm these conclusions, but what amounts to a more conservative substitution, in terms of the observed effect of the substitution, provides additional insight. Rates of reactivation of R117A and R117D KatG<sup>N</sup> by KatG<sup>C</sup> are essentially the same ( $\sim 2 \times 10^{-5} \text{ s}^{-1}$ ); both of them lack the initial rapid phase of reactivation observed in KatG<sup>N</sup>. So, R117 is important in the reactivation process. At the same time, the extent of R117D KatG<sup>N</sup> active site restructuring is clearly greater than that of R117A variant and compares closely with unmodified KatG<sup>N</sup>. It would seem that aspartate at position 117 preserves more of KatG<sup>N</sup> in a conformation that can be addressed by KatG<sup>C</sup> than an alanine at the same position.

The companion modification to reverse the polarity of the R117/D597 ion pair (D597R) had a highly detrimental impact on the ability of KatG<sup>C</sup> to reactivate KatG<sup>N</sup> and R117D KatG<sup>N</sup>. This is not entirely surprising in the case of the unmodified N-terminal

domain as two arginine residues would be expected to point toward one another at the interdomain interface. However, little difference in reactivation was observed when R117D KatG<sup>N</sup> was used in place of KatG<sup>N</sup>. Inspection of CD spectra at far UV wavelengths indicated that the D597R substitution was highly disruptive to secondary structural content. This is somewhat surprising given that the D597A substitution is well tolerated, and it is expected that in the absence of the N-terminal domain, D597 would be in a solvent exposed position. Nevertheless, these data make it clear that the N-terminal domain responds to a properly folded C-terminal domain for reactivation, but the reverse does not appear to be the case.

## CHAPTER FIVE

### ROLE OF Y111 AND R484 IN CATALASE-PEROXIDASE REACTIVATION

#### 5.1 Abstract

In spite of being positioned 30 Å away from the active site, the C-terminal domain is essential for catalase-peroxidase (KatG) function. Addition of equimolar amounts of separately expressed and isolated C-terminal domain (KatG<sup>C</sup>) to the active-site bearing N-terminal domain (KatG<sup>N</sup>) restores KatG function. There are highly conserved interdomain residue interactions that could be essential for the reactivation of KatG<sup>N</sup>. Previous kinetic and spectroscopic studies indicate that the Arg 117-Asp597 (R117-D597) salt-bridge interaction is not essential for KatG catalytic function. However, the R117 and D597 individually appear to play a significant role in stabilizing a loop that connects the N-terminal B (contains the active site distal histidine (His 106)) and C helices. This loop (BC) could play a role in maintaining the structural integrity of the active site. To further explore this hypothesis, we investigated the strictly conserved Tyr111 (Y111) residue on the N-terminal domain BC loop and the strictly conserved Arg484 (R484) on the B'C' loop of the C-terminal domain. Spectroscopic and kinetic evaluation revealed minimal changes in the catalase and peroxidase activities upon reactivation of the Y111A KatG<sup>N</sup> variant with KatG<sup>C</sup>. However, the kinetics of Y111A

catalase recovery were considerably slower than all other features of reactivation, indicating that a feature unique to catalase activity was impaired by the substitution. A 10-fold decrease in catalase and a total loss of peroxidase activity was observed for the reactivation of KatG<sup>N</sup> and Y111A KatG<sup>N</sup> with the R484A variant. These results suggest that R484 may play a role in supporting the B'C' loop structure. This loop may be essential for proper interaction with the N-terminal domain's BC loop, which in turn plays a major role in maintaining proper active site architecture for KatG function.

## 5.2 Introduction

Catalase-peroxidases (KatGs) are hemoproteins capable of decomposing hydrogen peroxide by two distinct reaction pathways using a single active site. The first step in both the catalase and peroxidase reaction cycles involve the two-electron oxidation of the resting enzyme by one equivalent of H<sub>2</sub>O<sub>2</sub> producing H<sub>2</sub>O and the ferryl porphyrin/protein radical intermediate known as compound **I**. In the catalase reaction cycle, compound **I** is reduced back to the ferric enzyme by a second equivalent of H<sub>2</sub>O<sub>2</sub>, releasing O<sub>2</sub> and a second molecule of H<sub>2</sub>O. On the other hand, compound **I** undergoes two one-electron reduction steps by an exogenous substrate donor in the peroxidase cycle to return the enzyme to its resting state, releasing H<sub>2</sub>O and two oxidized donor substrate molecules.

The bifunctional nature of the KatG active site is noteworthy due to the fact that the catalatic and peroxidatic reaction cycles are comparable yet these activities very rarely coincide in enzyme catalysis. Typical heme enzymes that have extensive catalase



activity usually exhibit weak peroxidase activity. Likewise, enzymes that have strong peroxidase activity usually have insubstantial catalase activity. The fact that monofunctional peroxidases and catalase-peroxidases have highly similar active sites but strikingly different functions is due to structures that are peripheral to and at a distance from the KatG active site.

Catalase-peroxidases consist of three structural features absent from monofunctional peroxidases that are necessary for KatG function: two interhelical insertions and a C-terminal domain. The interhelical insertions each contain about 35 amino acids. One (the DE insertion) connects helices D and E and the other (the FG insertion) connects helices F and G. Previous studies of variants produced by removing both insertions resulted in loss of catalase activity whereas peroxidase activity was maintained [81].

Catalase-peroxidases contain two fused copies of the primordial peroxidase gene [43, 78]. The N-terminal domain copy is similar to monofunctional peroxidase and contains a heme prosthetic group cofactor for catalysis. The C-terminal domain, believed to have been derived from a monofunctional peroxidase gene duplication and fusion event [69-70], is also structurally similar to its evolutionary predecessor, but does not bind heme. Nevertheless, this domain is a conserved structure across all catalase-peroxidases, suggesting that it has a significant role in KatG function.

Proper function of monofunctional peroxidases depends on the presence of a calcium cation ( $\text{Ca}^{2+}$ ) supporting the structure of a loop (BC) that is a part of the active site helix [106-107]. Previous studies showed that removal of the  $\text{Ca}^{2+}$  ion destabilizes the BC loop resulting in collapsed active site, rendering the enzyme inactive [116, 110,

125, 108-109]. The C-terminal domain appears to play a similar role in catalase-peroxidase structure and function. Variants of *E. coli* KatG lacking the C-terminal domain (KatG<sup>N</sup>) [79] have spectroscopic, catalytic, and ligand binding properties demonstrating that of KatG<sup>N</sup> demonstrate that the C-terminal domain is essential in supporting the active site by preventing the coordination of the distal histidine (His106) to the heme iron. This is accomplished some 30Å from the active site. Addition of the separately expressed and isolated C-terminal domain (KatG<sup>C</sup>) to KatG<sup>N</sup> decreased the hexacoordinate low-spin species and increased the active high spin species. Consistent with the restructuring of the active site, both catalase and peroxidase activities were detected.

Residues at the interdomain interface have an important role in maintaining structures necessary for the reactivation process (Chapters 3 and 4). In particular the loop connecting the B and C helices (BC loop) is a structure present in both domains. This structure is strongly conserved in both domains of all catalase-peroxidases. Moreover, the KatG structure is organized such that the BC loop of each domain is positioned at the interface.

To further investigate the function of conserved residues on these loop structures, we produced variants of Tyr111 on the BC loop of the N-terminal domain and Arg484 on the B'C' loop of the C-terminal domain. The spectral and kinetic properties of Y111A KatG<sup>N</sup> + KatG<sup>C</sup> revealed a mixture of high- and low-spin heme states with the former being the more dominant. Therefore, this reactivation process was highly similar to that observed for the wild-type recombined domains. However, the kinetics of Y111A catalase reactivation were considerably slower than all other features of reactivation,

indicating that a feature specific to catalase activity was impaired by the substitution. Furthermore, a 10-fold decrease in catalase and a total loss of peroxides activity was observed for the reactivation of KatG<sup>N</sup> and Y111A KatG<sup>N</sup> with R484A KatG<sup>C</sup>. These results suggest that R484 may play a role in supporting the B'C' loop structure. This loop may be essential for proper domain interaction, which in turn plays a major role in maintaining the structural integrity of the active site.

### 5.3 *Materials and Methods*

#### 5.3.1 *Reagents*

Hydrogen Peroxide (30%), imidazole, hemin, ampicillin, chloramphenicol, sodium dithionite, and 2,2'-azino-bis(3-ethylbenzthiazoline-6-sulfonic acid) (ABTS) were purchased from Sigma (St. Louis, MO). Isopropyl- $\beta$ -D-thiogalactopyranoside (IPTG), mono- and di-basic sodium phosphate, acetic acid, and sodium acetate were obtained from Fisher (Pittsburgh, PA). Potassium cyanide was purchased from Mallinckrodt (Paris, KY). Benzonase was purchased from Novagen (Madison, WI). All restriction enzymes were purchased from New England Biolabs (Beverly, MA). All oligonucleotide primers were purchased from Invitrogen (Carlsbad, CA). All *E. coli* strains (BL-21 [DE3] and XL-1 Blue) and *Pfu* polymerase were obtained from Stratagene (La Jolla, CA). Nickel-nitrilotriacetic acid (Ni-NTA) resin was purchased from Qiagen (Valencia, CA). All buffers and media were prepared using water purified through a Millipore QPak-II system (18.2 M $\Omega$ /cm resistivity).

### 5.3.2 Cloning of $KatG^C$ and R484A $KatG^C$ Expression Plasmids

Generation of an expression construct for  $KatG^C$  was accomplished using a deletion mutagenesis procedure developed in our laboratory [71] as previously described in Chapter Two. Site-directed mutagenesis was used to produce the R484A  $KatG^C$  variant utilizing blunt-end primers ECCP M 310+ (ACT GCT GAT CGC GAA AGC ACA GC) and ECCP M 310- (GCT GTG CTT TCG CGA TCA GCA GT).

### 5.3.3 Cloning of $KatG^N$ and Y111A $KatG^N$ Expression Plasmids

Generation of an expression construct for  $KatG^N$  was accomplished as previously described in Chapter 2. Site-directed mutagenesis was used to produce the Y111A  $KatG^N$  variant utilizing ECCP M 05+ (5'-GCG GGG ACT GCA CGT TCA ATC GAT GG-3') and ECCP M 04- (3'-CGC CCC TGA CGT GCA AGT TAG CTA CC-5') for p $KatG^N$  according to the QuikChange procedure (Stratagene, La Jolla, CA). Amplification products were used to transform *E. coli* XL-1 Blue by electroporation (BIO-RAD MicroPulser, Hercules, CA). Plasmids from candidate colonies were evaluated by diagnostic restriction digest and DNA sequence analysis. Correctly mutated plasmid was used to transform *E. coli* (BL-21 [DE3] pLysS).

#### 5.3.4 *Expression and Purification of the KatG Domains and their Variants*

Expression of the KatG domains and their variants were carried out as previously described in Chapter Two. Isolation of KatG<sup>C</sup> and R484A KatG<sup>C</sup> was carried out as previously described for another catalase-peroxidase [93]. Purification of KatG<sup>N</sup> and Y111A KatG<sup>N</sup> was performed as previously described in Chapter 2, except that the supernatant was diluted 1:2 with 1M NaCl prior to being added to the Ni-NTA resin.

#### 5.3.5 *Domain Mixing and Incubation Procedures*

The concentrations of KatG<sup>N</sup> and Y111A KatG<sup>N</sup> as well as KatG<sup>C</sup> and R484A KatG<sup>C</sup> were determined using molar absorptivities below. Solutions containing KatG<sup>N</sup> and KatG<sup>C</sup> were incubated at 4°C for times ranging from 0 to 48 hours in the presence of 100 mM phosphate buffer, pH 7.0. Following a given incubation time, aliquots were removed, and activity was measured according to the assays described below.

#### 5.3.6 *UV-Visible absorption spectra and activity assays*

Enzyme was reconstituted with 0.95 equivalents of hemin. Reconstituted enzyme solution incubated for 72 hours at 4°C to allow unincorporated heme to precipitate out of solution. The solution was then spun and removed from the precipitated heme. This was to ensure that free heme did not interfere with any spectral or kinetic data. Concentration of reconstituted enzyme was determined using the pyridine hemichrome assay [90]. The

determined concentration was used to convert absorption into molar absorptivity according to Beer's Law. Protein containing heme in the ferrous state was prepared by adding a small (< 10 mg) amount of sodium dithionite to the native enzyme. All spectra were obtained at room temperature on a Shimadzu UV-1601 spectrophotometer (Columbia, MD) with a cell pathlength of 1.0 cm. Catalase and peroxidase activity assays were performed as previously described [80]. Initial velocities were fit to Michaelis-Menten equation by non-linear regression analysis to determine the apparent kinetic parameters. If inhibition was evident for the peroxidase assays, the fitting equation was modified to a general excess substrate dependent inhibition model:

$$V_0/[E]_T = k_{cat}[S]/K_M + [S] + [S]^2/K_N \quad (1)$$

Where  $K_N$  is a macroscopic constant that reflects the ability of the substrate to act as an inhibitor.

### 5.3.7 *Circular Dichroism Spectroscopy (CD)*

All spectra were obtained using 5  $\mu$ M enzyme in 5 mM phosphate (pH 7.0.) Spectra were recorded at 23 °C in a quartz cell (0.5 mm path length) from 250 – 195 nm on a Jasco J-810 spectrophotometer (Tokyo, Japan.) Baseline and analysis were done using Jasco J-720 software.

### 5.3.8 *Magnetic Circular Dichroism Spectroscopy (MCD)*

All ferric and ferrous spectra were obtained using 1.0 and 15  $\mu$ M recombinant proteins, respectively, in 100 mM phosphate buffer, pH 7.0. Enzyme containing ferrous heme was prepared by adding a small amount (<10 mg) of sodium dithionite to the native enzyme. Spectra were recorded at 23 °C in a quartz cell (5.0 mm path length) with 1.4 Tesla magnetic cell holder from 700 – 350 nm on a Jasco J-810 spectrophotometer (Tokyo, Japan). Baseline and analysis were done using Jasco J-720 software.

### 5.3.9 *Electron Paramagnetic Resonance Spectroscopy*

Spectra were recorded using a Bruker EMX instrument equipped with an Oxford ESR 900 cryostat and ITC temperature controller. Additional sample concentration was performed using Amicon Ultra-4 centrifugal filter devices (Beverly, MA.) The settings for the spectrometer were as follows: temperature, 10 K; microwave frequency, 9.38 GHz; microwave power, 0.1 mW; modulation amplitude, 10 G; modulation frequency, 100 kHz; time constant, 655.36 ms; conversion time, 655.36 ms; and receiver gain,  $1.0 \times 10^5$ .

## 5.4 Results

### 5.4.1.1 Spectroscopic Evaluation of Reactivated Y111A KatG<sup>N</sup>

#### 5.4.1.1 Far-UV Circular Dichroism (CD) Spectra of Y111A KatG<sup>N</sup> and R484A KatG<sup>C</sup>

To evaluate the composition of secondary structural features of the stand- alone Y111A KatG<sup>N</sup> and R484A KatG<sup>C</sup>, far-UV CD spectra of the substituted domains were recorded and compared with those of their respective unmodified domains. The CD spectrum of Y111A KatG<sup>N</sup> resembles that of KatG<sup>N</sup> (Figure 5.1). The strong negative signals at around 222 nm and 208 nm represent substantial  $\alpha$ -helical content in the structure, and the strong positive signal at 190 nm is also contributed by  $\alpha$ -helix and potentially some  $\beta$ -sheet. On the other hand, the CD spectrum of R484A KatG<sup>C</sup> reveals a near complete loss of CD signal, consistent with a substantial disruption of secondary structure (Figure 5.2).

### 5.4.2 UV-visible spectroscopy

The heme absorption spectra for ferric Y111A KatG<sup>N</sup> before and after incubation with a single equivalent of KatG<sup>C</sup> are shown in Figure 5.3. In the absence of KatG<sup>C</sup>, the spectrum is clearly that of a hexacoordinate low-spin heme complex similar to that of KatG<sup>N</sup>. Incubation of Y111A KatG<sup>C</sup> resulted in a substantial shift of absorption spectra consistent with the appearance of high-spin species. The spectral characteristics of ferric



Y111A KatG<sup>N</sup> following incubation with KatG<sup>C</sup> bore a strong resemblance to reactivated KatG<sup>N</sup> (Table 5.1).

Reduction of Y111A KatG<sup>N</sup> before its incubation with equimolar KatG<sup>C</sup> produced spectra consistent with the unmodified KatG<sup>N</sup>. Reduction following incubation with KatG<sup>C</sup> also produced similar spectra to KatG<sup>N</sup> following its reactivation with KatG<sup>C</sup> (Figure 5.4). However, in this case there were notable differences (Table 5.2). Primarily, the ferrous Y111A showed a broad Soret band that appeared to contain two peaks, ~427 nm and ~440 nm, corresponding to low-spin and high-spin ferrous heme, respectively. This was confirmed in the  $\beta$  and  $\alpha$  absorption bands (500 – 625 nm). The most intense absorption was observed at 560 nm, but absorption features were also evident at ~530 nm and ~585 nm, consistent with the presence of low-spin and high-spin ferrous heme, respectively.

The separately expressed and isolated C-terminal domain (KatG<sup>C</sup>) does not bind heme or catalyze a reaction directly. Thus, heme spectra cannot be compared for KatG<sup>C</sup> and its variants. However, the influence of KatG<sup>C</sup> or its variants on the absorption spectra of KatG<sup>N</sup> (and its variants) can be compared. Indeed, as shown above, KatG<sup>C</sup> promotes a substantial shift in the heme environment of Y111A KatG<sup>N</sup>. The R484A variant of KatG<sup>C</sup> shows no such ability. Following incubation of either KatG<sup>N</sup> or Y111A KatG<sup>N</sup> with R484A KatG<sup>C</sup>, the Soret band remains at 414 nm. Likewise, absorption due to  $\beta$  and  $\alpha$  bands is clearly indicated at 535 and 570 nm, respectively, and no charge transfer band is observed between 600 and 650 nm (Figure 5.5). All these features are consistent with an exclusively hexacoordinate low-spin heme complex, exactly what

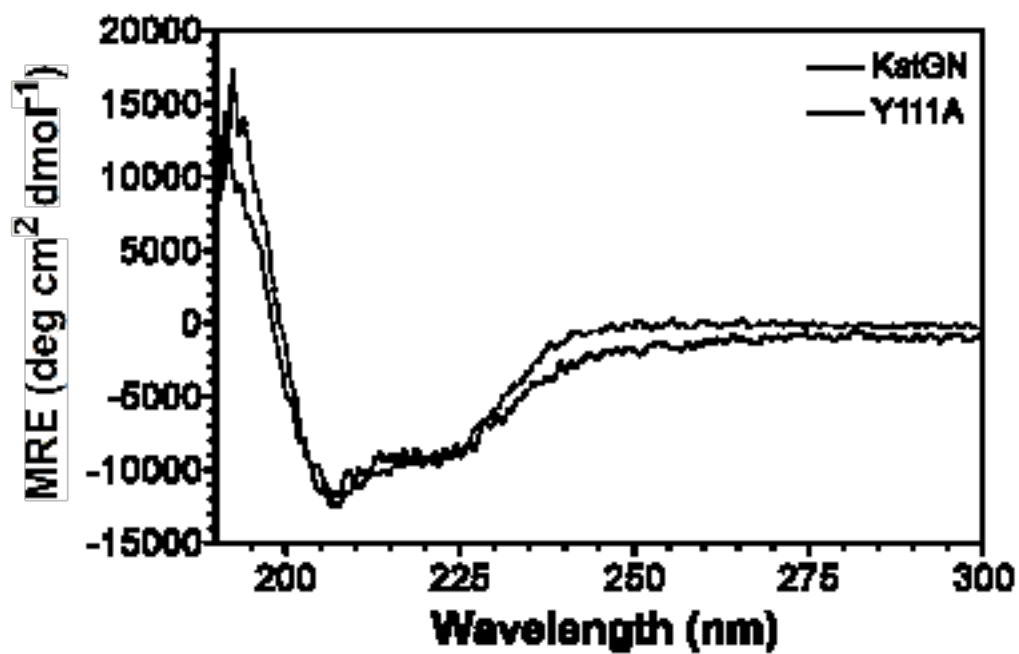


Figure 5.1. Far-UV CD spectra of KatG<sup>N</sup> and Y111A KatG<sup>N</sup>.

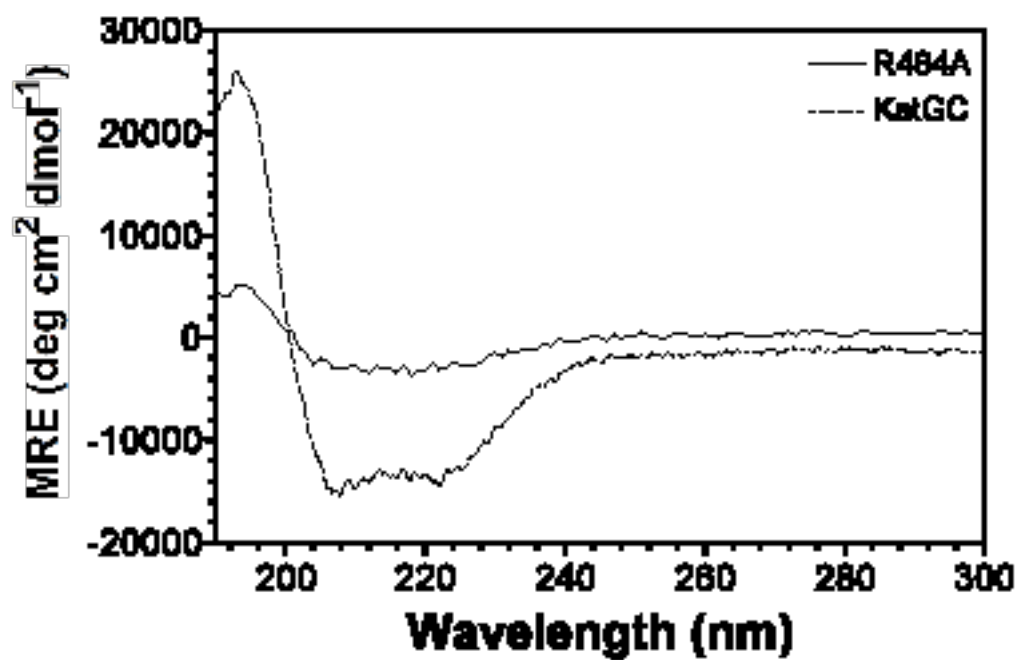


Figure 5.2. Far-UV CD spectra of KatG<sup>C</sup> and R484A KatG<sup>C</sup>.

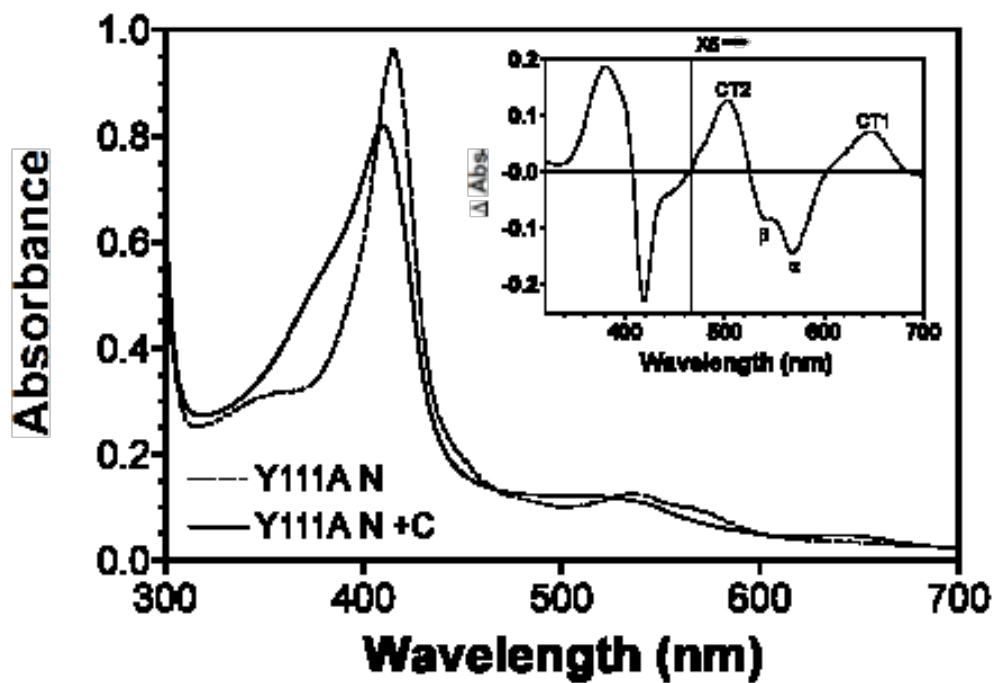


Figure 5.3. UV-visible absorption spectra of ferric Y111A KatG<sup>N</sup> before (dashed line) and after (solid line) incubation with KatG<sup>C</sup>. The difference spectrum (after – before) is shown in the inset.

Domain Variants		Absorption band maxima (nm [ $\text{mM}^{-1} \text{cm}^{-1}$ ])				
N	C	Soret ( $\gamma$ )	$\beta$	$\alpha$	CT2 <sup>b</sup>	CT1 <sup>c</sup>
KatG <sup>N</sup>	KatG <sup>C</sup>	408 (61.4)	----- <sup>d</sup>	-----	507 (7.52)	645 (2.27)
Y111A	KatG <sup>C</sup>	408 (81.0)	-----	-----	508 (13.4)	645 (4.58)
Y111A	R484A	414 (55.4)	533 (8.02)	-----	-----	-----
KatG <sup>N</sup>	R484A	414 (51.8)	534 (8.06)	-----	-----	-----

**Table 5.1.** Ferric spectral features<sup>a</sup> of KatG<sup>N</sup> and Y111A KatG<sup>N</sup> recombined with KatG<sup>C</sup> an R484A KatG<sup>C</sup>.

<sup>a</sup> Phosphate buffer (200mM, pH 7.0) was used for all spectral measurements.

<sup>b</sup> CT2 = short wavelength charge transfer transition (between 490 and 510 nm).

<sup>c</sup> CT1 = long wavelength charge transfer transition (between 600 and 650 nm).

<sup>d</sup> Absorption bands that were not observed were too weak to make definite assignments are indicated by a dash

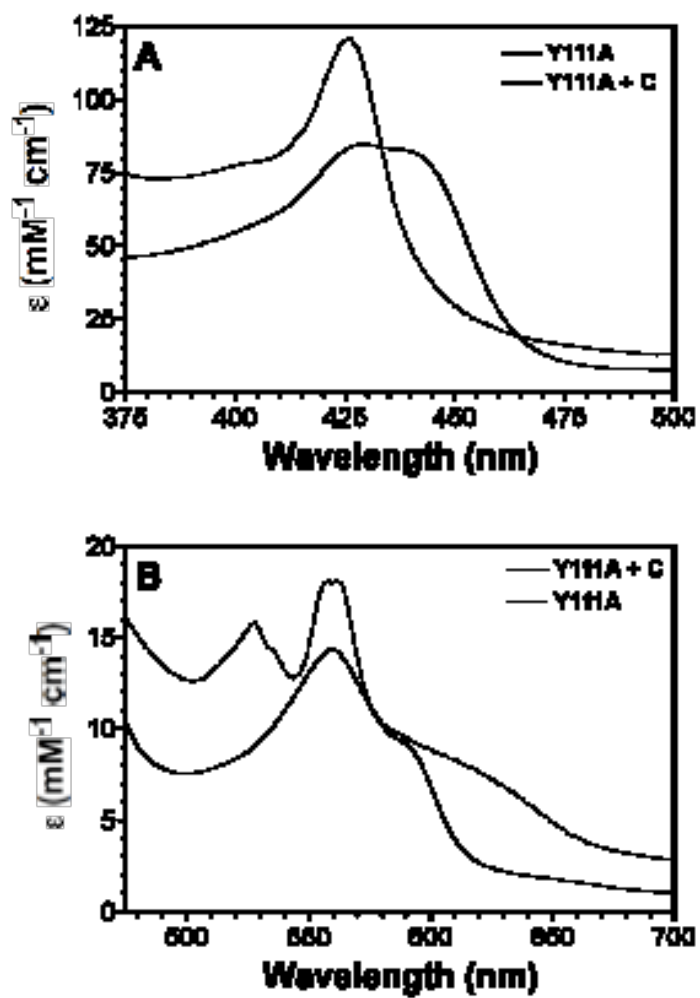


Figure 5.4. UV-visible absorption spectra of ferrous Y111A KatG<sup>N</sup> before (dashed line) and after (solid line) incubation with KatG<sup>C</sup>. The wavelength range corresponding to the Soret ( $\gamma$ ) band (A), as well as the wavelength range of the  $\alpha$ ,  $\beta$ , and charge transfer bands (B) are shown.

Table 5.2. Ferrous spectral features<sup>a</sup> of KatG<sup>N</sup> and Y111A KatG<sup>N</sup> recombined with KatG<sup>C</sup> and R484A KatG<sup>C</sup>.

Domain Variants		Absorption band maxima (nm [mM <sup>-1</sup> cm <sup>-1</sup> ])				
N	C	Soret ( $\gamma$ )	$\beta$	$\alpha$	CT2 <sup>b</sup>	CT1 <sup>c</sup>
KatG <sup>N</sup>	KatG <sup>C</sup>	435 (81.6)	538 (10.1)	568 (12.4)	----- <sup>d</sup>	-----
Y111A	KatG <sup>C</sup>	429 (84.7)	560 (14.4)	580 (9.2)	-----	-----
		440 (82.6)				
Y111A	R484A	427 (59.2)	532 (14.2)	559 (15.8)	-----	-----
KatG <sup>N</sup>	R484A	427 (48.5)	530 (6.75)	559 (9.10)	-----	-----

<sup>a</sup> Phosphate buffer (200mM, pH 7.0) was used for all spectral measurements.

<sup>b</sup> CT2 = short wavelength charge transfer transition (between 490 and 510 nm).

<sup>c</sup> CT1 = long wavelength charge transfer transition (between 600 and 650 nm).

<sup>d</sup> Absorption bands that were not observed were too weak to make definite assignments are indicated by a dash

KatG<sup>N</sup> and Y111A KatG<sup>N</sup> display on their own. The reduced spectra for KatG<sup>N</sup> and Y111A KatG<sup>N</sup> following incubation with R484A KatG<sup>C</sup> confirm these results (Figure 5.6). The Soret absorption at 426 nm, a prominent  $\beta$  band at 530 nm, and a clear  $\alpha$  band at 560 nm, are all features consistent with exclusively hexacoordinate low spin heme.

#### 5.4.3 *Magnetic Circular Dichroism Spectroscopy (MCD)*

Spectra obtained by MCD for the ferrous state more clearly showed the distribution of spin states in Y111A KatG<sup>N</sup> following its incubation with KatG<sup>C</sup> (Figure 5.7). Prior to the addition of KatG<sup>C</sup>, the spectrum was dominated by a derivative feature near 560 nm, indicating an entirely hexacoordinate low-spin complex. Indeed, the position of this feature is most consistent with a bis-histidine coordinated heme. Following incubation with KatG<sup>C</sup>, new features were observed near 440 nm and 590 nm, indicating the presence of high-spin species. Nevertheless, the feature at 560 nm was still present suggesting that a significant population of hexacoordinate low-spin heme remained. When R484A KatG<sup>C</sup> was used in place of KatG<sup>C</sup>, no shift to high spin heme intermediates in Y111A or even unmodified KatG<sup>N</sup> (Figure 5.8).



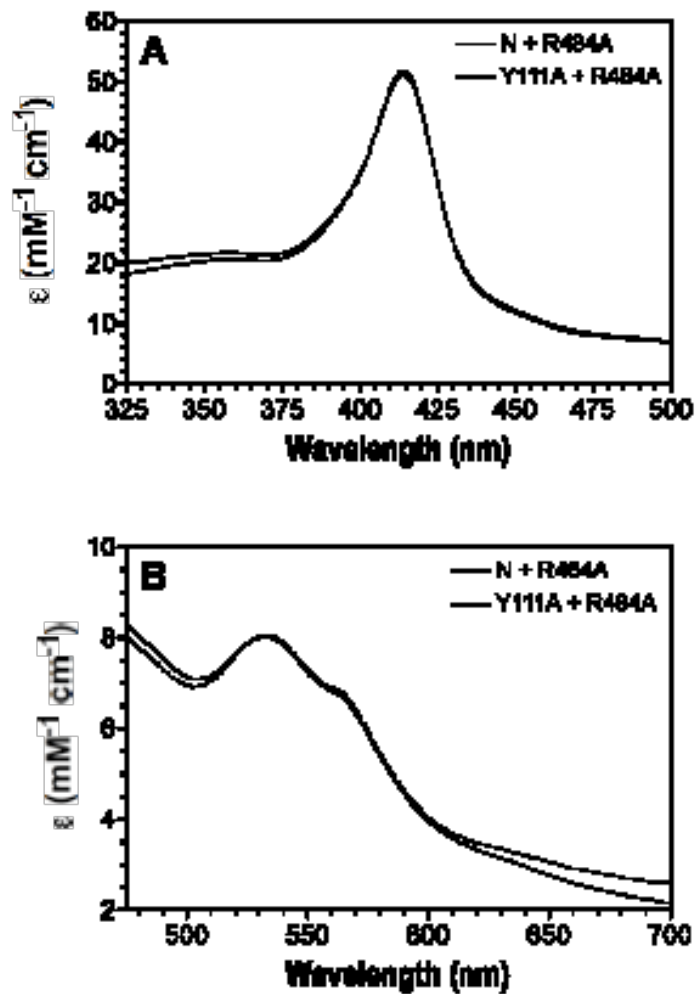


Figure 5.5 UV-visible absorption spectra of ferric KatG<sup>N</sup> (dashed line) and Y111A KatG<sup>N</sup> (solid line) after incubation with R484A KatG<sup>C</sup>. The wavelength range corresponding to the Soret ( $\gamma$ ) band (A), as well as the wavelength range of the  $\alpha$ ,  $\beta$ , and charge transfer bands (B) are shown.

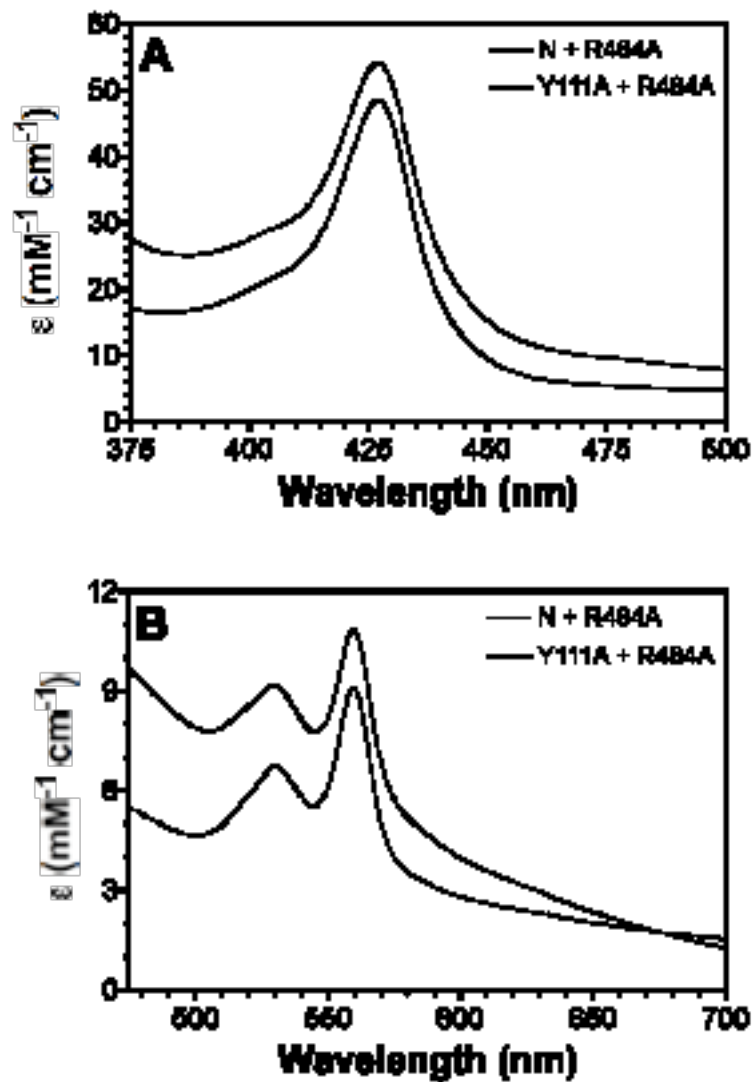


Figure 5.6 UV-visible absorption spectra of ferrous KatG<sup>N</sup> (dashed line) and Y111A KatG<sup>N</sup> (solid line) after incubation with R484A KatG<sup>C</sup>. The wavelength range corresponding to the Soret ( $\gamma$ ) band (A), as well as the wavelength range of the  $\alpha$ ,  $\beta$ , and charge transfer bands (B) are shown.

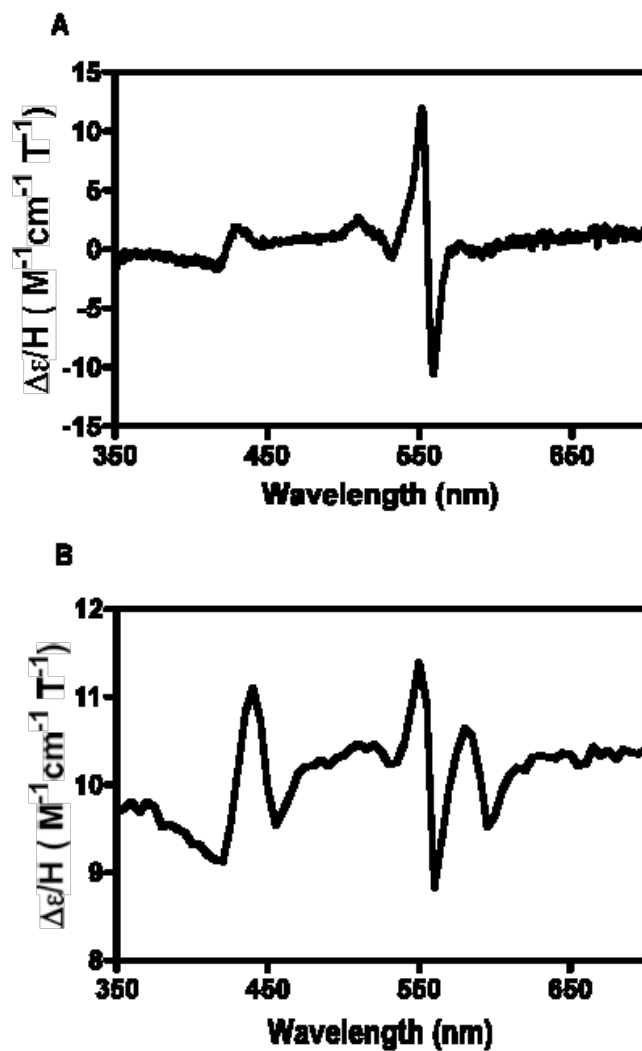


Figure 5.7. Ferrous magnetic circular dichroism (MCD) spectra of Y111A KatG<sup>N</sup>. The MCD spectra were recorded of Y111A KatG<sup>N</sup> (A) immediately following mixture with equimolar KatG<sup>C</sup> and (B) following a 24-hr incubation period at 4°C with equimolar KatG<sup>C</sup>. Domain mixtures were reduced by adding a small amount of dithionite. Spectrometer settings were as described in Materials and Methods.

#### 5.4.4 *Electron paramagnetic resonance (EPR) spectroscopy*

By EPR spectroscopy, the most prominent feature for Y111A KatG<sup>N</sup> following incubation with KatG<sup>C</sup> (Figure 5.9) is the increase in the intensity of high-spin signals. These spectra are highly similar to the EPR spectra for wild type KatG as well as that of KatG<sup>N</sup> following its reactivation by KatG<sup>C</sup>. The contribution of axial ( $g_{\perp} = 5.97$ ;  $g_{\parallel} = 1.99$ ) and rhombic ( $g_x = 6.65$ ;  $g_z = 1.95$ ) species are clearly observed and their distribution appears to be similar to that of KatG<sup>N</sup> following its reactivation by KatG<sup>C</sup>. It should also be noted that spectral components arising from the hexacoordinate low-spin species concomitantly diminish. In contrast, exclusively low-spin signals ( $g = 2.92, 2.27, 1.53$ ) are the significant features for KatG<sup>N</sup> and Y111A KatG<sup>N</sup> following their 24-hour incubation with R484A KatG<sup>C</sup> (Figure 5.10).

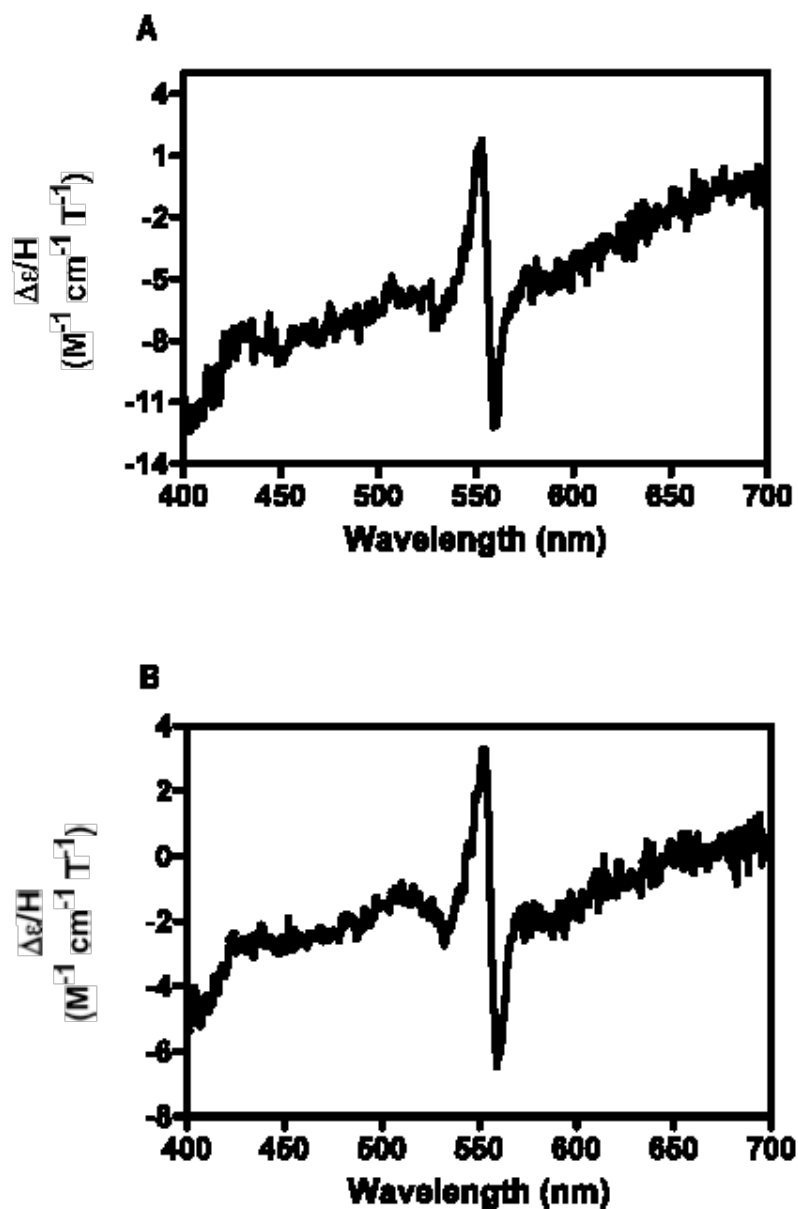


Figure 5.8. Effect of incubation of R484A KatG<sup>C</sup> on the ferrous magnetic circular dichroism (MCD) spectra of Y111A KatG<sup>N</sup>. The MCD spectra were recorded of Y111A KatG<sup>N</sup> (A) immediately following mixture with equimolar R484A KatG<sup>C</sup> and (B) following a 24-hr incubation period at 4°C with equimolar R484A KatG<sup>C</sup>. Domain mixtures were reduced by adding a small amount of dithionite. Spectrometer settings were as described in Materials and Methods.

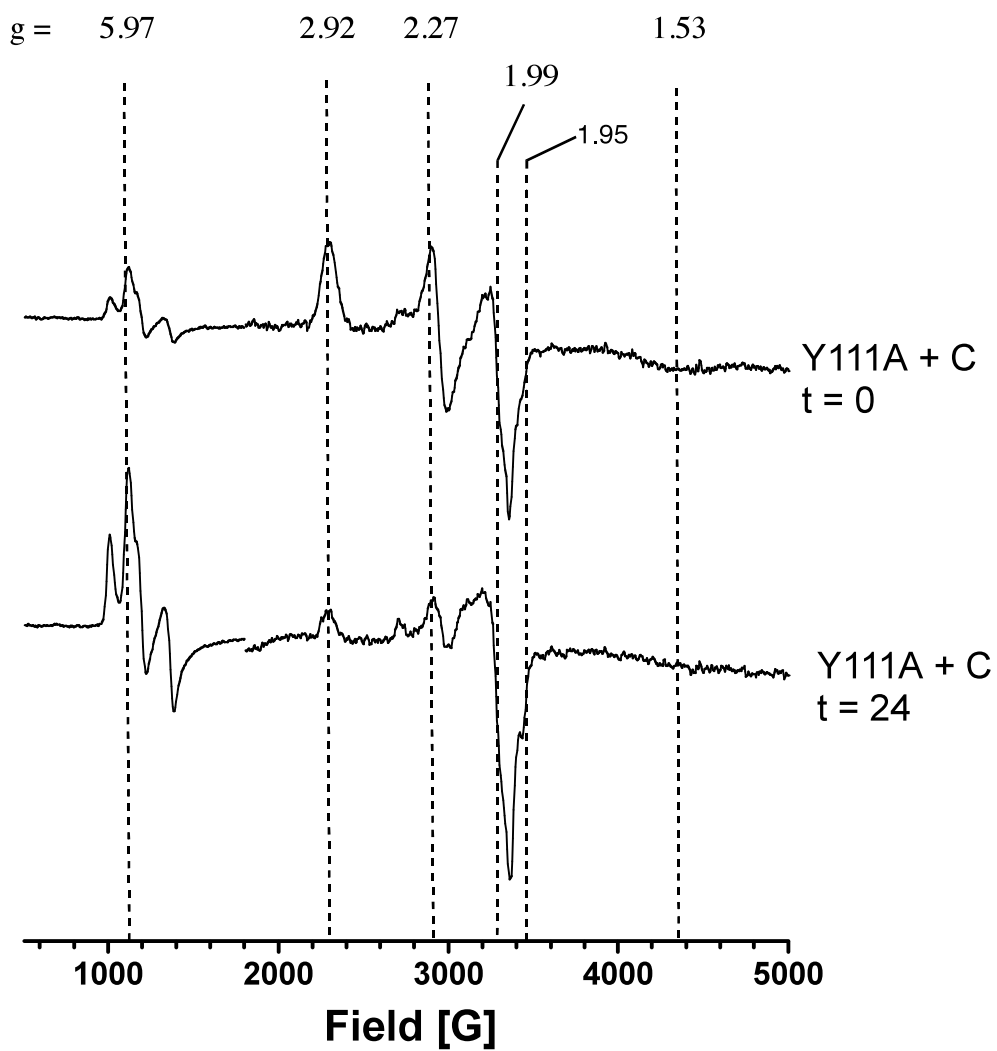


Figure 5.9. EPR Spectra of Y111A KatG<sup>N</sup> recombined with KatG<sup>C</sup>. Spectra were recorded immediately after mixing equimolar amounts of Y111A KatG<sup>N</sup> and KatG<sup>C</sup> and after a 24-hr incubation period at 4°C.

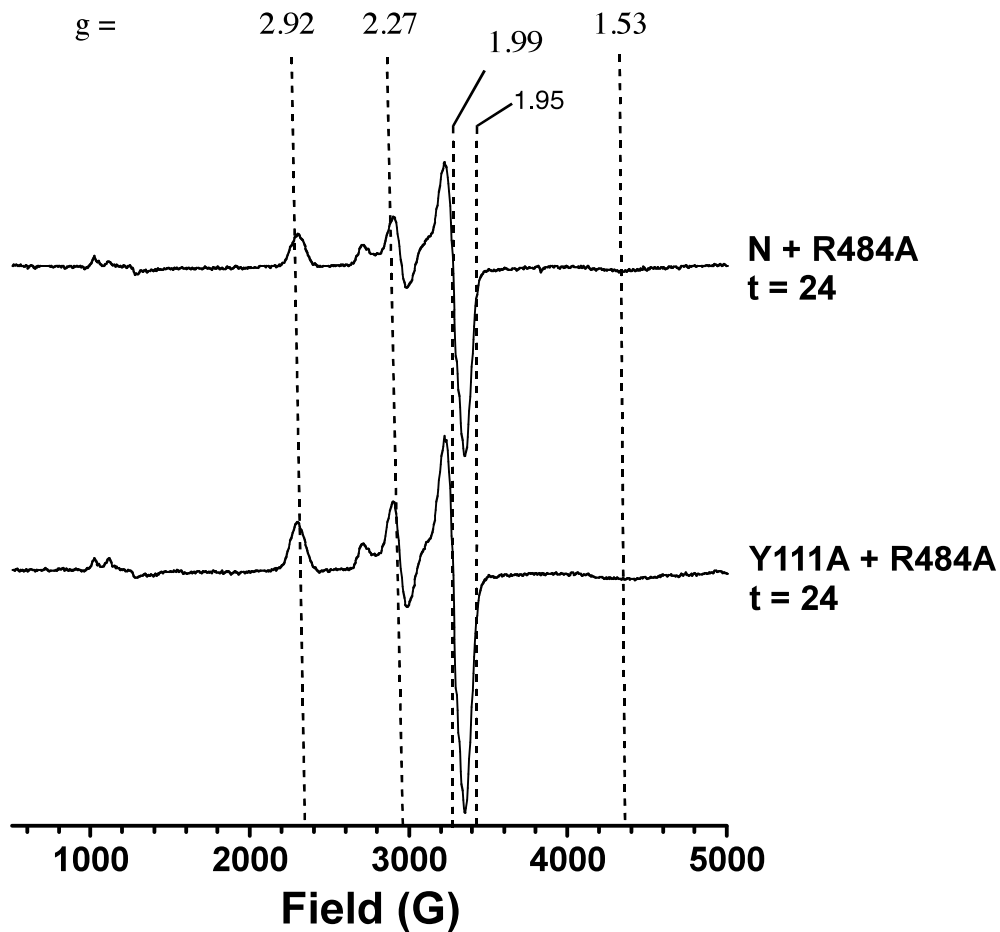


Figure 5.10. EPR Spectra of KatG<sup>N</sup> and Y111A KatG<sup>N</sup> following a 24-hour incubation with R484A KatG<sup>C</sup>. incubation period at 4°C.

#### 5.4.5 Time Course of Y111A KatG<sup>N</sup> Reactivation and Kinetic Parameters of Reactivated Y111A KatG<sup>N</sup>

##### 5.4.5.1 Catalase

Incubation of Y111A KatG<sup>N</sup> with an equimolar concentration of KatG<sup>C</sup> resulted in a return of catalase activity (Figure 5.11). Two phases in catalase reactivation were evident. Fitting the data to a two-exponential equation produced a rate constant ( $k_1$ ) for the initial more rapid phase of  $2.3 \times 10^{-4} \text{ s}^{-1}$  and a second rate constant ( $k_2$ ) of  $1.5 \times 10^{-5} \text{ s}^{-1}$  for the second slower phase. The biphasic behavior was similar to that observed for the reactivation of unmodified KatG<sup>N</sup> by KatG<sup>C</sup> (Table 5.3). The primary difference in the reactivation of Y111A KatG<sup>N</sup> was in the first phase whose rate and amplitude were two- and three-fold smaller than that observed with unmodified KatG<sup>N</sup>, respectively. Most of the activity was recovered in the second slow phase of reactivation. In contrast, KatG<sup>N</sup> catalase recovery by KatG<sup>C</sup> is evenly split between the two phases.

When R484A KatG<sup>C</sup> was used in place of KatG<sup>C</sup> with either KatG<sup>N</sup> or Y111A KatG<sup>N</sup>, a single phase was observed whose rate constants were most similar to the  $k_2$  values obtained from reactivation using unmodified KatG<sup>C</sup> (Table 5.3). Most importantly, in both cases, the extent of activity recovery using R484A KatG<sup>C</sup> (i.e., amplitude) was at least ten-fold lower than reactivations observed with KatG<sup>C</sup> (Figure 5.11).



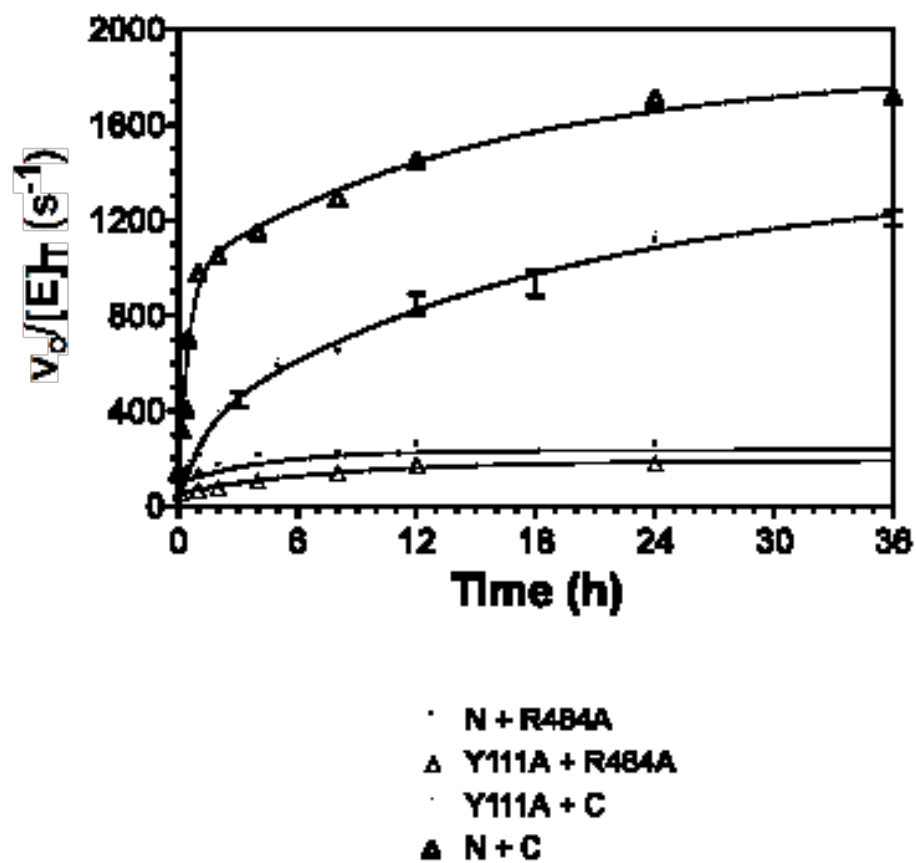


Figure 5.11 Reactivation of KatG<sup>N</sup> and Y111A KatG<sup>N</sup>.

Catalase activities were measured for equimolar mixtures of each domain.

**Table 5.3.** Rate constants and catalase activity recovered for KatG<sup>N</sup> and Y111A KatG<sup>N</sup> paired with KatG<sup>C</sup> and R484A KatG<sup>C</sup>.

Domain Variants		Rate constants (s <sup>-1</sup> )		Amplitudes { $v_o/[E]_T$ (s <sup>-1</sup> )} <sup>a</sup>		
N	C	$k_1$ (s <sup>-1</sup> )	$k_2$ (s <sup>-1</sup> )	$Amp_1$	$Amp_2$	$Amp_T$
KatG <sup>N</sup>	KatG <sup>C</sup>	5.9 x 10 <sup>-4</sup>	1.8 x 10 <sup>-5</sup>	970	870	1840
Y111A	KatG <sup>C</sup>	2.3 x 10 <sup>-4</sup>	1.5 x 10 <sup>-5</sup>	320	1048	1368
Y111A	R484A	-	3.4 x 10 <sup>-5</sup>	-	138	138
KatG <sup>N</sup>	R484A	-	6.0 x 10 <sup>-5</sup>	-	138	138

<sup>a</sup>Amplitudes correspond to catalase activity recovered and are reported as ( $v_o/[E]_T$ ). Amplitude corresponding to  $k_1$  ( $Amp_1$ ) and  $k_2$  ( $Amp_2$ ) are summed to give total recovered catalase activity ( $Amp_T$ ).

The effect of H<sub>2</sub>O<sub>2</sub> concentration on the activity of each of the domain pairs was evaluated (Figure 5.12), and the kinetic parameters for recovered catalase activity were determined (Table 5.4). The  $k_{cat}$  values obtained for the recovered catalase activity of each domain pairing compared well with the total amplitudes of reactivation seen in Figure 5.11. All kinetic parameters for Y111A KatG<sup>N</sup> reactivated by KatG<sup>C</sup> were similar to those obtained from the pairing of unmodified KatG<sup>N</sup> with KatG<sup>C</sup>. The lost activity of domain pairings including R484A KatG<sup>C</sup> was accounted for primarily in the decrease of  $k_{cat}$ , however, an increase in  $K_M$  was observed for KatG<sup>N</sup> when it was incubated in the presence of R484A KatG<sup>C</sup> rather than unmodified KatG<sup>C</sup>.

#### 5.4.5.2 Peroxidase

The time courses for recovery of peroxidase activity by KatG<sup>N</sup> and its Y111A variant in the presence of KatG<sup>C</sup> were highly similar in terms of rate and amplitude (Figure 5.13). It was difficult to distinguish whether the data were best fit by a single exponential or double exponential equation. The values obtained from the single-exponential fit are presented in Table 5.5. The value of  $k$  provides a composite measure of the rate obtained with each domain pairing. It is noteworthy that the value falls between the  $k_1$  and  $k_2$  values observed in the more clearly biphasic processes (see Table 5.3). The amplitudes obtained from the fit of each trace provide a good comparative estimate of activity returned but are likely to be underestimated. The incubation of KatG<sup>N</sup> and Y111A KatG<sup>N</sup> with R484A KatG<sup>C</sup> also produced results similar to one another but clearly distinct from those involving unmodified KatG<sup>C</sup>. The R484A

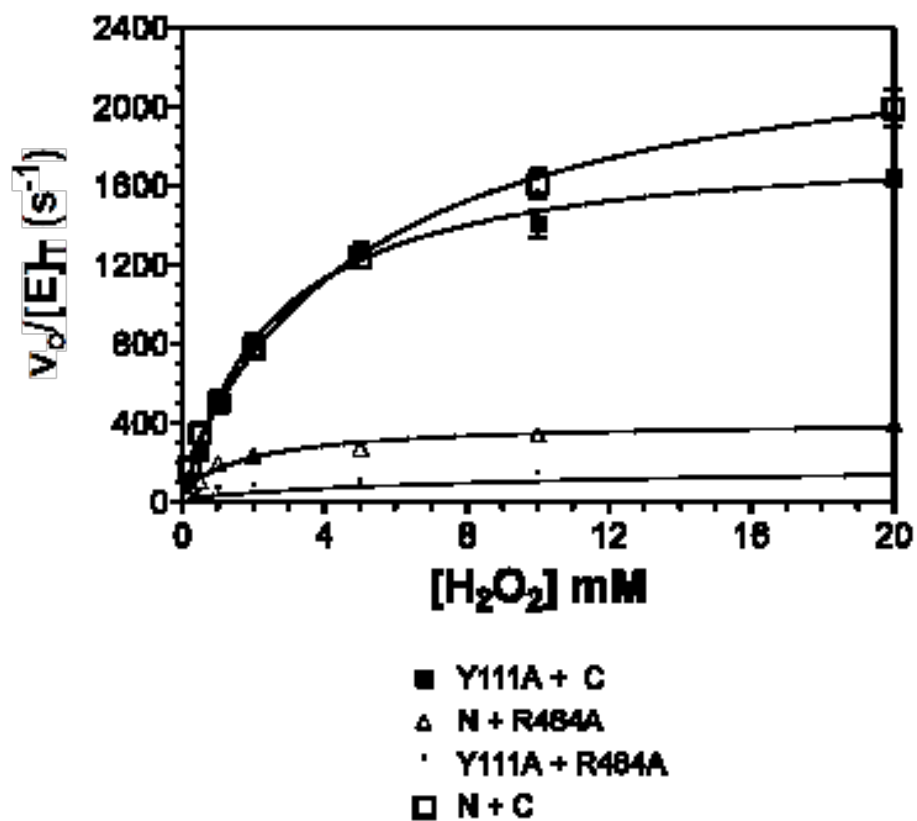


Figure 5.12 Comparison of Catalase Activity of KatG<sup>N</sup> and Y111A KatG<sup>N</sup> after a 24-hr incubation period with the C-terminal domain and the R484A variant with respect to H<sub>2</sub>O<sub>2</sub> as the substrate.

**Table 5.4.** Apparent kinetic parameters for the recovered catalase activity in KatG<sup>N</sup> or Y111A KatG<sup>N</sup> paired with KatG<sup>C</sup> or R484A KatG<sup>C</sup>.

Domain Variants		Catalase kinetic parameters		
N	C	$k_{cat}$ (s <sup>-1</sup> )	$K_M$ (mM H <sub>2</sub> O <sub>2</sub> )	$k_{cat}/K_M$ (M <sup>-1</sup> s <sup>-1</sup> )
KatG <sup>N</sup>	KatG <sup>C</sup>	2312 ± 78	3.9 ± 0.4	5.9 x 10 <sup>5</sup>
Y111A	KatG <sup>C</sup>	1841 ± 51	2.5 ± 0.2	7.4 x 10 <sup>5</sup>
Y111A	R484A	351 ± 17	2.2 ± 0.2	1.6 x 10 <sup>5</sup>
KatG <sup>N</sup>	R484A	178 ± 15	10 ± 2	1.7 x 10 <sup>4</sup>

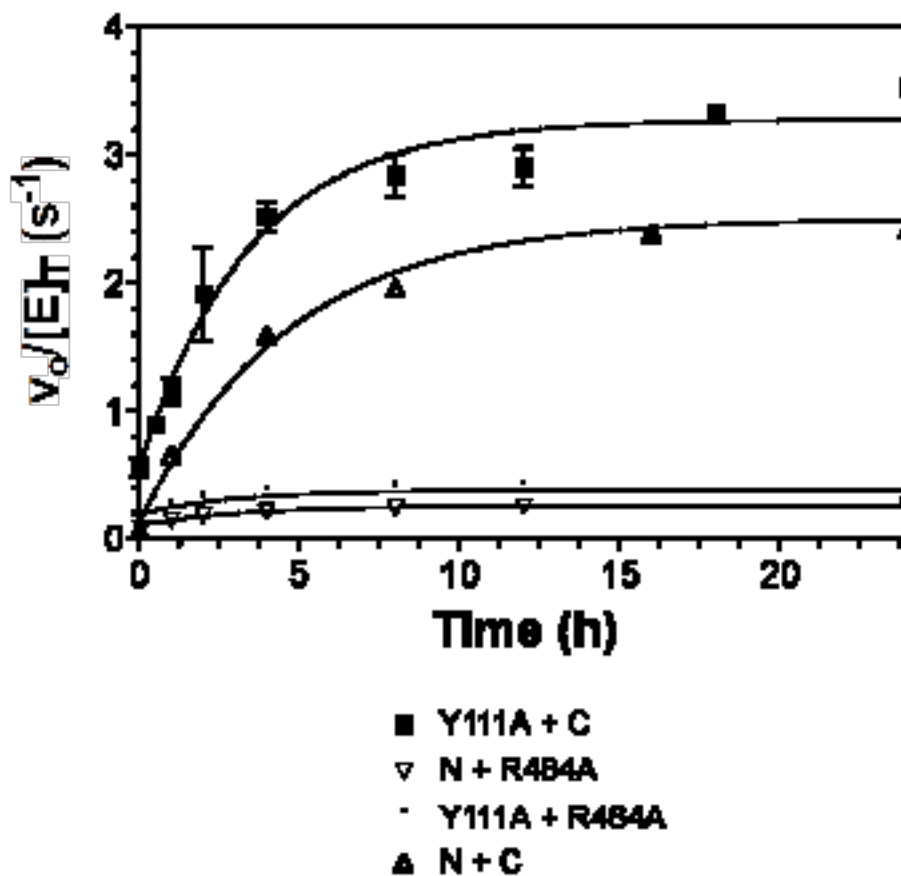


Figure 5.13 Reactivation of KatG<sup>N</sup> and Y111A KatG<sup>N</sup>.

Peroxidase activities were measured for equimolar mixtures of each domain.

**Table 5.5.** Rate constants and activity recovered for the peroxidase restoration in KatG<sup>N</sup> or Y111A KatG<sup>N</sup> paired with KatG<sup>C</sup> or R484A KatG<sup>C</sup>.

Domain Variants		Rate constants (s <sup>-1</sup> )		Amplitudes { $v_o/[E]_T$ (s <sup>-1</sup> )} <sup>a</sup>		
N	C	$k_1$ (s <sup>-1</sup> )	$k_2$ (s <sup>-1</sup> )	$Amp_1$	$Amp_2$	$Amp_T$
KatG <sup>N</sup>	KatG <sup>C</sup>	1.3 x 10 <sup>-4</sup>	4.0 x 10 <sup>-5</sup>	1.50	1.20	2.70
Y111A	KatG <sup>C</sup>	-	8.0 x 10 <sup>-5</sup>	-	2.71	2.71
Y111A	R484A	-	8.9 x 10 <sup>-5</sup>	-	0.15	0.15
KatG <sup>N</sup>	D597R	-	9.5 x 10 <sup>-5</sup>	-	0.19	0.19

<sup>a</sup>Amplitudes correspond to peroxidase activity recovered and are reported as ( $v_o/[E]_T$ ). Amplitude corresponding to  $k_1$  ( $Amp_1$ ) and  $k_2$  ( $Amp_2$ ) are summed to give total recovered peroxidase activity ( $Amp_T$ ).

substitution caused a 10 to 20-fold decrease in activity recovery with very little change in the observed rate as estimated by  $k$ .

The effect of  $\text{H}_2\text{O}_2$  concentration on the peroxidase activity of each of the domain pairs following their incubation together was evaluated (Figure 5.14), and the kinetic parameters for recovered peroxidase activity were compared (Table 5.6). Following its reactivation by  $\text{KatG}^{\text{C}}$ , the peroxidase activity of Y111A  $\text{KatG}^{\text{N}}$  was lower than that of the unmodified  $\text{KatG}^{\text{N}}$  at all  $\text{H}_2\text{O}_2$  concentrations tested. This can be attributed entirely to a  $k_{\text{cat}}$  for Y111A  $\text{KatG}^{\text{N}}$  that was roughly half that of  $\text{KatG}^{\text{N}}$ . The  $K_M$  for hydrogen peroxide and the constant describing  $\text{H}_2\text{O}_2$ -dependent inhibition ( $K_N$ ) were nearly identical for the two activated  $\text{KatG}^{\text{N}}$  proteins. In contrast, the same  $\text{KatG}^{\text{N}}$  variants incubated in the presence of R484A  $\text{KatG}^{\text{C}}$  showed very poor peroxidase activity due again, primarily, to a substantially diminished  $k_{\text{cat}}$  (50 to 100-fold compared with reactivation carried out with unmodified  $\text{KatG}^{\text{C}}$ ).

#### *5.4.5.3 Parallel Comparison of Heme Coordination, Catalase Activity, and Peroxidase Activity During Y111A $\text{KatG}^{\text{N}}$ Reactivation by $\text{KatG}^{\text{C}}$*

Alteration of heme coordination environment can be monitored over time by the MCD signal of the ferric state. Ferric low-spin heme shows a strong derivative-like signal centered near 413 nm. The high-spin ferric heme species show only a weak signal in this wavelength range. In the presence of  $\text{KatG}^{\text{C}}$ , Y111A  $\text{KatG}^{\text{N}}$  shows a loss of the ferric low-spin heme spectrum (Figure 5.15A). The kinetics of the spectral shift much



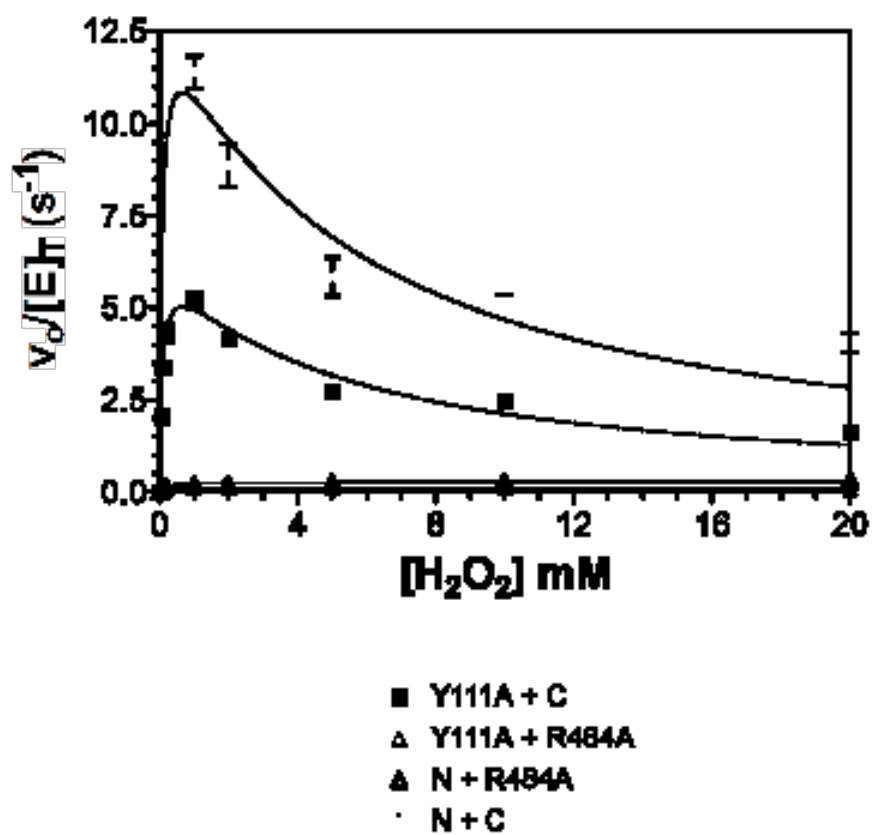


Figure 5.14 Comparison of peroxidase activity of KatG<sup>N</sup> and Y111A KatG<sup>N</sup> after a 24-hr incubation period with KatG<sup>C</sup> and the R484A variant with respect to H<sub>2</sub>O<sub>2</sub> as the substrate.

**Table 5.6.** Apparent kinetic parameters for the recovered peroxidase activity in KatG<sup>N</sup> or Y111A KatG<sup>N</sup> paired with KatG<sup>C</sup> or R484A KatG<sup>C</sup>.

Domain Variants		Peroxidase kinetic parameters			
N	C	$k_{\text{cat}}$ (s <sup>-1</sup> )	$K_M$ (mM H <sub>2</sub> O <sub>2</sub> )	$k_{\text{cat}}/K_M$ (M <sup>-1</sup> s <sup>-1</sup> )	$K_N$ (mM H <sub>2</sub> O <sub>2</sub> )
KatG <sup>N</sup>	KatG <sup>C</sup>	13.6 ± 0.9	0.084 ± 0.02	1.6 x 10 <sup>5</sup>	5.3 ± 0.9
Y111A	KatG <sup>C</sup>	6.4 ± 0.4	0.09 ± 0.01	6.9 x 10 <sup>4</sup>	5.0 ± 0.8
Y111A	R484A	0.28 ± 0.01	0.19 ± 0.03	1.5 x 10 <sup>3</sup>	-
KatG <sup>N</sup>	R484A	0.12 ± 0.03	0.031 ± 0.01	3.9 x 10 <sup>3</sup>	-

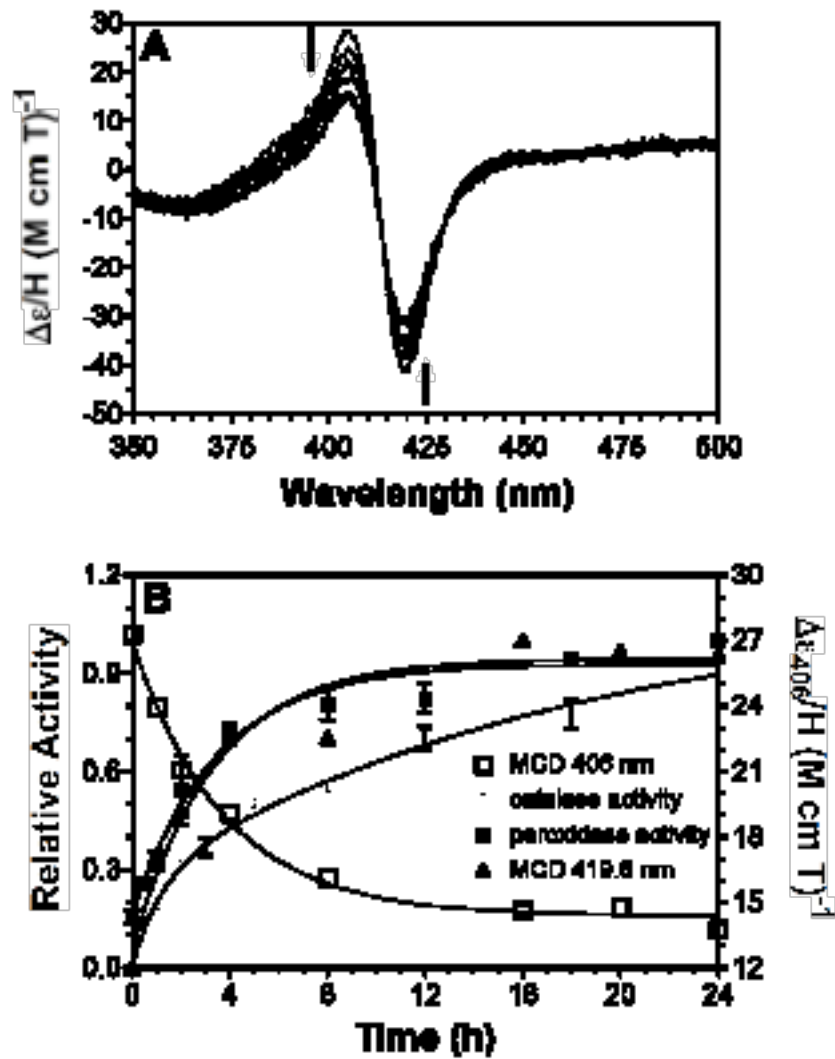


Figure 5.15 (A) Change in the ferric MCD spectrum of Y111A KatG<sup>N</sup> over a 24-hr incubation period with KatG<sup>C</sup>. (B) Comparison of the return of catalase and peroxidase activity for Y111A KatG<sup>N</sup> + KatG<sup>C</sup> with the decrease in low-spin heme monitored by ferric MCD.

more closely mimic the return of peroxidase activity rather than catalase activity (Figure 5.15B). The spectral shift for Y111A KatG<sup>N</sup> is best fit by a single exponential equation with a relatively fast rate constant. In contrast, catalase restoration is biphasic with a majority of activity returning in the slower of the two phases. Thus, it would seem that in the case of Y111A KatG<sup>N</sup> reactivation the shift in coordination environment precedes the return of most catalase activity, but peroxidase activity returns concomitant with the shift in spin state detected by MCD. This is in contrast with restoration of unmodified KatG<sup>N</sup> by KatG<sup>C</sup>. Here MCD spectral shifts are biphasic and the rate constants closely match the biphasic return of catalase activity. Inclusion of R484A KatG<sup>C</sup> in place of the unmodified KatG<sup>C</sup>, produces only negligible shifts in ferric MCD spectra (data not shown) consistent with the minimal return of catalase and peroxidase activities.

## 5.5 Discussion

A series of strictly conserved residues at an interdomain interface in KatG is hypothesized to be critical to the function of an active site over 30 Å away. The ability of the separately expressed and isolated N- and C-terminal KatG domains to associate non-covalently and convert the inactive stand alone N-terminal domain to an active catalase-peroxidase provides for a unique method to probe the structure and function of these interactions. It is an approach that allows for insight into important mechanisms for active site control that cannot be addressed with the intact KatG enzyme. The side chains targeted for substitution for this chapter were Tyr 111 and Arg 484 from the N- and C-

terminal domains, respectively. Both are strictly conserved across all catalase-peroxidases.

Substitution of Arg 484 with alanine (i.e. R484A KatG<sup>C</sup>) resulted in a substantial decrease in KatG<sup>N</sup> reactivation. At best, a ten percent recovery of either catalase or peroxidase activity was observed. Consistent with these results, all spectroscopic measurements of KatG<sup>N</sup> (or its Y111A variant) following incubation with R484A KatG<sup>C</sup> demonstrated dominance of hexacoordinate low-spin heme. The CD spectrum of R484A KatG<sup>C</sup> showed a clear disruption of secondary structural content, suggesting that the compromised ability of the domain to reactivate its partner was due to a globally misfolded domain.

This is interesting in several respects. First, R484 forms part of a motif that is common to both domains of ALL known catalase-peroxidases (RXXDXRGG). This motif forms indistinguishable loop structures in each domain: the BC loop in the N-terminal domain and the B'C' loop in the C-terminal domain. In fact, R484 and R117 (evaluated in Chapters 3 and 4 as R117A and R117D KatG<sup>N</sup>, respectively) are analogous within that consensus (RXXDXR<sub>117/484</sub>GG). As shown in Chapter 3, R117 is essential for KatG<sup>N</sup> reactivation. This appears to be due to local misfolding of the R117A protein rather than the inability to ion pair with D597 per se. The comprehensive structural disruption of R484A KatG<sup>C</sup> would confirm that the BC loop structure is an essential one for each domain. Interestingly, R117 is directed more external to the N-terminal domain, while R484 is oriented more to the interior of the C-terminal domain. This may explain the more comprehensive structural disruption observed in R484A KatG<sup>C</sup> than R117A KatG<sup>N</sup>.

The results with R484A KatG<sup>C</sup> also indicate that KatG<sup>N</sup> is not sufficient to serve as a folding platform for its aberrant KatG<sup>C</sup> partner. The slow biphasic reactivation kinetics observed when KatG<sup>N</sup> encounters KatG<sup>C</sup> suggests that KatG<sup>C</sup> is able to address multiple conformers of its KatG<sup>N</sup> partner. This would be consistent with one of the proposed roles of this “inactive” C-terminal domain. Indeed, it would appear that folding defects in the BC loop (or B’C’ loop) cannot be addressed in either direction.

Substitution of tyrosine 111 clearly affects the reactivation process. As followed by catalase activity, Y111A KatG<sup>N</sup> reactivation by KatG<sup>C</sup> lags behind the unmodified KatG<sup>N</sup>. Biphasic kinetics are still observed, but a decreased rate constant for the first, more rapid phase, and more importantly, a decreased amplitude for that phase account for the difference. The catalase kinetic parameters observed following Y111A KatG<sup>N</sup> reactivation by KatG<sup>C</sup> confirm this conclusion. They indicate a distribution of pentacoordinate and hexacoordinate high spin species similar to the wild type intact KatG as well as KatG<sup>N</sup> following its reactivation by KatG<sup>C</sup>.

A unique feature observed in Y111A KatG<sup>N</sup> reactivation is monophasic shift in MCD spectrum over time. This contrasts with the biphasic return of catalase activity and biphasic shift in MCD spectrum observed with KatG<sup>N</sup>. Notably, the return of peroxidase activity and the shift in MCD spectrum are kinetically indistinguishable from one another but clearly outpace the majority of catalase recovery. This is the first instance where there is a clear difference between the return of catalase activity and the shift in spin-state of the active site heme. The Y111A substitution does appear to marginally slow active site recovery, but the more important effect is observed *after* the shift in heme

coordination environment. A structural change uniquely essential for catalase activity is apparently limited by the Y111A substitution.

There are a couple of likely candidates for such a structural shift. One is that the Y111A substitution impeded efficient crosslink formation between Trp 105, Tyr 226, and Met 252. The W-Y-M crosslink is essential for catalase activity but not for peroxidase activity [75, 76]. A defect in restoring the crosslink would not be observed in MCD spectra nor the return of peroxidase activity. A second possibility is a subtle structural perturbation that slows the correct placement of Arg 426. This arginine is purported to occupy two orientations [134]. The orientation of this residue is affected by, among other things, pH. One orientation of the residue favors peroxidase activity while the other is observed more prominently in catalase active KatG conformations. Structurally, Y111 is in close proximity to this arginine residue, and its absence may decrease the efficiency with which the catalase-active conformation may be achieved. The data in hand do not allow one to distinguish between these two possibilities.

In either case, however, our data show that conserved residues at the interdomain interface not only regulate the “macro” features of active site structure such as the position of the distal histidine as a heme ligand versus an active site base, but also in much more subtle arrangements that contribute to the bifunctional behavior of catalase-peroxidases.

## CHAPTER 6

### DISCUSSION

Although substantial progress has been made in understanding the relationship between a given enzyme structure and its catalytic ability and cellular function, several significant questions remain. What roles do distant and peripheral protein structures have in the catalytic function of enzyme active sites? To what extent do such structures direct catalytic function? What mechanisms are employed to communicate the effects of distant structures to the active site? What is required to introduce new enzyme activities into an existing protein framework? How is this accomplished in nature? How can these mechanisms be duplicated or modified to accomplish the rational redesign of enzymes for new catalytic function? Not only do these unanswered questions impede progress in the fundamentals of protein structure/function, but they also remain under-explored due, in part, to a lack of good models for study. In answer to this, we suggest that catalase-peroxidases (KatGs) offer a unique model to investigate these and other fundamental questions surrounding enzyme structure and catalysis.

Several convergent features make catalase-peroxidases ideal enzyme structure-function models. First, they utilize a single active site to catalyze two mechanistically distinctive reactions, catalase and peroxidase. It is true that the reaction cycles of these



two activities have several common features. However, it is important to remember that, aside from these bifunctional enzymes, the two activities poorly overlap in nature. Typical catalases have poor peroxidase activity, and typical peroxidases have very poor catalase activity. Interestingly, the catalase-peroxidases are clearly distinct and unrelated to all other enzymes known to possess significant catalase activity. There is no discernable sequence homology between typical catalases and the bifunctional enzymes. Furthermore, the global as well as active site structures (other than the presence of heme) bear little resemblance to one another. At the same time, it is abundantly clear that the catalase-peroxidases are derived from proteins that have little or no catalase activity, that is, the monofunctional peroxidases. Indeed, the catalase-peroxidase active site virtually superimposes on those of Class I plant peroxidases (e.g., cytochrome c peroxidase and ascorbate peroxidase) and even bears a strong resemblance to horseradish peroxidase, the canonical plant peroxidase. That being said, the catalase-peroxidases do show some significant differences in protein structure in comparison to the monofunctional peroxidases. The vast majority of these differences are present in catalase-peroxidases and absent in monofunctional peroxidases and lie peripheral to and distant from the catalase-peroxidase active site. The most obvious of these structural differences are two interhelical insertions, one of which participates in an unusual triamino acid crosslink, and a C-terminal domain. Importantly, the Goodwin laboratory has collected evidence that all three of these structures are critical for the full catalytic function of catalase – peroxidases.

### *6.1 Role of the C-terminal domain in Catalase-Peroxidase Structure and Function*

The focus of the research presented in this dissertation is on the C-terminal domain. As mentioned in earlier chapters, this domain has arisen from gene duplication and fusion, assigning a well understood mechanism for its evolutionary origin. This domain no longer has a functioning active site or any heme binding capability, nevertheless the general scaffolding for a peroxidase active site remains. Immediately preceding the research described in this dissertation, two possible accounts could be made for this domain. The first was that the C-terminal domain was a vestigial structure possibly required at one time for function but in the process of being phased out. In support of this hypothesis, the monofunctional peroxidases are purported to have arisen after catalase-peroxidases. Given that none of the other plant peroxidases have two-domain subunit structure, the truncation of the second domain could conceivably be accomplished without loss of function. Against this hypothesis is the conservation of a C-terminal domain across all catalase-peroxidases. This would support the second possibility that the C-terminal domain was essential for catalase-peroxidase function.

In order to begin addressing this question, Ruletha Baker, another member of the laboratory at the time had produced a KatG variant lacking its C-terminal domain. (This protein has been identified as KatG<sup>N</sup> throughout this document.) KatG<sup>N</sup> was expressed in inclusion bodies. It was purified under denaturing conditions, and Dr. Baker demonstrated that the protein could be refolded and reconstituted with heme. These preparations of KatG<sup>N</sup> had neither catalase nor peroxidase activity. Spectroscopic

measurements were consistent with a hexacoordinate low spin complex, and binding of cyanide by the KatG<sup>N</sup> heme was dramatically reduced. Site-directed mutagenesis studies suggested that KatG<sup>N</sup> supplied active site His106 and His 267 as ligands to the heme.

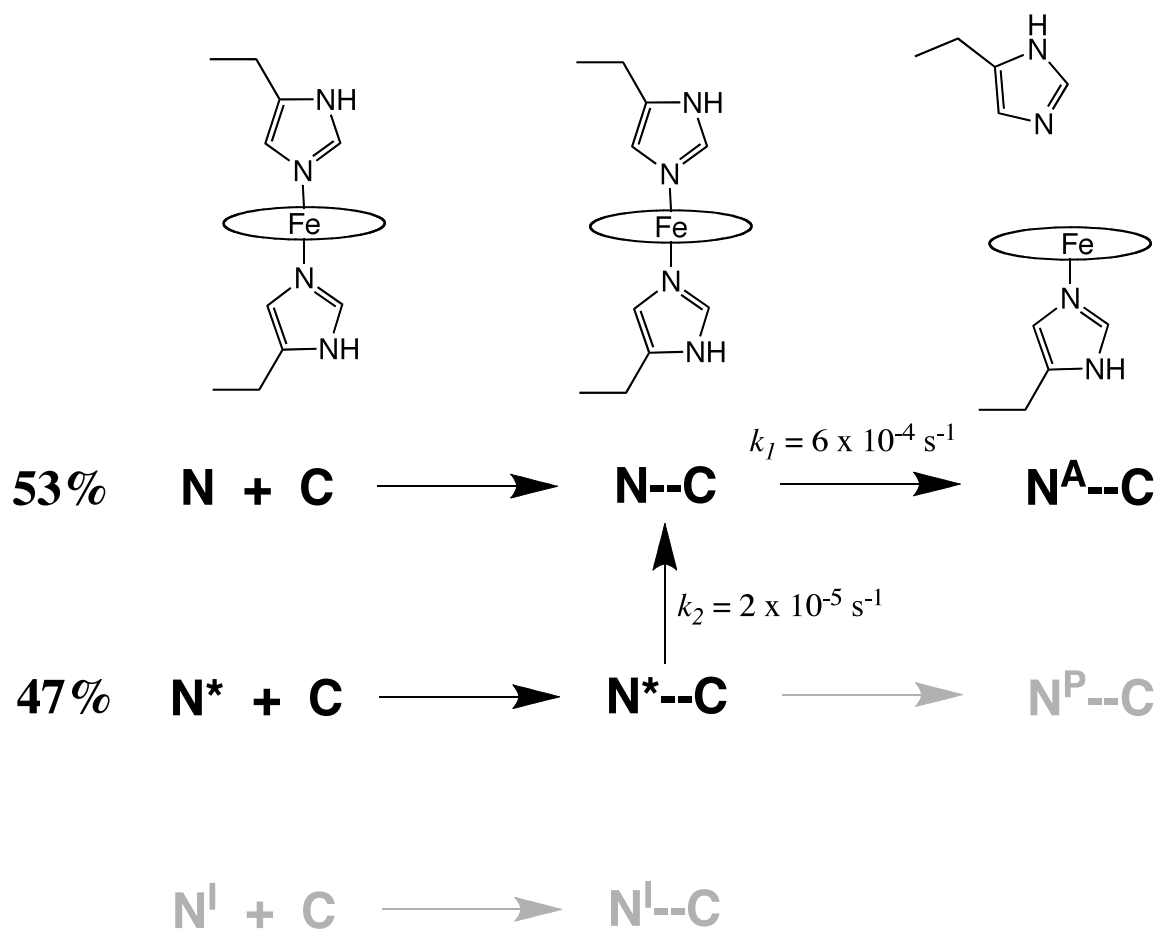
The first step in the research comprising this dissertation was the production of a construct for the expression of the KatG C-terminal domain as a stand-alone protein (KatG<sup>C</sup>). Contrary to KatG<sup>N</sup>, KatG<sup>C</sup> was expressed and isolated in its soluble form. As described in Chapter 2, KatG<sup>C</sup> is able to affect the reactivation of KatG<sup>N</sup>. The restoration of a typical KatG active site as evident from UV-vis and especially EPR spectroscopy was confirmed by the return of peroxidase and catalase activity. The return of catalase activity is particularly significant because amino acid substitutions to KatG have significantly compromised catalase activity, whereas peroxidase activity was not hindered [67-68, 71-72, 81-82, 104-104, 117]. It is clear that the catalase activity is far more sensitive to subtle protein modification than is the peroxidase activity. This seems to highlight the principle that both catalase and peroxidase activities require a common set of components for function, but catalase also requires additional features (e.g., the W-Y-M crosslink). In any case, it is clear that the C-terminal domain is able to direct the correct alignment of ALL of these features from its distant position from the active site. This must be accomplished by way of hydrophobic, hydrogen bonding, and ionic interactions because a covalent linkage between the domains is not critical to the process.

The C-terminal domain makes highly conserved intrasubunit interdomain contacts with the BC loop of the N-terminal domain [86-87, 100-101]. Because the BC loop extends from the B helix, a major part of the KatG active site, these contacts between the BC loop and the C-terminal domain may be necessary for the proper structural integrity

of the heme-dependent active site. Furthermore, the N-terminal domain makes several interactions with the B'C' loop of the C-terminal domain. To determine the roles of these interactions, we have used site-directed mutagenesis to make substitutions to several interdomain residues. The purpose of this dissertation is to determine the effect of these substitutions on the reactivation and the structural integrity of the catalase-peroxidase active site.

Based on the spectroscopic and kinetic measurements of the reactivation process (chapters 2 and 3), a model for reactivation of  $\text{KatG}^{\text{N}}$  by  $\text{KatG}^{\text{C}}$  is proposed (Figure 6.1). For the unmodified  $\text{KatG}^{\text{N}}$  and  $\text{KatG}^{\text{C}}$ , the return of catalase and peroxidase activity occurs on the same time scale. This suggests that restoration of features required for both activities are rate limiting in the process. Moreover, the kinetics of active site restoration as viewed by MCD spectroscopy indicate that either the opening of the coordination sphere (i.e., removal of His 106 as a ligand) or some prior step is rate-determining. This is further supported by the pH dependence of reactivation of the active site. A decrease in pH increases recovery rates (up to a point). The estimated  $\text{pK}_a$  would be consistent with the protonation of a histidine residue which would disfavor its coordination to heme iron, facilitating its removal from the coordination sphere.

One of the more interesting and surprising features of reactivation is its biphasic nature. Each phase accounts for roughly half of the recovered activity, and each phase is rather slow, especially the second phase at  $2 \times 10^{-5} \text{ s}^{-1}$ . Given that changes in active site



Scheme 6.1. Model for reactivation of  $\text{KatG}^{\text{N}}$  in the presence of  $\text{KatG}^{\text{C}}$ .

structure appear rather uniform (i.e., activities return together, isosbestic points in spectroscopic measurements), two phases would appear to arise from the presence of multiple conformations of the N-terminal domain. The first phase involves a conformation accounting for roughly 50% of the  $\text{KatG}^{\text{N}}$  present (shown as N in Scheme 6.1). According to this model, N is readily activated when incubated with  $\text{KatG}^{\text{C}}$ . A complex between the two (N-C) rapidly forms after which the C-terminal domain induces conversion of  $\text{KatG}^{\text{N}}$  to a catalase and peroxidase active state (labeled as  $\text{N}^{\text{A}}$  in Scheme 6.1). The limiting feature of this process could well be that of repositioning of the B-helix to remove His 106 from coordination with the heme iron. The slower phase by activity and spectroscopic changes looks indistinguishable from the first phase except for the substantially slower rate. This suggests a  $\text{KatG}^{\text{N}}$  conformation (labeled as  $\text{N}^*$  in scheme 6.1) that requires a more substantial structural rearrangement before the active coordination environment of the heme can be established.

It is important to point out that although this model accounts for the data currently in hand, other viable models could also be put forward. For example it is possible that in both cases opening the coordination sphere is rate determining, but that the  $\text{N}^*$  conformation impedes  $\text{KatG}^{\text{C}}$ 's ability to affect the change necessary for reactivation. The data are not currently in hand to distinguish these two possibilities. Nevertheless, the data do suggest an intriguing role for the gene duplicated and fused C-terminal domain: a platform able to address multiple errant N-terminal domain conformations and return them to fully active catalytic function.

## 6.2 *Effect of N-terminal Domain substitutions on catalase-peroxidase reactivation*

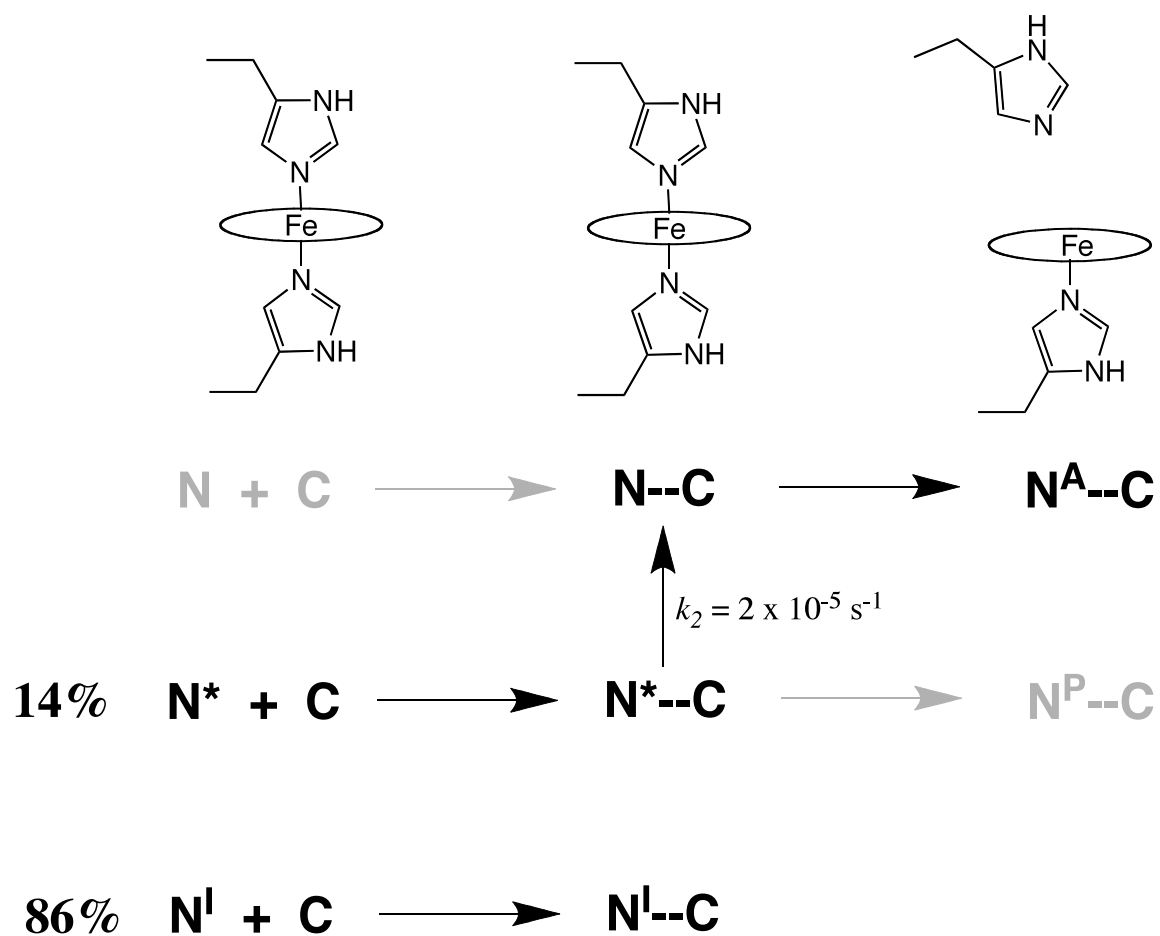
This raises a number of natural follow-up questions. How does the C-terminal domain support N-terminal domain function? What interactions are required? By what mechanisms does the C-terminal domain serve to support the active site? How might gene duplication and fusion be a particularly advantageous way of addressing the needs of the N-terminal domain? The remainder of this dissertation set out to explore such questions. The ability for the separately expressed and isolated KatG domains to interact, leading to active site restoration in the N-terminal domain is a particular advantage. It afforded an opportunity to explore the effect of side-chain substitution by site-directed mutagenesis on the rate and extent of reactivation as well as the catalytic and spectroscopic properties of the reactivated enzymes. Of course, one must always determine which amino acids should be targeted for substitution.

The structures of catalase-peroxidases show a set of intrasubunit interactions between the N- and C-terminal domains. These are particularly compelling for study for at least three reasons. First, the main structure from the N-terminal domain involved at this interdomain interface is the C-terminal end of the B-helix and the subsequent BC loop. It will be remembered that the new His ligand to the heme iron in KatG<sup>N</sup> is His106 which is found on the B-helix. Second, other peroxidases employ mechanisms which support this same structure. Though these mechanisms are dramatically different than a C-terminal domain, their disruption by a number of methods results in similar active site changes as observed for catalase-peroxidases without a C-terminal domain. Third,

residues forming a network of hydrogen bonds at the interface between the KatG N- and C-terminal domains are strictly conserved across all catalase-peroxidases.

One of these residues is Arg 117, part of a strictly conserved motif in catalase-peroxidases (i.e., Y<sub>111</sub>RXXDGR<sub>117</sub>GG<sub>119</sub>). The results presented here indicate that R117 is critical to reactivation, but not by virtue of its interaction with the C-terminal domain *per se*. Substitution of R117 with alanine dramatically diminished reactivation. The rapid phase observed with KatG<sup>N</sup> was replaced by a lag phase silent for changes in activity. The total returned catalase activity was about 10% of that observed for KatG<sup>N</sup> all of which returned in a slow phase following a pronounced lag. These features can be fit onto the model proposed for KatG<sup>N</sup> reactivation according to Scheme 6.2. The majority of R117A KatG<sup>N</sup> was not in a conformation reactivatable by KatG<sup>C</sup>. This is referred to as N<sup>I</sup>. The remaining R117A KatG<sup>N</sup> could only be reactivated slowly, suggesting its conformation was classified more appropriately as N\*. Finally, because conformations that can be rapidly activated are absent for this KatG<sup>N</sup> variant, additional insight may be obtained for activation of more difficult N-terminal domain conformational states. Notably a lag phase is present which would indicate a silent conformational adjustment preceding active site restoration. Interestingly, it would not be possible to observe this for the N\* populations of unmodified KatG<sup>N</sup> reactivation because it would be overshadowed by the rapidly activating fraction (Figure 6.1). Surprisingly, the value of Arg117 is not in its ability to form a salt bridge with Asp597 of the C-terminal domain. KatG<sup>N</sup> reactivation by D597A KatG<sup>C</sup> differs minimally from that observed with unmodified KatG<sup>C</sup> and differs markedly from R117A KatG<sup>N</sup> reactivation by either KatG<sup>C</sup> or its D597A variant.





Scheme 6.2 Proposed mechanism for the reactivation of R117A KatG<sup>N</sup> with KatG<sup>C</sup>

This was further confirmed by the remarkable features of the R117D variant of KatG<sup>N</sup>. At first glance, the rate of reactivation by KatG<sup>C</sup> would seem comparable to R117A KatG<sup>N</sup>. It is relatively slow and relatively little catalase activity is recovered (~30% of that observed for KatG<sup>N</sup>). However, R117D is reactivated in a monophasic process, and most surprisingly, the peroxidase activity of the recovered active site is indistinguishable from KatG<sup>N</sup>, not only in maximum turnover (i.e.,  $k_{\text{cat}}$ ), but also in apparent  $K_M$  and parameters governing substrate-dependent inhibition (i.e.,  $K_N$ ). All of R117D KatG<sup>N</sup> is restored to an active conformation by KatG<sup>C</sup>, but the active site conformation produced is one that substantially limits catalase activity (designated as N<sup>P</sup> in Scheme 6.3). The presence of aspartate at position 117 seems to have two effects. The first is to impede rates (but not extents) of reactivation in comparison to arginine (i.e., unmodified KatG<sup>N</sup>). The second is to influence the conformation of the active site following reactivation as evident from a markedly different EPR spectrum for the reactivated enzyme as well as a shift in favor of peroxidase activity.

Thus, Arg 117 would seem to be optimal for producing N-terminal domain structures that are responsive to the C-terminal domain. A nonpolar residue at this position is highly disruptive in this respect, but a charged residue (even of opposite polarity) is tolerated, albeit with slower responses to the C-terminal domain. More importantly, the conservation of Arg 117 would also seem to be necessary for preserving a fully bifunctional active site. Thus, these data demonstrate that the interdomain interface is not only necessary for ensuring a heme coordination environment for any activity, but also fine-tuning for bifunctionality.

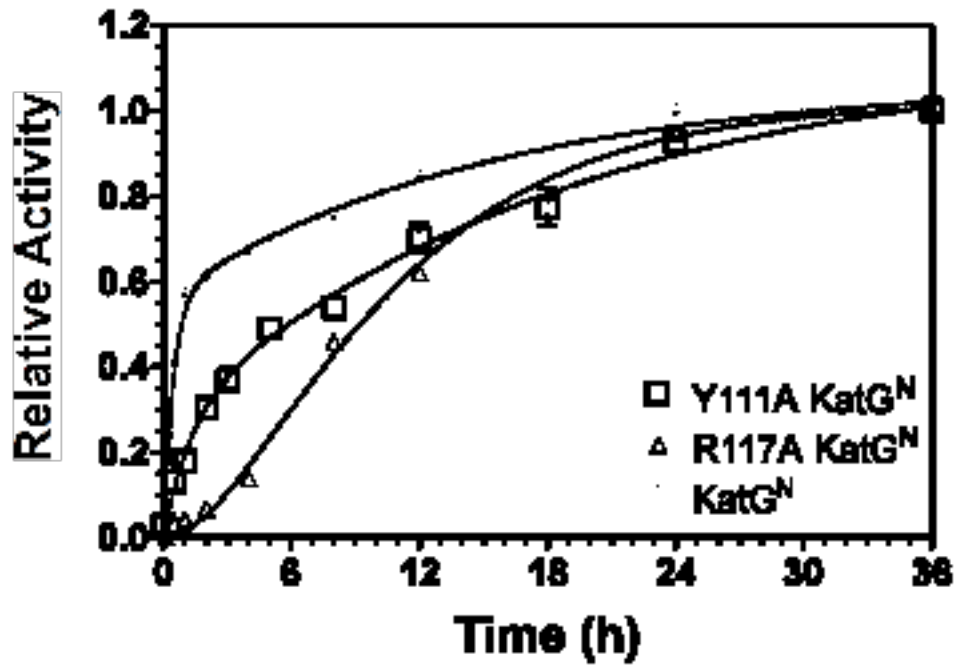
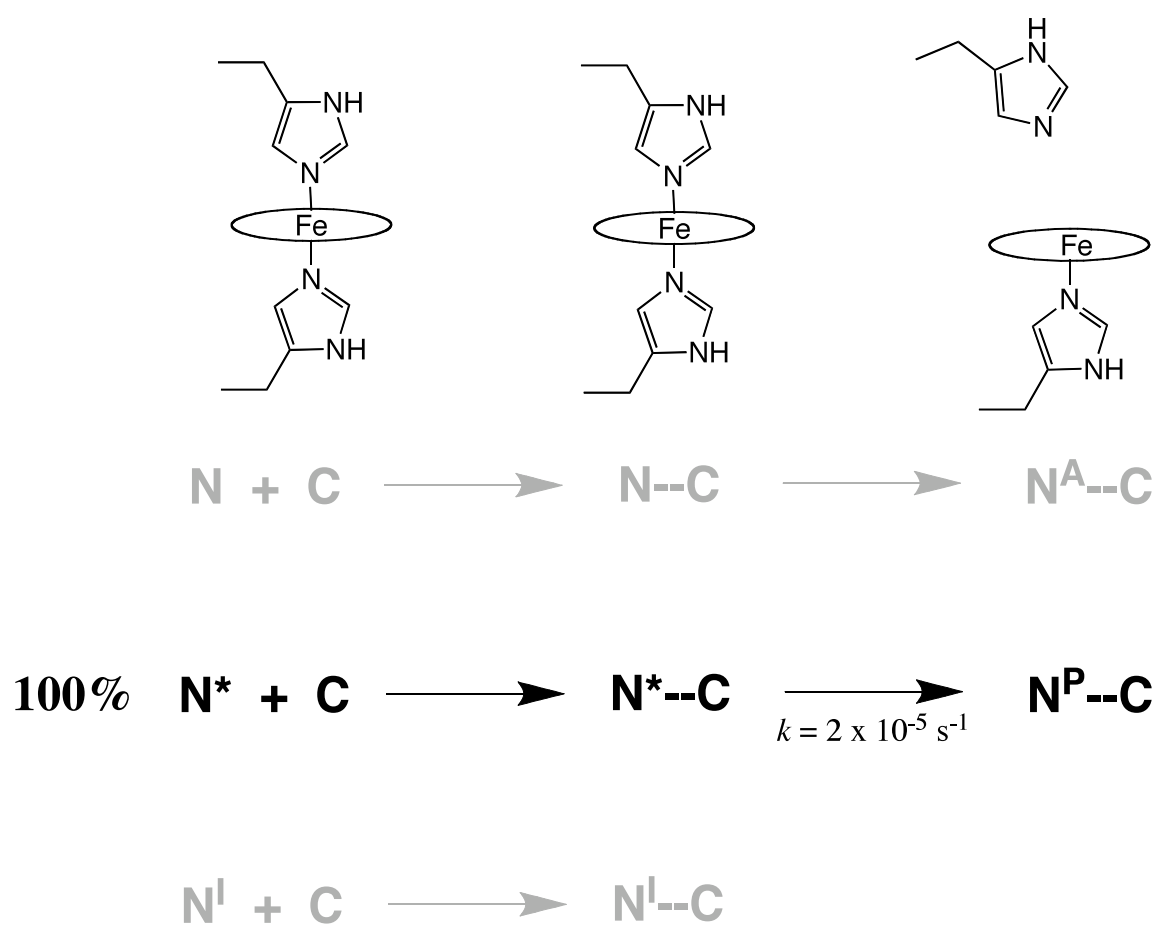


Figure 6.1 Normalized return of catalase activity for KatG<sup>N</sup>, R117A KatG<sup>N</sup>, and Y111A KatG<sup>N</sup> in the presence of KatG<sup>C</sup>. All three display biphasic kinetics in the return of catalase activity, the first phase is “silent” with R117A KatG<sup>N</sup>.

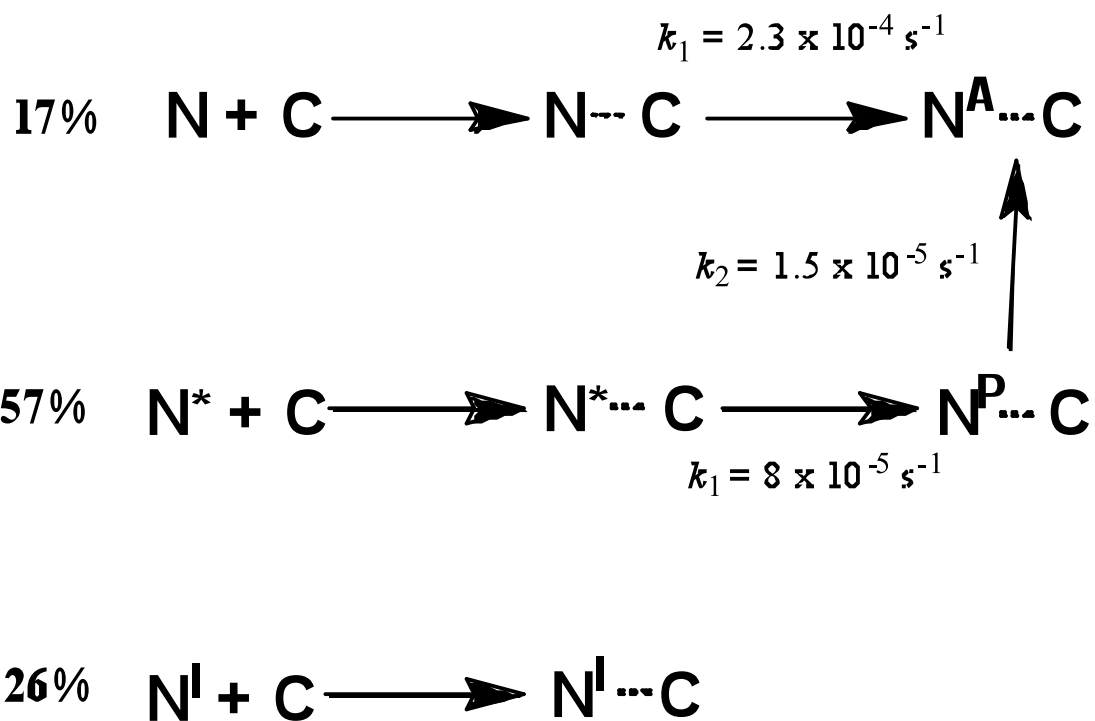
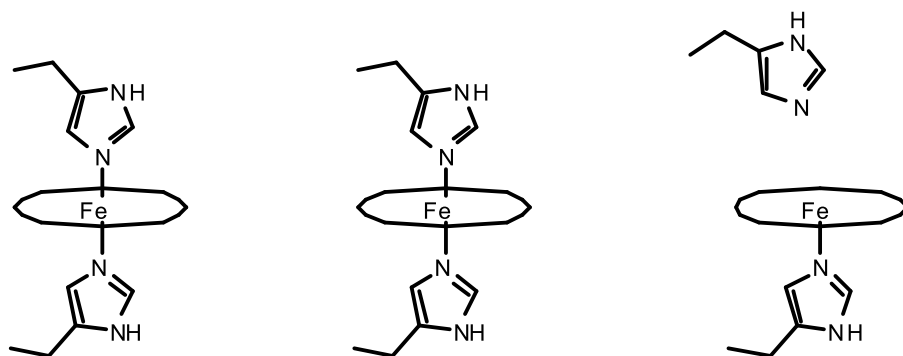


Scheme 6.3. Proposed mechanism for the reactivation of R117D KatG<sup>N</sup> with KatG<sup>C</sup>.

For Y111A KatG<sup>N</sup> catalase activity returns in two phases as observed for KatG<sup>N</sup>. The first phase is somewhat slower and has a three fold lower amplitude than KatG<sup>N</sup>. This would indicate a lower population of easily reactivating conformational states in Y111A KatG<sup>N</sup> (~18%). The majority of Y111A activity appears in a second slower phase, and in one important respect, this compares most closely with R117D KatG<sup>N</sup>: the most striking effect is observed following the opening of the coordination sphere. The majority of recovered catalase activity is observed to lag behind the return of the active site to its high spin state. In contrast to R117D KatG<sup>N</sup>, a majority of catalase activity is eventually recovered (~80%). The return of the high spin heme states as well as peroxidase activity follow virtually identical kinetics to one another. A single phase is observed governed by a rate constant of  $\sim 8 \times 10^{-5} \text{ s}^{-1}$ . For Y111A KatG<sup>N</sup>, the majority of catalase activity returns in a second slower phase with a rate constant ( $1.5 \times 10^{-5} \text{ s}^{-1}$ ) that lags behind the restoration of heme coordination state. This indicates that an active site conformation for peroxidase (indicated as N<sup>P</sup> in Scheme 6.4) is established first and subsequent steps bring catalase-specific element(s) on line. The end result is a reactivated domain with activity comparable to that observed for unmodified KatG<sup>N</sup> in the presence of KatG<sup>C</sup>. What catalase-specific elements lag behind in the activation of the Y111A KatG<sup>N</sup> variant are not known, but one likely possibility is the formation of the unique W-Y-M crosslink.

These studies provide strong evidence that the conserved residues appearing at the interdomain interface are essential in a number of roles in supporting the unique catalytic properties of catalase-peroxidases. Arginine 117 appears as part of a loop whose

*Y 111A KatG<sup>N</sup> + KatG<sup>C</sup>*



Scheme 6.4 Proposed mechanism for the reactivation of Y111A KatG<sup>N</sup> by KatG<sup>C</sup>.

structure appears to be essential for catalytic function. Replacement with a nonpolar residue renders the majority of the N-terminal domain unresponsive to its C-terminal domain partner. Conversion of the alanine at 117 to a negative charge fully restores response to the C-terminal domain, albeit with slower rates of reactivation. However, with the opposite charge at position 117, the active site is unable to support full catalase activity. Substitution of tyrosine 111 impedes formation of structures uniquely necessary for catalase activity, but these appear to be kinetic rather than thermodynamic barriers as near full catalase activity is eventually observed. Importantly, the ability to evaluate the effect of these substitutions in the reactivation of the separately expressed and isolated domains allowed for insight that would not have been possible with the intact catalase-peroxidase enzyme.

### *6.3 Effect of C-terminal domain substitutions on catalase-peroxidase reactivation*

Arginine 117 appears to form an ionic interaction with aspartate 597 which is located on the E' helix of the C-terminal domain. The results presented in this dissertation clearly indicate important roles for Arg 117. Surprisingly, the effects of Arg 117 substitution were not duplicated by Asp 597 substitution, indicating that the functions of Arg 117 do not arise primarily because of the ion pairing interaction. The R117A KatG<sup>N</sup> variant shows minimal reactivation, but D597A KatG<sup>C</sup> is capable of reactivating KatG<sup>N</sup> at the same rates and to the same extent as unmodified KatG<sup>C</sup>. Indeed, there was little discernable difference between the reactivation of R117D KatG<sup>N</sup> by KatG<sup>C</sup> or its D597A variant. It is important to point out, however, that there are some

constraints imposed on position 597. Although a small aliphatic can be tolerated at this position with little discernable effect on the ability of the C-terminal domain to direct KatG<sup>N</sup> reactivation, arginine is clearly not tolerated. The CD spectra recorded for D597R KatG<sup>C</sup> showed substantial disruption of secondary structure and along with this very little ability to reactivate KatG<sup>N</sup>.

This result highlights an important feature of the two-domain structure of catalase-peroxidases. A properly folded stand-alone C-terminal domain is able to address at least some range of N-terminal domain conformers. However, thus far, it appears that KatG<sup>N</sup> has a limited ability in this regard. The results reported for R484A KatG<sup>C</sup> confirm these results. This substitution also resulted in a rather dramatic disruption of C-terminal domain structure. Here again, KatG<sup>N</sup> was not able to restore R484A KatG<sup>C</sup> to a functional state.

The particularly interesting feature of R484 in KatG<sup>C</sup> is its analogous position to R117 in KatG<sup>N</sup>. Both arginines are part of a loop between the second (B) and third (C) helices of a typical peroxidase structure (i.e., the BC loop in N-terminal domain and the B'C' loop of the C-terminal domain). A sequence of RXXDXR<sub>(117/484)</sub>GG is strictly conserved in both domains of all catalase-peroxidases. This is remarkable given the substantial diversification in the domains that appears to have occurred since gene duplication and fusion. The C-terminal domain has since lost its ability to bind heme, and the residues of the former active site necessary for catalysis have been replaced. The N-terminal domain has gained the two large-loop interhelical insertions. It is interesting to note as well that the RXXDXR<sub>117/484</sub>GG motif is absent from all other plant peroxidases, including the closely related Class I enzymes (ascorbate peroxidase and



cytochrome c peroxidase). The data presented here indicate that this motif (in particular R117/484) is essential to proper function of each domain, but apparently for differing reasons.

#### 6.4 *Advancing catalytic function by gene-duplication and fusion*

Gene duplication and fusion has been proposed to contribute to the development of new catalytic function in other enzymes. In order to put the results of this research in a broader context and to understand the role of gene duplication and fusion in catalase-peroxidase catalysis, it is important to consider these other cases.

The eightfold  $\beta/\alpha$  barrel forms the structural scaffold of a vast number of enzymes from transaldolase to ornithine decarboxylase to isocitrate lyase. Indeed, it has been estimated that over 10% of all enzymes have this domain structure [136]. One suggested mechanism for the origin of the eightfold  $\beta/\alpha$  barrel is that these enzymes arose from a series of gene duplication and fusions of  $(\beta/\alpha)_2$  structures, culminating with a fusion of two  $(\beta/\alpha)_4$  structures [137-138]. Current  $(\beta/\alpha)_8$  structures show extensive integration of the two halves into a single cohesive domain structure. Accordingly, it is postulated that the initial gene duplication and fusion was succeeded by a series of modifications leading to an ancestral  $(\beta/\alpha)_8$  protein. Subsequent gene duplication (but not fusion) of the ancestral  $(\beta/\alpha)_8$  enzyme and subsequent divergence gave rise to the broad spectrum of  $(\beta/\alpha)_8$  proteins currently known [139]. In this respect the role of gene duplication and fusion in the development of  $(\beta/\alpha)_8$  enzymes is distinct from catalase-peroxidases. In the  $(\beta/\alpha)_8$  proteins, most if not all of the components derived from gene

duplication and fusion contribute directly to the function of the active site because the active site is located at the C-terminal ends of the  $\beta$ -strands [139]. In catalase-peroxidases gene duplication and fusion produced a structure separated by a considerable distance from the active site.

Another example is provided in the pyridoxal phosphate-independent aspartate racemase (AspR). Here gene duplication and fusion of an  $\alpha/\beta$  structure (not a  $[\beta/\alpha]_8$  barrel) has generated active site symmetry to catalyze the reversible racemization of D- and L- aspartate [141]. Each domain contributes a single cysteine to the active site that acts as a general acid/general base [140]. The domains remain considerably less integrated than in the  $(\beta/\alpha)_8$  enzymes, and in this respect is more similar to catalase-peroxidase enzymes [140]. Indeed, the C-terminal domain of *Pyrococcus horikoshii* AspR can be separately expressed as a soluble protein [141]. Once again, however, each domain contributes one of the catalytic cysteine residues to the active site. This is distinct from the “inactive” C-terminal domain of catalase-peroxidases.

A group of arginine kinases (AK) are distinct in their size (80 kD) and structure, both of which result from gene duplication and fusion [142-144]. The typical AK is a 40 kD monomeric enzyme. The contribution of each of the domains to AK activity has been difficult to assess and the subject of some controversy. For AK from *Ensis directus* (razor clam) the intact protein is expressed in a soluble and active form, but neither domain is soluble when expressed on its own [145]. However, expression of each domain fused to NusA is soluble and enterokinase cleavage of each domain from the NusA tag leaves each domain in a soluble form [145]. Strikingly, the soluble N-terminal domain has no activity, but the soluble C-terminal domain has full AK activity [145]. A

two-domain AK from a deep-sea clam (*Calymene kaikoi*) showed activity in both domains, but the N-terminal domain was considerably less active than the C-terminal domain, and it is apparent that N-terminal domain activity and stability is heavily dependent on the C-terminal domain [146].

This, in many respects, bears a strong resemblance to the function of gene duplication and fusion in catalase-peroxidases. However, there are distinct differences evident. The first is that in the two-domain AKs, both domains have the necessary side chains for activity in each domain's active site. In the catalase-peroxidases, the C-terminal domain has the scaffold of an active site, but none of the residues essential for heme binding or catalysis are present. The catalase-peroxidase C-terminal domain could never be regarded as an active stand-alone enzyme. Along these lines, it is interesting to note that the majority of AK enzymes are actually monomeric 40 kD enzymes. Clearly, activity is not predicated on gene duplication and fusion. Nevertheless, it is an event that has occurred independently in the AKs of four separate groups of organisms. In the case of catalase-peroxidases, there are similar monomeric single domain enzymes, typical peroxidases. However, this cannot be regarded in the same light as AK enzymes. In the catalase-peroxidases, gene duplication and fusion coincides with a clear distinction in function from the monomeric single domain enzymes (i.e., catalase activity).

Finally, bacterial luciferase provides an instructive comparison. The functional enzyme is a heterodimeric protein with an  $\alpha$  and a  $\beta$  subunit. Each subunit has a  $(\beta/\alpha)_8$  fold, and the two are virtually superimposable on one another [147]. A rather high level of sequence identity between the structures indicates a gene duplication event. The most striking structural difference between the two is the presence of about 25 amino acids in a

flexible loop in the  $\alpha$  subunit that are absent in the  $\beta$  subunit [147]. Interestingly, it is the  $\alpha$  subunit that contains the functioning active site, but the  $\alpha$  subunit is inactive unless the  $\beta$  subunit is also present [148]. The  $\beta$  subunit is inactive and, in the absence of the  $\alpha$  subunit, can dimerize to form  $\beta_2$  dimers [148]. Indeed, the interface between the  $\alpha$  and  $\beta$  subunits in luciferase is separate from the  $\alpha$  subunit active site [147]. In almost every respect, the luciferase protein system is analogous to catalase-peroxidase except that in nature the two subunits remain as separate polypeptides. There has been gene duplication, but fusion has not been observed. Interestingly, the fusion of the luciferase  $\alpha$  and  $\beta$  subunits has been accomplished artificially, generating active two-domain luciferase enzymes [157].

#### *6.5 Catalase-peroxidases: Novel roles for gene duplication and fusion in advancing catalytic function.*

While there are substantial similarities with the examples noted above (particularly in arginine kinases and luciferase), in catalase-peroxidases it appears that gene duplication and fusion has been applied for a unique outcome. First, in the context of the plant peroxidases, the C-terminal domain fulfills a role that is addressed by much more simple mechanisms in other enzymes of the family.

A histidine is required as a general base for catalysis. Without it, hydrogen peroxide cannot be deprotonated to assist in the heterolytic cleavage of the O-O bond [135]. Peroxidases and catalase-peroxidases are both inactivated by the substitution of this histidine [73-74, 156]. In order to fulfill its catalytic function, this distal histidine

( $\epsilon\text{N}$ ) must be poised  $\sim 5 \text{ \AA}$  above and perpendicular the plane of the heme. The problem is that imidazoles are highly favorable toward coordination of iron. One need look no further than the proximal side of the heme in the peroxidases to observe this, and there are abundant examples of bis-histidine coordinated hemes in nature. Typical plant peroxidases use a strategically placed calcium coordination site to support the pentacoordinate active site environment and prevent alteration of the B-helix to allow distal histidine coordination to the heme. In the fungal peroxidases, displacement of this calcium (by chelators or site-directed mutagenesis) results in formation of the inactive bis-histidine coordinated heme [158, 159, 108, 62]. The spectroscopic and catalytic properties of these proteins are highly similar to those of  $\text{KatG}^{\text{N}}$ . In the Class III plant peroxidases like horseradish peroxidase and peanut peroxidase, the loss of calcium is much less dramatic [108], but this is only because the coordination of calcium is backed up by a disulfide bond that provides additional support to the B-helix and BC loop [63].

One of the key points of contact between the two domains of the catalase-peroxidase involves the BC-loop of the N-terminal domain. The absence of the C-terminal domain produces similar effects as the fungal peroxidases lacking the critical calcium atom. As has been amply demonstrated in this dissertation, the addition of separately expressed and isolated C-terminal domain effectively reverses inactivation. The inactive bis-histidine coordinated low-spin heme is replaced by high spin species that show substantial catalase and peroxidase activities.

The ability of other peroxidase enzymes to address this fundamental structural requirement with a simple calcium-binding site (and in some cases a disulfide bridge), suggests a broader role for the C-terminal domain in catalase-peroxidases. The results of

the research described here indicate side chains at the interdomain interface (separated by a considerable distance from the active site) are integral for the bifunctional catalytic ability that is the hallmark of these enzymes. Substitution of side chains at this interface result in selectively diminished catalase activity (R117D), and diminished rates for establishing structures uniquely required for catalase activity (Y111A). However, the R117A substitution resulted in a conformation that yielded no substantially reduced return of catalase or peroxidase activities.

A third function accomplished by gene duplication and fusion is the provision of a cofactor-independent folding platform for the active-site bearing domain. The loss of catalytic and heme binding function following the duplication event has produced a remarkably robust and stable protein. The separately expressed and isolated C-terminal domain is soluble, highly stable, and does not depend on a cofactor for correct folding. Indeed, a crystal structure for the *E. coli* catalase-peroxidase C-terminal domain has been determined [118]. Conversely, the *E. coli* N-terminal domain enzyme is resistant to all attempts at crystallization, and therefore, a structure has yet to be successfully solved. As the Goodwin laboratory has observed, catalase-peroxidase variants lacking a C-terminal domain are expressed in inclusion bodies. Upon purification under denaturing conditions, refolding, and reconstitution, a structure approximating the N-terminal domain of intact KatG can be obtained. From here the addition of the C-terminal domain as a separate protein is sufficient to result in conversion of the N-terminal domain to a catalase- and peroxidase-active state. Indeed, the kinetics of the C-terminal domain-driven reactivation of KatG<sup>N</sup> uncovered in this research indicates that multiple

conformational states are present and manipulated by the C-terminal domain to an active state observed in wild type KatG.

In this respect two requirements must be met for the C-terminal domain to function in this role. First, the N-terminal domain must occupy conformational states that can be addressed by the C-terminal domain, and second, the C-terminal domain must maintain a conformation complementary to the N-terminal domain.

#### *6.6 Impact of gene duplication and fusion on catalase-peroxidase reactivation*

Catalase-peroxidases, along with cytochrome *c* peroxidase and ascorbate peroxidase, belong to Class I of the plant, bacterial and fungal peroxidase superfamily. A 230-residue long homologous region exists in all of Class I peroxidase family members. This conserved region exists in both domains of catalase-peroxidases [78]. This makes catalase-peroxidases the only subclass of peroxidases that exists as duplicates of the ancestral peroxidase gene. All structurally significant parts of the peroxidase gene were conserved in the duplicated C-terminal domain due to the fact that when separately expressed and isolated, it is a soluble protein. It is believed that natural selection protected the second copy of the ancestral peroxidase gene from random mutagenesis after duplication until the process of fusion developed it to function as the C-terminal half of catalase-peroxidases [78].

It is widely accepted that the evolution of catalase-peroxidases was a single gene duplication event in the common peroxidase ancestry line. Duplication of genes is the most important mechanism by which new genes are created that lead to enhancing the

structural and functional properties as compared to the original protein. Catalase-peroxidase evolution provided a second, perhaps more efficient mechanism by which organisms can eliminate toxic reactive oxygen species from their environment. This enhancement of function was accompanied by loss and gain of certain structural elements. The gene-duplicated C-terminal domain copy lost its ability to bind heme or catalyze any discernable reaction. However, the N-terminal domain derived from the ancestral gene gained certain structural features that are absent in monofunctional peroxidases that imparted catalase activity to KatGs. This makes catalase-peroxidases unique from their fellow class I peroxidase superfamily members such as cytochrome c peroxidase. Catalase-peroxidases are two-domain homodimers with one active site that catalyze two distinctive reaction pathways. Therefore, gene duplication is the major mechanism by which new genes are developed to give rise to enhanced or novel structural and functional protein properties.

The time lapse between the duplication event and the fusion event in catalase-peroxidases is not known. However, because the C-terminal domain has retained more than half of the sequence homology as its ancestral gene, it can be assumed that the fusion event occurred immediately after duplication or almost simultaneously as duplication. It is clear that the fusion of these two domains is necessary in order for the C-terminal half to contribute to the bifunctionality of KatGs because the separately expressed and isolated KatG<sup>C</sup> has no apparent catalytic function. This contribution appears to be in the form of controlling substrate access to the active site by serving as a structural support scaffold for the N-terminal domain loops and insertions near the active site that control substrate access to the heme pocket.



It has been determined by the work presented in this dissertation that the gene duplicated C-terminal domain serves in a structural support role to impart bifunctionality to the KatG active site. It has also been shown that the structural stability of the BC loop in the N-terminal domain and that of the B'C' loop in the C-terminal domain is modulated by interdomain arginine residues (R117 and R484). Because catalase peroxidases exist as dimers, the intersubunit residues should also be examined to determine their role in stabilizing catalytically significant peripheral structures. In addition, the crystal structure of KatG<sup>C</sup> shows it lost its ability to bind heme and no longer has an active site [118]. The residues that once comprised the active site's catalytic triad were replaced by mainly hydrophobic residues as a result of the gene duplication and fusion event. The new role for this duplicated domain is to act as a structural support scaffold. Therefore, further research should be done to use this domain as a scaffold to engineer new hemoprotein catalysts which includes restoring the ancestral peroxidase activity to KatG<sup>C</sup> to support the gene duplication theory.

In conclusion, the C-terminal domain of catalase-peroxidases is essential for its catalase and peroxidase activity. The two-domain structure of KatGs evolved from gene duplication and fusion. Both genes undergo changes during these evolutionary processes: the N-terminal domain gains peripheral structures and associations (i.e., interhelical insertions and covalent crosslink) that its peroxidatic predecessor gene does not provide, which are necessary for imparting catalase activity. On the other hand, the C-terminal domain has lost the active site residue architecture that is necessary for heme-binding so that it can perform its new functions that include supporting the new peripheral structures gained by the N-terminal domain that are essential for controlling active site access and

acting as a folding platform. In order for both gene duplicated domains to perform their new KatG roles, there are certain residues in the interdomain space that must be present. The two arginine residues that reside on the BC loop of the N-terminal domain (R117) and the B'C' loop of the C-terminal domain (R484) are essential for these two loops to synergistically support the N-terminal domain's catalytically essential peripheral structures.

## REFERENCES

1. R.E. Huie and P. Neta, Chemistry of Reactive Oxygen Species, in *Reactive Oxygen Species in Biological Systems*, D.L. Gilbert and C.A. Colton (Ed. D.), Kluwer Academic/Plenum Publishers, New York, 1999, pp. 33.
2. M. K. Eberhardt, Basic Chemistry of Radicals, in *Reactive Oxygen Metabolites: Chemical and Medical Consequences*, CRC Press, Boca Raton, FL, 2001, pp. 14-15.
3. A.O. Allen, *The Radiation Chemistry of Water and Aqueous Solutions*, Van Nostrand-Reinhold, Princeton, N.J., 1969.
4. I.G. Draganic and Z.D. Draganic, *The Radiation Chemistry of Water*, Academic Press, New York, 1979.
5. R.M. Sellers and M.G. Simic, Pulse radiolysis study of the reactions of some reduced metal ions with molecular oxygen in aqueous solution, *J. Am. Chem. Soc.*, 98, 1976, pp. 6145.
6. D.H. Flint, J.F. Tuminello, and M.H. Emptage, The inactivation of Fe-S cluster containing hydrolyases by superoxide, *J. Biol. Chem.*, 268(22), 1993, pp. 369.
7. C.F. Kou, T. Mashino, and I. Fridovich, a,b-Dihydroxy isovalerate dehydratase; a superoxide-sensitive enzyme, *J. Biol. Chem.*, 262, 1987, pp. 4724.
8. P.R. Gardner and I. Fridovich, Superoxide sensitivity of the *Escherichia coli* 6-phosphogluconate dehydratase, *J. Biol. Chem.*, 266, 1991, pp. 1478.
9. P.R. Gardner and I. Fridovich, Superoxide sensitivity of the *Escherichia coli* aconitase, *J. Biol. Chem.*, 266(19), 1991, pp. 328.
10. S.A. Woods, S.D. Schwartzbach, and J.R. Guest, Two biochemically distinct classes of fumarase in *Escherichia coli*, *Biochim. Biophys. Acta*, 954, 1988, pp. 14.

11. D. H. Flint, M. H. Emptage, and J.R. Guest, Fumarase A from *Escherichia coli*: purification and characterization as an iron-sulfur cluster containing enzyme, *Biochemistry*, 31, 1992, pp. 10331.
12. S.I. Liochev and I. Fridovich, Modulation of the fumarases of *Escherichia coli* in response to oxidative stress, *Arch. Biochem. Biophys.*, 301, 1993, pp. 379.
13. P.R. Gardner and I. Fridovich, Quinolinate synthasae: The oxygen-sensitive site of de novo NAD<sup>+</sup> biosynthesis, *Arch. Biochem. Biophys.*, 284, 1991, pp. 106.
14. J.S. Beckman, T.W. Beckman, J. Chen, P.A. Marshall, and B.A. Freeman, Apparent hydroxyl radical production by peroxynitrite: Implications for endothelial injury from nitric oxide and superoxide, *Proc. Natl. Acad. Sci. USA* 87, 1990, pp. 1620.
15. J.M. McCord and I. Fridovich, The reduction of cytochrome c by milk xanthine oxidase, *J. Biol. Chem.*, 243, 1968, pp. 5753.
16. J.M. McCord and I. Fridovich, Superoxide dismutase: An enzyme function for erythrocyte hemocuprein (hemocuprein), *J. Biol. Chem.*, 244, 1969, pp. 6049.
17. S.K. Nelson, S.K. Bose, and J.M. McCord, The toxicity of high-dose superoxide dismutase suggests that superoxide can both initiate and terminate lipid peroxidation in the reperfused heart, *Free Radical Biol. Med.* 16, 1994, pp. 195.
18. S.B. Farr, R. D'Arin, D. Touati, Oxygen-dependent mutagenesis in *Escherichia coli* lacking superoxide dismutase, *Proc. Natl. Acad. Sci. USA*, 83, 1986, pp. 8268.
19. A. Carlouz and D. Touati, Isolation of superoxide dismutase mutants in *Escherichia coli*: is superoxide dismutase necessary for aerobic life?, *EMBO J.* 5, 1986, pp. 623.
20. D.R. Rosen, T. Siddique, D. Patterson, et al., Mutations in Cu/Zn superoxide dismutase gene are associated with familial amyotrophic lateral sclerosis, *Nature*, 362, 1993, pp. 59.
21. M.E. Gurney, H. Pu, A.Y. Chiu, et al., Motor neuron degeneration in mice that express a human Cu/Zn superoxide dismutase mutation, *Science* 264, 1994, pp. 1772.
22. W. Robberecht, P. Sapp, M.K. Viaene, et al., Cu/Zn superoxide dismutase activity in familial and sporadic amyotrophic lateral sclerosis, *J. Neurochem.* 63, 1994, pp. 384.

23. Y. Kono and I. Fridovich, Superoxide radical inhibits catalase, *J. Biol. Chem.* 257, 1982, pp. 5751.
24. D. Metodiewa and H.B. Dunford, The reactions of horseradish peroxidase, lactoperoxidase and myeloperoxidase with enzymatically generated superoxide, *Arch. Biochem. Biophys.* 272, 1989, pp. 245.
25. O. Loew, *US Dept of Agriculture Reports* 65, 1900, pp. 5.
26. P. Nicholls, I. Fita, and P.C. Loewen, Enzymology and structure of the catalases in *Advances in Inorganic Chemistry* Volume 51, Academic Press, New York, 2001, pp. 52.
27. M.M. Whitaker, V.V. Barynin, S.V. Antonyuk, J.W. Whittaker, The oxidized (3, 3) state of manganese catalase: comparison of enzymes from *Thermus thermophilus* and *Lactobacillus plantarum*, *Biochemistry* 38, 1999, pp. 9126.
28. M.M. Whitaker, V.V. Barynin, S.V. Antonyuk, J.W. Whittaker, Outer sphere mutagenesis of *Lactobacillus plantarum* manganese catalase disrupts the cluster core, *Eur J. Biochem.* 270, 2003, pp. 1102-1116.
29. M. Zamocky, P.G. Furtmuller, and C. Obinger, Evolution of catalases from bacteria to humans, *Antioxidants and Redox Signaling* 10(9), 2008, pp. 1539-1542.
30. C. Teutloff, K-O Schafer, S. Sinnecker, V. Barynin, R. Bittl, K. Wieghardt, F. Lendzian, and W. Lubitz, High-field EPR investigations of Mn(III)Mn(IV) and Mn(II)Mn(III) states of dimanganese catalase and related model systems, *Magn. Reson. Chem.* 43, 2005, S51-S64.
31. M.G. Klotz, G.R. Klassen, and P.C. Loewen, Phylogenetic relationships among prokaryotic and eukaryotic catalases, *Mol. Biol. Evol.* 14, 1997, pp. 951.
32. S. Shigeoka, T. Ishikawa, M. Tamoi, Y. Miyagawa, T. Takeda, Y. Yabuta, and K. Yoshimura, Regulation and function of ascorbate peroxidase isoenzymes, *J. Exp. Bot.* 53, 2002, pp. 1305-1319.
33. K. Asada, The role of ascorbate peroxidase and monodehydroascorbate reductase in H<sub>2</sub>O<sub>2</sub> scavenging in plants, In *Oxidative Stress and the Molecular Biology of Antioxidant Defences* (J.G. Scandalios, ed), Cold Spring Harbor Laboratory Press, Cold Spring Harbor, NY, 1997, pp. 715-735.
34. C.F. Schonbein, Ueber die Katalytische Wirksamkeit organischer Materien und deren Vebretung in der Pflanzen-und Thierwelt, *J. Prakt. Chem.* 98, 1863, pp. 323-344.

35. G. Linossier, Contribution a l'etude des ferments oxidants, Sur la peroxidase du pups, *C. R. Soc. Biol, Paris* 50, 1898, pp. 373-375.
36. G.C. Mills, Hemoglobin catabolism: glutathione peroxidase, an erythrocyte enzyme which protects hemoglobin from oxidative breakdown, *J. Biol. Chem.* 229, 1957, pp. 189-197.
37. M. Maiorino, F. Ursini, V. Bosello, S. Toppo, S.C. Tosatto, P. Mauri, K. Becker, A. Roveri, C. Bulato, L. Benazzi, A. De Palma, and L. Flohe, The thioredoxin specificity of Drosophila GPx: a paradigm for a peroxiredoxin-like mechanism of many glutathione peroxidases, *J. Mol. Biol.* 365, 2007, pp. 1033-1046.
38. O. Epp, R. Ladenstein and A. Wendel, The refined structure of the selenoenzyme glutathione peroxidase at 0.2-nm resolution, *Eur. J. Biochem.* 133, 1983, pp. 51-69.
39. S.C.E. Tosatto, V. Bosello, F. Fogolari, P. Mauri, A. Roveri, S. Toppo, L. Flohe, F. Ursini, and M. Maiorino, The catalytic site of glutathione peroxidase, *Antiox. Redox. Signal.* 10, 2008, pp. 1515-1525.
40. F. Ursini, M. Maiorino, R. Brigelius-Flohe, K.D. Augman, A. Roveri, D. Schomburg, and L. Flohe, Diversity of glutathione peroxidases, *Methods Enzymol.* 252, 1995, pp. 38-53.
41. F. Passardi, G. Theiler, M. Zamocky, C. Cosio, N. Rouhier, F. Teixeira, M. Margis-Pinheiro, V. Ioannidis, C. Penel, L. Falquet, and C. Dunand, PeroxiBase: the peroxidase database, *Phytochemistry* 68, 2007, pp. 1605-1611.
42. L. Flohe, W.A. Gunzler and H.H. Schock, Glutathione peroxidase: a selenoenzyme. *FEBS LETT* 32, 1973, pp. 132-134.
43. K.G. Welinder, Superfamily of plant, fungal, and bacterial peroxidases, *Curr. Opin. Struct. Biol.* 222, 1992, pp. 388-393.
44. M.J. Davies, C.L. Hawkins, D.I. Pattison, and M.D. Rees, Mammalian Heme Peroxidases: From molecular mechanisms to healthy implications, *Antioxidants and Redox Signaling* 10(7), 2008, pp. 1199-1234.
45. P.J. O'Brien, Peroxidases, *Chemico-Biological Interactions* 129, 2000, pp. 113-119.
46. T.J. Fiedler, C.A. Davey, and R.E. Fenna, X-ray crystal structure and characterization of halide-binding sites of human myeloperoxidase at 1.8 Å resolution, *J. Biol. Chem.* 275, 2000, pp. 11964-11971.

47. P.G. Furtmuller, M. Zederbauer, W. Jantschko, J. Helm, M. Bogner, C. Jakopitsch, and C. Obinger, Active site structure and catalytic mechanisms of human peroxidases, *Arch. Biochem. Biophys.* 445, 2006, pp. 199-213.
48. J. Zeng and R.E. Fenna, X-ray crystal structure of canine myeloperoxidase at 3 Å resolution, *J. Mol. Biol.* 226, 1992, pp. 185-207.
49. T.L. Poulos and J. Kraut, The stereochemistry of peroxidase catalysis, *J. Biol. Chem.* 255, 1980, pp. 8199-8205.
50. T.L. Poulos, Heme enzyme crystal structures, *Adv. Inorg. Biochem.* 7, 1988, pp. 1-36.
51. T.L. Poulos and R.E. Fenna in: *Metals in Biological Systems*, H. Siegel, ed., Marcel Dekker, New York, Vol. 30, 1994, pp. 25-75.
52. A. Hochman in *Plant Peroxidases, Biochemistry and Physiology*, K.G. Welinder, S.K. Rasmussen, C. Penel, and J. Greppin, eds., University of Geneva, Geneva, 1993, pp. 103-112.
53. N. Effolk, Cytochrome *c* Peroxidase. 1. Preparation of the Crystalline Enzyme from Baker's Yeast, *Acta Chem. Scand.* 21, 1967, pp. 175-181.
54. M. Sivaraja, D.B. Goodin, M. Smith, and B.M. Hoffman, Identification by ENDOR of Trp191 as the free-radical site in cytochrome *c* peroxidase compound ES, *Science* 245, 1989, pp. 738-740.
55. J.E. Huyett, P.E. Doan, R. Gurbiel, A.L.P. Houseman, M. Sivaraja, D.B. Goodin, and B.M. Hoffman, Compound ES of Cytochrome *c* Peroxidase Contains a Trp  $\pi$ -Cation Radical: Characterization by Continuous Wave and Pulsed Q-Band External Nuclear Double Resonance Spectroscopy, *J. Am. Chem. Soc.* 117, 1995, pp. 9033-9041.
56. H.B. Dunford, Yeast cytochrome *c* Peroxidase. I: Properties and reactions with small molecules in *Heme Peroxidases*, Wiley-VCH, New York, 1999, pp. 235-236.
57. W.R. Patterson and T.L. Poulos, Crystal structure of recombinant pea cytosolic ascorbate peroxidase, *Biochemistry* 34, 1995, pp. 4331-4341.
58. T.L. Poulos, S.L. Edwards, H. Wariishi, and M.H. Gold, Crystallographic refinement of lignin peroxidase at 2Å, *J. Biol. Chem.* 268, 1993, pp. 4429-4440.
59. M. Sundaramoorthy, K. Kishi, M.H. Gold, and T. L. Poulos, The crystal structure of manganese peroxidase from *Phanerochaete chrysosporium* at 2.06-Å

- resolution, *J. Biol. Chem.* 269, 1994, pp. 32759-32767.
60. L. Marquez, H. Wariishi, H.B. Dunford, and M.H. Gold, Spectroscopic and kinetic properties of the oxidized intermediates of lignin peroxidase from *Phanerochaete chrysosporium*, *J. Biol. Chem.* 263, 1988, pp. 10549-10552.
  61. M. Sundaramoorthy, H.L. Youngs, M.H. Gold, and T.L. Poulos, High-resolution crystal structure of manganese peroxidase: substrate and inhibitor complexes, *Biochemistry* 44, 2005, pp. 6463-6470.
  62. L. Banci, I. Bertini, C. Capannoli, R. Del Conte, and M. Tien, Spectroscopic characterization of active mutants of manganese peroxidase: mutations on the proximal side affect calcium binding of the distal side, *Biochemistry* 38, 1999, pp. 9617-9625.
  63. D.J. Schuller, N. Ban, R.B. van Huystee, A. McPherson, and T.L. Poulos, The crystal structure of peanut peroxidase, *Structure* 4(3), 1996, pp. 311-321.
  64. M. Rodriguez, M.J. Stillman, and R.B. van Huystee, Codependency of calcium and porphyrin for an integrated molecular structure of peanut peroxidase: a circular dichroism analysis, *Biochem. Biophys. Res. Commun.* 194, 1993, pp. 326.
  65. N.S. Reading and S.D. Aust, Engineering a disulfide bond in recombinant manganese peroxidase results in increased thermostability, *Biotech. Prog.* 16, 2000, pp. 326-333.
  66. R.A. Ghiladi, K.F. Medzihradzky, and P.R. Ortiz de Montellano, Role of the Met-Tyr-Trp crosslink in *Mycobacterium tuberculosis* catalase-peroxidase (KatG) as revealed by KatG (M255I), *Biochemistry* 44, 2005, 15093-15105.
  67. Y. Yamada, T. Fujiwara, T. Sato, N. Igarashi, and N. Tanaka, The 2.0 Å crystal structure of catalase-peroxidase from *Haloarcula marismortui*, *Nat Struct Biol* 9, 2002, pp. 691-695.
  68. X. Carpena, S. Loprasert, S. Mongkolsuk, J. Switala, P. C. Loewen, and I. Fita, Catalase-peroxidase KatG of *Burkholderia pseudomallei* at 1.7Å resolution, *J Mol Biol* 327, 2003 pp. 475-489.
  69. M. Zamocky, G. Regelsberger, C. Jakopitsch, and C. Obinger, The molecular peculiarities of catalase-peroxidases, *FEBS Lett* 492 (2001), pp. 177-182.
  70. K. G. Welinder, Bacterial catalase-peroxidases are gene duplicated members of the plant peroxidase superfamily, *Biochim Biophys Acta* 1080 (1991), 215-220.



71. Y. Li and D.C. Goodwin, Vital roles of an interhelical insertion in catalase-peroxidase bifunctionality, *Biochem. and Biophys. Res. Commun.* 318 (2004), pp. 970-976.
72. T. Bertrand, N. A. Eady, J. N. Jones, Jesmin, J. M. Nagy, B. Jamart-Gregoire, E. L. Raven, and K. A. Brown, Crystal structure of Mycobacterium tuberculosis catalase-peroxidase, *J Biol Chem* 279 (2004) 38991-38999.
73. G. Regelsberger, C. Jakopitsch, F. Rümer, D. Krois, G.A. Peschek and C. Obinger, Effect of distal cavity mutations on the formation of compound I in catalase-peroxidases, *J. Biol. Chem.* 275 (2000), pp. 22854–22861.
74. A. Hillar, B. Peters, R. Pauls, A. Loboda, H. Zhang, A.G. Mauk and P.C. Loewen, Modulation of the activities of catalase-peroxidase HPI of Escherichia coli by site-directed mutagenesis, *Biochemistry* 39 (2000), pp. 5868–5875.
75. S. Yu, S. Giroto, X. Zhao and R.S. Magliozzo, Rapid formation of compound II and a tyrosyl radical in the Y229F mutant of Mycobacterium tuberculosis catalase-peroxidase disrupts catalase but not peroxidase function, *J. Biol. Chem.* 278 (2003), pp. 44121–44127.
76. C. Jakopitsch, M. Auer, A. Ivancich, F. Ruker, P.G. Furtmüller and C. Obinger, Total conversion of bifunctional catalase-peroxidase (KatG) to monofunctional peroxidase by exchange of a conserved distal side tyrosine, *J. Biol. Chem.* 278 (2003), pp. 20185–20191.
77. E. Santoni, C. Jakopitsch, C. Obinger and G. Smulevich, Comparison between catalase-peroxidase and cytochrome c peroxidase. The role of the hydrogen-bond networks for protein stability and catalysis, *Biochemistry* 43 (2004), pp. 5792–5802.
78. M. Zamocky, S. Janecek, F. Miller, Common phylogeny of catalase-peroxidases and ascorbate peroxidases, *Gene* 256 (2000) pp. 169-182.
79. R.D. Baker, C.O. Cook, and D.C. Goodwin, Properties of catalase-peroxidase lacking its C-terminal domain, *Biochem. Biophys. Res. Commun.* 320 (2004), pp. 833-839.
80. R.D. Baker, C.O. Cook, and D.C. Goodwin, Catalase-peroxidase active site restructuring by a distant and “inactive” domain, *Biochemistry* 45:23 (2006), pp. 7113-7121.
81. Y. Li, Roles of two interhelical insertions in catalase–peroxidase catalysis: tracing the impact of peripheral protein structures on heme enzyme function. Doctoral Dissertation, Auburn University, Auburn, AL, (2005), 108 – 110.

82. K. Wada, T. Tada, Y. Nakamura, T. Kinoshita, M. Tamoi, S. Shigeoka, K. Nishimura, Crystallization and preliminary X-ray diffraction studies of catalase-peroxidase from *Synechococcus* PCC7942, *Acta Crystallogr. D Biol. Crystallogr.* 58 (2002), 157 – 159.
83. A. Rattan, A. Kalia, and N. Ahmad, Multidrug-resistant Mycobacterium tuberculosis: molecular perspectives, *Emerging Infect. Dis.* 4 (1998) pp. 195-209.
84. W. Brunder, H. Schmidt, and H. Karch, KatP, a novel catalase-peroxidase encoded by the large plasmid of enterohaemorrhagic *Escherichia coli* O157:H7, *Microbiology* 142 (Part 11), 1996, pp. 3305-3315.
85. E. Garcia, Y.A. Nedialkov, J. Elliott, V.L. Motin, and R.R. Brubaker, Molecular characterization of KatY (antigen 5), a thermoregulated chromosomally encoded catalase-peroxidase of *Yersinia pestis*, *J. Bacteriol.* 181 (1999) pp. 3114-3122.
86. R.J. Mehigh and R.R. Brubaker, Major stable peptides of *Yersinia pestis* synthesized during the low-calcium response, *Infect. Immun.* 61 (1993) pp. 13-22.
87. B.A. Chromy, M.W. Choi, G.A. Murphy, A.D. Gonzales, C.H. Corzett, B.C. Chang, J.P. Fitch, and S.L. McCutchen-Maloney, Proteomic characterization of *Yersinia pestis* virulence, *J. Bacteriol.* 187 (1993) pp. 8172-8180.
88. C. Jakopitsch, M. Auer, G. Regelsberger, W. Jantschko, P.G. Furtmuller, F. Ruker, and C. Obinger, Distal site aspartate is essential in the catalase activity of catalase-peroxidases, *Biochemistry* 42 (2003) pp. 5292-5300.
89. J. M. Sambrook, and E. F. Fritsch, *Molecular cloning: a laboratory manual*, ed., Cold Spring Harbor, NY 1989.
90. J. K. Falk, *Porphyrins and Metalloporphyrins*, ed., Elsevier Publishing, New York 1964.
91. S.L. Scott, W.J. Chen, A. Bakac, and J.H. Espenson, Spectroscopic parameters, electrode potentials, acid ionization constants, and electron exchange rates of the 2, 2'-azinobis(3-ethylbenzothiazoline-6-sulfonate) radicals and ions, *J. Phys. Chem.* 97 (1993) pp. 6710-6714.
92. S.C. Gill and P.H. von Hippel, Calculation of protein extinction coefficients from amino acid sequence data, *Anal. Biochem.* 182, (1989) pp. 319-326
93. C.L. Varnado, K.M. Hertwig, R.Thomas, J.K. Roberts, and D.C. Goodwin, Properties of a novel periplasmic catalase-peroxidase from *Escherichia coli* O157:H7, *Arch. Biophys.* 421, (2004) pp. 166-174.

94. J. W. Allen, N. Leach, and S. J. Ferguson, The histidine of the c-type cytochrome CXXCH heme-binding motif is essential for heme attachment by the *Escherichia coli* cytochrome *c* maturation (Ccm) apparatus, *Biochem. J.* (2005).
95. P. Kotsonis, L. G. Frohlich, C. S. Raman, H. Li, M. Berg, R. Gerwig, V. Groehn, Y. Kang, N. Al-Masoudi, S. Taghavi-Moghadam, D. Mohr, U. Munch, J. Schnabel, P. Martasek, B. S. Masters, H. Strobel, T. Poulos, H. Matter, W. Pfeleiderer, and H. H. Schmidt, Structural basis for pterin antagonism in nitric-oxide synthase. Development of novel 4-oxo-pteridine antagonists of (6R)-5, 6, 7, 8-tetrahydrobiopterin, *J. Biol. Chem.* 276 (2001) 49133-49141.
96. R. E. Dickerson, T. Takano, D. Eisenberg, O. B. Kallai, L. Samson, A. Cooper, and E. Margoliash, Ferricytochrome *c*. 1. General features of the horse and bonito proteins at 2.8 Å resolution, *J. Biol. Chem.* 246 (1971) 1511-1535.
97. C. Jakopitsch, A. Wanasinghe, W. Jantschko, P.G. Furtmuller, and C. Obinger, Kinetics of interconversion of ferrous enzymes, compound II and compound III, of wild-type *Synechocystis* catalase-peroxidase and Y249F: proposal for the catalytic mechanism, *J. Biol. Chem.* 280 (2005) pp. 9037-9042.
98. P.M. Gadsby and A.J. Thomson, Assignment of the axial ligands of ferric ion in low-spin hemoproteins by near-infrared magnetic circular dichroism and electron paramagnetic resonance spectroscopy, *J. Am. Chem. Soc.* 112 (1990) pp. 5003-5011.
99. G. Palmer, *The porphyrins: physical chemistry, part B* (Dolphin, D., Ed.) (1979) pp. 313-350.
100. S. Chouchane, S. Giroto, S. Kapetanki, J.P. Schelvis, S. Yu, and R.S. Magliozzo, Analysis of Heme Structural Heterogeneity in *Mycobacterium tuberculosis* Catalase-Peroxidase (KatG), *J. Biol. Chem.* 278 (2003) pp.8154-8162.
101. C. Jakopitsch, A. Ivancich, F. Schmuckenschlager, A. Wanasinghe, P.G. Furtmüller, F. Rümer and C. Obinger, Influence of the unusual covalent adduct on the kinetics and formation of radical intermediates in *synechocystis* catalase peroxidase: a stopped-flow and EPR characterization of the MET275, TYR249, and ARG439 variants, *J. Biol. Chem.* 279 (2004), pp. 46082–46095.
102. C. Jakopitsch, M. Auer, G. Regelsberger, W. Jantschko, P.G. Furtmuller, F. Ruker, and C. Obinger, The catalytic role of the distal site asparagine-histidine couple in catalase-peroxidases, *Eur. J. Biochem.* 270 (2003) pp. 1006-1013.
103. R.A. Ghiladi, G.M. Knudsen, K.F. Medzihradzky and P.R. Ortiz de Montellano, The Met-Tyr-Trp cross-link in *Mycobacterium tuberculosis* catalase-peroxidase (KatG): autocatalytic formation and effect on enzyme catalysis and spectroscopic properties, *J. Biol. Chem.* 280 (2005), pp. 22651–22663.

104. L. Donald, O.V. Krokhin, H.W. Duckworth, B. Wiseman, T. Deemagarn, R. Singh, J. Switala, X. Carpena, I. Fita, and P.C. Loewen, Characterization of the catalase-peroxidase KatG from *Burkholderia pseudomallei* by mass spectrometry, *J. Biol. Chem.* 278 (2003) pp. 35687-35692.
105. N.A.J. Eady, N.A.J. Jesmin, S. Servos, A.E.G. Cass, J.M. Nagy, K.A. Brown, Probing the function of *Mycobacterium tuberculosis* catalase-peroxidase by site-directed mutagenesis, *Dalton Transl.* 2005 (2005) pp. 3495-3500.
106. T.L. Poulos, S.L. Edwards, H. Wariishi, and M.H. Gold, Crystallographic refinement of lignin peroxidase at 2 Å, *J. Biol. Chem.* 268 (1993) pp.4429-4440.
107. M. Sundaramoorthy, K. Kishi, M.H. Gold, and T.L. Poulos, The crystal structure of manganese peroxidase from *Phanerochaete chrysosporium* at 2.06-Å resolution, *J. Biol. Chem.* 269 (1994) pp. 32759-32767.
108. G.R. Sutherland, L.S. Zapanta, M. Tien, and S.D. Aust, Role of calcium in maintaining the heme environment of manganese peroxidase, *Biochemistry* 36 (1997) pp. 3654-3662.
109. G. Nie and S.D. Aust, Spectral changes of lignin peroxidase during reversible inactivation, *Biochemistry* 36 (1997) pp. 5113-5119.
110. G. Nie and S.D. Aust, Effect of calcium on the reversible thermal inactivation of lignin peroxidase, *Arch. Biochem. Biophys.* 337 (1997) pp. 225-231.
111. D.J. Schuller, N. Ban, R.B. Huystee, A. McPherson, T.L. Poulos, The crystal structure of peanut peroxidase, *Structure*, **1996**, 4(3), 311 – 321.
112. M. Gajhede, D.J. Schuller, A. Henriksen, A.T. Smith, and T.L. Poulos, Crystal structure of horseradish peroxidase C at 2.15Å resolution, *Nat. Struct. Biol.* 4 (1997) pp. 1032-1038.
113. Y. Shiro, M. Kurono, and I. Morishima, Presence of endogenous calcium ion and its functional and structural regulation in horseradish peroxidase, *J. Biol. Chem.* 261 (1986) pp. 9382-9390.
114. Van Huystee, R.B., Y. Xu, and J.P. O'Donnell, Preliminary crystallographic studies of peanut peroxidase, *Plant Physiol. Biochem.* 30 (1992) pp. 293-297.
115. N.S. Reading and S.D. Aust, Engineering a disulfide bond in recombinant manganese peroxidase results in increased thermostability, *Biotech. Prog.* 16 (2000) pp. 326-333.
116. G.R. Sutherland and S.D. Aust, Thermodynamics of binding of the distal calcium

- to manganese peroxidase, *Biochemistry* 36 (1997) pp. 8567-8573.
- 117.C. Jakopitsch, D. Kolarich, G. Petutschnig, P.G. Furtmuller and C. Obinger, Distal side tryptophan, tyrosine and methionine in catalase-peroxidases are covalently linked in solution, *FEBS Lett.* 552 (2003), pp. 135–140.
- 118.X. Carpena, W. Melik-Adamyanyan, P.C. Loewen, and I. Fita, Structure of the C-terminal domain of the catalase-peroxidase KatG from *Escherichia coli*, *Acta Crystallogr., Sect. D: Biol. Crystallogr.* 60, 2004, pp. 1824-1832.
- 119.L. Tang, L. Stith, and E.K. Jaffe, Substrate-induced interconversion of protein quaternary structure isoforms, *J. Biol. Chem.* 280 (2005) pp. 15786-15793.
- 120.Y. Li, Roles of two interhelical insertions in catalase–peroxidase catalysis: tracing the impact of peripheral protein structures on heme enzyme function. Doctoral Dissertation, Auburn University, Auburn, AL, (2005), 108 – 110.
- 121.M.R.Cheesman, C. Greenwood, and A.J. Thomson, Magnetic Circular Dichroism of Hemoproteins; *Advances in Inorganic Chemistry Vol. 36* (Academic Press: New York, NY) (1991) pp. 201-255.
- 122.E.W. Svastis, J.H. Dawson, Models for ferrous cytochrome *b<sub>5</sub>*: sign inversions in the magnetic circular dichroism spectra of bis-imidazole ferrous porphyrin systems, *Inorganica Chimica Acta* 123 (1986) pp. 83-86.
- 123.J. Cheek, D. Mandelman, T.L. Poulos, J.H. Dawson, A study of the K<sup>+</sup>-site mutant of ascorbate peroxidase: mutations of protein residues on the proximal side of the heme cause changes in iron ligation on the distal side, *J. Biol. Inorg. Chem.* 4 (1999) pp. 64-72.
- 124.A. Ivancich, C. Jakopitsch, M. Auer, S. Un, C. Obinger, . Protein-based radicals in the catalase-peroxidase of *Synechocystis* PCC6803: A multifrequency EPR Investigation of wild-type and variants on the environment of the heme active site, *J. Am. Chem. Soc.* 125(46) (2003) pp. 14093-14102.
- 125.Banci, L.; Bartolesi, I.; Ciofi-Baffoni, S.; Tien, M. Unfolding and pH studies on manganese peroxidase: role of heme and calcium on secondary structure stability, *Biopolymers*, **2003**, 72(1), 38-47.
- 126.Cook, C.O., Moore, R.L., and Goodwin, D.C., The effect of R117 and D597 interdomain residue substitutions on the reactivation of *Escherichia coli* catalase-peroxidase, *2008 Proceedings of the 35<sup>th</sup> Annual Conference of the National Organization for the Professional Advancement of Black Chemists and Chemical Engineers*, Philadelphia, PA, April 2008.

127. A.E. Pond, M. Sono, Elenkova, E.A., D.B. Goodin, A.M. English, J.H. Dawson, Influence of protein environment on magnetic circular dichroism spectral properties of ferric and ferrous ligand complexes of yeast cytochrome *c* peroxidase, *Biospectroscopy* 5 (1999) 542-552.
128. L. Vickery, T. Nozawa, K. Sauer, Magnetic circular dichroism studies of low-spin cytochromes. Temperature dependence and effects of axial coordination on the spectra of cytochrome *c* and cytochrome *b5*, *J. Am. Chem. Soc.* 98 (1976) 351-357.
129. M.K. Johnson, in Que (Ed.) *Physical methods in Bioinorganic Chemistry: Spectroscopy and Magnetism, CD, and MCD Spectroscopy*, University Science Books (2000) pp. 233-285.
130. Moore, R.L., Cook, C.O., Williams, R., Goodwin, D.C. Substitution of strictly conserved Y111 in catalase-peroxidases: Impact of remote interdomain contacts on active site structure and catalytic performance, *J. Inorg. Biochem.* 2008, pp. 1819-1824.
131. Y. Cao, R. A. Musah, S. K. Wilcox, D. B. Goodin, and D. E. McRee, Protein conformer selection by ligand binding observed with crystallography, *Protein Science* 7 (1998) 72-78.
132. E. Garcia-Fruitos, N. Gonzalez-Montalban, M. Morell, A. Vera, R.M. Ferraz, A. Aris, S. Ventura, and A. Villaverde, Aggregation as bacterial inclusion bodies does not imply inactivation of enzymes and fluorescent proteins, *Microbial Cell Factories* 4(27), 2005, pp. 1-6.
133. M. Bertin, S.M. Pomponi, C. Kokuhuta, N. Iwasaki, T. Suzuki, and W.R. Ellington, Origin of the genes for the isoforms of creatine kinase, *Gene* 392(1-2), 2007, pp. 273-282.
134. X. Carpena, B. Wiseman, T. Deemagarn, R. Singh, J. Switala, A. Ivancich, I. Fita, and P.C. Loewen, A molecular switch and electronic circuit modulates catalase activity in catalase-peroxidases, *EMBO reports* 6, 2005, pp. 1156-1162.
135. J.E. Erman, L.B. Vitello, M.A. Miller, A. Shaw, K.A. Brown, J. Kraut, Histidine 52 is a critical residue for rapid formation of cytochrome *c* peroxidase compound I, *Biochemistry* 32, 1993, pp. 9798-9806.
136. G.K. Farber, An  $\alpha/\beta$ -barrel full of evolutionary trouble, *Curr. Opin. Struc. Biol.* 3(3), 1993, pp. 409-12.

137. C. Yanofsky, E. W. Miles, T. Bauede, and K. Kirschner, The trp Operon and Tryptophan Biosynthesis in *Escherichia coli* and *Salmonella enterica*, T. E. Creighton, Ed., Vol. 4 of *The Encyclopedia of Molecular Biology* (Wiley, New York, 1999), pp. 2676-2689.
138. T. Dandekar, B. Snel, M. Huynen, and P. Bork, Conservation of gene order: a fingerprint of proteins that physically interact, *Trends Biochem. Sci.* 23, 1998, pp. 324.
139. J.A. Gerlt and F.M. Raushel, Evolution of function in (b/a)<sub>8</sub>-barrel enzymes, *Current Opinion in Chemical Biology* 7, 1007, pp. 252-264.
140. L. Liu, K. Iwata, A. Kita, Y. Kawarabayasi, M. Yohda and K. Miki, Crystal structure of aspartate racemase from *Pyrococcus horikoshii* OT3 and its implications for molecular mechanism of PLP-independent racemization, *J. Mol. Biol.* 319, 2002, pp. 479–489.
141. L. Liu, K. Iwata, M. Yohda, and K. Miki, Structural insight into gene duplication, gene fusion, and domain swapping in the evolution of PLP-independent amino acid racemases, *FEBS Letters* 528(1), 2002, pp. 114-118.
142. T. Suzuki, Y. Kawasaki, and T. Furukohri, Evolution of phosphagen kinase: isolation, characterization and cDNA-derived amino acid sequence of two-domain arginine kinase from sea anemone *Anthopleura jopnicus*, *Biochem. J.* 328, pp. 301-306.
143. T. Suzuki, Y. Kawasaki, Y. Unemi, Y. Nishimura, T. Soga, M. Kamidochi, Y. Yazawa, and T. Furukohri, Gene duplication and fusion have occurred frequently in the evolution of phosphagen kinases – a two-domain arginine kinase from the clam *Pseudocardium sachalinensis*, *Biochim. Biophys. Acta.*, 1388, 1998, pp. 253-259.
144. T. Suzuki, N. Sugimura, T. Taniguchi, Y. Kawasaki, Y. Unemi, T. Murata, M. Haysahida, K. Yokouchi, and T. Furukohri, Two-domain arginine kinases from the clams of *Solen strictus* and *Corbicula japonica*. Exceptional amino acid replacement of the functionally important D62, *G. Int. Biochem. Cell. Biol.* 34, 2002, pp. 1221-1229.
145. D.M. Compann and W.R. Ellington, Functional consequences of a gene duplication and fusion event in an arginine kinase, *J. Exp. Biol.* 206, 2003, pp. 1545-1556.
146. K. Uda, K. Yamamoto, N. Iwasaki, M. Iwai, K. Fujikura, W.R. Ellington, and T. Suzuki, Two-domain arginine kinase from the deep-sea clam *Calyptogena kaikoi* – Evidence of two active domains, *Comparative Biochem. and Physiol., Part B* 151, 2008, pp. 176-182.

147. T.O. Baldwin, J.A. Christopher, F.M. Raushel, J.F. Sinclair, M.M. Ziegler, A.J. Fisher, and I. Rayment, Structure of bacterial luciferase, *Curr. Opin. Struc. Biol.* 5, 1995, pp. 798-809.
148. T.O. Baldwin and M.M. Zieger, The biochemistry and molecular biology of bacterial bioluminescence. In: F Müller, Editor, *Chemistry and Biochemistry of Flavoenzymes III*, CRC Press, Boca Raton, FL, 1992, pp. 467-530.
149. W.W. Parson, Electron transport and oxidative phosphorylation, in *Biochemistry*, G.L. Zubay, ed., pp. 379-413, third edition, W.C. Brown Publishers, Dubuque, Iowa, 1993.
150. H.J. Forman and M.J. Thomas, Oxidant production and bactericidal activity of phagocytes, *Ann. Rev. Physiol.* 48, (1986), pp. 669.
151. P. Chelikani, I. Fita, and P.C. Loewen, Diversity of structures and properties among catalases, *Cell Mol. Life Sci.* 61(2), 2004, pp. 192-208.
152. M.G. Klotz and P.C. Loewen, The molecular evolution of catalatic hydroperoxidases: evidence for multiple lateral transfer of genes between prokaryota and from bacteria into eukaryote, *Mol. Biol. Evol.* 20(7), 2003, pp. 1098-1112.
153. J. Bravo, P.C. Loewen, and I. Fita, Crystal structure of catalase HP11 from *Escherichia coli*, *Structure* 3(1995), pp. 491-502.
154. J. Wang, J.M. Mauro, S.L. Edwards, S.J. Oatley, L.A. Fishel, V.A. Ashford, N.-H. Xuong, and J. Kraut, X-ray structures of recombinant yeast cytochrome *c* peroxidase and three heme-cleft mutants prepared by site-directed mutagenesis, *Biochemistry* 29 (1990), pp. 7160-7173.
155. K.G. Welinder, Superfamily of plant, fungal and bacterial peroxidases, *Current Opinion in Structural Biology* 2 (1992), pp. 388-393.
156. J. Hirst, S.K. Wilcox, J. Ai, P. Moenne-Loccoz, T.M. Loehr, and D.B. Goodin, Replacement of the axial histidine ligand with imidazole in cytochrome *c* peroxidase. 2. Effects on heme coordination and function, *Biochemistry* 40(5), 2001, pp. 1274-1283.
157. M.O. Boylan, J. Pelletier, S. Dhepagnon, S. Trudel, N. Sonenberg, and E.A. Meighen, Construction of a fused LuxAB gene by site-directed mutagenesis, *J. Biolumin. Chemilumin.* 4(1), 1989, pp. 310-316.
158. G. Smulevich, M.A. Miller, J. Kraut, and T.G. Spiro, Conformational change and histidine control of heme chemistry in cytochrome *c* peroxidase: resonance



Raman evidence from Leu-52 and Gly-181 mutants of cytochrome c peroxidase, *Biochemistry* 30(39), 1991, pp. 9546-9558.

- 159.K. Kishi, D.P. Hildebrand, M. Kusters-van Someren, J. Gettemy, A.G. Mauk, and M.H. Gold, Site-directed mutations at phenylalanine-190 of manganese peroxidase: effects on stability, function, and coordination, *Biochemistry* 36(14), 1997, pp. 4268-4277.